Nonlinearities in the quantum measurement process of superconducting qubits

Ioana Şerban

München, 2008

Nonlinearities in the quantum measurement process of superconducting qubits

Ioana Şerban

Dissertation
an der Fakultät für Physik
der Ludwig–Maximilians–Universität
München

vorgelegt von
Ioana Şerban
aus Bukarest, Rumänien

München, Mai 2008

Erstgutachter: Prof. Dr. Jan von Delft
Zweitgutachter: Prof. Dr. Frank K. Wilhelm
Tag der mündlichen Prüfung: 09.07.2008

Contents

List of Figures

Abstract

As condensed matter systems become smaller, and ultimately reach the nanoscale, quantum electrodynamical effects become more important. Mesoscopic systems such as quantum dots and ultra-small Josephson junctions can, e. g., be used as artificial atoms or molecules. Compared to natural atoms, they present the significant advantage that their optical and electronic properties can be designed and controlled with high flexibility. Such artificial quantum systems offer an attractive combination of high engineering potential and quantum properties, thus being an ideal test-bed for fundamental physics. These properties make solid state devices promising candidates in the realization of a scalable quantum computer.

It has been shown that solid-state quantum bits (qubits) present quantum-coherent features such as Rabi oscillations and Ramsey fringes. Nevertheless, the preservation of such a coherent behavior in the presence of the many degrees of freedom in the environment of such mesoscopic devices remains an important issue, as well as the detection of the quantum state of the qubit.

The work described in this thesis focuses on the investigation of decoherence and measurement backaction, on the theoretical description of measurement schemes and their improvement. It is motivated by the importance of improving detection schemes for the field of quantum computing, but also by the fundamental interest in the physics of quantum measurement and the implications of nonlinearities for this process.

The study presented here is centered around quantum computing implementations using superconducting devices and most important, the Josephson effect. The measured system is invariantly a qubit, i. e. a two-level system. The objective is to study detectors with increasing nonlinearity, e. g. coupling of the qubit to the frequency a driven oscillator, or to the bifurcation amplifier, to determine the performance and backaction of the detector on the measured system and to investigate the importance of a strong qubit-detector coupling for the achievement of a quantum non-demolition type of detection.

The first part gives a very basic introduction to quantum information, briefly reviews some of the most promising physical implementations of a quantum computer before focusing on the superconducting devices. It also gives a short summary for the theory of decoherence, which offers powerful tools for the description of open quantum systems, thus providing an insight into the physics of quantum measurement.

The second part presents a series of studies of different qubit measurements, describing the backaction of the measurement onto the measured system and the internal dynamics of the detector. The chapters follow closely publications in peer reviewed journals, or still under review, and have a self contained structure, with separate introduction and conclusion.

Methodology adapted from quantum optics and chemical physics (master equations, phase-space analysis etc.) combined with the representation of a complex environment yielded a tool capable of describing a nonlinear, non-Markovian environment, which couples arbitrarily strongly to the measured system. This is described in chapter 3 along with a theoretical description of the the dispersive readout protocol of Ref. [1]. The developed tool allows the investigation of the non-linear coupling between qubit and its detector beyond the weak measurement limit. Chapter 4 focuses on the backaction on the qubit and presents novel insights into the qubit dephasing in the strong coupling regime.

Chapter 5 uses basically the same system and technical tools to explore the potential of a fast, strong, indirect measurement, and determine how close such a detection would ideally come to the quantum non-demolition regime.

Chapter 6 focuses on the internal dynamics of a strongly driven Josephson junction. The nonlinearity of this device (or rather of the very similar Josephson bifurcation amplifier, JBA) has been already used as a significant ingredient for a qubit measurement, achieving remarkable resolution. However, this feature may be a source of novel macroscopic quantum features such as macroscopic dynamical tunneling, and thus worth attention by itself. Dynamical tunneling refers to tunneling between two patterns of motion rather than the conventional tunneling between two points in space. The possibility for such an phenomenon to be detected, in the presence of noise, with present day technological means is investigated. The analytical results are based on phase-space methods, a modified version of the WKB approximation and the Caldeira-Leggett approach.

Returning to the application of the JBA as a qubit detector, chapter 7 describes the relaxation of the qubit in contact with its detector.

The last chapter is concerned with optimal control of a qubit in the presence of a two level fluctuator. The two level fluctuator represents e. g. a resonator in the amorphous material of a Josephson junction. The theory of optimal control is applied to a qubit Z gate. The optimization takes into account the environment represented by the fluctuator and thus expands the limits of coherent control for solid state qubits.

Part I

Introduction

Chapter 1

Quantum measurement

Within the frame of quantum mechanics, the process of *measurement* has been and remains a topic of discussion [2]. It is usually introduced in the form of a separate, fundamental postulate, which involves an irreversible time evolution for the measured system. Thus, the standard textbook description of a quantum measurement states that a system $\mathbb{S}$ evolves continuously according to a unitary, deterministic dynamics, determined only by the properties of the system Hamiltonian, as long as no measurement is made. However, if a measurement is made, the system instantaneously and randomly changes its state into a state that corresponds to the value of the measurement outcome.

Mathematically this can be formulated as follows (the *Born rule*): the measurement process instantaneously transforms an initial quantum state described by a Hilbert space vector $|\Psi\rangle$ into one of the eigenstates $|o_n\rangle$ of the operator $\hat{O}$ that describes the measured observable. Within the traditional interpretation of quantum mechanics, this instantaneous, irreversible and non-unitary evolution is known as "wavefunction collapse". The outcome o_n of the measurement, where $\{o_n\}$ are the eigenvalues of $\hat{O}$, emerges randomly with a probability $|\langle\Psi|o_n\rangle|^2$. Ideally, the measurement leaves the measured quantity unperturbed. It follows that, by repeating the measurement, the outcome of the second measurement is the same as the first. However, this does not describe the most general type of measurement and has been extended to the idea of a positive operator-valued measure [3].

According to the Heisenberg uncertainty principle, the precise values of a pair of conjugate variables, e. g. position and momentum, cannot be simultaneously determined with arbitrary precision. In the context of quantum measurement this has consequences for the precision with which an observable can be measured. More precisely, the reason for this limitation is that one cannot always prevent, in the design of the measuring device, the simultaneous gain of information about the observable conjugate to $\hat{O}$, see also Ref. [4]. Thus a perturbation of the measured quantity occurs, limited by the uncertainty relation. Even in the ideal case, where the desired observable $\hat{O}$ alone is being monitored, limitations can occur, e. g. in the case of a continuous measurement. Here the perturbation on the conjugate observable can induce a perturbation of $\hat{O}$ at a later time, leading to the standard quantum limit [5]. The term quantum non-demolition (QND) refers to a measurement where no such perturbation of the measured observable occurs, nor is there any fundamental constraint on the measurement precision. In other words, this corresponds to the textbook description of measurement. It should be noted here that (in most cases) only observables that are conserved during the free evolution of the system and certain classes of interactions of the measured system with its detector permit a QND type of detection [5].

In reality, the measurement is performed by another physical system, the measurement apparatus $\mathbb{A}$, which itself can be described quantum-mechanically and is immersed in "the rest of the world", e. g. a large, closed environment $\mathbb{B}$. Measurements can be viewed as a class of interactions between the measured system $\mathbb{S}$ and its detector. The complete system $\mathbb{S} \otimes \mathbb{A} \otimes \mathbb{B}$ can be viewed as closed and described by the Schrödinger equation. However, the individual degrees of freedom associated with the environment $\mathbb{B}$ will remain unobserved and only a collective degree of freedom, associated with the measurement outcome, is detected.

A closed quantum system will have an unitary evolution, conserving quantum properties such as coherence. This is a property of waves to exhibit interference, e. g. of a quantum mechanical system to exist in a superposition of eigenfunctions of the observable to be measured. This property of a microscopic, closed, quantum mechanical system $\mathbb{S}$ is usually lost when the system becomes open, in contact with a dissipative environment $\mathbb{B}$, as is the case during the measurement. This local, subsystem specific suppression of interference is known as environment-induced decoherence. The complete wave function, describing the total system $\mathbb{S} \otimes \mathbb{B}$, remains coherent at all times. In general, the effect of decoherence increases with the size of the system, marking the transition between the quantum and classical worlds. A remarkable counterexample is given by superconducting devices [6], where superpositions of macroscopic[1] currents are observable. Effects of decoherence in such devices will be the main focus of this thesis.

Due to the interaction, correlations between the system $\mathbb{S}$ and the measurement apparatus $\mathbb{B}$ emerge in time. This interaction leaves a set of so-called pointer states of the system unchanged [9, 10] while their quantum superpositions are damped. The process of decoherence-induced selection of a preferred set of "robust" pointer states is called environment-induced superselection. The pointer states are uniquely determined by the form of the interactions between system, measurement apparatus and environment. They represent a small set of properties of the system, perceived as "classical". In the standard, textbook interpretation of the quantum measurement, they would be associated with the eigenstates of the measured observable. However, depending on the relative strengths of the Hamiltonians describing the complete system, different cases can be distinguished [11]. For example, if the dynamics are dominated by the system-environment Hamiltonian, then the pointer states will be eigenstates of this interaction Hamiltonian. If the interaction is weak, the pointer states are eigenstates of the system Hamiltonian.

This approach provides insight into the measurement problem, avoiding the arbitrariness of the boundary between the quantum and classical world. It sheds light onto the

[1] The question of macroscopically distinct superpositions, so called Schrödinger cat-states has been discussed e. g. in Refs. [7, 8].

mechanism of wave function collapse, but does not explain the randomness in the outcome of the final eigenstate.

The decoherence theory provides a good understanding of weak measurements, which only marginally perturb the measured system while extracting some information, i. e. a "weak value" about it [12, 13]. Indirect measurements are of interest for the work presented in this thesis. By introducing an intermediate, weakly damped quantum system $\mathbb{A}$ and measuring one of its observables directly influenced by the the system observable $\hat{O}$, one can investigate the effects of strong, nonlinear coupling between the system and its environment with tools commonly used for the description of weak measurements, such as master equations.

1.1 Quantum decoherence

The loss of quantum coherence is an irreversible process, associated with entropy increase, that takes place at the boundary between the quantum and classical world.

A standard treatment of decoherence is to let the system of interest, $\mathbb{S}$, interact with an environment $\mathbb{B}$ containing an infinite number (continuum) of degrees of freedom acting as a heath bath [14, 15]. The evolution of the complete system is unitary, and reversible, but the periodicity of this evolution is given by the energy splittings of the entire system. A continuous, infinite environment will then be periodic only on an infinite time scale. The dynamics of the reduced system $\mathbb{S}$ will be characterized by energy dissipation and local loss of coherence.

A good candidate for an environment is a bath of harmonic oscillators. The interaction with such an environment induces a reduced dynamics of $\mathbb{S}$ that reproduces the damped classical evolution of the system in certain limits [16]. Situations where the oscillator bath is an appropriate model include the case where the perturbation on the system is weak such that the bath can be treated within linear response theory, i. e. it is infinite, cannot be energetically saturated and remains in thermal equilibrium at all times. This is the case of interest for this thesis. The oscillator bath is introduced artificially as a tool to describe fluctuations and dissipation, and can be tailored to ensure, in the weak perturbation limit, the fulfillment of the dissipation-fluctuations theorem [17]. It can play the role of a Bosonic environment, e. g. phonons, or a Fermionic environment such as a the electrons in a resistor, where the electron-hole excitations behave like Bosons [18] up to high orders [19]. The main phenomenological quantity describing the bath is the spectral density of oscillators $J(\omega)$. Examples where such a model of the environment is not appropriate include, among others, spin baths which can saturate and shot noise which is not in thermal equilibrium.

It has been suggested (see Ref. [20] and the references therein) that the effects of a *low dimensional, chaotic* environment can be, in many ways, similar to those produced by thermal baths, pointing out the importance of ergodicity.

1.1.1 Open quantum systems

The time evolution of a closed quantum-mechanical system must be unitary. One considers a quantum mechanical system $\mathbb{S}$ in contact with an unobserved environment (bath) $\mathbb{B}$. The evolution of the total system obeys the Liouville-von Neumann equation

$$\mathbb{i}\hbar\dot{\hat{\rho}} = \left[\hat{H}, \hat{\rho}\right], \;\; \hat{H} = \hat{H}_S + \hat{H}_I + \hat{H}_B. \tag{1.1}$$

One can describe the effective evolution of the *reduced* system of interest, $\mathbb{S}$, by integrating over (tracing out) the unobserved degrees of freedom of the bath, $\hat{\rho}_s = \mathrm{Tr}_B\hat{\rho}$. This evolution is described by the formally exact Nakajima-Zwanzig equation [21, 22], which is an inhomogeneous integro-differential equation in time and can be solved by further approximations.

From the multitude of methods used for the treatment of quantum dissipative systems [19] we focus henceforth on the standard example of the master equation in the Born-Markov approximation. This equation will be the starting point of most calculations presented in this thesis. It reads

$$\dot{\hat{\rho}}_S(t) = \frac{1}{\mathbb{i}\hbar}[\hat{H}_S, \hat{\rho}_S(t)] + \frac{1}{(\mathbb{i}\hbar)^2}\int_0^\infty dt'\mathrm{Tr}_B[\hat{H}_I, [\hat{H}_I^I(t, t-t'), \rho_S(t)\hat{\rho}_B(0)]]. \tag{1.2}$$

For a detailed derivation of Eq. (1.2) see appendix A. The assumptions entering its derivation are:

1. $\mathbb{B}$ has many degrees of freedom such that the effects of the interaction with $\mathbb{S}$ dissipate quickly and do not act back on $\mathbb{S}$. $\mathbb{B}$ remains in equilibrium, independent on how much energy is being exchanged with $\mathbb{S}$.

2. The system-bath coupling is weak. Eq. (1.2) is basically a consistent expansion in $\hat{H}_I$ up to the second order, known as the Born approximation.

3. The coupling Hamiltonian is separable in system and bath operators, i. e. $\hat{H}_I = \sum_i \hat{S}_i \otimes \hat{B}_i$.

4. Before the interaction is turned on at $t = 0$ the system and bath are uncorrelated such that the initial state is factorized $\hat{\rho}(0) = \hat{\rho}_S \otimes \hat{\rho}_B(0)$.

5. The Markov approximation implies that the coupling to the environment destroys the information about previous evolution of the system, such that $\dot{\hat{\rho}}_S(t)$ depends on $\hat{\rho}_S(t)$ alone. The correlations that arise in the environment decay on a much faster time scale τ than all other processes in the system, i. e. the memory of the interaction is wiped out

$$\tau \ll 1/\lambda, \tag{1.3}$$

where λ describes the system-bath interaction strength. On a time scale shorter than τ, Eq. 1.2 is no longer reliable.

6. $\langle \hat{H}_i \rangle_B = 0$, i. e. the interaction produces no classical frequency shift, and the bath produces unbiased noise.

These are the assumptions under which the results presented in this work have been derived.

From a mathematical point of view, the evolution of the density matrix describing the reduced system must be completely positive [23, 24]. The most general form of generators $\hat{\mathcal{L}}$ that preserve complete positivity during the irreversible time evolution $\dot{\hat{\rho}} = \hat{\mathcal{L}}\hat{\rho}$ has been given by Lindblad [23]. The Born-Markov master equation usually (with some exceptions which imply e. g. the secular approximation) violates the complete positivity on the short time scale, when the Markov approximation is not valid.

1.2 Quantum optical methods for the solid state

This section will give an overview of the ingredients adapted from quantum optics which will be employed to describe solid state systems.

Using techniques such as the P-representation [25, 26] or the Wigner representation [27], harmonic systems can be reduced to quasiprobability distributions in the phase-space spanned by position x and momentum p.

A single electromagnetic mode is described in the second quantization by the Hamiltonian

$$\hat{H}_c = \hbar\Omega\left(\hat{a}^\dagger\hat{a} + \frac{1}{2}\right), \tag{1.4}$$

with eigenstates $|n\rangle$ (number states or Fock states).

The *coherent state* [25] plays a role central importance for quantum optics and is a basic ingredient for all phase-space techniques. It is the quantum state of the harmonic oscillator which most closely reproduces the classical motion of a particle in a quadratic potential. This is also the minimum-uncertainty eigenstate of the annihilation operator $\hat{a}$. It can be expressed in terms of the Fock states as follows

$$|\alpha\rangle = \mathrm{e}^{-\frac{1}{2}|\alpha|^2}\sum_{n=0}^{\infty}\frac{\alpha^n}{\sqrt{n!}}|n\rangle. \tag{1.5}$$

Here α is a complex number $\langle\hat{a}\rangle = \alpha$. The real and imaginary parts of α are associated with the position and momentum coordinates in the phase-space. Using the displacement operator $\hat{D}(\alpha) = \exp(\alpha\hat{a}^\dagger - \alpha^*\hat{a})$, the coherent state can be written as a unitary transformation of the vacuum state

$$|\alpha\rangle = \hat{D}(\alpha)|0\rangle. \tag{1.6}$$

Two coherent states are not orthogonal to each other, but satisfy the relation

$$\langle\beta|\alpha\rangle = \exp\left(\alpha^*\beta - \frac{1}{2}|\alpha|^2 - \frac{1}{2}|\beta|^2\right). \tag{1.7}$$

Coherent states also satisfy the completeness formula

$$\hat{\mathbb{1}} = \int d^2\alpha |\alpha\rangle\langle\alpha|. \tag{1.8}$$

Of particular importance for future discussion will be the representation of the density operator $\hat{\rho}$ of e. g. a harmonic oscillator in terms of coherent states. Among the various phase-space representations, the Wigner representation has proven most useful. By comparison to the P-representation, the Wigner representation is well defined for all density operators, and its characteristic function has, in the worst case, a delta singularity. Moreover, it turns out that the Wigner representation applied to noisy systems yields simpler forms of the differential equations that describe its time evolution.

For any operator $\hat{\rho}$ with finite norm (here one uses the Hilbert-Schmidt norm $\parallel \hat{\rho} \parallel = \left(\mathrm{Tr}\left\{\hat{\rho}^\dagger\hat{\rho}\right\}\right)^{1/2}$) has been shown [27] that following representation is possible

$$\hat{\rho} \;=\; \frac{1}{\pi}\int d^2\, \alpha \chi(\alpha)\hat{D}(-\alpha). \tag{1.9}$$

Here the phase-space distribution (or Wigner characteristic function) $\chi(\alpha)$ is the Fourier transform of the Wigner function

$$W(\alpha,\alpha^*) \;=\; \frac{1}{\pi^2}\int d^2\lambda \mathrm{e}^{-\lambda\alpha^*+\lambda^*\alpha}\chi(\lambda,\lambda^*), \tag{1.10}$$

$$W(x_0,p_0) \;=\; \frac{1}{\pi\hbar}\int dy\langle x_0+y|\hat{\rho}\, \mathrm{e}^{-2\mathrm{i}yp_0}|x_0-y\rangle. \tag{1.11}$$

It should be noted that the operator $\hat{\rho}$ in Eq. (1.9) does not necessarily need to have a trace constantly equal to unity, as it is the case of well-behaved density operators. The trace of $\hat{\rho}$ is given by

$$\langle\hat{\rho}\rangle \;=\; 4\pi\chi(0). \tag{1.12}$$

The Wigner function can have negative values, therefore it is not, in the true sense, a probability distribution. Nevertheless, it is useful for the evaluation of expectation values. When the representation (1.9) is introduced in the master equation (1.2), one transforms it into a partial differential equation for χ. For the case of a harmonic oscillator ($\mathbb{S}$) in contact with a bath of oscillators ($\mathbb{B}$) this becomes a simple Fokker-Planck equation [28] with an analytic solution.

Chapter 2

Quantum computing with superconducting devices

In a classical computer information is stored in form of bits which ideally take only the well defined values 0 and 1. By contrast, a quantum mechanical system with states $|0\rangle$ and $|1\rangle$ can exist in a continuum of linear combinations $\alpha|0\rangle + \beta|1\rangle$ of these states, until it is observed. The measurement collapses (or, in the language of the previous chapter, decoheres) the quantum bit (qubit) into one of the eigenstates, the chance for the outcome to be either $|0\rangle$ or $|1\rangle$ being given by the coefficients $|\alpha|^2$, $|\beta|^2$ of the superposition. Despite the fact that the measurement outcome can only be 0 or 1 as in a classical computer, in a closed quantum mechanical system nature keeps track of the coefficients of the superposition. Therefore, in principle, a computer operating according to the principles of quantum mechanics can perform a large number of computations in parallel.

The idea of making use of this advantage in the context of information processing has gained interest due to the substantial speedup for certain problems such as the search of an unsorted database [29] or the factorization of large numbers into primes [30], of importance for secure communication. Before that, it has been suggested by Feynman [31] that a quantum computer may efficiently simulate the behavior of another quantum system in cases where this task proves too difficult for a classical computer. Moreover, the laws of quantum mechanics can be exploited in the context of communication and cryptography [32].

The elementary building block of a quantum computer is the qubit. Operations on a quantum computer are described by unitary transformations that can be defined via the time evolution of a Hamiltonian. It has been shown that any n qubit operation can be decomposed into a set of universal one- and two-qubit gates with ability to entangle the two qubits, see Refs. [3, 33] and references therein.

In principle, the quantum computation is reversible. In practice nevertheless, this reversible time evolution is restricted by decoherence, which originates in the coupling to the surrounding environment. The practical realization of a quantum computer faces the challenge posed by the tendency for qubit superpositions of $|0\rangle$ and $|1\rangle$ to decohere (see also chapter 1) into either $|0\rangle$ or $|1\rangle$ due to the interaction with their environment.

A set of five general criteria are established guidelines in the search for a feasible physical implementation of a quantum computer. These (the DiVincenzo criteria [34–36]) request

1. a scalable physical system of well-characterized qubits
2. the ability to initialize the state of the qubits to a simple state such as $|000..\rangle$
3. long (relative) decoherence times, much longer than the gate-operation time
4. a universal set of quantum gates
5. a qubit-specific measurement capability

Promising physical systems for the implementation of a quantum computer include

- **optical-wavelength photons**. The qubits are represented by photons with different polarisation or in different modes of the light field. A scheme for efficient quantum computation with linear optics has been proposed [37]. Recently Shor's algorithm [30] has been demonstrated experimentally [38].

- **trapped ions**. Qubits are stored in stable states of each ion, the individual atoms can be manipulated by laser pulses and measured with photodetectors. Scalability can be achieved by use of ion-trap arrays that are interconnected with photons or by moving ions between trap nodes [39]. An experimental realization of the controlled-NOT gate with trapped ions has been proposed [40] and demonstrated [41] and the Deutsch-Jozsa [3] algorithm has been implemented [42]. Experimental quantum error correction [43] has also been implemented in ion traps.

- **neutral atoms**. Optical lattices can be loaded with cooled atoms and the qubits are defined as hyperfine states of these atoms or as their motional states in the trapping potential. Low decoherence is achieved for both internal and motional states due to the neutral charge. For the same reason, qubit interactions [44] are more difficult.

- **cavity QED**. The interaction between an atom-like, material qubit and the quantized field (single photon) of a optical or microwave resonator can be achieved in various systems ranging atoms, ions, solid state and superconducting devices. The common feature of all these implementations is the ability to coherently convert quantum states between material and photon qubits.

- **nuclear magnetic resonance (NMR)**. The qubits consist of distinct nuclear spins in liquid or solid state, have long coherence times. The detection occurs through an ensemble weak measurement which requires a large number of spins. Shor's algorithm [45] and quantum error correction [46] has been experimentally demonstrated. The liquid state approach is limited in scalability by chemistry and qubit initialization is problematic.

- **electrons on helium**. Electrons float above the surface of the helium, attracted to it by the helium dielectric image, and are prevented from entering the liquid by the Pauli exclusion principle. Their states can be manipulated by microwaves and by circuits embedded in the substrate below the helium film [47]. The quantized states associated with motion normal to the helium surface represent the qubit.

- **solid state based implementations** such as

  - *quantum dots* (semiconductor nanostructure, e. g. AlGaAs/GaAs that confines the motion of conduction band electrons) [48]. Here the intrinsic spin-1/2 degree of freedom of a single electron confined to the quantum dot represents the qubit. The qubits are controlled by local magnetic fields and interact via Heisenberg-exchange interaction. The readout occurs via direct measurement of the spin using a spin-filter such as a magnetic semiconductor or by converting the spin information to charge information (which can be detected by sensitive electrometers) through a spin-dependent tunnelling process. Alternatively, the qubit can be represented by the electron position in a double quantum well. First steps towards graphene quantum dots have been taken [49].
  - *impurities in solid state* (e. g. phosphorus donors embedded in silicon) [50]. In this case the nuclear spins of the donors (qubit encoding) and the spins of the electrons (qubit interaction) contribute to the computation.
  - *nuclear spins in diamond.* Coherent interactions between individual nuclear spin qubits were observed and their coherence properties were demonstrated [51].

- **superconducting devices**. Recently significant progress has been made with qubits in superconducting structures. They present good scalability prospects and flexibility in fabrication parameters. Coherent quantum control of single qubits [52–54] and a conditional operation for two coupled qubits [55, 56] have been demonstrated. Entanglement of two superconducting qubits was measured [57]. Nevertheless, because of to the many degrees of freedom in a solid-state system, decoherence remains an important challenge.

We will focus henceforth on the superconducting devices and their application for the practical realization of a quantum computer. These devices are based on the charge or phase degree of freedom associated with the Cooper pair condensates in superconductors separated by Josephson junctions.

2.1 The Josephson effect

It has been shown by Bardeen, Cooper and Schrieffer [59] that in a superconductor all the Cooper pairs of electrons that contribute to the supercurrent are condensed into a macroscopic state described by a single wave function $\Psi(\vec{r},t) = |\Psi(\vec{r},t)|\mathrm{e}^{\mathrm{i}\varphi(\vec{r},t)}$, and thus

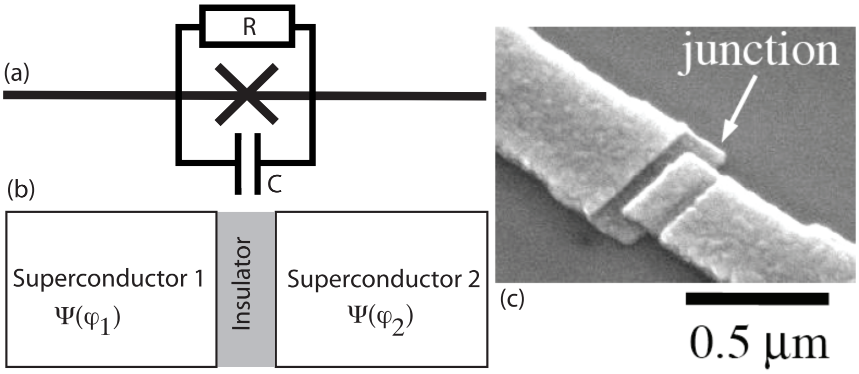

Figure 2.1: (a) Schematic representation of a resistively and capacitively shunted Josephson junction. (b) A basic Josephson junction consists of two superconductors connected by a weak link e. g. a piece of insulator. (c) Picture of a Josephson junction fabricated with shadow-evaporation techniques [58].

behaving as a single degree of freedom. This behavior confers to the (macroscopic) superconducting circuits many features common to microscopic systems such as quantized energy levels, superpositions of states. It is crucial for the operation of superconducting devices as qubits. In particular the phase φ plays an essential role in the Josephson effect.

The basic building block for superconducting devices, the Josephson junction, Fig. 2.1 (b) and (c), is a thin tunnel barrier between two superconductors, e. g. an insulating layer such an oxide layer, a normal metal or a constriction region. In 1962, B. D. Josephson [60] predicted that even at zero applied voltage, a finite DC supercurrent will flow between the two superconductors,

$$I_{\mathrm{s}} = I_{\mathrm{c}} \sin(\Delta\varphi), \tag{2.1}$$

where $\Delta\varphi = \varphi_1 - \varphi_2$ is the phase difference between the Cooper-pair condensate wavefunctions in the two superconductors, and I_{c} is the critical current, i. e. is the maximum supercurrent that the junction can support. In the presence of an applied voltage, the phase difference $\Delta\varphi$ evolves according to

$$\frac{d}{dt}\Delta\varphi = \frac{2eV}{\hbar}, \tag{2.2}$$

such that the flowing supercurrent alternates with frequency $2eV/h$. In terms of the gauge invariant phase difference

$$\gamma = \Delta\varphi - \frac{2\pi}{\Phi_0}\int \vec{A}\cdot d\vec{s}, \tag{2.3}$$

with the flux quantum $\Phi_0 = h/2e$, $\vec{A}$ the vector potential, and the integration running from one electrode of the weak link to the other, the expression for the supercurrent becomes

$$I_{\mathrm{s}} = I_{\mathrm{c}} \sin\gamma. \tag{2.4}$$

Eqs. (2.2, 2.4) show that the Josephson junction behaves like a nonlinear inductance. This inductance is obtained from the time derivative of Eq. (2.4)

$$\frac{dI_{\mathrm{s}}}{dt} = I_{\mathrm{c}} \cos\gamma \frac{d\gamma}{dt} = I_{\mathrm{c}} V \frac{2e}{\hbar} \cos\gamma, \tag{2.5}$$

applying Faraday's law $V = -LdI/dt$ the Josephson inductance is found to be

$$|L_J| = \frac{\hbar}{2eI_{\mathrm{c}} \cos\gamma}. \tag{2.6}$$

At high frequencies the shunting capacitance between the two superconductors starts to play a role. Also the normal current through the junction adds a contribution V/R to the total current (here R depends on the voltage V, temperature T and material properties). Therefore, a realistic junction behaves like an ideal one described by Eqs. (2.2, 2.4) shunted by a resistor R and a capacitor C, (the resistively and capacitively shunted junction model, RCSJ) see also Fig. 2.1 (a). The time dependence of the phase γ in the presence of a bias current I_B fulfills the equation of motion

$$\frac{I_B}{I_{\mathrm{c}}} = \sin\gamma + \frac{1}{Q}\frac{d\gamma}{d\tau} + \frac{d^2\gamma}{d\tau^2}, \tag{2.7}$$

where $\tau = \Omega t$, $\Omega = \sqrt{2eI_{\mathrm{c}}/(\hbar C)}$ is the plasma frequency of the junction and $Q = \Omega RC$ is the quality factor. This is identical to the equation of motion of a particle of mass $(\hbar/2e)^2$ in a *titled washboard* potential, see also Fig. 2.2,

$$U(\gamma) = -E_J \cos\gamma - \frac{\hbar I_B}{2e}\gamma, \tag{2.8}$$

where $E_J = \hbar I_{\mathrm{c}}/2e$ is the Josephson energy. In the absence of damping (for the single junction modeled above, this translates to $R \to \infty$), and for $I_B < I_{\mathrm{c}}$ the phase particle is trapped in one of the wells and the junction is in the zero-voltage state, according to Eq. (2.2). At $I_B = I_{\mathrm{c}}$ the wells disappear, and the particle can move freely down the washboard generating a finite voltage across the junction. The particle will be re-trapped only when the bias current is reduced to zero, in order to overcome the inertia of the moving mass, and the current-voltage characteristic is hysteretic.

In the absence of dissipation, quantization of a circuit containing Josephson junctions can be performed as follows. Starting with the the classical equations of motion for an electrical circuit, based on Kirchhoff's laws, see e. g. Eq. (2.7), one can derive the corresponding Lagrangian function. Using a Legendre transformation one obtains a classical Hamiltonian. The quantum mechanical Hamiltonian is then obtained by imposing the usual commutation relations between canonical variables [61, 62].

For a single junction with infinite shunt resistance, the Hamiltonian reads

$$\hat{H} = 4E_C\hat{n}^2 - E_J \cos\hat{\gamma} - \frac{\hbar I_B}{2e}\hat{\gamma}, \tag{2.9}$$

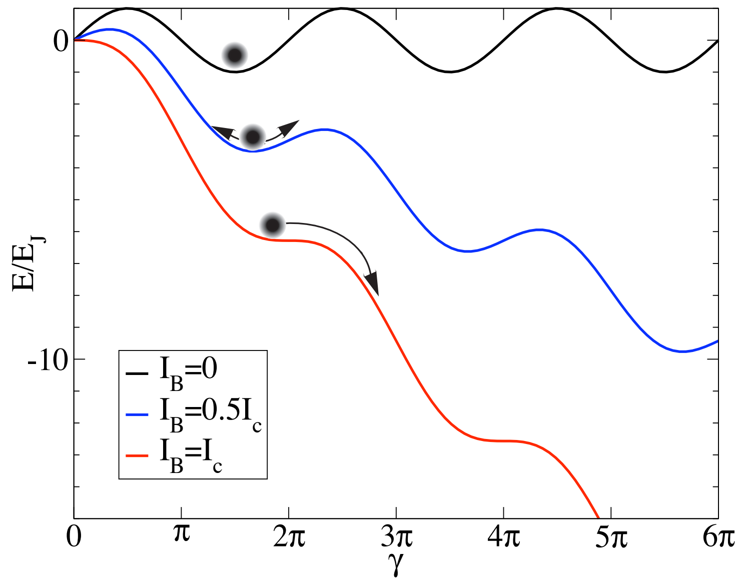

Figure 2.2: Tilted washboard potential of a Josephson junction for different values of the bias current. For values close to the critical current of the junction, the phase particle starts rolling down the washboard generating a finite voltage.

where $E_C = e^2/(2C)$ is the charging energy. The operator $\hat{n}$ represents the number of Cooper pairs. In this system the charge and flux form a pair of conjugate variables and satisfy the same commutation relation as position and momentum.

Experimental evidence of quantum behavior of a Josephson junction [63, 64] was produced by the observation of macroscopic quantum tunneling of the phase particle out of a metastable well, see Fig. 2.2, at $I_B < I_\mathrm{c}$. After tunneling, the particle moves down the washboard potential, generating a finite voltage which can be detected. The quantization of energy levels in the metastable well [65] was investigated by microwave absorption experiments. The escape rate from the zero-voltage state was enhanced when the microwave radiation was in resonance with the energy difference between two levels. Due to the anharmonic nature of the junction, the energy spacing decreases for higher energy levels, and each transition has a distinct frequency. Following this demonstration, the research focused on the experimental investigation of quantum coherence which involves the superposition of macroscopically distinct quantum states [66], as its observation tests the validity boundaries of quantum mechanics. The first such experiment [67] has demonstrated spectroscopically the superposition of different Cooper pair states. The superposition of states in the flux qubit were later demonstrated in Refs. [6, 68].

2.2 Superconducting qubits

Recently, due to the advantages resulting from the freedom in design parameters and scalability, the interest has moved in the direction of circuits with application as quantum bits. For $E_J \gg E_C$, $\hat{\gamma}$ is well defined while $\hat{n}$ has large quantum fluctuations such that the Josephson behavior dominates. In the opposite case $E_J \ll E_C$ the charging behavior of the capacitor dominates as $\hat{n}$ is well defined and $\hat{\gamma}$ has large quantum fluctuations. As E_J and E_C are determined by the junction fabrication parameters, one can use this flexibility to design a variety of superconducting devices.

The **charge qubit** consists of a small superconducting island (Cooper pair box) connected to a potential via a gate capacitance and to ground through a small Josephson junction with $E_J \ll E_C$. The qubit states are represented by consecutive Cooper pair number states on the island. The Josephson junction allows Cooper pairs to tunnel to the island, i. e. couples number states $|n\rangle$ and $|n+1\rangle$, which are used as the two qubit states. The readout is performed by coupling the charge qubit capacitively to a single electron transistor (SET), which consists of an island connected to two Josephson junctions. The charge on the qubit island changes the SET gate voltage.

Cooper pair boxes are sensitive to low-frequency noise from electrons moving among defects. This problem has been reduced in devices such as the *transmon* [69] and *quantronium* [53]. The transmon is a small Cooper pair box that is made insensitive to charge noise by an increased ratio of Josephson energy and charging energy which is achieved by a large shunt capacitance and large gate capacitance. The quantronium circuit includes a superconducting island connected to two small tunnel junctions. These are connected via a third, larger junction and form a loop to which an external flux is applied. The two qubit states are characterized by persistent currents flowing around the loop in opposite directions. The impact of charge and flux noise is reduced by keeping the qubit at a double degeneracy point.

The **phase qubit** [54] consists of a single Josephson junction biased below the critical current. The qubit states are the ground and first excited levels in one of the metastable wells of the washboard potential. Detection occurs by monitoring the tunneling rate out of the well and into the running state with finite voltage. This rate decreases exponentially with the height of the barrier. To determine the state of qubit, one applies a microwave pulse in resonance with the transition between the first and second excited states. If the qubit is in the excited state, this pulse brings the junction in the second excited state from which a high tunneling rate causes the junction to switch to the voltage state. If the qubit is in the ground state no such transition is observed. The operation of this qubit relies heavily on the anharmonicity of the potential which makes the levels in the metastable well unequally separated.

The **flux qubit**, Fig. 2.3, consists of a superconducting loop interrupted by one (or three) Josephson junction(s) with $E_J \gg E_C$ [6, 68, 70–72]. Both designs operate in similar ways. For simplicity we focus on the one-junction design.

For a superconducting loop, Fig. 2.3, with inductance L and circulating current I interrupted by a Josephson junction with capacitance C, using Kirchhoff's and Ampere's laws one obtains

$$I = C\ddot{\gamma}\frac{\hbar}{2e} + I_c \sin\gamma = -\frac{\Phi - \Phi^{(x)}}{L} = -\frac{\gamma\hbar}{2eL} + \frac{\Phi^{(x)}}{L}, \tag{2.10}$$

where Φ is the total flux enclosed by the loop, $\Phi^{(x)}$ the external flux applied to the loop and the last equality results from the fluxoid quantization [73]. Thus the phase particle

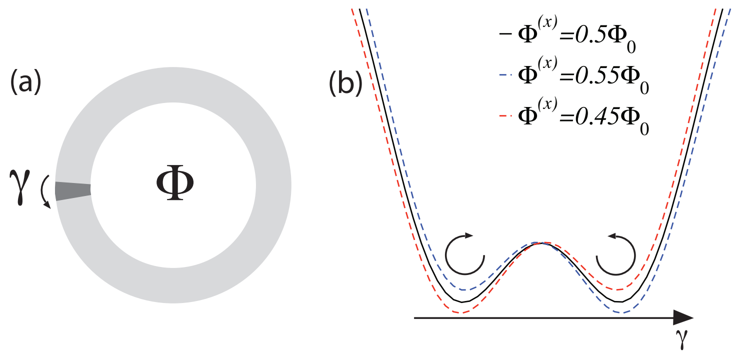

Figure 2.3: (a) Schematic representation of a superconducting flux qubit. (b) Effective potential of the flux qubit. The asymmetry can be tuned by the external flux $\Phi^{(x)}$.

moves in a potential

$$U(\gamma) = -E_J \cos\gamma + \frac{\gamma^2\Phi_0^2}{8\pi^2 L} - \frac{\Phi^{(x)}\Phi_0\gamma}{2\pi L}, \tag{2.11}$$

which can be tuned by $\Phi^{(x)}$ to become a double-well potential. The asymmetry of the double well is tuned by the external flux, while the height of the barrier is determined by the ratio $\beta_L = 2\pi I_c L/\Phi_0$. The qubit states are the two lowest quantum states localized in each well $|\Psi_L\rangle$ and $|\Psi_R\rangle$. They are characterized by supercurrent flowing in an clockwise or anti-clockwise direction through the superconducting loop and coupled by tunneling through the barrier between the wells. The qubit Hamiltonian, truncated to these two states, reads

$$\hat{H}_\mathrm{q} = \hbar\left(\omega\hat{\sigma}_z + \delta\hat{\sigma}_x\right), \tag{2.12}$$

where $\hat{\sigma}_i$ are the usual Pauli operators. For an appropriate choice of parameters these lowest two states of the full potential are separated by a significant gap from the higher levels, such that this two-state approximation is valid.

A natural candidate for the measurement of the current in the qubit loop is the superconducting quantum interference device (SQUID) [74]. This device consists of two Josephson junctions connected in parallel and behaves much like a simple junction, with the difference that the critical current of this effective junction depends not only on the fabrication details but also on the external magnetic field applied to the area enclosed by the two junctions, see Fig. 2.4 (a).

From the condition that the phase φ of the condensate must be single valued one obtains a condition for the sum of the gauge-invariant phase differences γ_i around the contour in Fig. 2.4 (a)

$$\gamma_1 - \gamma_2 = 2\pi\frac{\Phi}{\Phi_0}\mathrm{mod}2\pi. \tag{2.13}$$

Thus, the maximum supercurrent of the parallel combination, for the case where the two junctions have the same critical current I_c is found to be

$$I_\mathrm{c}^\mathrm{eff} = 2I_\mathrm{c}\left|\cos\left(\frac{\pi\Phi}{\Phi_0}\right)\right|. \tag{2.14}$$

The different states of the flux qubit materialize in different values of the external magnetic flux Φ trough the superconducting loop. If a SQUID is wrapped around the

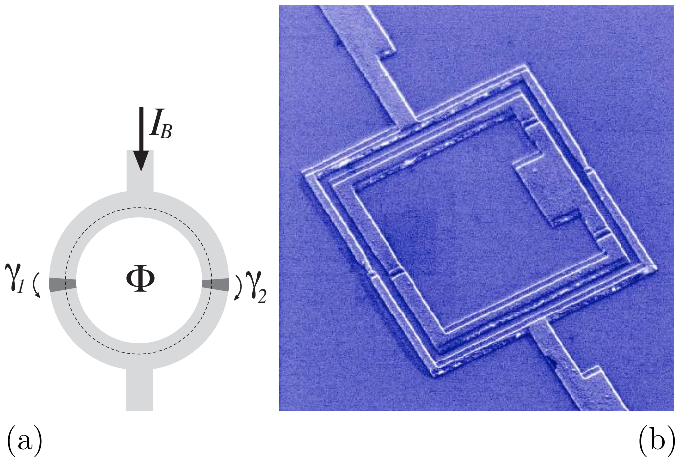

Figure 2.4: (a) Schematic representation of a superconducting quantum interference device. Two junctions described by the gauge-invariant phase difference γ_1 and γ_2 enclose the flux Φ. (b) Configuration of the original Delft flux qubit with a surrounding readout SQUID. The qubit state influences the critical current of the SQUID [75]. Image from TU Delft.

qubit as in Fig. 2.4 (b), also the flux through its loop, and ultimately I_c^{eff}, will depend on the qubit state.

2.2.1 Flux qubit readout

As the SQUID behaves like a large single junction, it can also be effectively modeled by a phase particle moving in the washboard potential described in section 2.1, Fig. 2.1. The applied bias current tilts the washboard up to the point $I_B = I_c^{\text{eff}}$ where the potential no longer has local minima. One measures the effective critical current I_c^{eff} of the SQUID as the maximum bias current the SQUID can sustain until it switches into the finite voltage state [70, 76]. Due to fluctuations of both classical and quantum-mechanical nature, the switching is a stochastic process (in the underdamped case, of interest for qubit detection). The two states of the qubit are distinguished by discriminating between the two averaged values of the maximum bias current. This detection scheme goes a long way, but has also some limitations. In this state the SQUID is no longer superconducting, it generates quasiparticles that recombine and release energy, and contribute to qubit decoherence. It also radiates strong, high frequency, broadband noise to the entire circuit. The long quasiparticle recombination times limit the reset of the qubit. The stochastic nature of the detection also imposes limits on the difference between the two average values of the switching current and thus the discrimination ability of the detector.

A significant improvement relative to the detection via SQUID switching is the dispersive readout, demonstrated in Ref. [1]. In this detection scheme, the SQUID remains trapped in one of the wells and avoids all the disadvantages associated with the switching into the dissipative state. One continuously drives the SQUID with a weak AC bias. When weakly AC driven, the SQUID behaves effectively like a harmonic oscillator. The frequency of this oscillator depends on the effective critical current of the SQUID and thus on the qubit state. By measuring either the phase or the amplitude of response to the drive, one can determine the frequency of the oscillator. This detection scheme has shown long qubit relaxation time ($80\mu s$). Nevertheless, this time is still comparable to the time necessary for reliable detection (one must wait until the transient oscillations in the response of the

SQUID have died out). This fact poses a significant limitation to this type of readout.

A similar (dispersive) readout was performed in Ref. [77] using a linear resonant circuit inductively coupled to the flux qubit. Dispersive readout of a Cooper pair box has been demonstrated in Ref. [78] and of quantronium in Ref. [79].

A further improvement relative to the dispersive readout is obtained when the SQUID is driven strongly enough to explore the anharmonicity of the well. Due to the intrinsic non-linearity of the Josephson junction, above a certain driving strength the device may respond to the drive with one of two possible stable oscillations. These are still trapped oscillations in one of the wells, and the device does *not* switch into the voltage state. Another type of swiching is involved in the detection, namely the switching between the two possible responses to drive, which have vastly different amplitudes. Depending on the qubit state, the system is more or less likely to switch between these stable oscillating states. Thus, fast, high contrast qubit detection is possible [80, 81]. It was experimentally verified that this type of detection is projective [82].

Part II

Flux qubit readout and control in the presence of decoherence

Chapter 3

Phase-space theory for dispersive detectors of superconducting qubits

I. Serban, E. Solano and F. K. Wilhelm

Motivated by recent experiments, we study the dynamics of a qubit quadratically coupled to its detector, a damped harmonic oscillator. We use a complex-environment approach, explicitly describing the dynamics of the qubit and the oscillator by means of their full Floquet state master equations in phase-space. We investigate the backaction of the environment on the measured qubit and explore several measurement protocols, which include a long-term full read-out cycle as well as schemes based on short time transfer of information between qubit and oscillator. We also show that the pointer becomes measurable before all information in the qubit has been lost.

Parts of this chaper have been published in *Physical Review B* **76**, 104510 (2007)

3.1 Introduction

The quantum measurement postulate is one of the most intriguing and historically controversial pieces of quantum mechanics. It usually appears as a separate postulate, as it introduces a non-unitary time evolution. A more detailed discussion of this background can be found in chapter 1.

On the other hand, at least in principle, qubit and detector can be described by a coupled manybody Hamiltonian and thus the measurement process can be investigated using the established tools of quantum mechanics of open systems. Even though this does not lead to a solution of the fundamental measurement paradox, such research gives insight into the *physics* of quantum measurement [2, 9, 10, 83–85].

This basic question has also gained practical relevance and has become a field of experimental physics in the context of quantum computing. Specifically, superconducting qubits have been proposed as building block of a scalable quantum computer [13, 86–88]. In these systems, the detector is based on the same technology — small, underdamped Josephson junctions — as the device whose state is to be detected. Thus these circuits are an ideal test-bed to investigate the physics of quantum measurement. Implementing a measurement which is fast and reliable, with a high (single-shot) resolution and high visibility is a topic of central importance to the practical implementation of these devices.

The basic textbook version of a quantum measurement is based on von Neumann's postulate [89, 90]. The state of the system is projected onto the eigenstate of the observable being measured corresponding to the eigenvalue being observed. This is not the only possible quantum measurement and has been generalized to the idea of a positive operator-valued measure [3].

From the microscopic, Hamiltonian-based perspective, intense research has been done on the measurement of small signals, which originated in the theory of gravitational wave detection [5]. The main challenge has been to identify how signals below the limitations of the uncertainty relation of the detector can be measured - a regime in which the detector response is also strictly linear. This work has resulted in the notion of a quantum nondemolition (QND) measurement [5], which is the closest to a microscopic formulation of a von Neumann measurement. This result has been generalized to many other systems, prominently atomic physics, and also found its way to the superconducting qubits literature. Here, the analogy of a tiny signal is the limit of weak coupling between qubit and detector. Another body of work [9, 10] takes a more general starting point and discusses the relevance of pointer state and environment induced superselection.

The measurement techniques used in superconducting qubits are covering many of the mentioned situations. Weak measurements can be performed using single electron transistors. Based on weak measurement theory, this is well understood (see Ref. [13] and the references therein) but only of limited use for superconducting qubits. These measurements are far from projective, their resolution is in practice rather limited and the whole process is very slow. In the case of qubit, the task is *not* to amplify an arbitrarily weak signal, but to discriminate two states in the best possible way. If the detector can be decoupled from the qubit when no measurement needs to be performed, this discrimination may involve strong qubit-detector coupling [91].

An opposite, generic approach is to perform a switching measurement — the detector switches out of a metastable state depending on the state of qubit. Switching is a highly nonlinear phenomenon, so this type of detection is far from the weak measurement scenario. In most of the early generic setup, this process is a switching of a superconducting device, e. g. a superconducting quantum interference device (SQUID), from the superconducting to the dissipative state [53, 54, 76, 92]. This technique goes a long way, and some experiments have proven that the switching type of readout can achieve high contrast [70, 93]. It has the drawback that it is not a projective readout and during the switching process hot quasiparticles with a long relaxation time are created. This limits the time between the consecutive measurements. Parts of this technique are well understood, such as the switching histogram [94], the pre-measurement backaction [95], and the influence of the shunt impedance to the SQUID [96, 97], but there is no full and single theory of this process on the same level of detail as the weak measurement theory.

Recent developments of detection schemes have lead to vast improvements based on following innovations. Instead of directly measuring a certain observable pertaining to a qubit state, one uses a pointer system, and measures one of its observables influenced by the state of the qubit. Thus this is an indirect measurement. The observation is usually materialized in the frequency shift of an appropriate resonator, whose response to an external excitation links to the measurement outcome [1, 71, 98, 99]. These measurements offer good sensitivity, high visibility [78], and fast repetition rates. They also allow to keep the qubit at a well-defined operation point, although not always the optimum one. In many cases, the resonators in use are nonlinear — based on Josephson junctions. Thus, at stronger excitation, generic nonlinear effects can be exploited. These nonlinear effects go up to switching, which in contrast to the critical current switching is between two dissipationless states [100]. Based on their performance and versatility, these devices also offer an ideal example for investigating the crossover between weak and strong measurements and the role of nonlinearity.

Analyzing the properties of quantum measurement is an application of open quantum systems theory. The backaction contains a variant of projection which can be viewed in an ensemble as dephasing. The resolution is determined by the behavior of the detector under the influence of the qubit viewed as an environment. For open quantum systems, a number of tools have been developed. Most of them, prominently Born and Born-Markov master equations (see e. g. [101] and references therein for a recent review) assume weak coupling between qubit and environment and are hence a priori unsuitable for studying strong qubit-detector coupling. Tools for stronger coupling have been developed [19, 102] but are largely restricted to harmonic oscillator baths and hence unsuitable to treat the generally nonlinear physics of the systems of interest. The Lindblad equation [23] is claimed to be valid up to strong coupling, however, due to its strong Markovian assumption it is unsuitable for strongly coupled superconducting systems at low temperature.

In this chapter we present a theoretical tool allowing to describe dispersive measurements involving nonlinearities. The tool is developed alongside the example of the experimental setup studied in Ref. [1]. It is based on the complex environments approach similar to what is used in cavity QED [103] but also in condensed-matter open quantum systems [104–106]. The idea is to introduce the potentially strongly and nonlinearly coupled component of the detector as part of the quantum system and only treat the weakly coupled part as an environment. In other words, we single out one prominent degree of freedom of the detector from the rest and treat it on equal footing with the qubit. This "special treatment" of one environmental degree of freedom is an essential point of this approach because it allows us to describe the dynamics of a qubit coupled arbitrarily strong to a specific non-Markovian environment. On the other hand it enhances the dimension of the Hilbert space to be captured. This technical complication can be handled using a phase-space representation of the extra degree of freedom — in our example, a harmonic oscillator.

In Section 3.2 we derive the model Hamiltonian motivated by Ref. [1]. For this Hamiltonian we derive in Section 3.3 a master equation and present a phase-space method which enables us to analyze the dynamics of an infinite level system. In Section 3.4 we demonstrate that our method enables to extract information about the measurement process of the qubit, such as dephasing and measurement time and also present three different measurement protocols.

3.2 From circuit to Hamiltonian

We consider a simplified version of the experiment described in Ref. [1]. The circuit consists of a flux qubit drawn in the single junction version, the surrounding SQUID loop, an AC source, and a shunt resistor, as depicted in Fig. 3.1. We note here that we later approximate the qubit as a two-level system. The qubit used in the actual experiment contains three junctions. An analogous but less transparent derivation would, after performing the two-state approximation, lead to the same model, parameterized by the two-state Hamiltonian, the circulating current, and the mutual inductance, in an identical way [92].

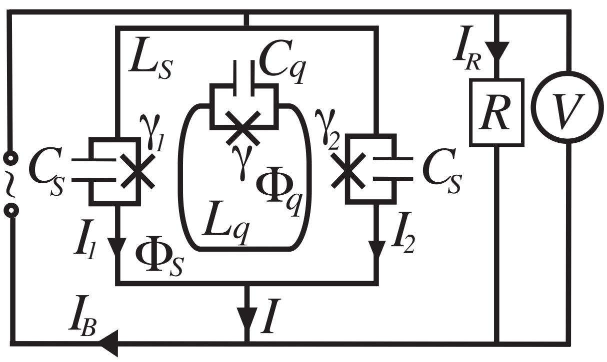

Figure 3.1: Simplified circuit consisting of a qubit with one Josephson junction (phase γ, capacitance C_q and inductance L_q) inductively coupled to a SQUID with two identical junctions (phases $\gamma_{1,2}$, capacitance C_S) and inductance L_S. The SQUID is driven by an AC bias $I_B(t)$ and the voltage drop is measured by a voltmeter with internal resistance R. The total flux through the qubit loop is Φ_q and through the SQUID is Φ_S.

The measurement process is started by switching on the AC source and monitoring the amplitude and/or phase of the voltage drop across the resistor.

The SQUID acts as an oscillator whose resonance frequency depends on the state of the qubit. When the measurement is started, the qubit entangles with the resonator and shifts its frequency. The value of the oscillator frequency relative to the frequency of the AC driving current determines the amplitude and phase of the voltage drop across the resistor.

The detector (voltmeter) contains an internal resistor. This is a dissipative element connecting the quantum mechanical system (qubit + SQUID) to the macroscopic observer. The resistor is needed for performing the measurement, defined as the transfer of quantum information encoded in a superposition of states to classical information encoded in the probabilities with which the voltmeter shows certain values, e. g. voltage amplitude or phase. Note that practically this resistor may be the distributed impedance of the coaxial line connected to the chip.

In this section we derive an effective Hamiltonian for this system. Our starting point is a set of current conservation equations for the circuit of Fig. 3.1.

The total magnetic fluxes through the SQUID and the qubit loops can be divided into screening (s) fluxes produced through circulating currents and external (x) fluxes from outside sources $\Phi_S = \Phi_S^{(x)} + \Phi_S^{(s)}$ and $\Phi_q = \Phi_q^{(x)} + \Phi_q^{(s)}$. Generally, Ampere's law for a system of current loops can be represented in matrix form

$$\begin{pmatrix} \Phi_q^{(s)} \\ \Phi_S^{(s)} \end{pmatrix} = -\begin{pmatrix} L_q & M_{Sq} \\ M_{Sq} & L_S \end{pmatrix} \begin{pmatrix} I_q \\ I_S \end{pmatrix}, \tag{3.1}$$

which can be inverted

$$\begin{pmatrix} I_q \\ I_S \end{pmatrix} = -\frac{1}{M_\Sigma^2} \begin{pmatrix} L_S & -M_{Sq} \\ -M_{Sq} & L_q \end{pmatrix} \begin{pmatrix} \Phi_q^{(s)} \\ \Phi_S^{(s)} \end{pmatrix}, \tag{3.2}$$

where M_{Sq} is the mutual inductance and M_Σ is the determinant of the inductance matrix $M_\Sigma^2 = L_q L_S - M_{Sq}^2 > 0$. The circulating current through the SQUID loop is given by the difference of the currents through the two branches $I_S = (I_1 - I_2)/2$ and the bias current is $I = I_1 + I_2$. The fluxoid quantization [73] in the two loops reads

$$\gamma_- = \gamma_1 - \gamma_2 = 2\pi \frac{\Phi_S}{\Phi_0} \mathrm{mod} 2\pi, \quad \gamma = 2\pi \frac{\Phi_q}{\Phi_0} \mathrm{mod} 2\pi, \tag{3.3}$$

where $\Phi_0 = h/2e$ is the magnetic flux quantum for a superconductor. To obtain the equations of motion for the phases $\gamma, \gamma_\pm$ with $\gamma_\pm = \gamma_1 \pm \gamma_2$ we start from the current conservation in each node

$$I_j = I_{cS} \sin\gamma_j + \dot{V} C_S = I_{cS} \sin\gamma_j + \ddot{\gamma}_j \frac{\Phi_0}{2\pi} C_S, \;\; j \in \{1, 2\}. \tag{3.4}$$

Here we assume that the two junctions have identical critical currents. This symmetry, as will be discussed below, has the consequence that at zero bias current through the SQUID, the qubit will be isolated from its environment. In experiment, the two SQUID junction will usually not be identical. In this case of an asymmetric SQUID the qubit can be protected from environmental noise [107] by applying an appropriate DC bias.

Using Eqs. (3.2) and (3.4) for the circulating current, we obtain

$$I_{cS}\cos\frac{\gamma_+}{2}\sin\frac{\gamma_-}{2}+\ddot{\gamma}_-\frac{\hbar}{4e}C_S=\frac{1}{M_\Sigma^2}\left(M_{Sq}\Phi_q^{(s)}-L_q\Phi_S^{(s)}\right). \tag{3.5}$$

Considering the analogy between Josephson junctions and inductors we introduce the Josephson inductance $L_{JS}=\Phi_0/(2\pi I_{cS})$ and rewrite Eq. (3.5) using the fluxoid quantization (3.3)

$$\frac{1}{L_{JS}}\cos\frac{\gamma_+}{2}\sin\frac{\gamma_-}{2}+\ddot{\gamma}_-\frac{C_S}{2}=\frac{1}{M_\Sigma^2}\left(M_{Sq}\gamma-L_q\gamma_-\right)+\Xi_1, \tag{3.6}$$

where the influence of external fields is captured in $\Xi_1=2\pi/(\Phi_0M_\Sigma^2)\left(-M_{Sq}\Phi_q^{(x)}+L_q\Phi_S^{(x)}\right)$.

For the bias current we have $I+V/R=I_B(t)$ and from Eq. (3.4) we obtain

$$\frac{1}{L_{JS}}\sin\frac{\gamma_+}{2}\cos\frac{\gamma_-}{2}+\ddot{\gamma}_+\frac{C_S}{2}+\frac{1}{4R}\dot{\gamma}_+=\frac{\pi}{\Phi_0}I_B(t). \tag{3.7}$$

For the circulating current in the qubit loop it follows from Eq. (3.2)

$$I_q=C_q\ddot{\gamma}\frac{\hbar}{2e}+I_{cq}\sin\gamma=-\frac{1}{M_\Sigma^2}\left(L_S\Phi_q^{(s)}-M_{Sq}\Phi_S^{(s)}\right). \tag{3.8}$$

Using $L_{Jq}=\Phi_0/(I_{cq}2\pi)$, Eq. (3.3), this becomes

$$C_q\ddot{\gamma}+\frac{1}{L_{Jq}}\sin\gamma \;=\; -\frac{L_S}{M_\Sigma^2}\gamma+\frac{M_{Sq}}{M_\Sigma^2}\gamma_-+\Xi_2, \tag{3.9}$$

where we defined $\Xi_2=2\pi/(M_\Sigma^2\Phi_0)\left(-M_{Sq}\Phi_S^{(x)}+L_S\Phi_q^{(x)}\right)$.

From Eqs. (3.6), (3.7), and (3.9), we observe that γ_+, the phase drop across the SQUID, serves as a pointer. It couples to the qubit degree of freedom γ and is read out by the classical observer, which appears in the classical equation of motion (3.7) as a dissipative term. Without bias current $I_B=0$, the classical solution for this degree of freedom becomes $\gamma_+=0$ independent of the internal degree of freedom γ_- and the qubit. It follows that, in the absence of I_B, there is no coupling between the quantum mechanical system and the environment, as the pointer is decoupled from the observer.

We start the derivation of the system Hamiltonian suppressing the dissipative term in Eq. (3.7). It will be later reintroduced in the form of an oscillator bath. Starting from the equations of motion (3.6), (3.7), and (3.9), for $\gamma_\pm$ and γ we first determine the Lagrangian such that $d_t(\partial_{\dot{\gamma}}\mathcal{L})=\partial_\gamma\mathcal{L}$ and $d_t(\partial_{\dot{\gamma}_\pm}\mathcal{L})=\partial_{\gamma_\pm}\mathcal{L}$. We introduce the canonically conjugate momenta $p=\partial_{\dot{\gamma}}\mathcal{L}=\hbar^2C_q\dot{\gamma}/e^2$ and $p_\pm=\partial_{\dot{\gamma}_\pm}\mathcal{L}=\hbar^2C_S\dot{\gamma}_\pm/(2e^2)$ and finally derive the

Hamiltonian using $\mathcal{H} = \dot{\gamma}p + \dot{\gamma}_- p_- + \dot{\gamma}_+ p_+ - \mathcal{L}$. This leads to

$$\begin{aligned}\mathcal{H} &= \left(\frac{p_+^2 + p_-^2}{C_S} + \frac{p^2}{2C_q}\right)\frac{e^2}{\hbar^2} - \left(\frac{2}{L_{JS}}\cos\frac{\gamma_-}{2}\cos\frac{\gamma_+}{2}\right. \\ &+ \left.\frac{M_{Sq}}{M_\Sigma^2}\gamma\gamma_- - \frac{L_q}{M_\Sigma^2}\frac{\gamma_-^2}{2} + \Xi_1\gamma_- + \frac{1}{L_{Jq}}\cos\gamma - \frac{L_S}{M_\Sigma^2}\frac{\gamma^2}{2} + \Xi_2\gamma + \frac{e}{\hbar}I_B(t)\gamma_+\right)\frac{\hbar^2}{e^2}.\end{aligned} \tag{3.10}$$

Now we proceed to simplify this Hamiltonian using the assumptions that $L_{JS} \gg L_S$, which applies to small SQUIDs as the ones used for qubit readout, and that the driving strength is small enough to remain in the harmonic part of the potential $|I_B| \ll I_{cS}$. Using the latter assumption, we can expand the potential energies to second order around the minimum and obtain two coupled harmonic oscillators (γ_+ and γ_-) with greatly different frequencies. γ_- evolves in a much narrower potential ($\propto 1/L_S$) than that of γ_+ ($\propto 1/L_{JS}$). Therefore we can perform an adiabatic approximation and substitute γ_- through its average position. We obtain the following potential for the remaining degree of freedom γ_+

$$\mathcal{U}(\gamma_+, \gamma) = \mathcal{U}_0 + \frac{\hbar^2}{e^2}\frac{1}{4L_{JS}}\cos\left(\Xi_1\frac{M_\Sigma^2}{2L_q} + \gamma\frac{M_{Sq}}{2L_q}\right)\left(\gamma_+ - \frac{I_B(t)}{I_{cS}}\frac{1}{\cos\left(\Xi_1\frac{M_\Sigma^2}{2L_q} + \gamma\frac{M_{Sq}}{2L_q}\right)}\right)^2. \tag{3.11}$$

In the next step, we perform the two-state approximation of the qubit along the lines of Ref. [19, 75], reducing its dynamics to the two lowest energy eigenstates. This space is spanned by wave functions centered around two values $\hat{\gamma} = \gamma_0\hat{\sigma}_z$ (γ either in the left or the right well of the potential). While the manipulation of the qubit is usually performed at the optimum working point [53], the readout can and should be performed in quantum nondemolition (QND) measurement i. e. in the pure dephasing limit. This reduces the qubit Hamiltonian to $\epsilon_0\hat{\sigma}_z$. We allow for a significant off-diagonal term $\propto \hat{\sigma}_x$ to have acted in the past in order to prepare superpositions of eigenstates of σ_z. Physically, this situation is achieved by either making one of the qubit junctions tunable, or imposing a huge energy bias to the qubit.

We note here that if, opposed to the case we will discuss in the following, the measurement interaction would not commute with the qubit Hamiltonian, a full analysis in terms of quantum measurement theory would be required. Similar to Refs. [108, 109] the action on the system given by each measurement result would need to be determined in order to quantify the information that the observer can obtain about the initial state of the qubit, as well as the state following the measurement.

After these approximations the qubit-SQUID Hamiltonian reads

$$\hat{H}_S = \epsilon(t)\hat{\sigma}_z + \frac{\hat{p}^2}{2m} + \frac{m(\Omega^2 + \Delta^2\hat{\sigma}_z)}{2}\hat{x}^2 - F(t)\hat{x}, \tag{3.12}$$

where $\hat{x}$ corresponds to the external degree of freedom of the SQUID γ_+, $\hat{p} = \hat{p}_+$ and $F(t) = F_0\sin(\nu t)$ originates in the AC driving by a classical field. The conversion of the parameters to circuit-related quantities can be found in section 3.6.1. Here Δ is the quadratic frequency shift (QFS).

An important property of this Hamiltonian is the absence of the commonly used linear coupling between the two-level system and the harmonic oscillator [92]. In our case the qubit couples to the squared coordinate of the oscillator, which leads to a qubit dependent change in the frequency of the harmonic oscillator instead of the shift of the potential minimum.

Because of the coupling to the driven oscillator the qubit energy splitting becomes time-dependent $\epsilon(t) = \epsilon_0 + \upsilon I_B^2(t)$.

To model the dissipation introduced by the resistor we follow the standard Caldeira-Leggett approach [19, 110–112] and include an oscillator bath to our Hamiltonian

$$\hat{H} = \hat{H}_S + \underbrace{\sum_i \left(\frac{\hat{p}_i^2}{2m_i} + \frac{m_i \omega_i^2}{2} \hat{x}_i^2 \right)}_{\hat{H}_B} + \underbrace{\hat{x} \sum_i \lambda_i \hat{x}_i}_{\hat{H}_I} . \tag{3.13}$$

with $J(\omega) = \sum_i \lambda_i^2 \hbar/(2m_i\omega_i)\delta(\omega - \omega_i) = m\hbar\kappa\omega\Theta(\omega - \omega_c)/\pi$ [16] where Θ is the Heaviside step function and $[\kappa] = s^{-1}$ the photon loss rate. The cut-off frequency ω_c is physically motivated by the high frequency filter introduced by the capacitors.

3.3 Method

Our goal is to analyze the resolution and measurement time and investigate the backaction on the qubit. The former requires tracing over the qubit and discuss the dynamics of the pointer variable of the detector, the latter requires tracing over the detector degrees of freedom.

It is well established how to do this in principle exactly [19] when the qubit couples to a Gaussian variable of the detector (i. e. sum of quadratures of the environmental coordinates). A method to map a damped harmonic oscillator to bath of uncoupled oscillators with a modified spectral density [113, 114] also exists. In our case, due to the quadratic coupling between the qubit and the damped oscillator (3.12), no such normal-mode transform leads to the usual Gaussian model and thus one cannot use many of the methods developed for the spin-boson model.

There are several approaches to dealing with this challenge. As long as the coupling is weak, $\Delta \ll \Omega$, one can still linearize the detector dynamics and make a Gaussian approximation as it was done in Ref. [98]. Nevertheless, weak coupling decoherence theory as reviewed e. g. in Refs. [13, 101] builds on two-point correlators and cannot distinguish Gaussian from non-Gaussian environments.

In this work we describe arbitrarily large couplings between qubit and oscillator going beyond the Gaussian approximation. The only small parameter we rely upon is the decay rate of the oscillator κ. This is justified by the fact that dispersive measurement only makes sense for large oscillator quality factors $Q > 1$. We treat a composite quantum system —

qubit $\otimes$ oscillator — weakly coupled to the heat bath represented by the resistor. This *complex environments approach* resembles the methods of, e. g. Refs. [98, 104].

We start with the standard master equation for the reduced density operator in Schrödinger picture and Born-Markov approximation [101, 115], assuming factorized initial conditions $\rho(0) = \rho_S(0) \otimes \rho_B(0)$

$$\frac{d}{dt}\hat{\rho}_S(t)(t) = \frac{1}{\mathbb{i}\hbar}[\hat{H}_S, \hat{\rho}_S(t)(t)] + \frac{1}{(\mathbb{i}\hbar)^2}\int_0^t dt' \, \mathrm{Tr}_B \left[\hat{H}_I, [\hat{H}_I(t, t-t'), \hat{\rho}_S(t)(t) \otimes \hat{\rho}_B(0)]\right], \tag{3.14}$$

where $\hat{H}_I(t,t') = \hat{U}^t_{t'}\hat{H}_I\hat{U}^{t'}_t$ and $\hat{U}^{t'}_t = \hat{\mathcal{T}}\exp\left(\int_t^{t'} d\tau(\hat{H}_S + \hat{H}_B)/(\mathbb{i}\hbar)\right)$ and $\hat{\mathcal{T}}$ is the time-ordering operator. In thermal equilibrium there will be correlations between the main oscillator and the oscillators of the bath, so the initial state is not strictly speaking factorized. In the low κ limit here, these correlations will affect the dynamics only in higher order κ^2 and can hence be neglected. This is a standard assumption in the perturbative treatment of open systems where here κ is the perturbative parameter, see e. g. Ref. [101]. This approach is valid at finite temperatures $k_BT \gg \hbar\kappa$, for times $t \gg 1/\omega_c$ [101, 116], which is the limit we will discuss henceforth. We assume unbiased noise $\langle\hat{H}_I\rangle = 0$. The Hamiltonian (3.12) describes a driven harmonic oscillator, therefore the Floquet modes (see e. g. Refs. [117, 118] for a short review) form the appropriate basis in which we express the master equation. For a driven harmonic oscillator the Floquet modes (see also appendix C and Ref. [118]), are given by

$$\begin{aligned}\Psi_n(x,t) &= \varphi_n(x-\xi(t))\exp\left[\frac{\mathbb{i}}{\hbar}\left(m\dot{\xi}(t)(x-\xi(t)) - E_nt + \int_0^t dt'\mathcal{L}(t',\xi,\dot{\xi})\right)\right] \\ &= \Phi_n(x,t)\mathbb{e}^{-\mathbb{i}E_nt/\hbar},\end{aligned} \tag{3.15}$$

where $E_n = \hbar\Omega(n+1/2)$, $\varphi_n(x)$ a number state, $\xi(t)$ is the classical trajectory and $\mathcal{L}(\xi,\dot{\xi},t)$ the classical Lagrangian of the driven undamped oscillator

$$\xi(t) = \frac{F_0\sin(\nu t)}{m(\Omega^2-\nu^2)}, \quad \mathcal{L}(\xi,\dot{\xi},t) = \frac{1}{2}m\dot{\xi}^2(t) - \frac{1}{2}m\Omega^2\xi^2(t) + \xi(t)F(t). \tag{3.16}$$

We also define the operator $\hat{A}$ as the annihilation operator corresponding to a Floquet mode

$$\hat{a} = \hat{A} + \zeta(t), \tag{3.17}$$

where $\zeta(t) = \sqrt{m/(2\hbar\Omega)}(\mathbb{i}\dot{\xi}(t) + \Omega\xi(t))$ so that $\hat{A}\Phi_n(x,t) = \sqrt{n}\Phi_{n-1}(x,t)$. After some algebra we obtain

$$\hat{x} = \sqrt{\frac{\hbar}{2m\Omega}}(\hat{A} + \hat{A}^\dagger) + \xi(t), \quad \hat{a}(t,t') = \mathbb{e}^{\mathbb{i}\Omega(t-t')}\hat{A} + \zeta(t'). \tag{3.18}$$

Eq. (3.18) has been obtained by calculating $\hat{a}(t,t')\Phi_n(x,t)$, where $\{\Phi_n(x,t)\}$ build a complete set of functions at any time t. Here one can interpret the sum $\hat{A}+\hat{A}^\dagger$ as the deviation of $\hat{x}$ from the classical trajectory $\xi(t)$.

Since we are describing a composite quantum mechanical system, the operators in Eq. (3.14) can be written in the qubit $\hat{\sigma}_z$ basis as follows

$$\hat{\rho}_S = \begin{pmatrix} \hat{\rho}_{\uparrow\uparrow} & \hat{\rho}_{\uparrow\downarrow} \\ \hat{\rho}_{\downarrow\uparrow} & \hat{\rho}_{\downarrow\downarrow} \end{pmatrix}, \; \hat{H}_S = \begin{pmatrix} \hat{H}_{S\uparrow} & 0 \\ 0 & \hat{H}_{S\downarrow} \end{pmatrix}, \; \hat{A} = \begin{pmatrix} \hat{A}_\uparrow & 0 \\ 0 & \hat{A}_\downarrow \end{pmatrix}, \; \hat{a}(t,t') = \begin{pmatrix} \hat{a}_\uparrow(t,t') & 0 \\ 0 & \hat{a}_\downarrow(t,t') \end{pmatrix}, \tag{3.19}$$

where all the matrix elements are operators in the oscillator Hilbert space

$$\hat{H}_{S\uparrow,\downarrow} = \pm\epsilon(t) + \left(\frac{\hat{p}^2}{2m} + \frac{m(\Omega^2 \pm \Delta^2)}{2}\hat{x}^2 - \hat{x}F(t)\right), \tag{3.20}$$

$$\hat{a}_\sigma(t,t') = \hat{A}_\sigma \mathbb{e}^{\mathbb{i}\Omega_\sigma(t-t')} + \zeta_\sigma(t'), \;\; \sigma \in \{\uparrow,\downarrow\}, \tag{3.21}$$

and $\hat{A}_{\uparrow,\downarrow}$ is the annihilation operator of a Floquet mode with frequency $\Omega_{\uparrow,\downarrow} = \sqrt{\Omega^2 \pm \Delta^2}$. The functions $\zeta(t)$ and $\xi(t)$ also depend on the frequency of the harmonic oscillator, therefore they become 2×2 diagonal matrices.

As we observed in the previous section, as long as $I_B = 0$ there is no direct coupling between the qubit and the oscillator in the second order approximation and thus no coupling to the environment. Therefore, at $t = 0$, before one turns on the AC driving, the harmonic oscillator has the frequency Ω independent of the qubit. Therefore the initial condition for the density matrix $\hat{\rho}_S$ is $\hat{\rho}_S(0) = \hat{\rho}_{\rm q} \otimes \hat{\rho}^{(\Omega)}_{\rm HO}$.

We introduce also the annihilation operator $\hat{A}_0$ for the Floquet modes with frequency Ω which relates to $\hat{A}_\sigma$ as follows

$$\hat{A}_\sigma = \frac{1}{2}\left(\hat{A}_0^\dagger\left(f_\sigma - f_\sigma^{-1}\right) + \hat{A}_0\left(f_\sigma + f_\sigma^{-1}\right)\right) - \zeta_\sigma^*(t) + \mathrm{Re}\zeta_0(t) f_\sigma - \mathbb{i}\mathrm{Im}\zeta_0(t)\frac{1}{f_\sigma}, \tag{3.22}$$

where $f_\sigma = \sqrt{\Omega_\sigma/\Omega}$.

Using the operators introduced above in Eq. (3.14), we obtain

$$\begin{aligned}
\dot{\hat{\rho}}_{\sigma\sigma'}(t) = & \frac{1}{\mathbb{i}\hbar}\left(\hat{H}_{S\sigma}\hat{\rho}_{\sigma\sigma'}(t) - \hat{\rho}_{\sigma\sigma'}(t)\hat{H}_{S\sigma'}\right) - \frac{1}{\hbar^2}\int_0^t dt' \int_0^\infty d\omega J(\omega) \\
\cdot & \left\{\left(\mathbb{e}^{\mathbb{i}\omega(t-t')} n(\omega) + \mathbb{e}^{-\mathbb{i}\omega(t-t')}(n(\omega)+1)\right)\right. \\
\cdot & \left(g_\sigma^2\left(\hat{a}_\sigma + \hat{a}_\sigma^\dagger\right)\left(\hat{a}_\sigma(t,t') + \hat{a}_\sigma^\dagger(t,t')\right)\hat{\rho}_{\sigma\sigma'}(t) - g_\sigma g_{\sigma'}\big(\hat{a}_\sigma(t,t') + \hat{a}_\sigma^\dagger(t,t')\big)\hat{\rho}_{\sigma\sigma'}(t)\Big(\hat{a}_{\sigma'} + \hat{a}_{\sigma'}^\dagger\Big)\right) \\
- & \left(\mathbb{e}^{-\mathbb{i}\omega(t-t')} n(\omega) + \mathbb{e}^{\mathbb{i}\omega(t-t')}(n(\omega)+1)\right)\left(g_\sigma g_{\sigma'}\left(\hat{a}_\sigma + \hat{a}_\sigma^\dagger\right)\hat{\rho}_{\sigma\sigma'}(t)\Big(\hat{a}_{\sigma'}(t,t') + \hat{a}_{\sigma'}^\dagger(t,t')\Big)\right. \\
- & \left.\left. g_{\sigma'}^2\hat{\rho}_{\sigma\sigma'}(t)\left(\hat{a}_{\sigma'}(t,t') + \hat{a}_{\sigma'}^\dagger(t,t')\right)\left(\hat{a}_{\sigma'} + \hat{a}_{\sigma'}^\dagger\right)\right)\right\},
\end{aligned} \tag{3.23}$$

where $g_\sigma = \sqrt{\hbar/(2m\Omega_\sigma)}$ and $n(\omega)$ is the Bose function. We observe that the equations of motion for the four components of $\hat{\rho}_S$ are not coupled to each other. This is the consequence of neglecting the tunneling in the qubit Hamiltonian Eq. (3.12). While the two diagonal components fulfill the same equations of motion as in the case of the well-known damped harmonic oscillator, each of them with a different frequency, the two off-diagonal elements of the density matrix have a more complicated evolution. Specifically, they are not Hermitian and do not conserve the norm. This is to be expected, as the norm of the off-diagonal elements measures the qubit coherence, which is not conserved during measurement.

One can handle master equations in an infinite-dimensional Hilbert space with the aid of phase-space pseudoprobability distribution functions [25, 27, 119], which encode any operator with a finite norm[1] [27] into a phase-space function. Here, we choose the characteristic function of the Wigner function $\chi(\alpha,\alpha^*,t)$ to represent the density matrix

$$\hat{\rho}_{\sigma\sigma'}(t) \;=\; \frac{1}{\pi}\int d^2\alpha\;\chi_{\sigma\sigma'}(\alpha,\alpha^*,t)\hat{D}(-\alpha), \tag{3.24}$$

where $\hat{D}(-\alpha) = \exp(-\alpha\hat{A}_0^\dagger + \alpha^*\hat{A}_0)$ is the displacement operator. For more detail, see also appendix B. By replacing this representation of $\hat{\rho}_{\sigma\sigma'}$ into the master equation (3.23) we obtain partial differential equations for the characteristic functions $\chi_{\sigma\sigma'}(\alpha,\alpha^*,t)$. Note that here $|\alpha\rangle$ is different from the coherent state as it is composed of Floquet modes instead of Fock states, i. e.

$$|\alpha\rangle \;=\; \mathbb{e}^{-|\alpha|^2/2}\sum_n \frac{\alpha^n}{\sqrt{n!}}|\Phi_n(t)\rangle. \tag{3.25}$$

3.4 Results

3.4.1 Measurement

In this section we propose three dispersive measurement protocols, all based on the detection of the oscillator momentum, from which the state of the qubit can be inferred.

We start by computing the measured observable of the detector, the voltage drop V across the SQUID. In our notation, the operator is found as the oscillator momentum, $V = \mathbb{i}V_0\hat{\mathbb{1}}_{\mathrm{q}}\otimes\left(\hat{a}-\hat{a}^\dagger\right)$, and involves a trace over the qubit. Here the momentum $\hat{p}$ is $2meV/\hbar$. Thus, we obtain the diagonal characteristic functions $\chi_{\sigma\sigma}$. For $\sigma=\sigma'$ we obtain from Eqs. (3.23), (3.24), and (3.22), a Fokker-Planck equation [28]

$$\begin{aligned}\dot{\chi}_{\sigma\sigma}(\alpha,\alpha^*,t) \;=\; & \Bigg(\left(\alpha\left(-\frac{\kappa}{2}+\mathbb{i}\tilde{\Omega}_\sigma^+\right)+\alpha^*\left(-\frac{\kappa}{2}+\mathbb{i}\tilde{\Omega}_\sigma^-\right)\right)\partial_\alpha \\ &+\left(\alpha^*\left(-\frac{\kappa}{2}-\mathbb{i}\tilde{\Omega}_\sigma^+\right)+\alpha\left(-\frac{\kappa}{2}-\mathbb{i}\tilde{\Omega}_\sigma^-\right)\right)\partial_{\alpha^*} \\ &-(1+2n_\sigma)\frac{\kappa\Omega_\sigma}{4\Omega}(\alpha+\alpha^*)^2+(\alpha+\alpha^*)f_\sigma(t)\Bigg)\chi_{\sigma\sigma}(\alpha,\alpha^*,t),\end{aligned} \tag{3.26}$$

where

$$f_\sigma(t) \;=\; \frac{\mathbb{i}F_0\left(\cos(\nu t)\kappa\nu+\sin(\nu t)\left(\Omega_\sigma^2-\Omega^2\right)\right)}{\sqrt{2m\Omega\hbar}\left(\Omega^2-\nu^2\right)}, \tag{3.27}$$

[1] Norm definition $\parallel\hat{O}\parallel = \left(\mathrm{Tr}\left\{O^\dagger O\right\}\right)^{1/2}$.

and $\tilde{\Omega}_\sigma^{\pm} = (\pm\Omega^2 + \Omega_\sigma^2)/(2\Omega)$. Note that we must express the operators in Eq. (3.14) in terms of $\hat{A}_0$ corresponding to frequency Ω as the oscillator has initially that frequency, in a particular case the thermal state of frequency Ω. Eq. (3.26) is consistent with the property $\chi_{\sigma\sigma'}(\alpha) = \chi^*_{\sigma'\sigma}(-\alpha)$ originating in the hermiticity of the density matrix. We perform the variable transformation $(\alpha, \alpha^*, t) \to (z, z^*, s)$ defined by means of following differential equations

$$\begin{aligned}
\partial_s \alpha &= \alpha\left(\frac{\kappa}{2} - \mathbb{i}\tilde{\Omega}_\sigma^{+}\right) + \alpha^*\left(\frac{\kappa}{2} - \mathbb{i}\tilde{\Omega}_\sigma^{-}\right), \ \partial_s\alpha^* = \alpha^*\left(\frac{\kappa}{2} + \mathbb{i}\tilde{\Omega}_\sigma^{+}\right) + \alpha\left(\frac{\kappa}{2} + \mathbb{i}\tilde{\Omega}_\sigma^{-}\right), \\
s &= t,
\end{aligned} \tag{3.28}$$

The solutions of these coupled differential equations will depend on some initial conditions i. e. $\alpha(s=0) = z$ and thus we obtain the transformation $\alpha \to \alpha(z, z^*, s)$. This transformation conveniently removes the partial derivatives with respect to α and α^* in Eq. (3.26) and we are left with

$$\begin{aligned}
\partial_s \chi_{\sigma\sigma}(z, z^*, s) &= (\alpha(z, z^*, s) + \alpha^*(z, z^*, s)) f_\sigma(t) \\
&- (1 + 2n_\sigma)\frac{\kappa\Omega_\sigma}{4\Omega}\left(\alpha(z, z^*, s) + \alpha^*(z, z^*, s)\right)^2,
\end{aligned} \tag{3.29}$$

which can be directly integrated. After performing the transformation back to the initial variables $\chi_{\sigma\sigma}(\alpha, \alpha^*, t)$ we can calculate the probability density of momentum $P(p_0, t) = \sqrt{\hbar m\Omega/2}\langle\delta(\hat{p} - p_0)\rangle$ where the qubit initial state is $q_\uparrow|\uparrow\rangle + q_\downarrow|\downarrow\rangle$ and

$$\begin{aligned}
P(p_0, t) &= \mu \sum_{\sigma\in\{\uparrow,\downarrow\}} \frac{|q_\sigma|^2}{2\pi^2} \int dk\, \mathbb{e}^{\mathbb{i}k(\dot{\xi}(t)m - p_0)} \int d^2\alpha\, \chi_{\sigma\sigma}(\alpha, \alpha^*, t) \int d^2\beta\, \langle\beta|\mathbb{e}^{-k\mu(\hat{A}_0^\dagger - \hat{A}_0)}\hat{D}(-\alpha)|\beta\rangle, \\
\mu &= \sqrt{\frac{\hbar m\Omega}{2}}.
\end{aligned} \tag{3.30}$$

Evaluating the integrals in Eq. (3.30) we obtain for the probability density of momentum

$$P(p_0, t) = \sum_{\sigma\in\{\uparrow,\downarrow\}} \frac{|q_\sigma|^2}{\sqrt{4\pi\mathcal{B}_\sigma(t)}} \exp\left(-\frac{(p_0 - \mathcal{C}_\sigma(t))^2}{4\mu^2\mathcal{B}_\sigma(t)}\right). \tag{3.31}$$

Here, assuming the oscillator initially in a thermal state, we have

$$\begin{aligned}
\mathcal{C}_\sigma(t) &= \frac{F_0\nu}{\kappa^2\nu^2 + (\nu^2 - \Omega_\sigma^2)^2}\Bigg(\cos(\nu t)(\Omega_\sigma^2 - \nu^2) + \sin(\nu t)\kappa\nu \\
&+ \mathbb{e}^{-\kappa t/2}\cos(\overline{\Omega}_\sigma t)\frac{\nu^2(\kappa^2 + \Omega^2) - (\nu^2 + \Omega^2)\Omega_\sigma^2 + \Omega_\sigma^4}{\Omega^2 - \nu^2} \\
&- \mathbb{e}^{-\kappa t/2}\sin(\overline{\Omega}_\sigma t)\frac{\kappa(\Omega_\sigma^4 + \nu^2(\kappa^2 + \Omega^2) + \Omega_\sigma^2(\Omega^2 - 3\nu^2))}{2\overline{\Omega}_\sigma(\Omega^2 - \nu^2)}\Bigg),
\end{aligned} \tag{3.32}$$

$$
\begin{aligned}
\mathcal{B}_\sigma(t) &= \frac{1+2n(\Omega_\sigma)}{2}\frac{\Omega_\sigma}{\Omega}\Big(1-\mathrm{e}^{-\kappa t}\frac{\Omega_\sigma^2}{\overline{\Omega}_\sigma^2}+\mathrm{e}^{-\kappa t}\cos(2\overline{\Omega}_\sigma t)\frac{\kappa^2}{4\overline{\Omega}_\sigma^2}+\mathrm{e}^{-\kappa t}\sin(2\overline{\Omega}_\sigma t)\frac{\kappa}{2\overline{\Omega}_\sigma}\Big) \\
&- \frac{1+2n(\Omega)}{2}\mathrm{e}^{-\kappa t}\Big(-\frac{\Omega_\sigma^2}{2\overline{\Omega}_\sigma^2}\left(1+\frac{\Omega_\sigma^2}{\Omega^2}\right)+\cos(2\overline{\Omega}_\sigma t)\frac{\Omega_\sigma^2\left(1+\frac{\Omega_\sigma^2}{\Omega^2}\right)-4\overline{\Omega}_\sigma^2}{4\overline{\Omega}_\sigma^2} \\
&+ \sin(2\overline{\Omega}_\sigma t)\frac{\kappa}{2\overline{\Omega}_\sigma}\Big).
\end{aligned}
$$

and $\overline{\Omega}_\sigma = \sqrt{\Omega_\sigma^2-\kappa^2/4}$. One can see that $\mathcal{B}(t)$ evolves from $\mathcal{B}_\sigma(0) = 1/2+n(\Omega)$ to $\mathcal{B}_\sigma(\infty) = (1/2+n(\Omega_\sigma))\Omega_\sigma/\Omega$ and for $\Omega=\Omega_\sigma$ $\langle\hat{p}\rangle_\sigma(t) = \mathcal{C}_\sigma(t)$ becomes the momentum of the classical damped oscillator with the initial conditions $\dot{p}(0) = -F_0\kappa\nu/(\Omega^2-\nu^2)$ and $p(0) = F_0\nu/(\Omega^2-\nu^2)$. Note that the value $\mathcal{B}_\sigma(\infty)$ is independent of the initial $\mathcal{B}_\sigma(0)$. Therefore the long time value of $\mathcal{B}$ is the same also for ground and coherent state.

In the following, when analyzing different types of measurement protocols, we have to differentiate between *discrimination* and *measurement* time. Measurement time is the total time needed to transfer the information from the qubit to the observer. In a sample-and-hold protocol, one imprints the qubit state into the oscillator, then decouples the two and observes the latter. The time needed for the first step is called discrimination time.

Long time, single shot measurement

In the measurement scheme of Ref. [1] one needs the voltage amplitudes corresponding to the two qubit states. For this one must wait until the transients in the momentum (voltage) oscillations have died out. From the amplitude of momentum one can then determine the state of the qubit.

Following Ref. [1] we define the measurement time as the time required to obtain enough information to infer the qubit state

$$\tau_{\mathrm{m}} = \frac{S_V}{(V_\uparrow - V_\downarrow)^2}, \tag{3.33}$$

where V_σ is the amplitude of the voltage for the qubit in the state $|\sigma\rangle$ and $S_V = 2k_BTR$ is the spectral density of the detector output. This is the time needed for discriminating two-long time amplitudes relative to a noise backgroud given by S_V. Therefore, in our notation,

$$\tau_{\mathrm{m}} = \frac{b}{\kappa(\mathcal{A}_\uparrow - \mathcal{A}_\downarrow)^2}, \tag{3.34}$$

where

$$\mathcal{A}_\sigma = \frac{\nu}{\sqrt{\kappa^2\nu^2+(\nu^2-\Omega_\sigma^2)^2}} \tag{3.35}$$

and $b = k_BTC_S/I_B^2$. Note that in this type of amplitude measurement it is advantageous to drive far from resonance, since at resonance the amplitudes $\mathcal{A}_\sigma$ become identical for the two qubit states. Off-resonance τ_{m} is a monotonically falling function of Δ, i. e. larger coupling leads to faster measurement. Close to resonance τ_{m} grows again for large values of Δ.

It is known that, when an harmonic oscillator is driven close to resonance, a *phase* measurement reveals most of the information about the oscillator frequency and leads to the best resolution and quantum limited measurement. Along the lines of Ref. [120] one can suppose that, for measurement closest to the quantum limit, the conjugate observable to the one being measured should deliver no information. In our case, for off-resonant driving and amplitude measurement, most of the information about the qubit is contained in the amplitude and almost none in the phase.

Short time, single shot measurement

In the measurement protocol of the previous section and Ref. [1] the desired information is extracted from the long-time $\mathcal{C}_\sigma = \langle\hat{p}\rangle_\sigma(t)$. The method has the advantage of being "single shot", but disadvantages resulting from long time coupling to the environment such as dephasing, relaxation and loss of visibility [121, 122].

In this section we present a different measurement protocol. It is based on the short time dynamics illustrated as follows. For the qubit initially in the state $1/\sqrt{2}(|\uparrow\rangle + |\downarrow\rangle)$ the probability distribution of momentum is plotted in Fig. 3.2 (a) and (b). In Fig. 3.2 one can see that the two peaks corresponding to the two states of the qubit split already during the transient motion of $\langle\hat{p}\rangle(t)$, much faster than the transient decay time. If the peaks are well enough separated, a single measurement of momentum gives the needed information about the qubit state, and has the advantage of avoiding decoeherence effects resulting from a long time coupling to the environment. Nevertheless the parameters we need to reduce the discrimination time also enhance the decoherence rate.

We define in this case the discrimination time as the first time when the two peaks are separated by more than the sum of their widths i.e.

$$|\mathcal{C}_\uparrow(\tau_{\mathrm{discr}}) - \mathcal{C}_\downarrow(\tau_{\mathrm{discr}})| \geq 3\sqrt{2m\hbar\Omega}\left(\sqrt{\mathcal{B}_\uparrow(\tau_{\mathrm{discr}})} + \sqrt{\mathcal{B}_\downarrow(\tau_{\mathrm{discr}})}\right). \tag{3.36}$$

A comparison between discrimination and dephasing rate will be given in Section 3.4.3.

Because of the oscillatory nature of $\mathcal{C}_\sigma(t)$ the problem of finding the first root of Eq. (3.36) is not trivial. We solve it by semi-quantitatively probing the function $|\mathcal{C}_\uparrow(t) - \mathcal{C}_\downarrow(t)| - 3\sqrt{2m\hbar\Omega}(\sqrt{\mathcal{B}_\uparrow(t)} + \sqrt{\mathcal{B}_\downarrow(t)})$ therefore the plot ist not very accurate. Nevertheless it gives a good idea about the dependence of τ_{discr} on Δ.

We observe in Fig. 3.3 that τ_{discr} is a discontinuous function of the coupling strength Δ, such that small adjustments in the parameters can give important improvement of the discrimination time.

For this type of measurement we are interested in the transients of $\mathcal{C}_\sigma(t)$ and we observe that the difference $|\mathcal{C}_\uparrow(t) - \mathcal{C}_\downarrow(t)|$ increases for values of the driving frequency ν close to resonance. For the ν far off-resonance the splitting of the peaks is increased by stronger driving.

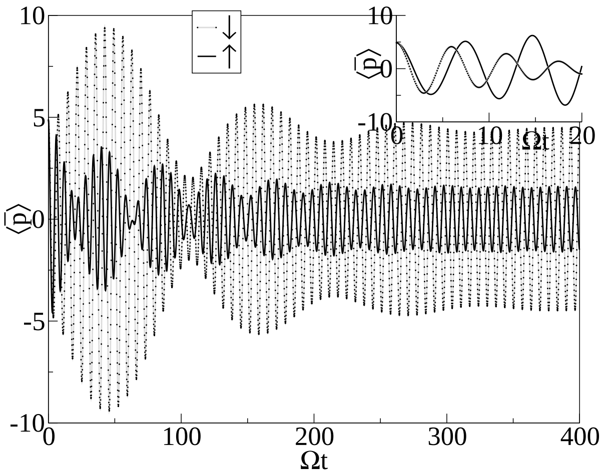

(a)

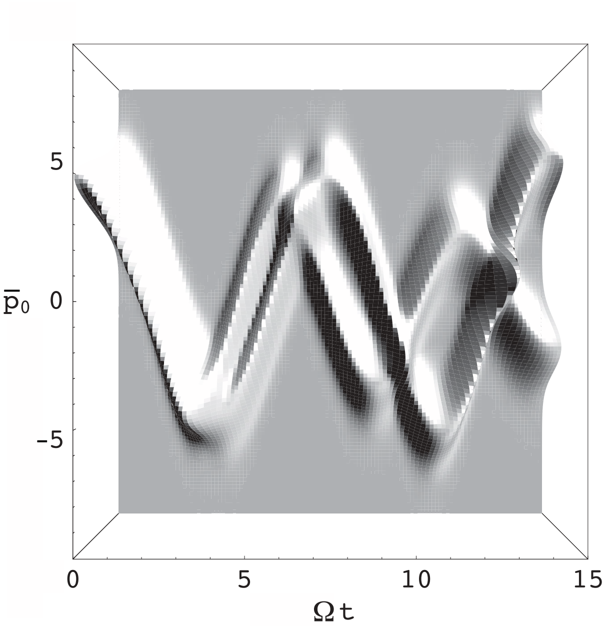

(b)

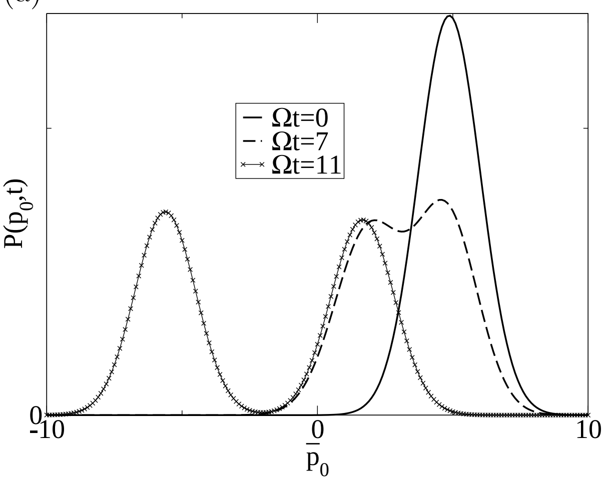

(c)

Figure 3.2: Expectation value of momentum for the two different qubit states (a), probability density of momentum $P(p_0, t)$ (b) and snapshots of it at different times (c). Here $\hbar\Omega/(k_B T) = 2$, $\Delta/\Omega = 0.45$, $\kappa/\Omega = 0.025$ and $\hbar\nu/(k_B T) = 1.9$ and $\overline{p}_0$ is the dimensionless momentum $p_0/\sqrt{k_B T m}$.

The discrimination time discussed here is not to be confused with the physical measurement time. In particular, the discrimination time remains finite even at vanishing κ and when the off-diagonal elements of the full density matrix in qubit space (3.19) still have finite norm at this time. The discrimination time is the time it takes to imprint the qubit state into the oscillator dynamics. For completing the measurement the oscillator itself needs to be observed by the heat bath and, as a consequence of that observation, the full density matrix will collapse further.

We note that in this kind of sample-and-hold measurement, the qubit spends only the discrimination time in contact with the environment. Keeping the discrimination time short may be of advantage in limiting bit flip errors during detection. We do not further describe such error processes in this chapter. However, in chapter 5 bit-flip errors in a similar setup are investigated, and a measurement protocol making full use of the advantages of fast and strong indirect measurements is presented.

As a technical limitation, it should be remembered that our theory is based on a Markov

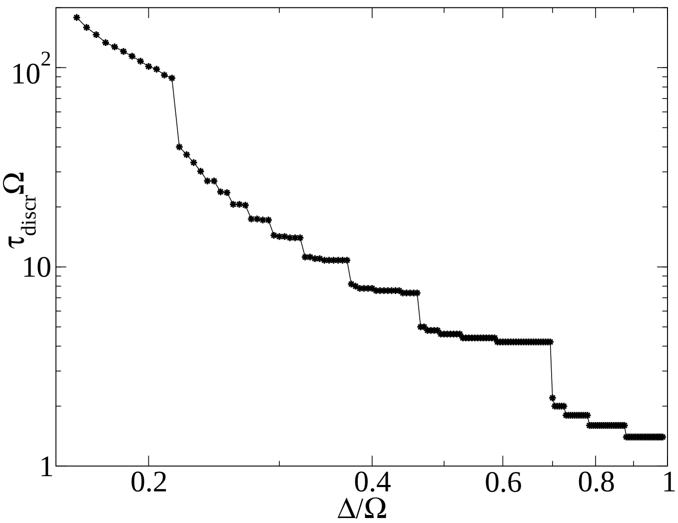

Figure 3.3: Discrimination time as function of the coupling strength between qubit and oscillator. Here $\hbar\Omega/(k_B T) = 2$, $\kappa/\Omega = 0.025$ and $\hbar\nu/(k_B T) = 1.95$.

approximation for the oscillator-bath coupling, hence it is not reliable for discrimination times lower than the bath correlation time.

Quasi-instantaneous, ensemble measurement

In this section, we are going to take this idea to the next level and analyze a measurement protocol that is based on extremely short qubit-detector interaction. In Refs. [123–125] has been shown that one can measure several field observables through infinitesimal-time probing of the internal states of the coupled qubit. In this section, we apply the same idea to the opposite setting. We show that the information about the state of the qubit is encoded in the expectation value of the momentum of our oscillator at only one point in time, leading to a fast weak measurement scheme.

We rewrite the Hamiltonian (3.13)

$$\begin{aligned} \hat{H} &= \hbar\Omega\left(\hat{a}^\dagger\hat{a}+\frac{1}{2}\right)+F(t)\sqrt{\frac{\hbar}{2m\Omega}}\left(\hat{a}+\hat{a}^\dagger\right)+\epsilon(t)\hat{\sigma}_z \\ &+ \hat{\sigma}_z\frac{\hbar\Delta^2}{4\Omega}\left(\hat{a}+\hat{a}^\dagger\right)^2+\frac{\hbar\left(\hat{a}+\hat{a}^\dagger\right)}{2\sqrt{m\Omega}}\sum_i\frac{\lambda_i\left(\hat{b}_i+\hat{b}_i^\dagger\right)}{\sqrt{m_i\omega_i}}+\sum_i\hbar\omega_i\left(\hat{b}_i^\dagger\hat{b}_i+\frac{1}{2}\right). \end{aligned} \tag{3.37}$$

In Schrödinger picture we have

$$\dot{\hat{\rho}} = \frac{1}{\mathbb{i}\hbar}[\hat{H},\hat{\rho}], \tag{3.38}$$

which leads, for any observable, to

$$\partial_t\langle\hat{O}\rangle = \langle\partial_t\hat{O}\rangle+\frac{1}{\mathbb{i}\hbar}\langle[\hat{O},\hat{H}]\rangle. \tag{3.39}$$

Setting $\hat{O} = \hat{a} - \hat{a}^\dagger$ we obtain:

$$\partial_t \langle \hat{a} - \hat{a}^\dagger \rangle = \frac{1}{\mathrm{i}\hbar} \left\langle \hbar\Omega(\hat{a} + \hat{a}^\dagger) + \frac{\hbar\Delta^2}{2\Omega}\hat{\sigma}_z(\hat{a} + \hat{a}^\dagger) - 2\sqrt{\frac{\hbar}{2m\Omega}}F(t) - 2\sqrt{\frac{\hbar}{2m\omega_i}}\lambda_i \left(\hat{b}_i + \hat{b}_i^\dagger\right) \right\rangle . \tag{3.40}$$

We assume unbiased noise and the qubit in the pure initial state $q_\uparrow|\uparrow\rangle + q_\downarrow|\downarrow\rangle$ which leads to

$$\hat{\rho}_{\mathrm{q}}(0) = \begin{pmatrix} |q_\uparrow|^2 & q_\uparrow q_\downarrow^* \\ q_\uparrow^* q_\downarrow & |q_\downarrow|^2 \end{pmatrix} . \tag{3.41}$$

For $t = 0$ Eq. (3.40) becomes

$$\partial_t \langle \hat{a} - \hat{a}^\dagger \rangle|_{t=0} = -\mathrm{i} \left\langle \hat{a} + \hat{a}^\dagger \right\rangle_{t=0} \left(\Omega + \frac{\Delta^2}{2\Omega}\langle\hat{\sigma}_z\rangle \right) - 2\sqrt{\frac{\hbar}{2m\Omega}}F(0), \tag{3.42}$$

$$\langle\hat{\sigma}_z\rangle = 2|q_\uparrow|^2 - 1. \tag{3.43}$$

If $\left\langle \hat{a} + \hat{a}^\dagger \right\rangle_{t=0} \neq 0$, the ensemble measurement of $\partial_t \langle \hat{a} - \hat{a}^\dagger \rangle|_{t=0}$ is sufficient to determine the state of the qubit.

In our case the oscillator is initially in a thermal state and $\left\langle \hat{a} + \hat{a}^\dagger \right\rangle_{t=0} = 0$. Nevertheless, calculating $\langle\hat{p}\rangle$ from Eq. (3.31) we obtain for the center of the Gaussians corresponding to the two qubit states $\mathcal{C}_\sigma$ of Eq. (3.32)

$$\langle\hat{p}\rangle(t) = \mathcal{C}_\downarrow(t) + (\mathcal{C}_\uparrow(t) - \mathcal{C}_\downarrow(t))|q_\uparrow|^2, \tag{3.44}$$

which is valid for *all* times. If $\mathcal{C}_\uparrow(t) \neq \mathcal{C}_\downarrow(t)$ we have

$$|q_\uparrow|^2 = \frac{\langle\hat{p}\rangle(t) - \mathcal{C}_\downarrow(t)}{\mathcal{C}_\uparrow(t) - \mathcal{C}_\downarrow(t)}. \tag{3.45}$$

At $t = 0$ we have, similar to the exact case $\mathcal{C}_\uparrow(0) = \mathcal{C}_\downarrow(0)$, independent of system parameters. This is again the consequence of the thermal initial state. Therefore one cannot infer from $\langle\hat{p}\rangle(0)$ the state of the qubit. For infinitesimal $\tau > 0$ we have $\mathcal{C}_\uparrow(\tau) \neq \mathcal{C}_\downarrow(\tau)$. Therefore quasi-instantaneous measurement of momentum still delivers the necessary information about the qubit, if the measurement is made at a infinitesimally small $\tau > 0$.

At $t = 0$ also the first derivative of $\mathcal{C}_\uparrow(t) - \mathcal{C}_\downarrow(t)$ is 0 due to the thermal initial state. A series expansion of Eq. (3.32) gives the short time result

$$\mathcal{C}_\uparrow(t) - \mathcal{C}_\downarrow(t) = \frac{2\nu F_0 \Delta^2}{\nu^2 - \Omega^2} \cdot t^2 + \mathcal{O}(t^3). \tag{3.46}$$

This gives a criterion for τ_{discr}, independent of κ, similar to observations of previous section, i. e. for short discrimination times we need large Δ and strong, close to resonance driving.

Moreover, it is sufficient to measure the expectation value of momentum, and not the first time derivative. The reason for this is the oscillator evolution, mediated by the interaction with the qubit, into a state with finite expectation value $\left\langle \hat{a} + \hat{a}^\dagger \right\rangle$, in other words the system is automatically creating its own measurement favorable "initial" condition. This is visible in Eq. (3.46) where the part of the signal proportional $|q_\uparrow|^2$ increases like t^2 which, for short times is slower than t, as it would be in the case where the favorable initial condition already exists.

This method leads to shorter discrimination times than the protocols presented in the previous sections which are independent of Δ and ν. Again, the read out of the oscillator in the end will be a separate issue and ultimately take a time $\propto \kappa^{-1}$.

On the other hand, in order to establish the expectation value with sufficient accuracy, this scheme requires a large ensemble average. According to the central limit theorem the uncertainty of the ensemble measurement is

$$\frac{\Delta y}{\langle y \rangle} = \frac{1}{\sqrt{N}} \frac{\Delta p}{\langle p \rangle} \tag{3.47}$$

where y is the ensemble averaged value of the measured momentum and N the number of measurements. For a given precision we have $N \propto \left(\Delta p / \langle p \rangle\right)^2$, therefore the number of measurements necessary to reach a given precision depends on Δ and time t. We have

$$N = \frac{\langle y \rangle^2}{(\Delta y)^2} \frac{|q_\uparrow|^2 |q_\downarrow|^2 (\mathcal{C}_\uparrow(t) - \mathcal{C}_\downarrow(t))^2 + m\Omega\hbar \sum_{\sigma\in\{\uparrow,\downarrow\}} |q_\sigma|^2 \mathcal{B}_\sigma(t)}{\left(\sum_{\sigma\in\{\uparrow,\downarrow\}} |q_\sigma|^2 \mathcal{C}_\sigma(t)\right)^2} \tag{3.48}$$

Eq. (3.45) shows that we need $\mathcal{C}_\uparrow \neq \mathcal{C}_\downarrow$ in order to determine the state of the qubit. At the same time, the number of measurements N necessary for high precision measurement of momentum is significantly reduced when $\mathcal{C}_\uparrow(t) = \mathcal{C}_\downarrow(t)$ (the two Gaussian distributions overlap completely). This reflects the tradeoff between the number of measurements and the signal strength $\mathcal{C}_\uparrow(t) - \mathcal{C}_\downarrow(t)$ which provides the information about the qubit.

The idea of a strong, quasi-instantaneous measurement will be pursued in more detail in chapter 5, taking into account also the possible bit-flip errors.

3.4.2 Back-action on the qubit

In order to complete the study of the measurement protocols presented in the previous section, we need insight into the measurement bakaction on the qubit. Since we are studying the QND Hamiltonian (3.12), the qubit decoherence consists only of dephasing. We start with the qubit in the initial pure state $(|\uparrow\rangle + |\downarrow\rangle)/\sqrt{2}$ and study the decay of the off-diagonal elements of the qubit density matrix. Such a superposition can be created by e. g. rapidly switching the tunnel matrix element from a large value to zero [126], or by ramping up the energy bias from zero to a large value. We compute the qubit coherence

$$\begin{aligned} C_x(t) &= \mathrm{Tr}\left\{\hat{\sigma}_x \otimes \mathbb{1}\hat{\rho}_S(t)(t)\right\} = 2\mathrm{Re}\mathrm{Tr}\left\{\hat{\rho}_{\uparrow\downarrow}(t)\right\} = 2\mathrm{Re}\int dx \langle x|\hat{\rho}_{\uparrow\downarrow}(t)|x\rangle \\ &= 2\mathrm{Re}\int dx \int dp\, W_{\uparrow\downarrow}(x,p,t) = 2\mathrm{Re}\int dx \int dp\, e^{\mathrm{i}x0} e^{\mathrm{i}p0} W_{\uparrow\downarrow}(x,p,t) \\ &= 8\pi \mathrm{Re}\,\chi_{\uparrow\downarrow}(0,0,t), \end{aligned} \tag{3.49}$$

where $W_{\sigma\sigma'}$ is the Wigner function

$$W_{\sigma\sigma'}(x_0, p_0) = \frac{1}{\pi\hbar}\int dy \langle x_0 + y|\hat{\rho}_{\sigma\sigma'} e^{-2\mathbb{i}yp_0}|x_0 - y\rangle. \quad (3.50)$$

We extract the dephasing time τ_ϕ from the strictly exponential long-time tail of $C_x(t)$.

We rewrite the master equation (3.23) for $\sigma \neq \sigma'$ using Eqs. (3.22) and (3.24) and obtain a partial differential equation for the characteristic function $\chi_{\uparrow\downarrow}$

$$\begin{aligned}\dot{\chi}_{\uparrow\downarrow}(\alpha,\alpha^*,t) &= \Big(\left(\alpha(k_1 + \mathbb{i}\Omega) + \alpha^* k_1 + B\sin(\nu t)\right)\partial_\alpha + \left(\alpha^*(k_2 - \mathbb{i}\Omega) + \alpha k_2 - B\sin(\nu t)\right)\partial_{\alpha^*} \\ &- \mathbb{i}\frac{\Delta^2}{2\Omega}(\partial_\alpha - \partial_{\alpha^*})^2 + (\alpha+\alpha^*)f_{\uparrow\downarrow}(t) + \mathcal{F}(t) + r(\alpha+\alpha^*)^2\Big)\chi_{\uparrow\downarrow}(\alpha,\alpha^*,t). \quad (3.51)\end{aligned}$$

The coefficients can be found in section 3.6.2. Eq. (3.51) is a generalized Fokker-Planck equation where the total norm is not conserved, i.e. $\int d^2\alpha \chi_{\uparrow\downarrow}(\alpha,\alpha^*,t)$ is *not* a constant of motion.

Solution of the generalized Fokker-Planck equation

Generalized Fokker-Planck equations (3.51) cannot in general be solved analytically with the established tools [28]. In our case, we are not interested in a fully general solution of the differential equation, but in the initial value problem where the $\chi_{\uparrow\downarrow}(\alpha,\alpha^*,0)$ is a Gaussian function, which covers thermal and coherent states of the oscillator. In this case one can show that $\chi_{\uparrow\downarrow}(\alpha,\alpha^*,t)$ remains a Gaussian at all time. This is the consequence of the QND Hamiltonian (3.12). We make the ansatz

$$\chi_{\uparrow\downarrow}(\alpha,\alpha^*,t) = A(t)\exp\big(-R_{11}(t)\alpha^2 - R_{22}(t)\alpha^{*2} - R_{12}(t)|\alpha|^2 + R_1(t)\alpha + R_2(t)\alpha^*\big), \quad (3.52)$$

and obtain for the time-dependent parameters of the Gaussian a closed system of nonlinear differential equations of the first order, thus proving that our ansatz is correct and complete if the initial characteristic function is a Gaussian.

We assume the oscillator initialy in a thermal state $\chi_{\uparrow\downarrow}(\alpha,\alpha^*,0) = (1/4\pi)\exp(-(1/2 + n(\Omega))|\alpha|^2)$ and obtain for the parameters of the Gaussian ansatz following equations of motion

$$\begin{aligned}\dot{A}_E(t) &= B\sin(\nu t)(R_1(t) - R_2(t)) + \mathcal{F}(t) \\ &+ \frac{\mathbb{i}\Delta^2}{\Omega}\left(R_{11}(t) + R_{22}(t) - R_{12}(t) - \frac{(R_1(t)-R_2(t))^2}{2}\right), \quad (3.53) \\ \dot{R}_1(t) &= (k_1 + \mathbb{i}\Omega)R_1(t) + k_2R_2(t) - B\sin(\nu t)(2R_{11}(t) - R_{12}(t)) \\ &- \frac{\mathbb{i}\Delta^2}{\Omega}(R_1(t) - R_2(t))(R_{12}(t) - 2R_{11}(t)) + f_{\uparrow\downarrow}(t) \quad (3.54)\end{aligned}$$

$$\begin{aligned}
\dot{R}_2(t) &= (k_2 - \mathbb{i}\Omega)R_2(t) + k_1 R_1(t) + B\sin(\nu t)(2R_{22}(t) - R_{12}(t)) \\
&- \frac{\mathbb{i}\Delta^2}{\Omega}(R_2(t) - R_1(t))(R_{12}(t) - 2\,R_{22}(t)) + f_{\uparrow\downarrow}(t) \qquad (3.55) \\
\dot{R}_{11}(t) &= 2(k_1 + \mathbb{i}\Omega)R_{11}(t) + k_2 R_{12}(t) + \frac{\mathbb{i}\Delta^2}{2\Omega}(R_{12}(t) - 2R_{11}(t))^2 - r, \qquad (3.56) \\
\dot{R}_{22}(t) &= 2(k_2 - \mathbb{i}\Omega)R_{22}(t) + k_1 R_{12}(t) + \frac{\mathbb{i}\Delta^2}{2\Omega}(R_{12}(t) - 2R_{22}(t))^2 - r, \qquad (3.57) \\
\dot{R}_{12}(t) &= (k_1 + k_2)R_{12}(t) + 2k_1 R_{11}(t) + 2k_2 R_{22}(t) \\
&- \frac{\mathbb{i}\Delta^2}{\Omega}(R_{12}(t) - 2R_{11}(t))(R_{12}(t) - 2R_{22}(t)) - 2r, \qquad (3.58)
\end{aligned}$$

where $A(t) = \mathbb{e}^{A_E(t)}$. This system of equations can be solved numerically, for example using a Runge-Kutta algorithm.

Chapter 4 gives a elaborate analysis of the various dephasing mechanisms in the case without driving and the parameter regimes where they come to play. There the weak qubit-oscillator coupling (WQOC) regime is associated to a phase Purcell effect [127] where the dephasing rate $1/\tau_\phi \propto 1/\kappa$. Beyond the weak coupling, chapter 4 explores a strong dispersive coupling regime with fundamentally different origin where the dephasing rate is proportional to κ.

In the following we want to apply and extend this results to the case of actual measurement, i. e. when the oscillator is driven in order to measure its frequency and from this information, to infere the state of the qubit.

Qubit dephasing

We start by studying the dependence of the qubit dephasing on the parameters of the oscillator driving field.

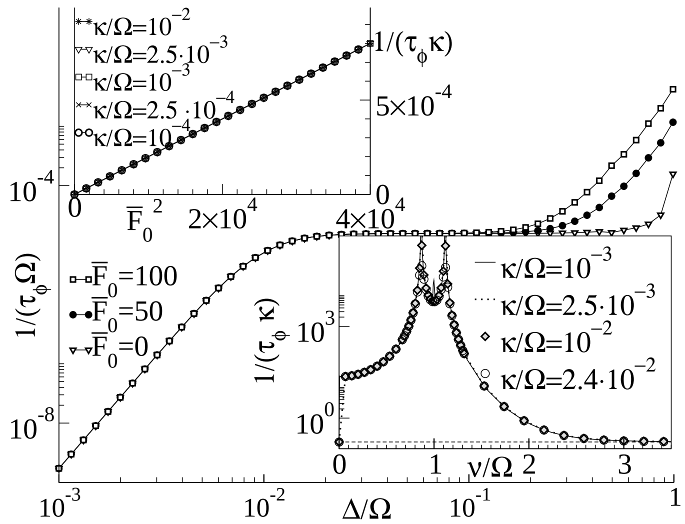

Figure 3.4: Dephasing rate dependence on driving: dependence on Δ for different driving strengths F_0 ($\kappa/\Omega = 10^{-4}$ and $\nu = 2\Omega$). Top inset: dependence of the decoherence rate on F_0 for different values of κ ($\Delta/\Omega = 5 \cdot 10^{-2}$ and $\nu = 2\Omega$). Bottom inset: dependence of the decoherence rate on driving frequency ν for different vales of κ ($\Delta/\Omega = 0.5$). Here $\hbar\Omega/k_B T = 2$ and $\overline{F}_0$ is the dimensionless force $F_0\hbar/(k_B T\sqrt{m k_B T})$.

In Fig. 3.4 we observe that the dependence of the dephasing rate $1/\tau_\phi$ on F_0 is quadratic.

For values of κ belonging to strong and weak coupling regime at $F_0 = 0$ we obtain the same driving contribution to the dephasing rate, proportional to κF_0^2, see the inset of Fig. 3.4. Here only the contribution of driving is shown. We have substracted from each curve the initial value of τ_ϕ at $F_0 = 0$. We observe that the decoherence rate must be of the form

$$\frac{1}{\tau_\phi} = \left.\frac{1}{\tau_\phi}\right|_{F_0=0} + \text{ct.} \cdot F_0^2 \kappa, \tag{3.59}$$

for both the weak and strong coupling regime.

This was to be expected since the qubit couples to the squared coordinate which (at least in the classical case) is proportional to F_0^2. In both regimes, the driving leads to a contribution to the dephasing rate that is proportional to κ because the driving leads to classical motion relative to the heat bath, which is fixed in the $\hat{x}$-coordinate space. This motion enhances the effect of the bath the stronger the friction coefficient κ is. Consequently, even if in the undriven case the dephasing rate scales as $1/\kappa$, strong driving can in principle cross it over to a decay rate $\propto \kappa$. This cross-over from $1/\kappa$ to κ inside the WQOC regime happens at either *very* strong driving or when the driving ν frequency approaches one of the system resonances Ω_σ.

The dependence on the driving frequency has also been analyzed in Fig. 3.4. Here we observe two peaks at $\Omega_\uparrow$ and $\Omega_\downarrow$. At $\nu = \Omega$ the classical driven and *un*damped trajectory $\xi(t)$ diverges. In terms of the calculation this means that the Floquet modes are not well-defined when the driving frequency is at resonance with the harmonic oscillator — we have a continuum instead. Physically this means that at $t = 0$ our oscillator has the frequency Ω because it has not yet interacted whit the qubit, and we are driving it at resonance, and by amplifying the oscillations of $\langle \hat{x} \rangle$ which is subject to noise we amplify the noise seen by the qubit. The dephasing rate is also expected to diverge. The peaks at $\Omega_\uparrow$and $\Omega_\downarrow$ show the same effect after the qubit and the oscillator build dressed states. The dephasing rate drops again for large driving frequencies to the value obtained in the case without driving.

3.4.3 Comparison of dephasing and measurement times

In this section we analyze the measurement times necessary for the measurement protocols described in section 3.4.1 and compare them with the dephasing times of the qubit obtained for the same parameters.

Long time, single shot measurement

For the long time measurement protocol (section 3.4.1) we observe that $1/\tau_\mathrm{m} \propto F_0^2 \Delta^4 + \mathcal{O}(\Delta^8)$.

Comparing $1/\tau_\phi$ and $1/\tau_\mathrm{m}$ we find that the measurement time depends more stronlgy on the driving strength F_0 than the dephasing time.

As one can see for the parameters of Fig. 3.5, in the WQOC regime the measurement time is longer than the dephasig time. Their difference decreases as we increase Δ due to the onset of the strong coupling plateau in the dephasing rate, approaching the quantum

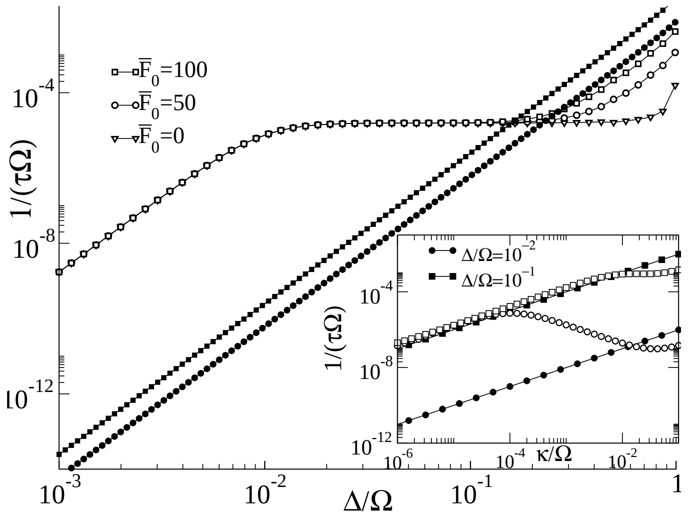

Figure 3.5: Comparison of dephasing / measurement rate. Open symbols: $1/(\tau_\phi\Omega)$ and filled symbols: $1/(\tau_{\rm m}\Omega)$. Here $\nu = 2\Omega$, $\kappa = 10^{-4}\Omega$ and $\hbar\Omega/(k_BT) = 2$. Inset: dependence on κ, $\overline{F}_0 = 200$. The crossings, conflicting with the quantum limit [5], are signaling the limits of the Born approximation, as described in text.

limit where the measurement time becomes comparable to the dephasing time. Note that, for superstrong coupling either between qubit and oscillator or between oscillator and bath, corrections of the order $(\kappa/\Omega_\downarrow)^2$ of the dephasing rate gain importance. These corrections are not treated in our Born approximation. Therefore the regions where the dephasing rate becomes lower than the measurement rate, in violation with the quantum limitation of Ref. [5], should be regarded as a limitation of our approximation.

The inset in Fig. 3.5 shows the dephasing and measurement times as function of κ. Again we observe improvement of the ratio of measurement and dephasing time as we increase Δ. On the other hand, if the tunning of κ should be easier to achieve experimentally, we also see that, at given Δ one can make use of the phase Purcell effect which reduces the dephasing rate as $1/\kappa$ while the measurement rate increases like κ. This will be investigated in more detail in chapter 4 where it will be shown that strong κ implies WQOC, i. e. phase Purcell effect.

Short time, single shot measurement

As already mentioned, for the short time, single shot measurement strong, close to resonance driving is needed for the rapid separation of the peaks. While the discrimination time is not very sensitive to the change of κ, we observe in Fig. 3.6 that one needs relatively strong coupling ($\Delta/\Omega \in (0.03, 0.1)$) for the discrimination time to become shorter than the decoherence time. The picture of the dephasing rate is also qualitatively different from the case without driving or with far off-resonant driving, since for $\Delta/\Omega \approx 0.4$, $\Omega_\uparrow$ becomes resonant with the driving frequency. In this region our numerical calculation also becomes unstable. Nevertheless, as one can see in Fig. 3.6, the dephasing rate is proportional to κ. Thus, by reducing the damping of the oscillator, one can extend the domain of values of Δ where the measurement can be performed.

We also observed that by further reducing Δ the discrimination rate suddenly drops to zero, i. e. for too small Δ the two peaks in Fig. 3.2 will never be well enough separated to

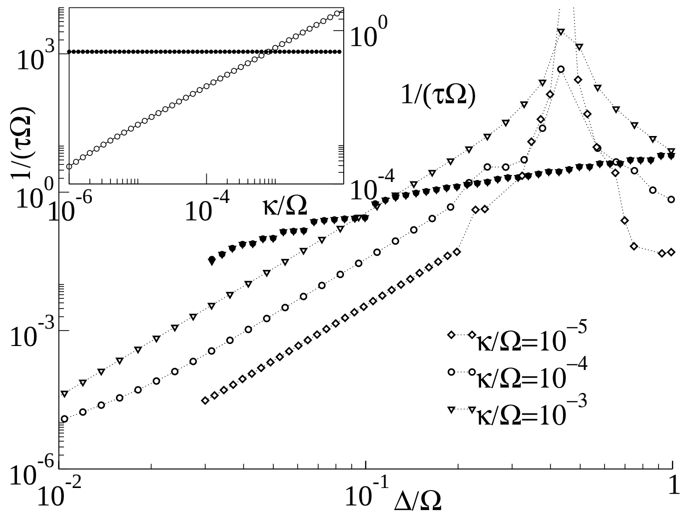

Figure 3.6: Comparison of dephasing / discrimination rates. Open symbols: $1/(\tau_\phi\Omega)$ and filled symbols: $1/(\tau_{\mathrm{discr}}\Omega)$. Here $\nu = 1.1\Omega$, $\overline{F}_0 = 200$ and $\hbar\Omega/(k_BT) = 2$. Inset: dependence on κ for $\Delta/\Omega = 0.1$.

allow a single shot measurement.

In this protocol what we call "discrimination time" is actually the time when the system becomes measurable, i. e. one can in principle extract from a single measurement the needed information about the qubit (and consequently collapse the wave function). We do not further describe this collapse here.

3.5 Conclusion

We have presented a phase-space theory of the measurement and measurement backaction on a qubit coupled to a dispersive detector.

We have studied the qubit coupled to an complex environment (weakly damped harmonic oscillator) with a quadratic coupling, which does not have to be weak. We solved the problem by considering the prominent degree of freedom of the environment, i. e. the main oscillator as part of the quantum mechanical system and explicitly solving its dynamics. Only at the end of the calculation we traced over this last degree of freedom of the environment in order to obtain the qubit dynamics.

We presented three measurement protocols and compared the measurement and decoherence times. The first measurement protocol described in section 3.4.1 requires long measurement time, such that the measurement can only be preformed in strong coupling regime, with far off-resonant driving. The second measurement protocol has the advantage of short discrimination times compared with the dephasing time, requires strong qubit-oscillator coupling and also close to resonance driving. Both this protocols can be performed as single shot measurement, and thus may be useful as a readout method for the scalable architecture with long range coupling using superconducting flux qubits [128]. The quasi-instantaneous measurement protocol presented in section 3.4.1 has the advantage of the shortest possible discrimination time and no restriction for the qubit-oscillator coupling, with the drawback that one needs to repeat the measurement a large number of times to obtain the momentum expectation value.

Chapter 5 will further explore the potential of a very similar setup and investigate qubit relaxation leading to possible bit flip errors. The possibility of a quantum non-demolition readout facilitated by a strong qubit-oscillator interaction will be studied.

We expect our results, with minor adaptations, to be applicable to various cavity systems, e. g. quantum dot or atom-based quantum optical schemes [129, 130]. The dispersive coupling of Hamiltonian (3.12) could have implications for the generation of squeezed states, quantum memory in the frame of quantum information processing, measurement and post-selection of the number states of the cavity.

3.6 Additional information

3.6.1 Parameter conversion

In this section we present the parameter conversion from the actual circuit to our model Hamiltonian. The plasma frequency and the mass of the oscillator are given by

$$\Omega = \sqrt{\frac{f_1}{L_{JS}C_S}}, \;\; m = \frac{\hbar^2 C_S}{2e^2}. \tag{3.60}$$

The qubit oscillator coupling strength is determined by

$$\Delta = \sqrt{\frac{\delta f_1}{L_{JS}C_S}}. \tag{3.61}$$

The harmonic driving force of the oscillator and the resulting indirect driving of the qubit read

$$F(t) = I_B(t)\frac{\hbar}{e}, \;\; \epsilon(t) = \epsilon_0 + \upsilon I_B^2(t). \tag{3.62}$$

The momentum and position of the oscillator are

$$p_+ \;\; = \;\; \frac{\hbar^2 C_S}{2e^2}\dot{\gamma}_+ = \frac{C_S \hbar V}{e}, \;\; x = \gamma_+. \tag{3.63}$$

The oscillator damping is given by $\kappa = 1/(2RC_S)$. From the relation $f(\hat{\gamma}) = f(\gamma_0\hat{\sigma}_z) = (f(\gamma_0) + f(-\gamma_0))/2 + \hat{\sigma}_z (f(\gamma_0) - f(-\gamma_0))/2$ we have:

$$\begin{aligned}
f_1 &= \frac{1}{2}\left(\cos\left(\frac{a+b\gamma_0}{2}\right) + \cos\left(\frac{a-b\gamma_0}{2}\right)\right), \; \delta f_1 = \frac{1}{2}\left(\cos\left(\frac{a+b\gamma_0}{2}\right) - \cos\left(\frac{a-b\gamma_0}{2}\right)\right), \\
a &= \Xi_1 \frac{M_\Sigma^2}{2L_q} = \frac{2\pi}{\Phi_0}\left(-M_{Sq}\Phi_q^{(x)} + L_q\Phi_S^{(x)}\right)\frac{1}{2L_q}, \; b = \frac{M_{Sq}}{2L_q}, \; \upsilon = \frac{1}{4L_{JS}I_{cS}^2}\delta f_2, \\
\delta f_2 &= \frac{1}{2}\left(\left(\cos\left(\frac{a+b\gamma_0}{2}\right)\right)^{-1} - \left(\cos\left(\frac{a-b\gamma_0}{2}\right)\right)^{-1}\right).
\end{aligned}$$

3.6.2 Parameters for the generalized Fokker-Planck equation

The parameters included in Eq. (3.51) are

$$
\begin{aligned}
k_{1,2} &= -\frac{\kappa}{2} \pm \kappa \frac{(1+2n_\uparrow)\Omega_\uparrow - (1+2n_\downarrow)\Omega_\downarrow}{4\Omega}, \\
r &= -\frac{\kappa}{8\Omega}\left(\Omega_\uparrow(1+2n_\uparrow) + \Omega_\downarrow(1+2n_\downarrow)\right) - \frac{\mathbb{i}\Delta^2}{8\Omega}, \;\; B = -\frac{2\mathbb{i}F_0\Delta^2}{\sqrt{2m\Omega\hbar}(\Omega^2-\nu^2)}, \\
\mathcal{F}(t) &= \frac{\mathbb{i}F_0^2\Delta^2}{2m\hbar(\nu^2-\Omega^2)^2}\left(\cos(2\nu t) - 1\right) - 2\frac{\mathbb{i}}{\hbar}\epsilon(t), \\
f_{\uparrow\downarrow}(t) &= \frac{\kappa F_0}{\sqrt{2m\hbar\Omega}}\left(\frac{\Delta^2\sin(\nu t)}{2(\nu^2-\Omega^2)}\sum_{\sigma\in\{\uparrow,\downarrow\}}\frac{\Omega_\sigma(1+2n_\sigma)}{\nu^2-\Omega_\sigma^2} - \frac{\nu\Delta^2\sin(\nu t)(1+2n_\nu)}{(\nu^2-\Omega_\uparrow^2)(\nu^2-\Omega_\downarrow^2)} + \frac{\mathbb{i}\nu\cos(\nu t)}{\Omega^2-\nu^2}\right).
\end{aligned}
$$

Chapter 4

Crossover from weak to strong coupling regime in dispersive circuit QED

I. Serban, E. Solano and F. K. Wilhelm

We study the decoherence of a superconducting qubit due to the dispersive coupling to a damped harmonic oscillator. We go beyond the weak qubit-oscillator coupling, which we associate with a *phase Purcell effect*, and enter into a strong coupling regime, with qualitatively different behavior of the dephasing rate. We identify and give a physically intuitive discussion of both decoherence mechanisms. Our results can be applied, with small adaptations, to a large variety of other physical systems, e. g. trapped ions and cavity QED, boosting theoretical and experimental decoherence studies.

Parts of this chaper have been published in *Europhysics Letters* **80**, 40011 (2007)

4.1 Introduction

With a thrust from applications in quantum computing, the manipulation of quantum states in superconducting nanocircuits has made tremendous progress over the last decade [13, 53, 107, 131–136]. A crucial step for these successes is the understanding of decoherence and the design of good measurement schemes. The latter is a particular challenge as the detector is made using the same technology as the system being detected i.e. the qubit. Also, the measurement timescale cannot be considered to be infinitesimally short as compared to the intrinsic scales of the qubit evolution. Thus, understanding the measurement process is crucial both fundamentally and for improving experiments.

A specifically attractive development is the emergence of circuit quantum electrodynamics (cQED) [95, 137–143], where effective Hamiltonians, similar to those of the coherent light-matter interaction of quantum optics and in particular of cavity QED, can be realized in the microwave frequency domain. There are many approaches to realize the qubit, including flux and charge, and the cavity, including a superconducting quantum interference device (SQUID) or a coplanar waveguide.

In this context, measurement protocols making use of dispersive qubit-oscillator interactions [107, 131] are useful for reducing the backaction on the qubit [1]. For example, in the flux qubit–SQUID combination, as in the Delft setup of Refs. [107, 144] discussed in chapter 3, the SQUID behaves like a harmonic oscillator. Its inductive coupling to the flux qubit leads to a frequency shift depending on the qubit state

$$\Omega_{\uparrow,\downarrow} = \sqrt{\Omega^2 \pm \Delta^2}. \tag{4.1}$$

Here, Ω is the bare oscillator frequency and Δ is the quadratic frequency shift. A measurement of the SQUID resonance frequency provides information of the qubit state. While the manipulation of the qubit is usually performed at the optimum working point [53], the readout can and should be performed in quantum nondemolition measurement i. e. in the pure dephasing limit.

In this chapter we study the decoherence of a qubit due to the dispersive coupling to a damped harmonic oscillator, taking the Delft setup as an example though our results may be adapted to several physical systems. In the Purcell effect a narrow oscillator linewidth enhances the absorbtion of the resonant photon emitted by the two-level atom and thus the energy relaxation of the latter. In the weak qubit-oscillator coupling regime (WQOC), we explain the behavior of dephasing in terms of a similar process, the phase Purcell effect. This regime is characterized, as we will be show later, by $\Delta/\Omega < \sqrt{\kappa/\Omega}/(1 + n(\Omega))^{1/4}$, where $n(\Omega)$ is the Bose function at the frequency Ω and environment temperature T. The main result of this work lays beyond the WQOC, in a regime where fast qubit-oscillator entanglement plays the dominant role. We find a qualitatively different behavior of the dephasing rate. The divergence of the qubit dephasing rate $1/\tau_\phi \propto 1/\kappa$ when the oscillator decay rate $\kappa \to 0$ is lifted by the onset of the strong coupling regime.

The Hamiltonian describing the Delft setup [144] can be written as

$$\hat{H} = \underbrace{\frac{\epsilon}{2}\hat{\sigma}_z + \hbar\Omega\left(\hat{a}^\dagger\hat{a} + \frac{1}{2}\right) + \frac{\hbar\Delta^2}{4\Omega}(\hat{a}+\hat{a}^\dagger)^2\hat{\sigma}_z}_{\hat{H}_S} + \hat{H}_D. \tag{4.2}$$

Here, $\hat{a}$ and $\hat{a}^\dagger$ are the annihilation and creation operators of the harmonic oscillator, $\hat{\sigma}_z$ acts in the Hilbert space of the qubit and $\hat{H}_D$ describes the damping of the oscillator. A full-length derivation of Hamiltonian (4.2) and discussion of the approximations used is given in chapter 3. It basically derives the Hamiltonian from the equations of motion of the Josephson phases across the junctions and truncates the SQUID potential to the second order.

We will show that key experiments [107, 131] are performed outside the WQOC. Moreover, a very recent experiment [145] explicitly relies on the use of a strong dispersive coupling regime. We demonstrate that the dephasing rate $1/\tau_\phi \propto 1/\kappa$ for WQOC, and $1/\tau_\phi \propto \kappa$ at strong coupling. We discuss the crossover between these regimes and its dependence on κ and temperature T. We provide physical interpretations of both regimes, the former as a phase Purcell effect and the latter as the onset of qubit-oscillator entanglement. The results of the present study may be extended straightforwardly to any system with similar dispersive qubit-oscillator coupling such as the charge-qubit–coplanar wave guide system (see Yale setup [131]), trapped ions [146] and 3D microwave cavity QED [129], quantum dots [130], among others.

4.2 Method

In studying the qubit dephasing we are facing the challenge of a complex non-markovian environment consisting in the main oscillator (i. e. SQUID) and the ohmic bath. Moreover, the qubit couples to a non-Gaussian variable of its environment. Therefore the tools developed for Gaussian baths [19] cannot be applied in this system for arbitrary strong coupling between the qubit and the oscillator.

We study the qubit dynamics under the Hamiltonian (4.2) for arbitrary Δ/Ω, assuming essentially the dimensionless oscillator decay rate κ/Ω as the *only* small parameter. In this regime we avoid over-damping of the oscillator and the strong backaction on the system which this would cause. We give in the following a brief description of the crucial steps and approximations of the calculation. We model the damping, associated with the oscillator decay rate κ, in the Caldeira-Leggett way by a bath of harmonic oscillators

$$\hat{H}_D = \underbrace{\sum_j \hbar\omega_j\left(\hat{b}_j^\dagger\hat{b}_j + \frac{1}{2}\right)}_{\hat{H}_B} + \underbrace{\sum_j \frac{\hbar(\hat{a}+\hat{a}^\dagger)}{2\sqrt{m\,\Omega}}\frac{\lambda_j(\hat{b}_j^\dagger+\hat{b}_j)}{\sqrt{m_j\,\omega_j}}}_{\hat{H}_I} + \hat{H}_c, \tag{4.3}$$

with $J(\omega) = \sum_j \lambda_j^2\hbar/(2m_j\omega_j)\delta(\omega-\omega_j) = m\hbar\kappa\omega\Theta(\omega-\omega_c)/\pi$ and $\hat{H}_c$ the counter term [16, 89, 101] where Θ is the Heaviside step function and ω_c an intrinsic high frequency cut-off. Our starting point is the Born-Markov master equation in the weak coupling to the bath limit for the reduced density matrix $\hat{\rho}_S$ in the qubit-oscillator Hilbert space

$$\dot{\hat{\rho}}_S(t) = \frac{1}{\mathbb{i}\hbar}\left[\hat{H}_S, \hat{\rho}_S(t)\right] + \int_0^\infty \frac{dt'}{(\mathbb{i}\hbar)^2}\,\mathrm{Tr}_B\left[\hat{H}_I, [\hat{H}_I(t, t-t'), \hat{\rho}_S(t)\otimes\hat{\rho}_B(0)]\right]. \tag{4.4}$$

This approach is valid at finite temperatures $k_BT \gg \hbar\kappa$, for times $t \gg 1/\omega_c$ [101, 116], which is the limit we will discuss henceforth. We start from a standard factorized initial state for all subsystems. We express $\hat{\rho}_S(t)$ in the qubit basis and represent its elements, which are still oscillator operators, in phase-space as

$$\hat{\rho}_S = \begin{pmatrix}\hat{\rho}_{\uparrow\uparrow} & \hat{\rho}_{\uparrow\downarrow}\\ \hat{\rho}_{\downarrow\uparrow} & \hat{\rho}_{\downarrow\downarrow}\end{pmatrix},\ \ \hat{\rho}_{\sigma\sigma'} = \int\frac{d^2\alpha}{\pi}\ \chi_{\sigma\sigma'}(\alpha,\alpha^*,t)\hat{D}(-\alpha),$$

where $\chi_{\sigma\sigma'}$ is the characteristic Wigner function and $\hat{D} = \exp(\alpha\hat{a}^\dagger - \alpha^*\hat{a})$ the displacement operator [27]. Independent of our work, Ref. [147] has used a different phase-space representation to calculate the qubit dephasing rate. We characterize the qubit coherence by $C_x(t) = \left\langle\hat{\sigma}_x\otimes\hat{\mathbb{1}}\right\rangle = 2\mathrm{Re}\ \mathrm{Tr}\hat{\rho}_{\uparrow\downarrow}(t)$ which can be easily shown to be $C_x(t) = 8\pi\mathrm{Re}\chi_{\uparrow\downarrow}(0,0,t)$. After a rather long but essentially straightforward calculation, one obtains for $\chi_{\uparrow\downarrow}$ a *generalized* Fokker-Planck equation

$$\begin{aligned}\dot{\chi}_{\uparrow\downarrow}(\alpha,\alpha^*,t) &= \Big(\left(\alpha(k_1+\mathbb{i}\Omega)+\alpha^*k_1\right)\partial_\alpha + \left(\alpha^*(k_2-\mathbb{i}\Omega)+\alpha k_2\right)\partial_{\alpha^*}\\ &- \frac{\mathbb{i}\Delta^2}{2\Omega}(\partial_\alpha-\partial_{\alpha^*})^2 + p(\alpha+\alpha^*)^2\Big)\chi_{\uparrow\downarrow}(\alpha,\alpha^*,t),\end{aligned} \tag{4.5}$$

where

$$k_{1,2} = -\frac{\kappa}{4}\left(2\mp\frac{\Omega_\uparrow}{\Omega}(1+2n_\uparrow)\pm\frac{\Omega_\downarrow}{\Omega}(1+2n_\downarrow)\right), \tag{4.6}$$

$$p = -\frac{\kappa}{8\Omega}\left(\Omega_\uparrow(1+2n_\uparrow)+\Omega_\downarrow(1+2n_\downarrow)\right) - \frac{\mathbb{i}\Delta^2}{8\Omega}, \tag{4.7}$$

and $n_\sigma = n(\Omega_\sigma)$ is the Bose function. To solve Eq. (4.5) we make a Gaussian ansatz for $\chi_{\uparrow\downarrow}$.

$$\chi_{\uparrow\downarrow} = A(t)\exp(-R_{11}(t)\alpha^2 - R_{22}(t)\alpha^{*2} - R_{12}(t)\alpha\alpha^*). \tag{4.8}$$

This ansatz includes coherent and thermal states. In the following we assume the oscillator to be initially in a thermal state, in equilibrium with its environment. This implies $R_{12}(0) = 1/2 + n(\Omega)$ and $R_{11}(0) = R_{22}(0) = 0$. Due to the quadratic (pure dephasing) form of the Hamiltonian (4.2), obtain a closed system of ordinary differential equations for the parameters of the Gaussian ansatz, see also chapter 3. This system can be easily solved perturbatively in Δ in the weak coupling regime, or numerically, (for arbitrarily strong coupling), and we can extract the dephasing time τ_ϕ from the strictly exponential long-time tail of $C_x(t) = 8\pi\mathrm{Re}A(t)$.

4.3 Weak qubit-oscillator coupling

Before solving Eq. (4.5) in a general manner, we revisit the case of small Δ. Up to the lowest non-vanishing order Δ^4, the analytically calculated WQOC dephasing rate is

$$\frac{1}{\tau_\phi} = \Delta^4 \frac{n(\Omega)\,(n(\Omega)+1)}{\Omega^2}\left(\frac{\kappa}{\kappa_m^2} + \frac{1}{\kappa}\right), \tag{4.9}$$

where $\kappa_m = \sqrt{2k_B T\Omega/(\hbar(1+2\,n(\Omega)))}$. The term $1/\kappa$ exactly reproduces the Golden Rule dephasing rate of Ref. [144], and is similar to the result of Ref. [98]. These previous results have been obtained considering only the two-point correlator of the fluctuating observable $(a+a^\dagger)^2$, i. e. assuming an Gaussian environment. The crossover point κ_m from $1/\kappa$ to κ in Eq. (4.9) is, at the Delft parameters [107], comparable to Ω, i. e. κ would dominate over $1/\kappa$ only in a regime where the Born approximation fails. Nevertheless, since the golden rule limit $\lim_{\kappa\to\infty} 1/\tau_\phi = 0$ is unphysical, such a term was to be expected.

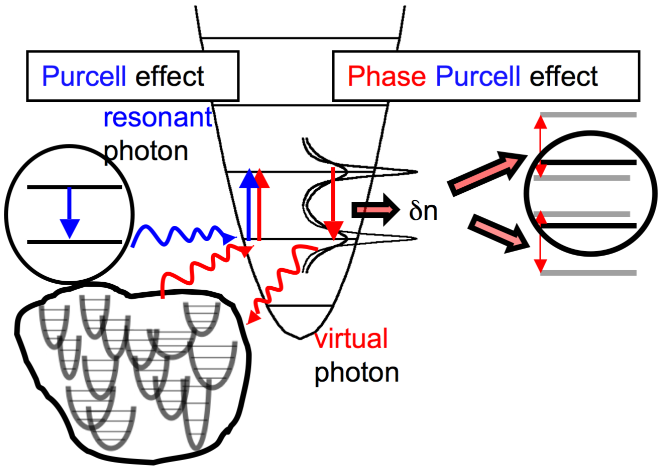

Figure 4.1: The Purcell effect (blue): absorption of a resonant photon emitted by the two-level atom; Dephasing in WQOC regime (red): virtual photon exchange between oscillator and bath.

In the WQOC regime, the enhancement of dephasing by weak coupling to the environment is analogous to the enhancement of spontaneous emission by the narrow cavity lines in the *resonant* Purcell effect, see Refs. [127, 148]. In the pure dephasing case we have no energy exchange between the qubit and the oscillator. Qubit decoherence is caused by fluctuations of $(\hat{a}+\hat{a}^\dagger)^2$. Since we are in the WQOC regime, the stronger coupling between the oscillator and the environment causes equilibrium between the oscillator and the bath on a shorter time scale than the qubit dephasing. In equilibrium, the main contribution to the fluctuations of $(\hat{a}+\hat{a}^\dagger)^2$ is the exchange of photons between oscillator and bath. The process is analogous to equilibrium fluctuations in canonical thermodynamics. A virtual photon returning from the environment (Fig. 4.1) is at resonance with the oscillator. The absorbtion of this photon, like in the resonant Purcell effect will be enhanced by narrow oscillator lines. Therefore, the entire dephasing process will be enhanced when the coupling to the environment is weak and this mechanism can be viewed as a phase Purcell effect. We give a more detailed discussion of this effect in section 4.6.

4.4 Strong qubit-oscillator coupling

The dephasing rate (4.9) obtained in the small κ and WQOC limit diverges for $\kappa \to 0$, i.e., in the absence of an environment. The solution to this apparent contradiction lies beyond the WQOC, therefore we solve Eq. (4.5) numerically using again the Gaussian ansatz for $\chi_{\uparrow\downarrow}$.

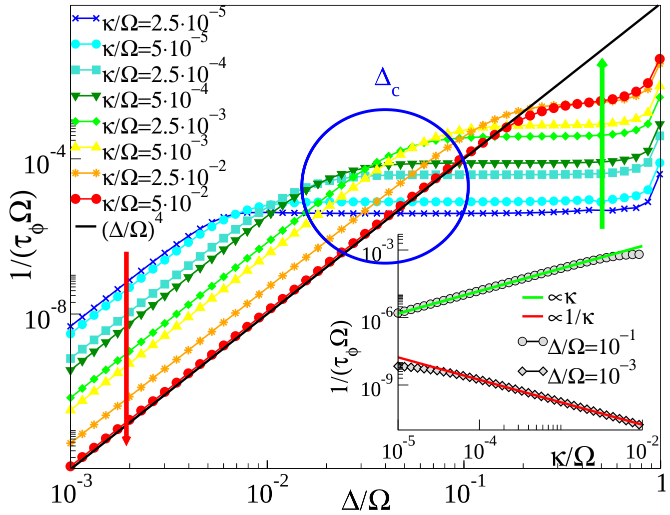

Figure 4.2: Dephasing rate $1/\tau_\phi$ as function of Δ for different values of κ. Power-law Δ^4 growth at low Δ crosses over to Δ-independence at strong coupling. Inset: dephasing rate as a function of κ in the weak coupling regime ($\Delta/\Omega = 10^{-3}$) showing $1/\tau_\phi \propto \Delta^4/\kappa$ and the strong coupling regime ($\Delta/\Omega = 10^{-1}$) with $1/\tau_\phi \propto \kappa$ dependence. Here $\hbar\Omega/k_BT = 2$ similar to experiments.

Fig. 4.2 shows the dependence of the dephasing rate on, Δ for various values of κ. The dimensionless parameter $\hbar\Omega/k_BT$ is 2, similar to the Delft and Yale setups. As predicted by Eq. (4.9) for $\kappa \ll \kappa_m$ and small Δ, the dephasing rate is proportional to Δ^4/κ. Further increasing Δ, we observe a saturation of the dephasing rate which marks the onset of the strong coupling regime. This regime is analogous to the strong coupling in linear cavity QED. Here $1/\tau_\phi$ is proportional to κ.

At strong qubit-oscillator coupling the oscillator couples to the qubit stronger than it couples to the heat bath, such that one cannot use the effective bath concept of WQOC. As the qubit-oscillator system becomes entangled, a fundamentally different dephasing mechanism emerges. The eigenstates of the Hamiltonian (4.2) at $\kappa = 0$ are the dressed states $\{|\sigma, m_\sigma\rangle\}$ where $|m_\sigma\rangle$ are the number states of the oscillator with frequency Ω_σ. Opposed to WQOC, these dressed states are built in the strong coupling regime on a shorter time scale than the re-thermalization of the oscillator. In the evolution from thermal state of oscillator with frequency Ω to an equilibrium between the new oscillator with Ω_σ and the bath, the state in the narrower potential tends to absorb and the one in the wider potential to emit photons to the bath in an incoherent manner, causing fluctuations of $(\hat{a} + \hat{a}^\dagger)^2$ and thus qubit decoherence. Thus we expect $1/\tau_\phi \propto \kappa n(\Omega)$. This simple picture is confirmed by numerical results in Fig. 4.3, for a wide range of values of κ.

The inset of Fig. 4.3 shows the crossover from strong coupling rate κ to WQOC rate $1/\kappa$. This indicates that, for fixed Δ, as κ decreases, Δ stops being "small" and the WQOC limit breaks down. Thus, approaching $\kappa = 0$ for any given Δ we eventually leave the domain of validity for eq. (4.9) avoiding the divergence at $\kappa \to 0$. As expected, dephasing will vanish

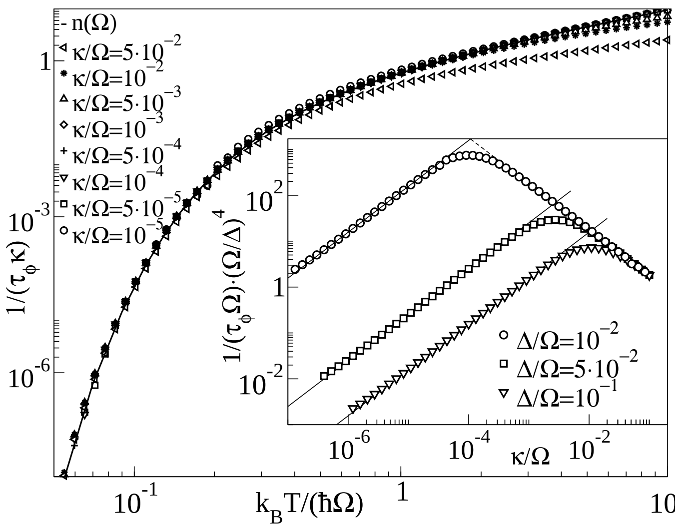

Figure 4.3: Scaling plot of the dephasing rate $1/\tau_\phi$ as function of temperature. For $\Delta/\Omega = 0.3$, i.e. in the strong coupling regime (see Fig. 4.2), for a wide range of κ's we show that $1/(\tau_\phi \kappa)$ is proportional to the Bose function $n(\Omega)$. Inset: dephasing rate $1/\tau_\phi$ as function of κ for different values of Δ and $\hbar\Omega/k_B T = 2$. Continuous lines correspond to $\kappa n(\Omega)$, dashed line corresponds to $n(\Omega)(n(\Omega)+1)\Delta^4/(\Omega^2\kappa)$.

as we go to a finite quantum system (qubit $\otimes$ single oscillator) at $\kappa = 0$. We observe that the criterion of "small" Δ in WQOC is valid only relative to κ. Using $1/\tau_\phi = \kappa n(\Omega)$ in the strong coupling regime and the $1/\kappa$ term of $1/\tau_\phi$ in Eq. (4.9) in the weak coupling regime, we determine the position of the crossover Δ_c between the two regimes

$$\frac{\Delta_c}{\Omega} = \sqrt{\frac{\kappa}{\Omega}} \frac{1}{(1+n(\Omega))^{1/4}} . \tag{4.10}$$

The position of the cross-over is controlled by the ratio of the coupling strengths between the three subsystems i.e. Δ^2/Ω and κ. Note that, with the in-situ tuning of the qubit-SQUID coupling, available in the Delft experiment, the position of the cross-over could be tested experimentally. Using the parameters from Ref. [107, 131] one finds $(\Delta/\Delta_c)_{\text{Yale}} \approx 1.4$ and $(\Delta/\Delta_c)_{\text{Delft}} \approx 1.3$ i.e., the strong coupling regime finds application in both setups .

If the oscillator is weakly driven off-resonance, as is the case in the dispersive measurement, the qualitative behavior remains the same as in Fig. 4.2, as shown in chapter 3. In general a tunneling $\hat{\sigma}_x$ term may occur in Eq. (4.2) and lead to energy relaxation as well as further reducing the matrix elements containing the dephasing rate. We expect that, as long as the energy splitting ϵ of the qubit is off-resonance with the oscillator, which in our case means $|\epsilon - \Omega| \gg \kappa$, the effect of the relaxation is rather weak and dephasing still dominates. On resonance, we expect a similar Purcell to strong coupling crossover as for the dephasing channel.

Our results have applications in other systems with similar dispersive qubit-oscillator coupling, e.g., the Yale setup [131], in the off-resonant dispersive regime. There, the system is described by a similar (Eq. (12) in Ref. [98]) quadratic coupling $\hat{a}^\dagger\hat{a}$ between qubit and cavity and a pure dephasing Hamiltonian. In particular, a strong dispersive regime of this system has been utilized to resolve number states of the electromagnetic field in Ref. [145]. The terms $\hat{a}^2$ and $\hat{a}^{\dagger 2}$ in Eq. (1) do not play a central role for our physical predictions, as confirmed by the numerical simulations. We expect our results, with minor adaptations, to be applicable to various cavity systems, e.g. quantum dot or atom-based quantum optical schemes [129, 130]. The dispersive coupling of Hamiltonian (4.2) could have implications for the generation of squeezed states, quantum memory in the frame of quantum information processing, measurement and post-selection of the number states of the cavity.

4.5 Conclusion

We have presented a concise theory of the dephasing of a qubit coupled to a dispersive detector spanning both strong and weak coupling. The phase-space method applied is based on treating the oscillator on the same level of accuracy as the qubit. We have discussed the dominating decoherence mechanism at weak qubit-oscillator coupling, where the linewidth of the damped oscillator plays the main role, analogous to the Purcell effect. At strong qubit-oscillator coupling we have identified a qualitatively different behavior of the qubit dephasing and discussed it in terms of the onset of the qubit-oscillator entanglement. We have provided a criterion delimitating the parameter range at which these processes dominate the qubit dephasing.

4.6 Additional information

Assuming the WQOC limit we use Fermi's Golden Rule in an otherwise exact manner to prove the analogy between the weak qubit-oscillartor coupling regime and the Purcell effect. One can map the damped oscillator by an exact normal mode transformation [114] onto an *effective* heat bath of *decoupled* oscillators denoted by $\hat{c}_j, \hat{c}_j^\dagger$ and with a spectral density

$$J_{\text{eff}}(\omega) = \frac{2\kappa\omega}{(\omega^2 - \Omega^2)^2 + \kappa^2\omega^2}. \tag{4.11}$$

J_{eff} corresponds to the effective density of electromagnetic modes in the cavity introduced in regular linear cavity QED for describing the Purcell effect. The WQOC decoherence rate is proportional to the two-point correlation function of the environmental operator coupling to the qubit [101, 149], in our case

$$\mathcal{K}_2(\omega) = \left\langle \hat{X}^2(t)\hat{X}^2(0) \right\rangle_\omega - \left(\langle \hat{X}^2 \rangle \right)^2, \tag{4.12}$$

where $\hat{X}$ is the sum of the *effective* bath coordinates $\hat{X} = \sum_j \sqrt{\hbar/(2m_j\omega_j)}(\hat{c}_j + \hat{c}_j^\dagger)$. For the pure dephasing situation described by the Hamiltonian (4.2) we only need to study $1/\tau_\phi \propto \mathcal{K}_2(\omega \to 0^+)$ because the qubit energy conservation implies energy conservation within its effective environment. The last term of Eq. (4.12) removes the noise bias. This is important since dephasing is caused only by processes that leave a trace in the bath [7], i.e. the exchanged boson spends a finite time in the environment. Terms of the structure $\left\langle \hat{c}_i^\dagger(t)\hat{c}_j^\dagger(t)\hat{c}_k\hat{c}_l \right\rangle$, $\left\langle \hat{c}_i(t)\hat{c}_j(t)\hat{c}_k^\dagger\hat{c}_l^\dagger \right\rangle$ contribute to $\mathcal{K}_2(0)$ only when $\omega_i = \omega_j = 0$, which are modes with density $J_{\text{eff}} \simeq 2\kappa\omega/\Omega^4$ each, leading to terms of order κ^2. Up to linear order in κ, the only terms in $\mathcal{K}_2(\omega \to 0^+)$ that fulfill the energy conservation and leave a trace in the bath are of the structure $\left\langle \hat{c}_l^\dagger(t)\hat{c}_j(t)\hat{c}_j^\dagger\hat{c}_l \right\rangle$, including the permutations among the operators taken at time t and those taken at time 0. The terms contributing to $\mathcal{K}_2(\omega \to 0^+)$ satisfy the condition $|\omega_l - \omega_j| \to 0^+$. Physically this corresponds to infinitesimal energy fluctuations which leave a trace in the bath. Or, in other words, the photon absorbed at t=0, $\hat{c}_l$, should spend finite time in the bath and be emitted back only at the later time t, but at the same time the energy change in the environment e.g. caused by $\hat{c}_j^\dagger\hat{c}_l$ should remain undetectable within the energy-time uncertainty at every time, therefore in the Golden Rule (long time) limit $\omega_l \approx \omega_j$. Taking the continuum limit we thus have

$$1/\tau_\phi \propto \int_0^\infty d\omega\; J_{\text{eff}}(\omega)(1+n(\omega))J_{\text{eff}}(\omega)n(\omega). \tag{4.13}$$

The integral in Eq. (4.13) can be rewritten as the convolution

$$\mathcal{K}(\omega') = \int d\omega J_{\text{eff}}(\omega)n(\omega)J_{\text{eff}}(\omega'-\omega)n(\omega'-\omega), \tag{4.14}$$

for $\omega' \to 0$. Using Eq. (4.11), $\mathcal{K}(\omega')$ becomes a function with resonances at $\omega' = 0$ and $\omega' = 2\Omega$, see Fig. 4.4. The the height of these resonances and consequently $1/\tau_\phi \propto \mathcal{K}_2(0)$ increases with decreasing κ, thus matching the behavior of the dephasing rate (4.9). At the same time, the tail of the peak at 2Ω enhances $\mathcal{K}_2(0)$ when κ increases. This corresponds to the κ term in Eq. (4.9). Analogous to $1/\tau_\phi$ in Eq. 4.9, $\mathcal{K}_2(\omega \to 0^+)$ vanishes for $T \to 0$.

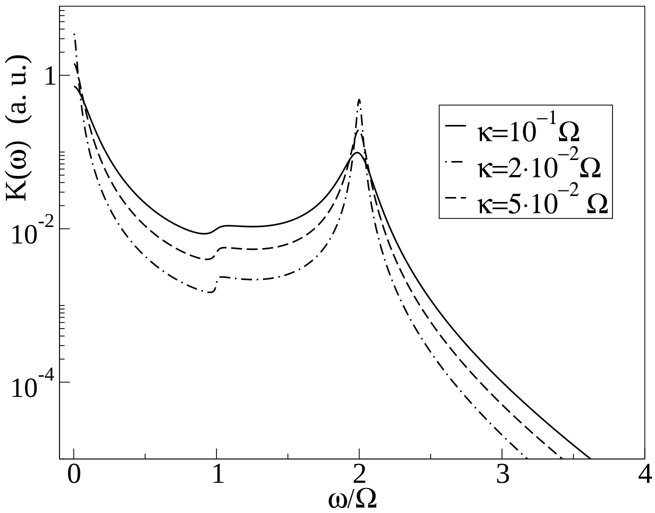

Figure 4.4: Illustrative plot of the function $\mathcal{K}(\omega)$ (in arbitrary units) for different values of κ

Chapter 5

Quantum nondemolition-like, fast measurement scheme for a superconducting qubit

I. Serban, B. L. T. Plourde and F. K. Wilhelm

We present a measurement protocol for a flux qubit coupled to a dc-Superconducting QUantum Interference Device (SQUID), representative of any two-state system with a controllable coupling to an harmonic oscillator quadrature, which consists of two steps. First, the qubit state is imprinted onto the SQUID via a very short and strong interaction. We show that at the end of this step the qubit dephases completely, although the perturbation of the measured qubit observable during this step is weak. In the second step, information about the qubit is extracted by measuring the SQUID. This step can have arbitrarily long duration, since it no longer induces qubit errors.

Parts of this chaper have been submitted to *Physical Review B* and are currently under review.

5.1 Introduction

The quantum measurement postulate is often viewed as the most intriguing assumption of quantum physics. Much of it has been demystified by the study of the physics of quantum measurements. The dynamics of the measurement process can be described by a coupled many-body Hamiltonian, consisting of the system to be measured and the detector with a heat bath component [4, 5]. Thus, the measurement process can be investigated using the established tools of quantum mechanics of open systems [19, 23, 101, 102].

Most interest has been focused on the physics of weak measurements, where the system-observer coupling can be treated within perturbation theory. Famously, this research has shown that only a certain class of measurements satisfy von Neumann's quantum measurement postulate [89, 90] and indeed project the system wavefunction onto an eigenstate of the measured observable. Measurements of this type are termed quantum nondemolition (QND) measurements. Within the weak measurement paradigm, the QND regime is achieved when the measured observable is a constant of the free motion and commutes with the system-detector coupling Hamiltonian. Weak QND measurements have been investigated in various systems, ranging spins, oscillators and even photons [150–158].

The dynamics of the weak measurement process has practical relevance in the context of quantum computing. Specifically, superconducting qubits have been proposed as building blocks of a scalable quantum computer [13, 86, 87], and a fast measurement with a high resolution and visibility is important for readout and also for error correction.

There are a variety of different measurement techniques used in superconducting qubits. Weak measurements can be performed using single-electron transistors [13]. A different approach is the switching measurement, where the detector switches out of a metastable state depending on the state of the qubit [53, 54, 76, 92, 93]. Such switching measurements have been a quite successful readout scheme for many superconducting qubit experiments to date. However, the dissipative nature of the switching process imposes limitations on the measurement speed and perturbs the qubit state.

A QND measurement could be achieved by using a pointer system, and measuring one of its observables influenced by the state of the qubit [95]. Recent developments of such detection schemes, using an oscillator as the pointer, have led to vast improvements [1, 71, 78, 82, 98, 99, 159] over previous measurement protocols.

It has previously been shown [123, 160–162] that infinitesimally short interaction between a qubit and an oscillator is sufficient to imprint information about the state of the oscillator onto the qubit. The similar idea of using a short interaction to transfer information about the qubit into the oscillator has been used, see chapter 3, in a dispersive readout scheme. In this case, after a short interaction, the state of the oscillator contains information about the qubit which can be extracted by further measuring one of its observables, for example, momentum. However, this scheme did not take possible bit flip errors into account. These errors may occur in the short yet finite time when the qubit is in contact with its environment. Thus, the full power of a quasi-instantaneous measurement has not yet been explored. Furthermore, if the aim is to apply the idea of this type of measurement, dispersive measurement, with all its potential advantages, may add unnecessary overhead.

In this paper we describe the effect of an ideally extremely short and arbitrarily strong interaction of a qubit with its environment (consisting of a weakly damped harmonic oscillator). We investigate the back-action on the qubit when the measured observable does not commute with the Hamiltonian describing the interaction with the environment, and study how close this result approximates the QND measurement.

We study a setup consisting of a flux qubit inductively coupled to a dc-SQUID magnetometer. The flux qubit consists of a superconducting loop with three Josephson junctions [75, 163]. For flux bias near odd half-integer multiple of $h/2e$, the qubit is represented by two circulating current states with opposite directions. During the entire measurement process the SQUID is coupled to measurement circuitry, with associated dissipative elements. However, during the entire measurement process, the SQUID never switches out of the zero dc-voltage state. The qubit-SQUID interaction of arbitrary strength is turned on only for a short time by applying a very short bias current pulse to the SQUID. During this time, information about the qubit is imprinted onto the SQUID. This information can later be extracted from the SQUID during the post-interaction phase by monitoring voltage oscillations across the SQUID. When the current pulse is switched off, the qubit-SQUID interaction ideally vanishes and the environment no longer perturbs the qubit. Thus, one can afford a long time to measure the SQUID and determine the state of the qubit.

In section 5.2, following Ref. [164], we model the qubit-SQUID system by a two-level system linearly coupled to a dissipative oscillator. We describe the evolution of this system by means of a master equation in the Born-Markov approximation [115], valid for the underdamped SQUID. In section 5.3 we discuss the qubit-oscillator evolution during both interaction and post-interaction phases. We study the qubit dephasing and relaxation during the interaction phase. We show that, at the end of this phase, the qubit appears completely dephased. In other words, the qubit has been measured and its information has been transferred in the form of a classical probability to the oscillator. During the same time interval, we find that qubit relaxation has remained negligible. For the post-interaction phase we describe the evolution of the oscillator under the influence of the environment, starting from the state prepared by the interaction with the qubit. Technically, extracting the qubit information amounts to measuring the amplitude of the ringdown of the oscillator momentum. In section 5.4 we discuss some of the details involved with implementing this measurement scheme.

5.2 Model and method

We study a flux qubit inductively coupled to a dc-SQUID, with one possible setup shown schematically in Fig. 5.1 (a). We describe a more realistic setup for implementing this scheme in section 5.4. The SQUID is characterized by a two-dimensional washboard potential for the two independent phases corresponding to the two junctions [165]. Their sum couples to bias current driven through the SQUID, while the difference of phases couples to the magnetic flux applied to the SQUID. The small oscillations in these two directions can have vastly different characteristic frequencies. In particular, a small geometric in-

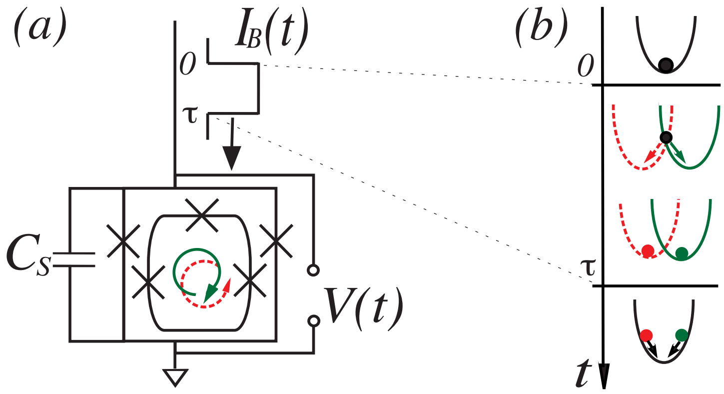

Figure 5.1: (a) Simplified circuit consisting of a flux qubit inductively coupled to a SQUID with two identical junctions and shunt capacitance C_S. The SQUID is driven by an bias step-like dc pulse $I_B(t)$ and the voltage drop $V(t)$ is measured by a device with internal resistance R. (b) Illustration of the measurement scheme: coupling ($t = 0$) and decoupling ($t = \tau$) of the qubit and the SQUID (oscillator) and the evolution of a point of mass in the transition of potential from one harmonic oscillator to a superposition of two displaced oscillators and back. The dashed (red) and the continuous (green) lines correspond to the different states of the qubit.

ductance and a low critical current can make the flux mode frequency large while a shunt capacitor can lower the bias current mode frequency substantially. In the limit of very different frequencies, as described in chapter 3, one can approximate the SQUID dynamics as that of a one-dimensional oscillator in the bias current direction, with the position of the oscillator minimum dependent on both I_B and the total flux coupled to the SQUID which, for example, could vary depending on the state of the qubit. The setup of Fig. 5.1 (a) can be described by the effective Hamiltonian [164]

$$\begin{aligned} \hat{H} &= \hat{H}_S + \hat{H}_I + \hat{H}_B, \qquad (5.1) \\ \hat{H}_S &= \hbar w \hat{\sigma}_z + \hbar\delta\hat{\sigma}_x + \hbar\Omega\left(\hat{a}^\dagger\hat{a} + \frac{1}{2}\right) + \hbar(\Theta(t) - \Theta(t-\tau))(\hat{a} + \hat{a}^\dagger)(\hat{\sigma}_z\gamma + K), \end{aligned}$$

where $\hat{H}_S$ is the Hamiltonian for the qubit-SQUID oscillator system, $\hat{H}_B$ is the Hamiltonian for the dissipative environment of the measurement circuitry, $\hat{H}_I$ describes the interaction between the SQUID oscillator and the environment, and Θ is the Heaviside step function.

We note that for a continuous shape of the current pulse similar results are expected, as long as the switching is not adiabatic. Here the SQUID is described, in the lowest-order approximation, by a harmonic oscillator with frequency Ω, i.e. the plasma frequency of the bias current degree of freedom. This frequency also depends on the applied bias current, as shown in section 5.6.2. This dependence leads to a slightly enhanced ring-down frequency after the pulse is switched off. Nevertheless, for simplicity, we assume this frequency to remain constant throughout the entire process. This is justified by the fact that this change in frequency does not, in the first approximation, depend on the qubit state, therefore it will not qualitatively affect this method of discrimination. The dispersive, next-to-leading order component of the qubit-oscillator coupling discussed in chapter 3 becomes significant in the absence of a linear component, for very weak bias pulse, which is *not* the limit we investigate here. In the following, the effects of the linear component are investigated in the regime where the qubit-SQUID interaction displaces the oscillator state by more than its zero-point fluctuation but does not yet explore the classical nonlinearity. The first consequence of the nonlinear component may be to add more phase shift to the ringdown oscillations. In the measurement protocol proposed here we assume a symmetric SQUID.

The qubit-oscillator coupling strength γ is tuned by the bias current I_B [167]. When $I_B = 0$, the qubit and the SQUID are decoupled. By using a fast current pulse, the qubit-oscillator interaction of arbitrary strength γ is turned on only for the short time τ allowing information about the qubit to be imprinted onto the oscillator. During this time, the SQUID oscillator is displaced according to the qubit state. After the coupling is switched off, the SQUID oscillator phase particle returns to the original position after undergoing ring-down oscillations that decay with a damping determined by the SQUID measurement circuitry. The parameter K describes the strength of the the bias current kick induced in the oscillator, caused by the abrupt shift in the minimum of the SQUID potential energy from the bias current pulse, in the absence of a qubit.

During the entire measurement process the oscillator is coupled via a linear Hamiltonian $\hat{H}_I$ to a dissipative environment described by a bath of harmonic oscillators described by $\hat{H}_B$

$$\hat{H}_I = \sum_i \frac{\hbar\lambda_i(\hat{a}\hat{b}_i^\dagger + \hat{a}^\dagger\hat{b}_i)}{\sqrt{2m\Omega}}, \quad \hat{H}_B = \sum_i \hbar\omega_i \left(\hat{b}_i^\dagger\hat{b}_i + \frac{1}{2}\right), \tag{5.2}$$

with Ohmic spectral density $J(\omega) = \sum_i \lambda_i^2 \hbar\delta(\omega - \omega_i) = m\hbar\kappa\omega\Theta(\omega - \omega_c)/\pi$ [16]. Here $[\kappa] = s^{-1}$ is the photon loss rate. The cut-off frequency ω_c is physically motivated by the high-frequency filter introduced by the capacitors. This environment represents the dissipative element contained in any measuring device.

We now describe the dynamics of the qubit and SQUID oscillator during the various phases of our measurement scheme.

5.2.1 The interaction phase

At $t = 0$, before the bias current is rapidly pulsed on and the qubit and SQUID interact strongly, we assume the factorized initial state $\hat{\rho}(0) = \hat{\rho}_S(0) \otimes \hat{\rho}_B(0)$. The oscillator interaction with the bath is supposed to be weak, and assuming a Markovian environment, we obtain the standard master equation for the qubit-oscillator reduced density matrix $\hat{\rho}_S(t) = \mathrm{Tr}_B\{\hat{\rho}(t)\}$ in the Born approximation

$$\dot{\hat{\rho}}_S(t) = \frac{1}{\mathrm{i}\hbar}\left[\hat{H}_S, \hat{\rho}_S(t)\right] - \frac{1}{\hbar^2}\int_0^t dt' \mathrm{Tr}_B\left[\hat{H}_I, \left[\hat{H}_I(t, t-t'), \hat{\rho}_S(t) \otimes \hat{\rho}_B(0)\right]\right], \tag{5.3}$$

where

$$\hat{H}_I(t,t') = \hat{U}^t_{t'}\hat{H}_I\hat{U}^{t'}_t, \;\; \hat{U}^{t'}_t = \mathcal{T}\exp\left(\int_t^{t'} d\tau \frac{\hat{H}_S + \hat{H}_B}{\mathbb{i}\hbar}\right), \tag{5.4}$$

and $\mathcal{T}$ is the time-ordering operator.

This approach is valid at finite temperatures $k_B T \gg \hbar\kappa$ and times $t \gg 1/\omega_c$ [101, 116], which is the limit we will discuss henceforth.

In the qubit $\hat{\sigma}_z$ eigen-basis the density matrix and the qubit-oscillator Hamiltonian read

$$\hat{\rho}_S = \begin{pmatrix} \hat{\rho}_{\uparrow\uparrow} & \hat{\rho}_{\uparrow\downarrow} \\ \hat{\rho}_{\downarrow\uparrow} & \hat{\rho}_{\downarrow\downarrow} \end{pmatrix}, \tag{5.5}$$

$$\hat{H}_{S\downarrow\uparrow} = \hat{H}_{S\uparrow\downarrow} = \hbar\delta, \quad r_\sigma = \langle\sigma|\hat{\sigma}_z|\sigma\rangle, \;\; \sigma \in \{\uparrow,\downarrow\}, \tag{5.6}$$

$$\hat{H}_{S\sigma\sigma} = \hbar(r_\sigma w + \Omega(\hat{a}^\dagger\hat{a} + 1/2) + (r_\sigma\gamma + K)(\hat{a} + \hat{a}^\dagger)). \tag{5.7}$$

In the following, we assume that the environment acts on each matrix element of (5.5) in the same way. This is a valid assumption in the case of very weak damping and $\delta/w \ll 1$ for an Ohmic bath. Within this assumption we obtain

$$\begin{aligned}
\dot{\hat{\rho}}_{\sigma\sigma} &= \frac{1}{\mathbb{i}\hbar}[\hat{H}_{\sigma\sigma}, \hat{\rho}_{\sigma\sigma}] - \mathbb{i}\delta r_\sigma(\hat{\rho}_{\downarrow\uparrow} - \hat{\rho}_{\uparrow\downarrow}) + \hat{\mathcal{L}}\hat{\rho}_{\sigma\sigma}, \\
\dot{\hat{\rho}}_{\uparrow\downarrow} &= \frac{1}{\mathbb{i}\hbar}(\hat{H}_{\uparrow\uparrow}\hat{\rho}_{\uparrow\downarrow} - \hat{\rho}_{\uparrow\downarrow}\hat{H}_{\downarrow\downarrow}) + \mathbb{i}\delta(\hat{\rho}_{\uparrow\uparrow} - \hat{\rho}_{\downarrow\downarrow}) + \hat{\mathcal{L}}\hat{\rho}_{\uparrow\uparrow} \\
\dot{\hat{\rho}}_{\downarrow\uparrow} &= \frac{1}{\mathbb{i}\hbar}(\hat{H}_{\downarrow\downarrow}\hat{\rho}_{\downarrow\uparrow} - \hat{\rho}_{\downarrow\uparrow}\hat{H}_{\uparrow\uparrow}) - \mathbb{i}\delta(\hat{\rho}_{\uparrow\uparrow} - \hat{\rho}_{\downarrow\downarrow}) + \hat{\mathcal{L}}\hat{\rho}_{\downarrow\uparrow},
\end{aligned} \tag{5.8}$$

where

$$\hat{\mathcal{L}}\hat{\rho}_{\sigma\sigma'} = -\kappa(\hat{a}^\dagger\hat{a}\hat{\rho}_{\sigma\sigma'} + \hat{\rho}_{\sigma\sigma'}\hat{a}^\dagger\hat{a} - 2\hat{a}\hat{\rho}_{\sigma\sigma'}\hat{a}^\dagger) - 2\kappa n(\hat{a}^\dagger\hat{a}\hat{\rho}_{\sigma\sigma'} + \hat{\rho}_{\sigma\sigma'}\hat{a}\hat{a}^\dagger - \hat{a}\hat{\rho}_{\sigma\sigma'}\hat{a}^\dagger - \hat{a}^\dagger\hat{\rho}_{\sigma\sigma'}\hat{a}). \tag{5.9}$$

At $t = 0$ we assume a factorized initial state for the qubit-oscillator reduced density matrix

$$\hat{\rho}_S(0) = \hat{\rho}_{\mathrm{q}}(0) \otimes \hat{\rho}_{\mathrm{HO}}(0), \tag{5.10}$$

and use the Wigner representation of the oscillator density matrix in phase-space [27]

$$\hat{\rho}_{\mathrm{HO}}(0) = \frac{1}{\pi}\int d^2\alpha\, \chi_0(\alpha)\hat{D}(-\alpha), \;\; \hat{D}(-\alpha) = \exp\left(-\alpha\hat{a}^\dagger + \alpha^*\hat{a}\right), \tag{5.11}$$

where χ_0 is the Fourier transform of the Wigner function. We assume the oscillator to be initially in a thermal state

$$\chi_0(\alpha) = \frac{1}{4\pi}\exp\left(-\frac{\eta}{2}|\alpha|^2\right), \;\; \eta = 1 + 2n(\Omega), \tag{5.12}$$

where $n(\Omega)$ is the Bose function at bath temperature T. The qubit is assumed to be initially in the pure state $|\Psi\rangle = q_\uparrow|\uparrow\rangle + q_\downarrow \mathbb{e}^{\mathbb{i}\phi}|\downarrow\rangle$ such that

$$\hat{\rho}_{\mathrm{q}}(0) = \begin{pmatrix} q_\uparrow^2 & q_\uparrow q_\downarrow \mathbb{e}^{-\mathbb{i}\phi} \\ q_\uparrow q_\downarrow \mathbb{e}^{\mathbb{i}\phi} & q_\downarrow^2 \end{pmatrix}. \tag{5.13}$$

For the corresponding Wigner characteristic functions we obtain the following coupled partial differential equations

$$\begin{aligned}
\dot{\chi}_{\sigma\sigma} &= (\mathbb{i}(r_\sigma\gamma + K)(\alpha + \alpha^*) + \mathbb{i}\Omega(\alpha\partial_\alpha - \alpha^*\partial_{\alpha^*}) + \mathcal{D})\chi_{\sigma\sigma} - r_\sigma \mathbb{i}\delta(\chi_{\downarrow\uparrow} - \chi_{\uparrow\downarrow})), \qquad (5.14)\\
\dot{\chi}_{\uparrow\downarrow} &= (2\mathbb{i}\gamma(\partial_{\alpha^*} - \partial_\alpha) + \mathbb{i}\Omega(\alpha\partial_\alpha - \alpha^*\partial_{\alpha^*}) - 2\mathbb{i}w + \mathbb{i}K(\alpha + \alpha^*) + \mathcal{D})\chi_{\uparrow\downarrow} - \mathbb{i}\delta(\chi_{\downarrow\downarrow} - \chi_{\uparrow\uparrow})),\\
\dot{\chi}_{\downarrow\uparrow} &= (-2\mathbb{i}\gamma(\partial_{\alpha^*} - \partial_\alpha) + \mathbb{i}\Omega(\alpha\partial_\alpha - \alpha^*\partial_{\alpha^*}) + 2\mathbb{i}w + \mathbb{i}K(\alpha + \alpha^*) + \mathcal{D})\chi_{\downarrow\uparrow} + \mathbb{i}\delta(\chi_{\downarrow\downarrow} - \chi_{\uparrow\uparrow})),
\end{aligned}$$

where the differential operator $\mathcal{D}$ is given by

$$\mathcal{D} = -\kappa(\alpha\partial_\alpha + \alpha^*\partial_{\alpha^*}) - \eta\kappa|\alpha|^2. \qquad (5.15)$$

To solve these equations, we approximate the inhomogeneous parts, in the limit of short time τ and weak tunneling δ, by

$$\chi_{\sigma\sigma'}(\alpha, t) \simeq \chi_{\sigma\sigma'}(\alpha, 0) + t\dot{\chi}_{\sigma\sigma'}(\alpha, 0), \quad \sigma, \sigma' \in \{\uparrow, \downarrow\}. \qquad (5.16)$$

For details on the solution see section 5.6.1.

5.2.2 The post-interaction phase

The state prepared by the interaction with the qubit at $t = \tau$, as the bias current pulse ends, is described by

$$\hat{\rho}(\tau) = \sum_{\sigma,\sigma' \in \{\uparrow,\downarrow\}} |\sigma\rangle\langle\sigma'|\hat{\rho}_{\sigma\sigma'}(\tau) \otimes \hat{\rho}_B(0). \qquad (5.17)$$

Since the system Hamiltonian no longer contains any qubit-oscillator interaction, we can write the time evolution of this density matrix as follows

$$\hat{\rho}(t) = \sum_{\sigma,\sigma' \in \{\uparrow,\downarrow\}} \hat{U}_{\mathrm{q}}(t)|\sigma\rangle\langle\sigma'|\hat{U}_{\mathrm{q}}^\dagger(t)\hat{U}_{\mathrm{HO}-B}(t)\hat{\rho}_{\sigma\sigma'}(\tau) \otimes \hat{\rho}_B(0)\hat{U}_{\mathrm{HO}-B}^\dagger(t), \qquad (5.18)$$

where the evolution operators are given by

$$\begin{aligned}
\hat{U}_{\mathrm{q}}(t) &= \exp(-\mathbb{i}(t-\tau)(\delta\hat{\sigma}_x + w\hat{\sigma}_z)), \qquad (5.19)\\
\hat{U}_{\mathrm{HO}-B} &= \mathcal{T}\exp\left(\int_\tau^t dt' \, \frac{\hat{H}_B + \hat{H}_I + \hbar\Omega\hat{a}^\dagger\hat{a})}{\mathbb{i}\hbar}\right). \qquad (5.20)
\end{aligned}$$

In the reduced density matrix

$$\hat{\rho}_S(t) = \mathrm{Tr}_B\hat{\rho}(t) = \sum_{\sigma,\sigma' \in \{\uparrow,\downarrow\}} \hat{U}_{\mathrm{q}}(t)|\sigma\rangle\langle\sigma'|\hat{U}_{\mathrm{q}}^\dagger(t)\mathrm{Tr}_B\left\{\hat{U}_{\mathrm{HO}-B}(t)\hat{\rho}_{\sigma\sigma'}(\tau) \otimes \hat{\rho}_B(0)\hat{U}_{\mathrm{HO}-B}^\dagger(t)\right\}, \qquad (5.21)$$

we can treat the time evolution of the oscillator components by means of a master equation in the Born-Markov approximation and, in a similar manner to Eq. (5.3), we obtain

$$\dot{\hat{\rho}}_{\sigma\sigma'}(t) = -\mathbb{i}\Omega[\hat{a}^\dagger\hat{a}, \hat{\rho}_{\sigma\sigma'}(t)] - \frac{1}{\hbar^2}\int_0^\infty dt' \mathrm{Tr}_B\left[\hat{H}_I, [\hat{H}_I(t, t-t'), \hat{\rho}_{\sigma\sigma'}(t) \otimes \hat{\rho}_B(0)]\right]. \qquad (5.22)$$

Using the Wigner representation

$$\hat{\rho}_{\sigma\sigma'}(t) = \frac{1}{\pi}\int d^2\alpha\, \tilde{\chi}_{\sigma\sigma'}(\alpha,t)\hat{D}(-\alpha), \tag{5.23}$$

we obtain the differential equation

$$\dot{\tilde{\chi}}_{\sigma\sigma'}(\alpha,t) = (\mathrm{i}\Omega(\alpha\partial_\alpha - \alpha^*\partial_{\alpha^*}) + \mathcal{D})\tilde{\chi}_{\sigma\sigma'}(\alpha,t), \tag{5.24}$$

with the initial condition prepared at the end of the interaction phase

$$\tilde{\chi}_{\sigma\sigma'}(\alpha,\tau) = \chi_{\sigma\sigma'}(\alpha,\tau), \tag{5.25}$$

and the analytic solution

$$\tilde{\chi}_{\sigma\sigma'}(\alpha,t) = \tilde{\chi}_{\sigma\sigma'}(\alpha \mathrm{e}^{-(t-\tau)(\kappa-\mathrm{i}\Omega)},\tau)\exp\left(\frac{\eta}{2}|\alpha|^2(\mathrm{e}^{-2(t-\tau)\kappa}-1)\right). \tag{5.26}$$

The reduced density matrix in the post-interaction phase is given by

$$\hat{\rho}_S(t) = \sum_{s,s'\in\{\uparrow,\downarrow\}} |s\rangle\langle s'|\frac{1}{\pi}\int d^2\alpha\chi_{ss'}(\alpha,t)\hat{D}(-\alpha), \tag{5.27}$$

where

$$\chi_{ss'}(\alpha,t) = \sum_{\sigma,\sigma'\in\{\uparrow,\downarrow\}}\langle s|\hat{U}_{\mathrm{q}}(t)|\sigma\rangle\langle\sigma'|\hat{U}_{\mathrm{q}}^\dagger(t)|s'\rangle\tilde{\chi}_{\sigma\sigma'}(\alpha,t). \tag{5.28}$$

5.3 Results

In this section we analyze the qubit decoherence and the evolution of its detector, the dissipative oscillator, during the entire measurement process.

5.3.1 Qubit decoherence

During the interaction phase, $t \in (0,\tau)$, the qubit is in contact with an environment represented by the dissipative oscillator, and thus subject to decoherence.

The qubit can be prepared in a well defined state by thermal relaxation or (if the temperature is too high) by measurement post-selection, and rotated by microwave pulses. We analyze the qubit relaxation described by

$$\langle\hat{\sigma}_z\rangle(t) = 4\pi(\chi_{\uparrow\uparrow}(0,t) - \chi_{\downarrow\downarrow}(0,t)), \tag{5.29}$$

and from Eq. (5.44) we obtain the analytic result

$$\langle\hat{\sigma}_z\rangle(t) = (q_\uparrow^2 - q_\downarrow^2)(1-2t^2\delta^2) + 4q_\uparrow q_\downarrow t\delta(tw\cos(\phi)+\sin(\phi)).$$

We observe that the above expression is identical with the expansion up to the second order in time of $\langle\hat{\sigma}_z\rangle(t)$ when the qubit evolves under the free Hamiltonian $\hat{H}_{\mathrm{q}}$ only. Thus, the evolution of $\langle\hat{\sigma}_z\rangle(t)$ in this short time expansion is indistinguishable from the free evolution of the unperturbed qubit. This can be understood as follows. The observable $\hat{\sigma}_z$ commutes with the environment coupling, but is not an integral of the free motion, as required for a QND measurement [5]. Thus, the perturbation of the measured observable comes only from the free evolution of the system. One can restrict this perturbation by reducing the time τ when it takes place. Fig. 5.2 (a) shows the evolution of $\langle\hat{\sigma}_z\rangle(t)$ for a set of parameters closely related to a feasible experiment, see also section 5.6.2. The initial state chosen for panel (a) was $|\uparrow\rangle$.

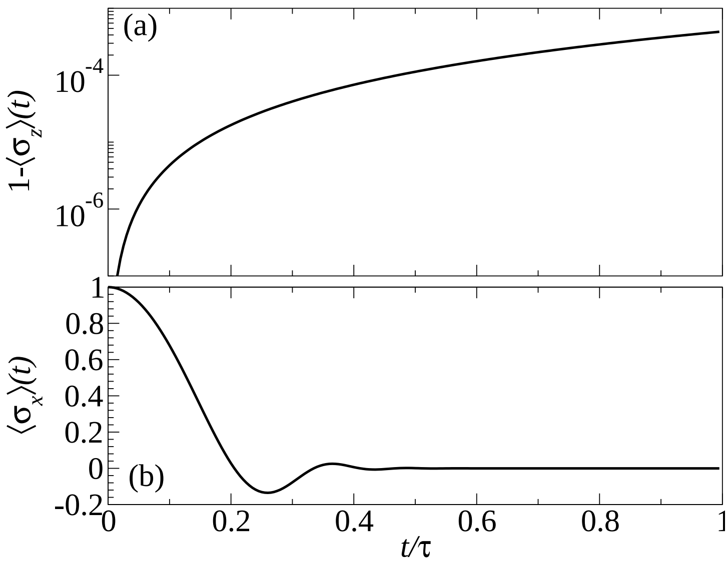

Figure 5.2: (a) Evolution of $\langle\hat{\sigma}_z\rangle$ with qubit initially in $|\uparrow\rangle$ state. (b) Dephasing from the $1/\sqrt{2}(|\uparrow\rangle+|\downarrow\rangle)$ state for the time τ that the qubit is in contact with the oscillator. For both plots, the following parameters were used: $\Omega/(2\pi) = 0.97$ GHz, $\kappa/\Omega = 10^{-2}$, $w = \Omega$, $\Omega\tau = 1.83$, $\delta\tau = 0.015$, $\gamma\tau = 3$, $T = 30$ mK. The values of the circuit parameters are given in section 5.6.2.

Furthermore, we analyze the qubit coherence $\langle\hat{\sigma}_x\rangle$ which is given by

$$\langle\hat{\sigma}_x\rangle(t) = 8\pi\mathrm{Re}\chi_{\uparrow\downarrow}(0,t), \tag{5.30}$$

and can be evaluated from Eqs. (5.53,5.54), where $\chi^{\mathrm{inh}}_{\uparrow\downarrow}(0,t)$ can be integrated numerically.

We observe that, if the interaction time τ is long enough to allow the oscillator a full period evolution, one finds a revival in the qubit coherence at the end of this period. As the oscillator returns to (almost) its initial state, the information about the qubit is "erased" from the oscillator, as the oscillator states corresponding to $|\uparrow\rangle$ and $|\downarrow\rangle$ are no longer discernible. The height of the coherence revival peaks at $\Omega t = 2\pi n$ decays in time as the information about the coupled qubit-oscillator system flows (irreversibly in this case) into the environment.

The qubit dephasing for the same parameters of section 5.6.2 is shown in Fig. 5.2 (b). The appropriate initial state for this study is the equal superposition $(1/\sqrt{2})(|\uparrow\rangle + |\downarrow\rangle)$. We observe that the qubit appears completely dephased after the strong interaction with the damped oscillator, such that only a classical probability is imprinted onto the latter.

In Fig. 5.2 (a) we observe that the relaxation from the excited qubit state is very weak during the interaction time. This combination of low coherence (b), indicating the fact that the information about the qubit has been imprinted onto the oscillator, and very low relaxation (a) demonstrates that the first step of the measurement protocol produces a good starting point for the second one, the oscillator readout. The negligible relaxation brings the qubit close to QND dynamics.

We observe that the qubit coherence time is essentially dominated by the coupling between the qubit and its complex environment γ^{-1} such that it is desirable to achieve $\gamma\tau \gg 1$. The relaxation of the qubit has been described in the first order in time, and essential to the almost-QND result is that $\tau\delta \ll 1$. We note that the implied condition $\gamma \ll \delta$ contradicts none of our approximations, and can also be realized in experiment.

5.3.2 Detector dynamics

In this section we study the evolution of the damped oscillator, which represents the detector. To achieve the strong qubit-oscillator coupling during the short interaction phase required to imprint the qubit state onto the oscillator, one needs a bias current pulse that approaches the critical current for the SQUID. Nonetheless, it is important that the SQUID does not switch out to the running state during the bias current pulse. For the parameters given in section 5.6.2, we can evaluate the SQUID escape rate [94] from the zero-voltage state during the bias current pulse in the regime of quantum assisted thermal activation ($k_B T \gtrsim \hbar\Omega$)

$$\Gamma_{\mathrm{sw}} = \frac{\sinh\left(\frac{\hbar\Omega}{2k_BT}\right)}{\sin\left(\frac{\hbar\Omega}{2k_BT}\right)}\frac{\Omega}{2\pi}\exp\left(\frac{-\Delta U}{k_BT}\right), \tag{5.31}$$

where ΔU is the potential barrier. We obtain, for the worst case, $\Gamma_{\mathrm{sw}} \approx 3.6 \cdot 10^7 s^{-1}$ such that the escape time is much larger than the duration of the bias current pulse.

The output of the detector is the time dependent voltage across the SQUID, which is proportional to the momentum of the oscillator. The probability distribution of momentum is given by

$$P(p,\tau,t) = \mu\langle\delta(\hat{p}-p)\rangle = 2\int d\alpha_x \sum_{\sigma\in\{\uparrow,\downarrow\}} \chi_{\sigma\sigma}(\alpha_x,t)\exp\left(\frac{\mathbb{i}p\alpha_x}{\mu}\right), \tag{5.32}$$

$$\mu = \sqrt{\frac{m\Omega\hbar}{2}},\ \ \alpha = \alpha_x + \mathbb{i}\alpha_y, \tag{5.33}$$

where, in the post-interaction phase ($t > \tau$), $\chi_{\sigma\sigma}(\alpha_x,t)$ also depends on τ via its initial condition. The expectation values for the nth moment of the oscillator momentum and position are then

$$\langle\hat{p}^n\rangle(t) = \frac{4\pi\mu^n}{\mathbb{i}^n}(-1)^n(\partial_{\alpha_x})^n\sum_{\sigma\in\{\uparrow,\downarrow\}}\chi_{\sigma\sigma}(\alpha_x,t)|_{\alpha_x=0}, \tag{5.34}$$

$$\langle\hat{x}^n\rangle(t) = \left(\sqrt{\frac{\hbar}{2m\Omega}}\right)^n\frac{4\pi}{\mathbb{i}^n}(\partial_{\alpha_y})^n\sum_{\sigma\in\{\uparrow,\downarrow\}}\chi_{\sigma\sigma}(\mathbb{i}\alpha_y,t)|_{\alpha_y=0}.$$

Furthermore, in the post-interaction phase we have, from Eq. (5.28),

$$\sum_{\sigma\in\{\uparrow,\downarrow\}} \chi_{\sigma\sigma} = \sum_{s,s',\sigma\in\{\uparrow,\downarrow\}} \langle\sigma|\hat{U}_{\rm q}(t)|s\rangle\langle s'|\hat{U}^{\dagger}_{\rm q}(t)|\sigma\rangle\tilde{\chi}_{ss'} = \sum_{s,s'}\langle s'|\hat{U}^{\dagger}_{\rm q}(t)\hat{U}_{\rm q}(t)|s\rangle\tilde{\chi}_{ss'} = \sum_{s}\tilde{\chi}_{ss}, \tag{5.35}$$

which shows, as expected, that no measurement of the oscillator can provide information about the post-interaction evolution of the qubit, provided this evolution is unitary (i. e. the qubit is not being measured by something else).

For the evaluation of both Eqs. (5.32, 5.34) the s-integration in $\chi^{\rm inh}_{\sigma\sigma}$, Eq. (5.46) should be evaluated last. Thus, one obtains an analytic (but rather long) expression for the expectation value of momentum, while for the probability density a numerical s-integration is required. Nevertheless, the components originating in $\chi^{\rm hom}_{\sigma\sigma}$ turn out to be dominant, and we give their analytic expressions in the following

$$\langle\hat{p}\rangle(\tau,t) = \langle\hat{p}\rangle_{\rm hom}(\tau,t) + \langle\hat{p}\rangle_{\rm inh}(\tau,t), \tag{5.36}$$

$$\langle\hat{p}\rangle_{\rm hom} = \left(K+\gamma q_{\uparrow}^2-\gamma q_{\downarrow}^2\right)\mu\mathbb{e}^{-(t-\tau)\kappa}\left(\mathbb{e}^{-(t-\tau)\mathbb{i}\Omega}\frac{1-\mathbb{e}^{-\tau(\kappa+\mathbb{i}\Omega)}}{-\kappa-\mathbb{i}\Omega}+\mathbb{e}^{(t-\tau)\mathbb{i}\Omega}\frac{1-\mathbb{e}^{-\tau(\kappa-\mathbb{i}\Omega)}}{-\kappa+\mathbb{i}\Omega}\right),$$

The explicit form of the probability distribution of momentum, Eq.(5.32), is given by

$$P(p,\tau,t) = P_{\rm hom}(p,\tau,t)+P_{\rm inh}(p,\tau,t), \tag{5.37}$$

where

$$P_{\rm hom}(p,\tau,t) = \sum_{\sigma}\frac{|\langle\sigma|\Psi\rangle|^2}{\sqrt{2\pi\eta}}\exp\left(\frac{\mathbb{i}p}{\sqrt{2\eta}\mu}-\mathbb{i}\frac{K+r_{\sigma}\gamma}{\sqrt{2\eta}}\mathbb{e}^{(\tau-t)\kappa}\right.$$
$$\left.\cdot\left(\mathbb{e}^{-(t-\tau)\mathbb{i}\Omega}\frac{1-\mathbb{e}^{-\tau(\kappa+\mathbb{i}\Omega)}}{-\kappa-\mathbb{i}\Omega}+\mathbb{e}^{(t-\tau)\mathbb{i}\Omega}\frac{1-\mathbb{e}^{-\tau(\kappa-\mathbb{i}\Omega)}}{-\kappa+\mathbb{i}\Omega}\right)\right)^2.$$

The results above refer to the post-interaction phase $t>\tau$. For the interaction phase, $t\in(0,\tau)$, the probability distribution of momentum is given by $P(p,t,t)$ in Eq. (5.37) and the expectation value of momentum by $\langle\hat{p}\rangle(t,t)$ in Eq. (5.36), i. e. by replacing τ by t.

The expectation value of momentum $\langle\hat{p}\rangle(\tau,t)$ in the post-interaction phase contains information about the qubit initial state. We observe that the momentum oscillations corresponding to the two different initial qubit states $|\uparrow\rangle$ and $\downarrow\rangle$ for $t>\tau$ are in phase. Disregarding the inhomogeneous contributions, which are relatively small in the limit of small $\tau\delta$, the envelope of the homogeneous part is given by

$$\mathcal{A}(q_{\uparrow},q_{\downarrow}) = \frac{2\mathbb{e}^{-(t-\tau)\kappa}(K+\gamma q_{\uparrow}^2-\gamma q_{\downarrow}^2)\mu}{\sqrt{\kappa^2+\Omega^2}}\sqrt{-2\mathbb{e}^{-\kappa\tau}\cos(\tau\Omega)+\mathbb{e}^{-2\kappa\tau}+1}. \tag{5.38}$$

Fig. 5.3 illustrates the phase-space trajectories of the oscillator corresponding to the qubit being in either the $|\uparrow\rangle$ or $|\downarrow\rangle$ state. During the interaction phase the system moves away from the origin. After switching off the interaction, the trajectories spiral back towards the origin, without crossing. For $K = 0$ the trajectories are symmetric with respect to the origin, while $K \neq 0$ introduces an asymmetry. We note that the artificial situation $K = 0$ includes only the bare oscillator response for the different qubit states. This situation has been introduced in order to more easily illustrate the difference between the two oscillations.

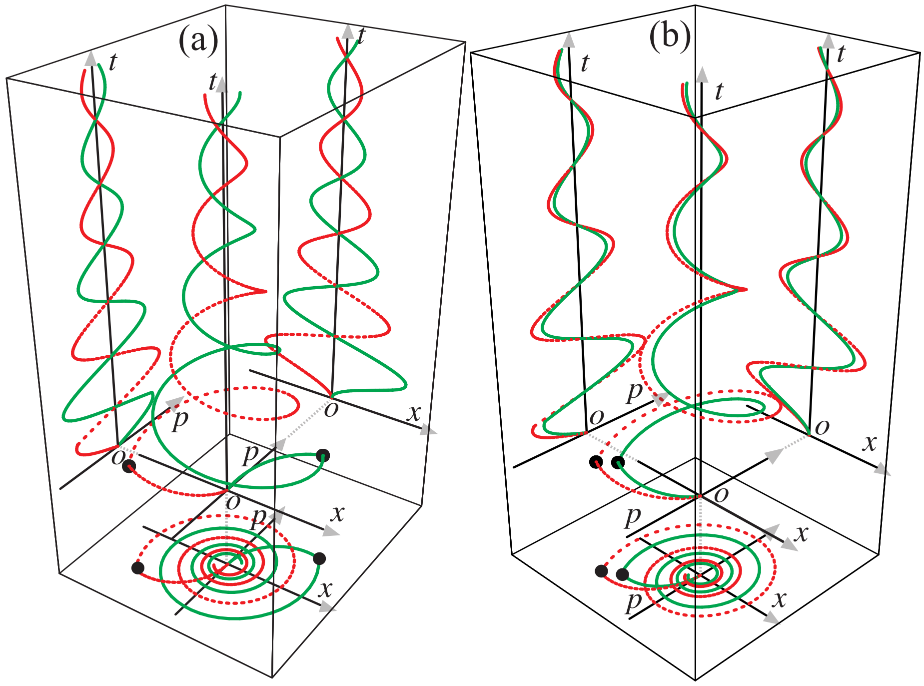

Figure 5.3: Phase space representation of the oscillator trajectories $(\langle\hat{x}\rangle(t), \langle\hat{p}\rangle(t), t)$ corresponding to the two qubit states $|\downarrow\rangle$ (dashed, red) and $|\uparrow\rangle$ (continuous, green) for the parameters given in section 5.6.2, an oscillator quality factor of 10, with $K = 0$ (a) and $K \neq 0$ (b). Projections on the (x, p), (x, t) and (p, t) planes are included. Both trajectories start at the origin and move away from it under the influence of the interaction with the qubit. At the point marked with $\bullet$ the interaction is switched off, and the system evolves freely spiraling around the origin. The trajectories circle around each other without crossing.

Fig. 5.4 shows the output of the detector for the two qubit states $\downarrow\rangle$ and $|\uparrow\rangle$.

The standard condition for the possibility of single-shot readout, i. e., the maximal separation of the two peaks corresponding to different qubit states in the probability distribution Eq. (5.32) should be larger than the peak width, is given by

$$\varepsilon \approx \frac{|\mathcal{A}(1,0) - \mathcal{A}(0,1)|}{3\mu\sqrt{\eta}} > 1, \tag{5.39}$$

where the envelope (5.38) has been evaluated at $t = \tau$. We note that $q_\uparrow$ and $q_\downarrow$ are continuous variables with values between 0 and 1 and the condition presented above takes

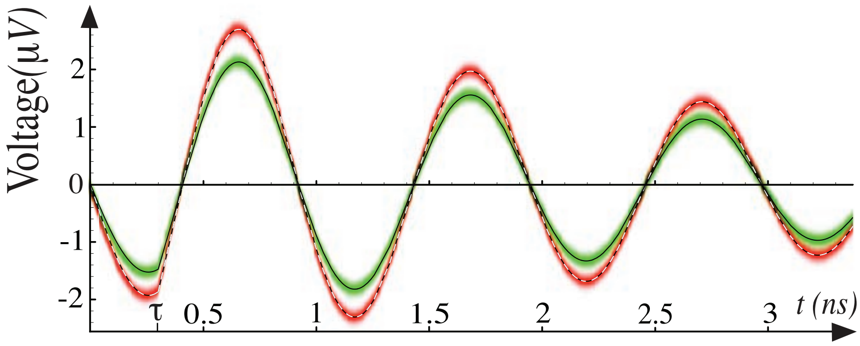

Figure 5.4: Probability distribution of output voltage (density plot, dark color indicates high and white low density) and expectation value of momentum for the two qubit states $|\downarrow\rangle$ (dashed, red) and $|\uparrow\rangle$ (continuous, green). Here $\Omega/(2\pi) = 0.97$ GHz, $\Omega/\kappa = 20$, $w = \Omega$, $\Omega\tau = 1.83$, $\delta\tau = 0.015$, $\gamma\tau = 3$, $T = 30$ mK. The values of the circuit parameters are given in section 5.6.2.

into account the extremal case of the difference between the states $|\uparrow\rangle$ and $|\downarrow\rangle$. The result is independent of K. For the parameters of Fig. 5.4 we have $\varepsilon \approx 2.5$.

5.4 Practical implementation

A possible measurement protocol involves discriminating the amplitudes of the ringdown oscillations corresponding to different qubit states. As demonstrated by Eq. (5.38), the amplitude difference is independent of K. This discrimination could be performed more accurately with an interferometric technique, where ringdown oscillations from a second, reference SQUID oscillator that is not coupled to the qubit are combined with those from the original SQUID oscillator.The reference SQUID is biased such that it undergoes ringdown oscillations with the same phase and amplitude as those of the measurement SQUID oscillator for one of the two qubit states. In this case, the resultant signal after the subtraction would be exactly zero for perfect cancellation when the qubit state causes the two SQUID oscillators to have identical ringdown signals. A residual ringdown oscillation would be produced for the other qubit state. This scheme requires that the two SQUIDs receive an identical kick and begin their ringdown oscillations at the same time. This can be achieved by splitting the bias current pulse signal along two separate lines, one going to each SQUID, as shown in Fig. 5.5, where the layout is such that the reference SQUID has a vanishing coupling to the qubit.

Fig. 5.6 shows the total signal, i. e. the difference of the ringdown oscillations from the measurement and reference SQUIDs for the two qubit states. We have considered the case where the total flux bias for the reference SQUID is equal to the total flux bias for the measurement SQUID in the case where the qubit state is $|\uparrow\rangle$. In this case the difference signal is smeared around 0 for the qubit in state $|\uparrow\rangle$. If the qubit is in the $|\downarrow\rangle$ state,

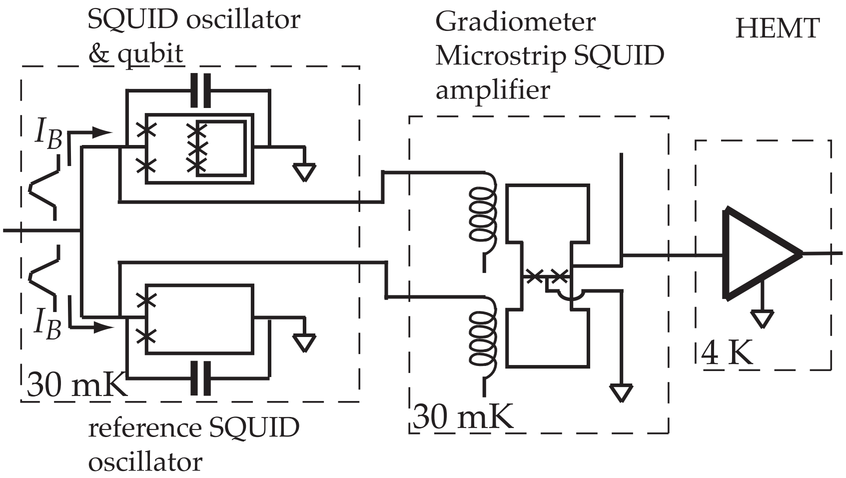

Figure 5.5: Circuit diagram for SQUID oscillator and qubit, along with reference SQUID oscillator, dual-input gradiometer microstrip amplifier and a cryogenic High Electron Mobility Transistor (HEMT). Dashed boxes indicate different chips and/or different temperatures.

the output signal oscillates with an amplitude is given by the difference between the two ringdown oscillations in Fig. 5.4.

The subtraction of the two ringdown signals can be achieved by using a microstrip SQUID amplifier arranged as a gradiometer with two separate microstrip inputs with their senses indicated in Fig. 5.5 [168]. The microstrip SQUID amplifier consists of a dc SQUID with a multi-turn superconducting input coil above a conventional SQUID washer, where the signal is connected between one side of the input coil and ground and the other end of the input coil is left open. Input signals near the stripline resonance frequency, related to the total length of the input coil, typically of the order of 1 GHz, couple strongly to the SQUID loop and the SQUID produces an output signal with a gain of $\sim 10 - 20$ dB [169]. A gradiometer microstrip SQUID amplifier for amplifying the difference between two separate signals near the stripline resonance can be produced as a straightforward extension from previous microstrip SQUID layouts by using a SQUID geometry with two loops and a separate stripline coil coupled to each of the loops, with one signal input connected to each stripline [168].

With no crosstalk between the two inputs, the circulating currents in the two loops of the SQUID amplifier cancel out when the input signals are identical, resulting in a vanishing output signal. Thus, with the arrangement in Fig. 5.5, the microstrip SQUID amplifier produces the difference between the two oscillator ringdowns. Of course, in any practical gradiometer, there will be non-zero crosstalk, where a signal at one input induces circulating currents in the other loop of the SQUID amplifier. However, for reasonable layouts of the device, this crosstalk could be kept at the 1% level, thus setting a limit on

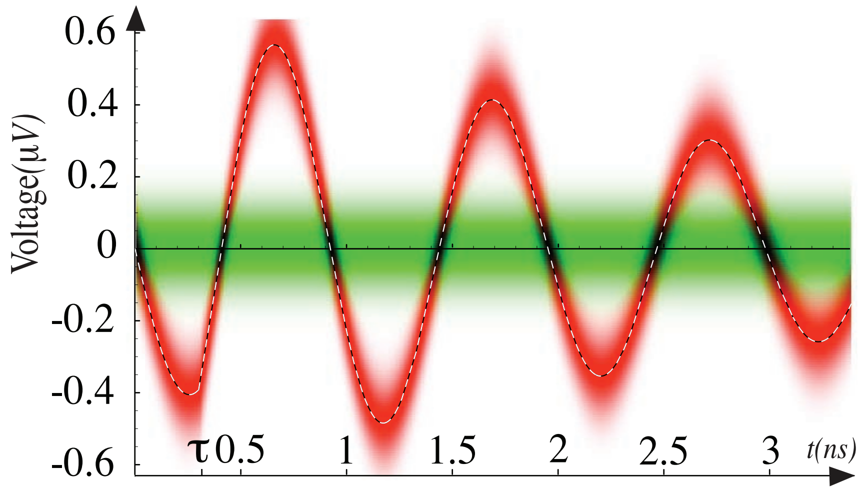

Figure 5.6: Probability distribution of output voltage (density plot, dark color indicates high and white low density) and expectation value of momentum for the two qubit states $|\downarrow\rangle$ (dashed, red) and $|\uparrow\rangle$ (continuous, green). Here the contribution of the reference SQUID has been introduced. Parameters: $\Omega/(2\pi) = 0.97$ GHz, $\Omega/\kappa = 20$, $w = \Omega$, $\Omega\tau = 1.83$, $\delta\tau = 0.015$, $\gamma\tau = 3$, $T = 30$ mK. The values of the circuit parameters are given in section 5.6.2.

the fidelity of the subtraction [168].

Based on the calculated difference signals for the ringdown oscillations in the two qubit states from Fig. 5.6, one must be able to discriminate the oscillations for the $|\downarrow\rangle$ qubit state from the non-oscillatory signal for the $|\uparrow\rangle$ state. Thus one needs to resolve a ~ 1 GHz signal with an amplitude of ~ 0.5 μV in a ~ 100 MHz bandwidth, i. e. before the ringdown is completed. Microstrip SQUID amplifiers operated at 20 mK have achieved noise temperatures as low as ~ 50 mK [170]. If we assume a conservative noise temperature estimate of 200 mK for our gradiometer microstrip SQUID amplifier, this would correspond to a noise of 150 nV in the 100 MHz bandwidth referred back to the SQUID oscillators. Thus, it should be possible to discriminate between the two possible output signals corresponding to the two qubit states in a single shot.

In the non-ideal case, the noise of the reference SQUID increases the broadening of the curves in Fig. 5.6 such that the single shot condition (5.39) must accommodate another width η. Still, at the parameters used in Fig. 5.6, this condition will still hold.

5.5 Conclusion

We have demonstrated that a non-QND Hamiltonian can induce a close to QND backaction on the qubit, despite arbitrarily strong interaction with the environment, provided that the interaction time is very short, i. e. the measurement is quasi-instantaneous. The relaxation of the qubit has been described in the first order in time and, essential to the almost-QND results presented above, is that $\tau\delta \ll 1$.

We observe that the measurement time, i. e., the time needed to reduce the qubit density matrix to a classical mixture is essentially dominated by the coupling between the qubit and its complex environment γ^{-1} such that it is desirable to achieve $\gamma\tau \gg 1$.

The readout time for the oscillator is restricted only by the ring-down of the two possible oscillations of momentum, i.e. κ^{-1}. The amplitude of these oscillations is proportional to γ, which again stresses the usefulness of a strong qubit-oscillator coupling. If the two peaks in $P(p,\tau,t)$ become separated by significantly more than their widths, single shot measurement may become possible.

5.6 Additional information

5.6.1 Solution for the Wigner characteristic functions

In this section we solve Eqs. (5.14) using the approximation (5.16).

The diagonal density matrix elements

We solve the diagonal equations needed for evaluation of expectation values such as $\langle\hat{p}\rangle(t)$, which characterize the output of the detector:

$$\dot{\chi}_{\sigma\sigma} = (\mathbb{i}(r_\sigma\gamma + K)(\alpha+\alpha^*) + \mathbb{i}\Omega(\alpha\partial_\alpha - \alpha^*\partial_{\alpha^*}) + \mathcal{D})\chi_{\sigma\sigma} - r_\sigma \mathbb{i}\delta\chi_0(\alpha)F(\alpha,t), \quad (5.40)$$

where

$$\begin{aligned} F(\alpha,t) &= 2q_\uparrow q_\downarrow \sin\phi(\mathbb{i} - K(\alpha+\alpha^*)t) - 2\mathbb{i}(q_\uparrow^2 - q_\downarrow^2)\delta t \\ &- 2\mathbb{i}q_\uparrow q_\downarrow \cos(\phi)t(\eta\gamma(\alpha^*-\alpha) - 2w). \end{aligned} \quad (5.41)$$

We perform a variable transformation in order to remove the first order derivatives in Eq. (5.40)

$$\alpha = z\mathbb{e}^{s(\kappa-\mathbb{i}\Omega)}, \quad \alpha^* = z^*\mathbb{e}^{s(\kappa+\mathbb{i}\Omega)}, \quad t = s, \quad (5.42)$$

and obtain

$$\begin{aligned} \partial_s\chi_{\sigma\sigma} &= (\mathbb{i}(r_\sigma\gamma + K)\mathbb{e}^{s\kappa}(z\mathbb{e}^{-s\mathbb{i}\Omega} + z^*\mathbb{e}^{s\mathbb{i}\Omega}) - \eta\kappa|z|^2\mathbb{e}^{2s\kappa})\chi_{\sigma\sigma} \\ &- r_\sigma\mathbb{i}\delta\chi_0(z\mathbb{e}^{s(\kappa-\mathbb{i}\Omega)})F(z\mathbb{e}^{s(\kappa-\mathbb{i}\Omega)}, s), \end{aligned} \quad (5.43)$$

which can be solved analytically, and transformed back to the initial variables α, t. The solution reads

$$\chi_{\sigma\sigma}(\alpha,t) = \frac{|\langle\sigma|\Psi\rangle|^2}{4\pi}\chi_{\sigma\sigma}^{\mathrm{hom}}(\alpha,t) - \frac{\mathbb{i}r_\sigma\delta}{4\pi}\chi_{\sigma\sigma}^{\mathrm{inh}}(\alpha,t), \quad (5.44)$$

where

$$\chi_{\sigma\sigma}^{\mathrm{hom}}(\alpha,t) = \exp\left(-\frac{|\alpha|^2\eta}{2} + \mathbb{i}(r_\sigma\gamma+K)\left(\frac{\alpha(1-\mathbb{e}^{-t(\kappa-\mathbb{i}\Omega)})}{\kappa-\mathbb{i}\Omega} + \frac{\alpha^*(1-\mathbb{e}^{-t(\kappa+\mathbb{i}\Omega)})}{\kappa+\mathbb{i}\Omega}\right)\right), \quad (5.45)$$

and

$$\chi^{\rm inh}_{\sigma\sigma}(\alpha,t)=\int_0^t ds\chi^{\rm hom}_{\sigma\sigma}(\alpha,s)F\left(\alpha\mathbb{e}^{-s(\kappa-\mathbb{i}\Omega)},t-s\right). \tag{5.46}$$

The off-diagonal density matrix elements

The method and approximations of the previous section can be used to solve the off-diagonal equations. From this solution we intend to extract information about the qubit coherence $\langle\hat{\sigma}_x\rangle(t)$. We start with

$$\dot{\chi}_{\uparrow\downarrow}=(2\mathbb{i}\gamma(\partial_{\alpha^*}-\partial_\alpha)+\mathbb{i}\Omega(\alpha\partial_\alpha-\alpha^*\partial_{\alpha^*})-2\mathbb{i}w+\mathbb{i}K(\alpha+\alpha^*)+\mathcal{D})\chi_{\sigma\sigma}-\mathbb{i}\delta\chi_0(\alpha)G(\alpha,t), \tag{5.47}$$

where

$$G(\alpha,t)=q_\downarrow^2-q_\uparrow^2-t\mathbb{i}(\gamma-K(q_\downarrow^2-q_\uparrow^2))(\alpha+\alpha^*)-4t\delta q_\uparrow q_\downarrow\sin(\phi). \tag{5.48}$$

The variable transformation in this case originates from

$$\partial_s\alpha=(-\mathbb{i}\Omega+\kappa)\alpha+2\mathbb{i}\gamma,\ \ \partial_s\alpha^*=(\mathbb{i}\Omega+\kappa)\alpha^*-2\mathbb{i}\gamma, \tag{5.49}$$

and reads

$$\begin{aligned}\alpha &= \frac{2\mathbb{i}\gamma}{\kappa-\mathbb{i}\Omega}\left(\mathbb{e}^{s(\kappa-\mathbb{i}\Omega)}-1\right)+z\mathbb{e}^{s(\kappa-\mathbb{i}\Omega)},\ \ \alpha^*=-\frac{2\mathbb{i}\gamma}{\kappa-\mathbb{i}\Omega}\left(\mathbb{e}^{s(\kappa+\mathbb{i}\Omega)}-1\right)+z^*\mathbb{e}^{s(\kappa+\mathbb{i}\Omega)},\\ t &= s.\end{aligned} \tag{5.50}$$

We obtain

$$\begin{aligned}\partial_s\chi_{\uparrow\downarrow} &= (-2\mathbb{i}w-\eta\kappa\alpha(z,s)\alpha^*(z^*,s)+\mathbb{i}K(\alpha(z,s)+\alpha^*(z^*,s)))\chi_{\uparrow\downarrow}\\ &- \mathbb{i}\delta\chi_0(\alpha(z,s))G(\alpha(z,s),s),\end{aligned} \tag{5.51}$$

which can be solved analytically, and transformed back to α,t. The solution reads

$$\chi_{\uparrow\downarrow}(\alpha,t)=\frac{q_\uparrow q_\downarrow\mathbb{e}^{-\mathbb{i}\phi}}{4\pi}\chi^{\rm hom}_{\uparrow\downarrow}(\alpha,t)-\frac{\mathbb{i}\delta}{4\pi}\chi^{\rm inh}_{\uparrow\downarrow}(\alpha,t), \tag{5.52}$$

where

$$\begin{aligned}\chi^{\rm hom}_{\uparrow\downarrow}(\alpha,t) &= \exp\left(-\frac{|\alpha|^2}{2}\eta-2\mathbb{i}tw-\frac{4t\gamma(\gamma\eta\kappa-\mathbb{i}K\Omega)}{\kappa^2+\Omega^2}+\frac{4\gamma(\gamma\eta(\kappa^2-\Omega^2)-2\mathbb{i}K\kappa\Omega)}{(\kappa^2+\Omega^2)^2}\right.\\ &+ \frac{K+\gamma\eta}{\kappa+\mathbb{i}\Omega}\left(\mathbb{i}(1-\mathbb{e}^{-t(\kappa+\mathbb{i}\Omega)})\alpha^*-\frac{2\mathbb{e}^{-t(\kappa+\mathbb{i}\Omega)}\gamma}{\kappa+\mathbb{i}\Omega}\right)\\ &+ \left.\frac{K-\gamma\eta}{\kappa-\mathbb{i}\Omega}\left(\mathbb{i}(1-\mathbb{e}^{-t(\kappa-\mathbb{i}\Omega)})\alpha+\frac{2\mathbb{e}^{-t(\kappa-\mathbb{i}\Omega)}\gamma}{\kappa-\mathbb{i}\Omega}\right)\right),\end{aligned} \tag{5.53}$$

and

$$\chi^{\rm inh}_{\uparrow\downarrow}(\alpha,t)=\int_0^t ds\chi^{\rm hom}_{\uparrow\downarrow}(\alpha,s)G\left(\mathbb{e}^{-s(\kappa-\mathbb{i}\Omega)}\alpha+\frac{2\left(1-\mathbb{e}^{-s(\kappa-\mathbb{i}\Omega)}\right)\gamma}{\mathbb{i}\kappa+\Omega},t-s\right). \tag{5.54}$$

From the density matrix calculated above we can extract information about the qubit relaxation and dephasing during the short interaction with the dissipative oscillator.

5.6.2 Conversion to circuit parameters

In the following we give a recipe (see also Ref. [164] for more detail) to obtain the parameters entering the calculation of this paper from the circuit components

$$\Omega = \sqrt{\frac{2\pi I_c^{\mathrm{eff}}}{C_S\Phi_0}}\left(1-\left(\frac{I_B}{I_{\mathrm{c}}^{\mathrm{eff}}}\right)^2\right)^{\frac{1}{4}}, \qquad m = \left(\tfrac{\Phi_0}{2\pi}\right)^2 C_S, \qquad \gamma = -\frac{M_{qS}I_{\mathrm{q}}I_B\tan\phi_m^0}{4\mu},$$
$$\kappa = \frac{1}{2RC_S}, \quad \tan\phi_m^0 = \frac{I_B}{\sqrt{I_{\mathrm{c}}^{\mathrm{eff}\,2}-I_B^2}}, \quad K = \frac{I_B}{2e}\sqrt{\frac{\hbar}{2m\Omega}},$$

where $\Phi_0 = h/2e$ is the magnetic flux quantum for a superconductor, M_{qS} is the qubit-SQUID mutual inductance, $I_{\mathrm{c}}^{\mathrm{eff}}$ is the effective critical current of the SQUID at the particular flux bias, I_B is the amplitude of the dc bias pulse applied to the SQUID, C_S the SQUID shunt capacitance, R the internal resistance of the measurement circuitry, and I_{q} is the circulating current of the localized states of the qubit. The momentum of the oscillator p and the voltage across the SQUID are related by

$$V = \frac{ep}{C_S\hbar}, \tag{5.55}$$

where e is the electron charge. The parameters used to generate Figs. 5.2, 5.3, 5.4 and 5.6 are

$$\begin{aligned} I_{\mathrm{c}}^{\mathrm{eff}} &= 0.5\cdot 10^{-6}A, & I_B &= 0.87 I_{\mathrm{c}}^{\mathrm{eff}}, & C_S &= 2\cdot 10^{-11}F, \\ M_{qS} &= 100\cdot 10^{-12}H, & I_{\mathrm{q}} &= 438\cdot 10^{-9}A, & \tau &= 0.3\cdot 10^{-9}s, \end{aligned}$$
$$\delta/(2\pi) = 0.8\cdot 10^{7}Hz.$$

Chapter 6

Macroscopic dynamical tunneling in a dissipative system

I. Serban and F. K. Wilhelm

We investigate macroscopic dynamical quantum tunneling (MDQT) in the driven Duffing oscillator, characteristic for Josephson junction physics and nanomechanics. Under resonant conditions between stable coexisting states of such systems we calculate the tunneling rate. In macroscopic systems coupled to a heat bath, MDQT can be masked by driving-induced activation. We compare both processes, identify conditions under which tunneling can be detected with present day experimental means and suggest a protocol for its observation.

Parts of this chaper have been published in *Physical Review Letters* **99**, 137001 (2007)

6.1 Introduction

The phase space of a classical system can have forbidden areas even in the absence of potential barriers, e. g. in the presence of external driving. Quantum-mechanically, these areas can be crossed in a process called dynamical tunneling [171, 172]. So far, dynamical tunneling has been observed experimentally in microscopic systems, i.e. cold atoms [173, 174] with very low damping. Recent experimental progress has demonstrated many basic quantum features in macroscopic systems such as Josephson junctions or nanomechanical oscillators, overcoming the limitations posed by their coupling to the environment. Important for this success was the ability to reduce noise and cool to very low temperatures.

In this chapter we discuss the possibility of macroscopic dynamical tunneling (MDQT) i. e. involving a macroscopic degree of freedom, like the phase difference across a driven Josephson junction. Classically, for certain parameters, this system has two stable coexisting oscillations with different amplitudes. This driven system will feel the influence of its dissipative environment strongly, even at temperature $T = 0$. We demonstrate that under experimentally accessible conditions the tunneling between the two classical states can indeed occur and be singled out from the background of thermal activation events. We suggest an experiment where MDQT can be directly observed. Our result can be applied to verify quantum physics in systems with weak nonlinearity such as nanomechanical oscillators. Quantum tunneling is also a potential dark count error process in the Josephson bifurcation amplifier. Here the classical switching between the two driving-induced, coexisting states in a Josephson junction was used for high resolution dispersive qubit state detection [79–81, 175].

Dynamical tunneling (in the absence of an environment) has been studied using the WKB approximation in the parametric driven oscillator [176]. Activation rates in the presence of an environment have been studied in bistable systems [177–179]. Dynamical tunneling with dissipation has been described numerically [180] and multiphoton resonances have been studied perturbatively [181].

6.2 The Duffing oscillator

We study a harmonically driven Duffing oscillator, as an approximate description of a wide range of macroscopic physical systems ranging Josephson junctions [81, 100] and nanomechanical oscillators [182, 183]. The classical Duffing oscillator fulfills following equation of motion

$$\ddot{x} + \kappa\dot{x} + \Omega^2 x + \frac{2F_0}{m}\cos(\nu t) - \frac{4\beta}{m}x^3 = 0 \tag{6.1}$$

The response of the oscillator to external harmonic driving $F(t)$ is shown schematically in Fig. 6.1 (a). Above a critical value the response to the driving presents two stable oscillations [184]. As we will show, this dynamical bistability can be mapped onto a static, bistable potential.

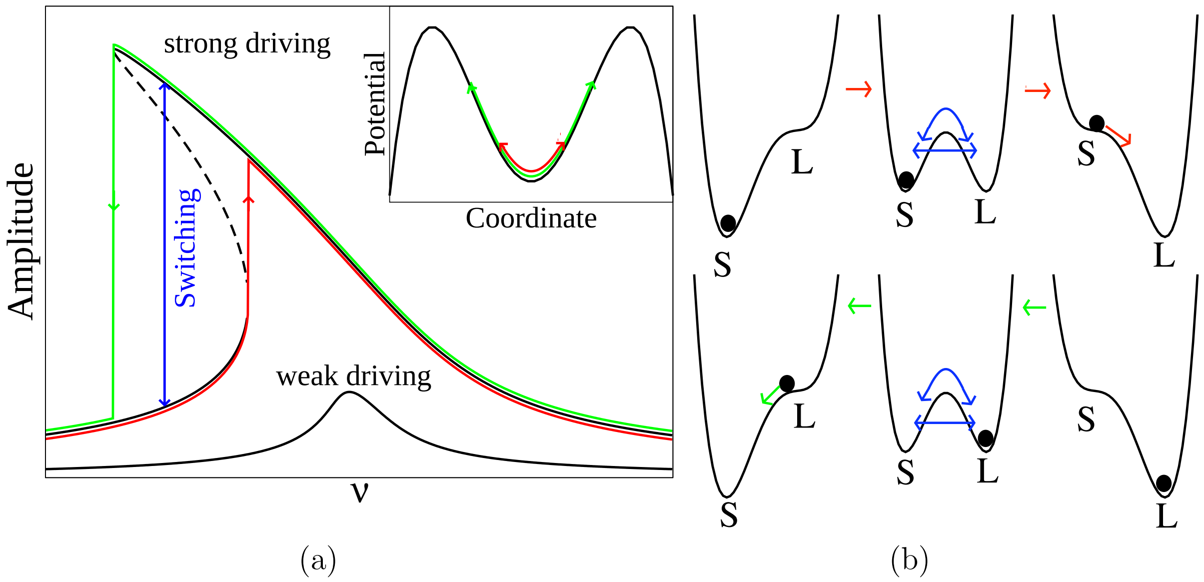

Figure 6.1: (a) Response of the Duffing oscillator (potential shown in the inset) to harmonic driving, as function of the driving frequency ν. For weak driving, a symmetric resonance peak centered around Ω can be observed. For strong, close to resonance driving, the peak becomes tri-valued, with two stable an one unstable solution. (b) The dynamical bistability can be mapped to a bistable static potential. Tilting the double-well corresponds to sweeping the driving frequency ν. Here "S" and "L" correspond to the large and small amplitude stable oscillations respectively.

The driven Duffing oscillator is described by the Hamiltonian

$$\hat{H}(t) \quad = \quad \frac{\hat{p}^2}{2m} + \frac{m\Omega^2}{2}\hat{x}^2 - \beta\hat{x}^4 + F(t)\hat{x}, \tag{6.2}$$

where $F(t) = F_0(\mathrm{e}^{\mathrm{i}\nu t} + \mathrm{e}^{-\mathrm{i}\nu t})$ is the driving field with frequency ν. For sub-resonant driving, $\nu < \Omega$, and below a critical driving strength $F_0 < F_c$ two classical oscillatory states with different response amplitudes coexist. Considering a Josephson junction with capacitance C, critical current I_c and driving current amplitude I_B we can identify x as the phase difference across the junction, $m = (\hbar/2e)^2 C$, $\Omega = \sqrt{2eI_c/(\hbar C)}$, $F_0 = \hbar I_B/(2e)$ and $\beta = m\Omega^2/24$.

Following the Caldeira-Leggett approach, we assume an Ohmic environment and describe it as a bath of harmonic oscillators

$$\hat{H}_B = \sum_i \left(\frac{m_i \omega_i^2 \hat{x}_i^2}{2} + \frac{\hat{p}_i^2}{2m_i} \right) - \hat{x} \sum_i \lambda_i \hat{x}_i + \hat{x}^2 \sum_i \frac{\lambda_i^2}{2m_i\omega_i^2},$$

with spectral density $J(\omega) = \pi \sum_i \lambda_i^2 \delta(\omega - \omega_i)/(2m_i\omega_i) = m\kappa\omega \exp(-\omega/\omega_c)$ and ω_c a high frequency cutoff. In the case of a Josephson junction $\kappa = 1/CR = \Omega/Q$.

6.3 Transformation to the rotating frame

We transform this Hamiltonian using the unitary operator $\hat{U} = \exp(\mathbb{i}\nu t(\hat{a}^\dagger\hat{a} + \sum_i \hat{b}_i^\dagger \hat{b}_i)$ similar to Ref. [177], where $\hat{a}$ and $\hat{b}_i$ are the annihilation operators for the system and bath oscillators. Dropping the fast rotating terms in the rotating wave approximation (RWA), we obtain

$$\hat{H}_{\mathrm{tot}} = \hat{H}_0^{(\delta)} - \hat{x}\sum_i \lambda_i \hat{x}_i + \sum_i \frac{\tilde{m}\tilde{\omega}_i^2 \hat{x}_i^2}{2} + \frac{\hat{p}_i^2}{2\tilde{m}_i}, \tag{6.3}$$

where, up to a constant we have

$$\hat{H}_0^{(\delta)} = \frac{\tilde{m}\tilde{\Omega}^2}{2}\hat{x}^2 + \frac{\hat{p}^2}{2\tilde{m}} - \frac{6\beta}{4\tilde{m}^2\tilde{\Omega}^4}\left(\frac{\tilde{m}\tilde{\Omega}^2}{2}\hat{x}^2 + \frac{\hat{p}^2}{2\tilde{m}}\right)^2 + F_0\hat{x}. \tag{6.4}$$

We thus obtain a time independent Hamiltonian at the expense of a form that is not separable in $\hat{p}$ and $\hat{x}$. This transformation reduces the frequency $\tilde{\Omega} = \Omega\delta$ and increases the mass $\tilde{m} = m/\delta$ of the oscillators by $\delta_i = (\omega_i - \nu)/\omega_i$ in the case of the bath and $\delta = (\Omega - \nu)/\Omega + \kappa\omega_c/(\pi\Omega^2)$ for the main oscillator, where the second term describes a deterministic force induced by dragging the system through its environment.

We note that the RWA is valid as long as the neglected terms, oscillating with frequency 2ν and indeed much faster than the degree of freedom moving according to the Hamiltonian (6.4), i. e. when $2\nu \gg \tilde{\Omega}$. This condition is best fulfilled close to resonance, when $\nu \approx \Omega$. Moreover, in (6.3) we have replaced the system-bath coupling $\lambda_i/2(\hat{x}\hat{x}_i - \hat{p}\hat{p}_i/(m\Omega m_i\omega_i)$ by $\lambda_i\hat{x}\hat{x}_i$. In the limit of weak coupling to the environment, the fast rotating terms $\hat{a}\hat{b}_i$ are can usually be discarded in RWA, thus we expect no quantitative chance of our results from their inclusion.

We concentrate at first on quantum tunneling in the absence of bath fluctuations and study the system in phase-space. The effect of dissipation on the tunneling rate [15] is expected to inhibit the tunneling. However, as it has been argued by Caldeira and Leggett, the environment acts as a “measurement” , continuously projecting the system and inhibiting its evolution. Therefore, the suppression of tunneling becomes significant only when the rate of “measurement” becomes comparable with the natural frequency of the system. In the limit of weak coupling to the environment, this correction should remain small.

The classical Hamilton function $H_0^{(\delta)}(x,p)$ is portrayed in Fig. 6.2(b) and (c) for a sub-critical driving strength $F_0 < F_c = 2/9(2\tilde{m}^3\tilde{\Omega}^6/\beta)^{1/2}$. It has three extremal points: saddle (s), minimum (m) and maximum (M) with phase space coordinates $(x_{\mathrm{e}}, p_{\mathrm{e}})$, where $\mathrm{e} \in \{\mathrm{m}, \mathrm{s}, \mathrm{M}\}$. The curves of constant quasi-energy $H_0^{(\delta)}(x,p) = E$ represent classical trajectories. In the bistability region $E \in (E_{\mathrm{m}}, E_{\mathrm{s}})$ where $E_{\mathrm{e}} = H_0^{(\delta)}(x_{\mathrm{e}}, p_{\mathrm{e}})$ there are always two periodic classical trajectories, around the two stable points (attractors) (m) and (M), with a small and large amplitude respectively. A classical damped system would evolve towards one of these attractors, and eventually stop. In the limit of $\kappa \to 0$, the positions x_{e} correspond to the amplitudes of the solutions of Eq. (6.1) see e.g. Fig. 6.1 as follows: (m) represents the small amplitude, (M) represents the large amplitude and (s) corresponds to the unstable solution.

Using this phase-space portrait, we outline an experiment to observe MDQT during the transient evolution of the system. Without driving, the system relaxes to its ground state centered around (m). Then, after turning on the driving field one records the time needed for a transition to the large orbit as a function of a parameter of the drive, e. g. frequency ν. When two quantized levels pertaining to the two oscillatory states are close in quasi-energy, tunneling can occur, and enhance the total switching rate.

We describe tunneling using the semiclassical WKB approximation which is an expansion in $\hbar$ close to the least action path. To find that path, we solve the equation $H_0^{(\delta)}(x,p) = E$ and obtain four coexisting momentum branches $\pm p_{L,S}(x,E)$ where

$$p_{S,L}(x,E) = \tilde{m}\tilde{\Omega}\sqrt{\frac{2\tilde{m}\tilde{\Omega}^2}{3\beta} - x^2 \mp \sqrt{\frac{8F_0}{3\beta}}\sqrt{x-X}}, \tag{6.5}$$

with $X = E/F_0 - (\tilde{m}\tilde{\Omega}^2)^2/(6F_0\beta)$. This configuration is reminiscent of Born-Oppenheimer surfaces in molecular physics where dynamical tunneling has also been studied [171].

A real-valued $p_{S,L}$ corresponds to a classically allowed area with an oscillating WKB wavefunction, a complex-valued one to a classically forbidden area with a decaying wavefunction. At $x = X$, both trajectories have the same momentum and position and connect. Here $\dot{x} = \partial_p H_0^{(\delta)}(x,p) = 0$ but $p \neq 0$ such that the motion changes direction and continues on a different momentum branch. At this point a transition from one branch to the other is possible [171].

For all $x < X$ both $p_{S,L}(x,E)$ are complex. The tunneling least-action trajectory which connects the two allowed regions only passes through the region $x > X$. Here the $p_{S,L}$ are either real or purely imaginary, i. e. $-p_{S,L}^2 \in \mathbb{R}$. Thus the forbidden area with $x < X$ does not influence the quantization rules within the WKB approximation.

To study the region where $x > X$, we mirror the solution $p_L(x,E)$ around the X point as shown in Fig. 6.2(a) and obtain a double well "potential". The small and large amplitude oscillation states are localized in the right and left-hand wells, respectively, and are separated by a "potential barrier" where the momentum is purely imaginary. We apply the WKB theory in this "potential" in order to determine the tunnel splitting in the limit of a low transmission through the forbidden region. The classical turning points x_i are given by $p_{S,L}(x_i,E) = 0$, see Fig. 6.2 (a). The bound state energies at zero transmission are given by the Sommerfeld energy quantization rules

$$S_{12}(E) = \pi n + \pi/2, \quad S_{4'3'}(E) = \pi m + \pi/2, \quad n, m \in \mathbb{Z}, \tag{6.6}$$

where $S_{ij}(E) = \int_{x_i}^{x_j} \mathrm{sign}(x-X)|p(x,E)|dx/\hbar$ and the negative sign on the left hand side of X is due to mirroring. Whenever a pair of energies from either well is degenerate, resonant tunneling through the barrier can occur. This induces coupling between the two wells and lifts the degeneracy. The level crossings become avoided crossings at finite transmission

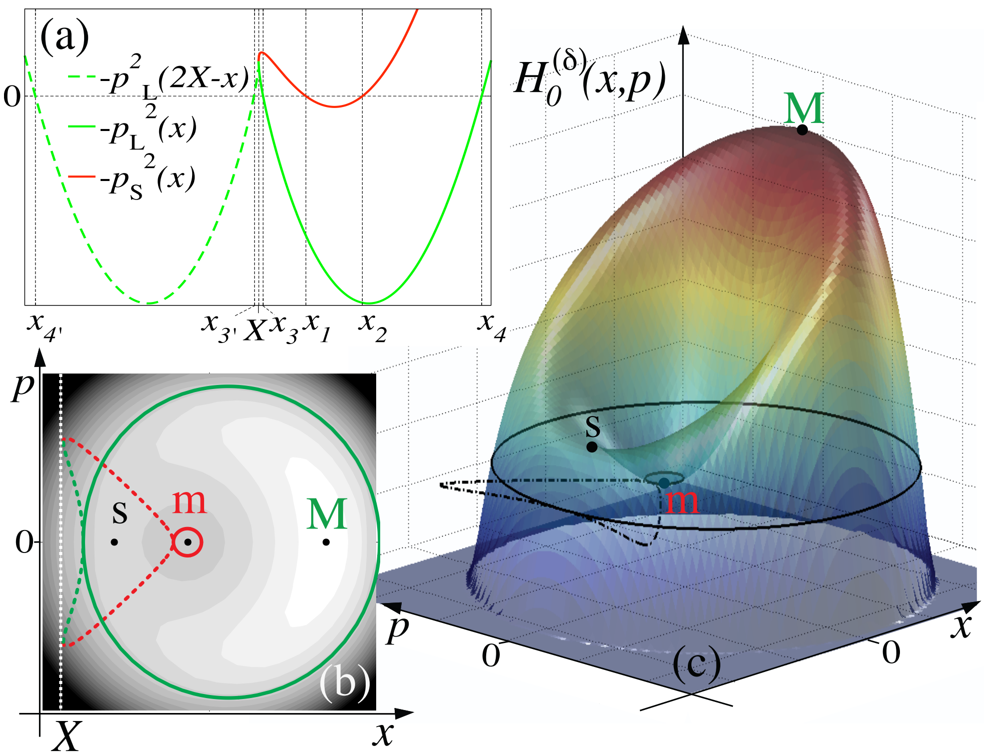

Figure 6.2: Illustration of the Hamilton function and the "potential" landscape. (a) $-p^2_{S,L}(x,E)$: the "potential" changes with E; classical turning points are found at $p(x_i,E)=0$. (b,c) $H_0^{(\delta)}(x,p)$; in (b) white corresponds to high, black to low quasi-energy; (c): green lines corresponds to the L, red ones to the S branch; continuous lines correspond to real and dashed ones to imaginary valued momentum.

and the full WKB condition reads

$$\cot S_{12}(E)\cot S_{4'3'}(E) = \exp(-2S_{3'1}(E))/4. \tag{6.7}$$

We expand the quasi-energy E and the actions S_{ij} in series of $\varepsilon = 1/4\exp(-2S_{3'1})$ around the level crossings with quasi-energy E_0 where Eqs. (6.6) are simultaneously satisfied. The first energy correction $E_1\varepsilon$ is obtained straightforwardly from $\partial_E S_{12}|_{E_0}\partial_E S_{4'3'}|_{E_0}(E_1\varepsilon)^2 = \varepsilon$, and the tunneling rate is obtained directly from the energy splitting at the avoided level crossings

$$\Gamma_{\mathrm{t}} = \frac{2E_1\varepsilon}{\hbar\pi} = \left.\frac{\exp(-S_{3'1})}{\hbar\pi\sqrt{\partial_E S_{12}\partial_E S_{4'3'}}}\right|_{E_0}. \tag{6.8}$$

This can be evaluated in closed form involving elliptic integrals for S_{ij} and we obtain the exact expressions

$$\begin{aligned} \partial_E S_{12}|_{\mathrm{m}} &= \partial_E S_{4'3'}|_{\mathrm{m}} = \pi/(\hbar\Omega_{\mathrm{m}}), \\ \partial_E S_{12}|_{\mathrm{s}} &= \partial_E S_{3'1}|_{\mathrm{m}} = \infty,\ \partial_E S_{3'1}|_{\mathrm{s}} = \pi/(\hbar|\Omega_{\mathrm{s}}|), \end{aligned}$$

where $\Omega_{\mathrm{e}} = \sqrt{\partial^2_{xx} H_0^{(\delta)} \partial^2_{pp} H_0^{(\delta)}}|_{\mathrm{e}}$ and $\mathrm{e} \in \{\mathrm{m}, \mathrm{s}, \mathrm{M}\}$. Thus, for S_{12} at (m) and $S_{3'1}$ at (s) we reproduce the harmonic oscillator result. The saddle point "frequency" Ω_{s} is imaginary as expected.

We simplify Eq. (6.8) by locally approximating $H_0^{(\delta)}$ close to the extremal points by harmonic oscillators, i. e. assuming that S_{ij} are linear functions of E. This approximation holds for all S_{ij} simultaneously when E is far enough from both extremal points $E_{\mathrm{s,m}}$, as it is the case for the ground state $E_{\mathrm{m}} + \hbar\Omega_{\mathrm{m}}/2$ of the small amplitude well. In this approximation $S_{3'1}(E) \approx \pi(E_{\mathrm{s}} - E)/(\hbar|\Omega_{\mathrm{s}}|)$ and thus we find a compact approximation

$$\Gamma_{\mathrm{t}} \approx \frac{\Omega_{\mathrm{m}}}{\pi^2} \exp\left(-\frac{\pi(E_{\mathrm{s}} - E_{\mathrm{m}} - \hbar\Omega_{\mathrm{m}}/2)}{\hbar|\Omega_{\mathrm{s}}|}\right). \tag{6.9}$$

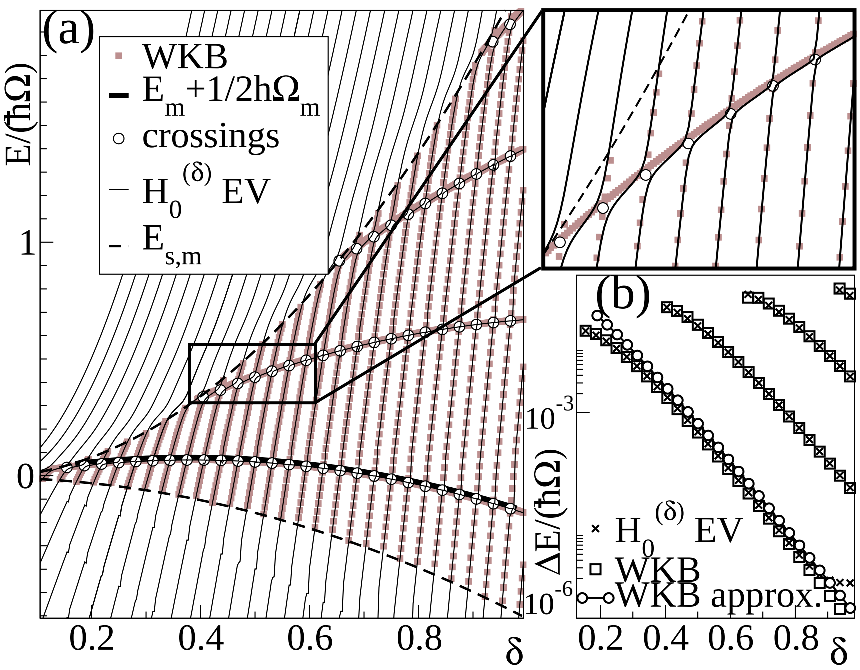

Figure 6.3: (a): Quantized energies: eigenvalues (EV) of $\hat{H}_0^{(\delta)}$ versus WKB. $\hat{H}_0^{(\delta)}$ was represented in the number state basis considering $2N$ levels. (b): Tunneling-induced energy splittings at level crossings. Frequency sweep at $m\Omega/\hbar = 2$, $\beta = m\Omega^2/24$, $\kappa\omega_c/\Omega^2 = 0.1$ and $F_0 = 0.5F_c(\nu)$.

Our calculations rely on a series of assumptions. To test them, we compare the results to a full numerical diagonalization of $\hat{H}_0^{(\delta)}$ taking a basis of the first $2N$ Fock states. At

$F_0 = 0$, the number of levels that cover the bistability region is $N = \hbar\Omega(2m\Omega)^2/(6\beta\hbar^2)$. As shown for a representative set of data in Fig. 6.3, we find good agreement between these numerically exact results and the predictions of Eqs. (6.6,6.8) and also (6.9).

We see good agreement between the WKB calculation (assuming separate wells) and the exact numerical diagonalization of the Hamiltonian $\hat{H}_0^{(\delta)}$. This indicates that far from the degeneracy points there is no tunneling between the wells. The agreement is excellent even when the system has only few quantized levels. The discrepancies occur close to the degeneracy points, where transmission between the wells starts playing an important role. The first correction in ε (i. e. the low transmission limit) to the degenerate energies agrees well with the exact numerical calculation.

In the experiment outlined previously for possible observation of MDQT we therefore expect for $\Gamma_{\mathrm{t}}(\delta)$ to present peaks centered around the degeneracy points. The values of δ where these anticrossings occur are found by minimizing $|\cot(S_{4'3'}(E_{\mathrm{m}}))|$ and are found in agreement with the weak driving result [181],

$$\delta = 3\hbar\beta n/(2m^2\Omega^3), \;\; n \in \mathbb{N}.$$

To estimate the width of the peaks of $\Gamma_{\mathrm{t}}(\delta)$ one may study the difference between the solution of Eq. (6.6), and given the good agreement between WKB calculation (assuming separate wells) and the exact numerical diagonalization of the Hamiltonian away from the anticrossings, we expect sharp periodic peaks in $\Gamma_{\mathrm{t}}(\delta)$.

6.4 Thermal activation

Quantum tunneling is significant only close to level crossings. It always competes with the activation over the barrier, which occurs at all energies and is based on classical fluctuations due to coupling to a heat bath. A rather detailed treatment of a similar process has been given in Refs. [178, 179]. We now estimate these effects and compare them to the quantum tunneling rate. When modeling activation, it is crucial to consider that we are working in a frame rotating relative to the heat bath, which is fixed in the laboratory.

We start from Eq. (6.3). As we will adopt the mean first passage time approach [185], it is sufficient to approximate the system Hamiltonian close to its minimum in phase space by $\hat{H}_0^{(\delta)} \approx \hat{p}^2/(2m_{\mathrm{eff}}) + V(\hat{x})$ where the effective mass is determined by the curvature of the Hamilton function $m_{\mathrm{eff}}^{-1} = \partial_{pp}^2 H_0^{(\delta)}(x,p)|_{\mathrm{m}}$ and the effective potential is $V(x) = H_0^{(\delta)}(x, p_{\mathrm{m}})$. In this approximation we obtain a quantum Langevin equation

$$m_{\mathrm{eff}}\ddot{x} + \partial_x V(x) - x\int_0^\infty d\omega \frac{2J(\omega)}{\pi\omega} + m_{\mathrm{eff}}\int_0^t \tilde{\kappa}(t-s)\dot{x}(s)ds = \xi(t), \tag{6.10}$$

where

$$\tilde{\kappa}(t) = \int_0^\infty \frac{2J(\omega)\cos((\omega-\nu)t)}{(\omega-\nu)\pi m_{\mathrm{eff}}} d\omega, \tag{6.11}$$

$$\xi(t) = \sum_i \lambda_i \left[\left(x_i(0) - \frac{\lambda_i x(0)}{\tilde{m}_i\tilde{\omega}_i^2} \right)\cos(\tilde{\omega}_i t) + \frac{p_i(0)}{\tilde{m}_i\tilde{\omega}_i}\sin(\tilde{\omega}_i t) \right]. \tag{6.12}$$

$\tilde{\kappa}(t)$ is peaked on a short time scale ω_c^{-1}. Its magnitude is characterized through the effective friction constant

$$\kappa_{\text{eff}} = \int_0^\infty \tilde{\kappa}(t)dt = 2\kappa \left(\delta - \frac{3\beta x_{\text{m}}^2}{2m\Omega^2}\right)(1 + \mathcal{O}(\nu/\omega_c)).$$

The factor of two difference between κ_{eff} and the damping constant of the undriven harmonic system accounts for the fact that in the rotating frame there are bath modes above and below $\omega = 0$ (see Eq. (6.3)) whereas for the undriven case the frequencies are strictly positive.

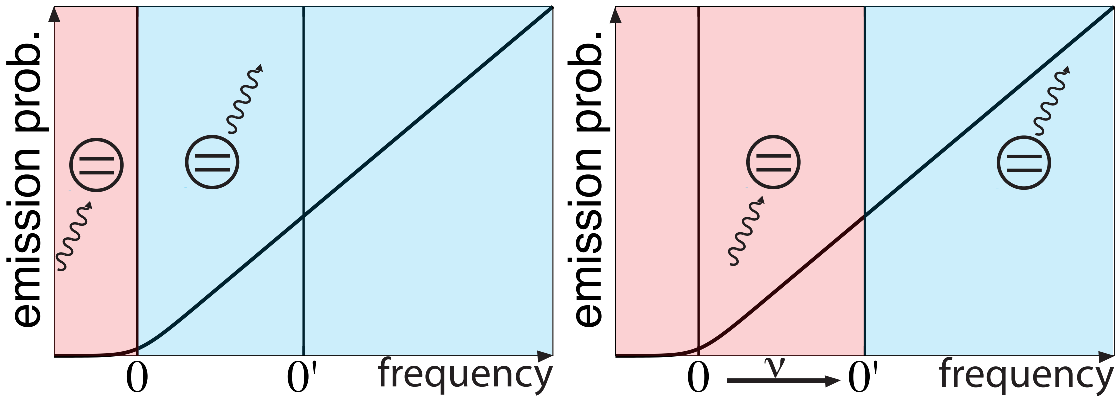

(a) (b)

Figure 6.4: Estimation of the effective temperature. In the description of the bath, the change to the rotating frame is equivalent to a translation of the frequency axis by ν. Panel (a) shows the probability of emission (blue, positive frequencies) and absorption (pink, negative frequencies) of a photon by a two level-system in the laboratory frame. The same is shown in panel (b) for the rotating frame.

Thus oscillators with frequency ω have the spectral density $J(\omega + \nu)$ and modes with negative frequencies have significant contribution to noise even at low temperatures. We use a detailed balance condition to determine the effective temperature of the bath as seen by a detector in the rotating frame (see Fig. 6.4), e. g. a two level system with level separation $\hbar\Omega_{\text{m}}$

$$\frac{P(\Omega_{\text{m}}, T)}{P(-\Omega_{\text{m}}, T)} = \exp\left(\frac{\hbar\Omega_{\text{m}}}{k_B T_{\text{eff}}}\right). \tag{6.13}$$

Here $P(\omega, T) = J(\omega+\nu)(1+n(\omega+\nu, T))$ is the probability for a quantum $\hbar\omega$ to be emitted to the bath in the rotating frame, see also Fig. 6.4. The effective temperature is enhanced at low T and finite even at $t = 0$. This accounts for the fact that what a detector in the rotating frame regards as (quasi-energy) absorption can actually be (energy) emission in the lab frame. In the case of constant acceleration in relativistic context this behavior is known as the Unruh effect [186].

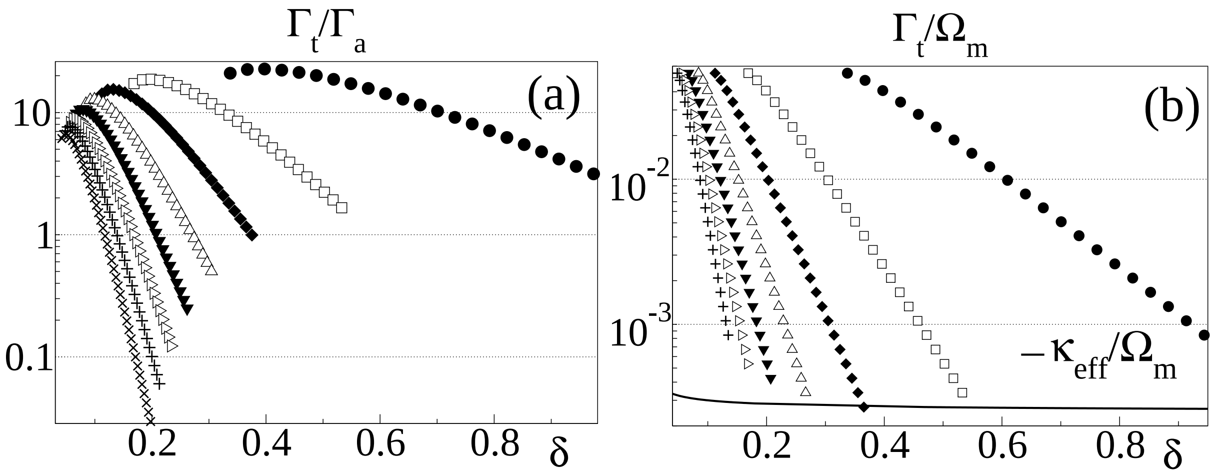

Figure 6.5: (a) The ratio of tunneling and activation rates from the small well at the avoided level crossings. (b) Corresponding tunneling rates compared to $\kappa_{\rm eff}$ (where $\Gamma_{\rm t}/\Gamma_{\rm a} > 1$). Driving frequency sweep at $F_0 = 0.7F_c(\nu)$; Values of Ω (in GHz): 1(●), 2(□), 3(⧫), 4(△), 5(▼), 6(▷), 7(+), 8(×), at parameters specified in text.

The barrier crossing problem for systems described by a quantum Langevin equation is well studied in the context of chemical reactions. For low damping, $\kappa_{\rm eff} \ll \Omega_{\rm m}$ mean-first-passage time theory predicts the activation rate [185]

$$\Gamma_{\rm a}^{-1} = \frac{1}{k_B T_{\rm eff}\kappa_{\rm eff}} \int_0^{S(E_{\rm s})} dS \mathrm{e}^{-E(S)/k_B T_{\rm eff}} \int_{E(S)}^{E_{\rm s}} dE' \frac{\mathrm{e}^{-E'/k_B T_{\rm eff}}}{S(E')}, \tag{6.14}$$

where $S(E) = \oint p(x,E)dx$. In the traditional low temperature limit $\kappa_{\rm eff} S(E_{\rm s}) \ll k_B T_{\rm eff} \ll E_{\rm s} - E_{\rm m}$ the activation rate becomes

$$\Gamma_{\rm a} = \frac{\kappa_{\rm eff}}{k_B T_{\rm eff}} \frac{\Omega_{\rm m}}{2\pi} \exp\left(-\frac{E_{\rm s} - E_{\rm m}}{k_B T_{\rm eff}}\right) S(E_{\rm s}). \tag{6.15}$$

In our case, the noise temperature $k_B T_{\rm eff}$ can be larger than the barrier height $E_{\rm s} - E_{\rm m}$. We justify the high temperature limit of expression (6.14) as follows:

- The weak coupling to the environment κ induces an energy bottleneck, i. e. even if the fluctuations of the environment may have large magnitude, the weak coupling to the system reduces the magnitude of the fluctuations the system actually feels. This allows for a separation of time scales [185]. In this case the energy is the slow varying variable, and we are in the energy diffusion regime.

- We deal here with a slightly different situation to the one described in Ref. [185]. There the system starts in thermal equilibrium, and one monitors the escape rate over the barrier which originates from equilibrium fluctuations. In our case the system starts in the ground state of the small well, which is not thermal equilibrium.

From this initial state it then thermalizes. When settled in the thermal equilibrium, it automatically escapes (due to the high temperature, the distribution in the small well is no longer restrained by the barrier).

- Our situation can be described by the same equations as the one described in Ref. [185] as follows from *Onsager's regression hypothesis*: the transition towards equilibrium from an initial constrained state is identical to the statistical evolution of the system (in particular, the same time constants govern both processes). Basically this hypothesis requires a Markovian system, i. e. a system that does not remember in which way it has reached a given state.

In this limit we obtain from Eq. (6.14)

$$\Gamma_{\mathrm{a}} = \kappa_{\mathrm{eff}} \left(F\left(\frac{E_{\mathrm{s}} - E_{\mathrm{m}}}{k_B T_{\mathrm{eff}}} \right) \right)^{-1}, \tag{6.16}$$

where $F(x) = \int dx(\exp(x) - 1)/x \equiv \mathrm{Ei}(x) - \log(x)$. Summarizing, in the rotating frame, as a consequence of driving, the bath appears with a quality factor $\Omega_{\mathrm{m}}/\kappa_{\mathrm{eff}}$ reduced by approximatively a factor of two and an enhanced effective temperature T_{eff}. Moreover, the bath shifts the detuning δ. We show that experimental observation of MDQT could still be possible. At the level anticrossings we calculate the WKB tunneling rate from the ground state and the activation rate from Eq. (6.16), see Fig. 6.5(a) where we have considered a Josephson junction with $\kappa = 10^{-4}\Omega$, the temperature $T = 10$ mK, shunt capacitance $C = 2 \cdot 10^{-12}$ F and $\beta = m\Omega^2/24$. We observe that the quantum tunneling rate can be one order of magnitude larger than the activation rate in the limit of relatively small detuning δ and low damping. By increasing the value of $\mathfrak{a} = m\Omega/\hbar$, we observe a reduction of the ratio $\Gamma_{\mathrm{t}}/\Gamma_{\mathrm{a}}$ as expected, since $\mathfrak{a}$ measures the number of quantized levels in the system and thus the "classicality" of its behavior. In Fig. 6.5 we have $\mathfrak{a} \in (2, 20)$, while in the experiment of Ref. [100] $\mathfrak{a}$ was larger than 100, at higher temperature and smaller quality factor, such that MDQT was probably masked by thermal activation.

We have argued at the beginning of the discussion of dynamical tunneling, that as long as the "measurement rate", which we now identify as the effective coupling to the environment κ_{eff} remains considerably smaller that the natural frequency of the system (a good estimate is Ω_{m}), the suppression of tunneling due to the dissipative environment should remain small. In Fig. rate (b) one can show that, at the chose parameters, this condition is indeed fulfilled, and that the rate of "measurement" remains significantly smaller that the tunneling rate. Thus, we expect that at the values of Fig. 6.5 the experiment we propose should produce direct evidence for MDQT.

6.5 Conclusion

We have investigated macroscopic dynamical tunneling by mapping it onto tunneling between two potential surfaces. We compared this process with the activation over the barrier using the mean first passage time approach. The values obtained suggest that dynamical tunneling can be singled out from the background of activation processes. We have proposed an experiment realizable within existing technology to demonstrate dynamical tunneling by monitoring the switching rate between the two dynamical states while tuning a parameter of the external driving.

6.6 Additional information

6.6.1 WKB quantisation

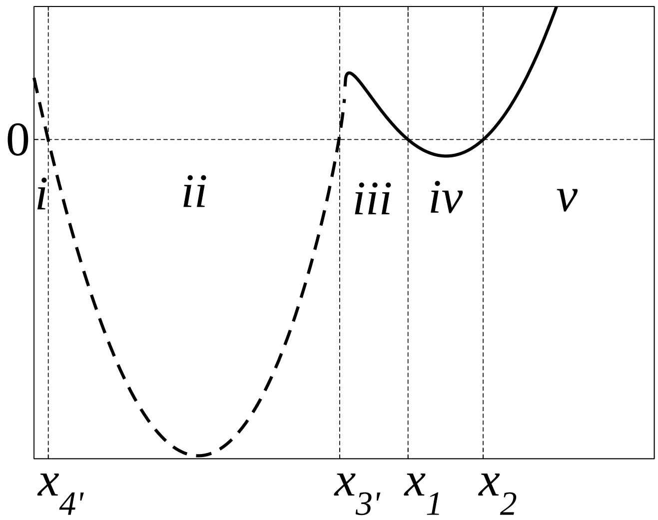

Figure 6.6: Effective double well potential in the rotating frame for WKB

The WKB conditions [187] in the "potential" of Fig. 6.6 are given in the following. At the turning point x_4' we have according to the Langer method [187, 188]

$$\Psi_i = \frac{\zeta_1}{2\sqrt{|p(x)|}} \exp\left(-\int_x^{x_4'} \frac{|p(x')|}{\hbar} dx'\right), \quad \Psi_{ii} = \frac{\zeta_1}{\sqrt{p(x)}} \cos\left(\int_x^{x_4'} \frac{p(x')}{\hbar} dx' + \frac{\pi}{4}\right). \quad (6.17)$$

At the turning point x_3' we have

$$\Psi_{ii} = \frac{\zeta_2}{\sqrt{p(x)}} \cos\left(\int_x^{x_3'} \frac{p(x')}{\hbar} dx' - \frac{\pi}{4} + \varphi_2\right), \quad (6.18)$$

$$\Psi_{iii} = \frac{\zeta_2}{\sqrt{|p(x)|}} \left(\frac{\cos\varphi_2}{2} \exp\left(-\int_{x_3'}^{x} \frac{|p(x')|}{\hbar} dx'\right) + \sin\varphi_2 \exp\left(\int_{x_3'}^{x} \frac{|p(x')|}{\hbar} dx'\right)\right).$$

At the turning point x_1 we have

$$\Psi_{iii} = \frac{\zeta_3}{\sqrt{|p(x)|}} \left(\frac{\cos\varphi_3}{2} \exp\left(-\int_x^{x_1} \frac{|p(x')|}{\hbar} dx'\right) + \sin\varphi_3 \exp\left(\int_x^{x_1} \frac{|p(x')|}{\hbar} dx'\right)\right),$$

$$\Psi_{iv} = \frac{\zeta_3}{\sqrt{p(x)}} \cos\left(\int_{x_1}^{x} \frac{p(x')}{\hbar} dx' - \frac{\pi}{4} + \varphi_3\right). \quad (6.19)$$

At the turning point x_2 we have

$$\Psi_{iv} = \frac{\zeta_4}{\sqrt{p(x)}} \cos\left(\int_x^{x_2} \frac{p(x')}{\hbar} dx' - \frac{\pi}{4}\right), \quad \Psi_v = \frac{\zeta_4}{2\sqrt{|p(x)|}} \exp\left(-\int_{x_2}^{x} \frac{|p(x')|}{\hbar} dx'\right). \quad (6.20)$$

We observe that for the regions ii, iii and iv, each connected to two turning points, the Langer method [187] prescribes two wave functions, pertaining to the two turning points. These wavefunctions of course have to be identical. Thus we obtain following conditions

$$\begin{aligned}
&\zeta_2 = \zeta_1 \cos n\pi, \quad \varphi_2 = -\int_{x_4'}^{x_3} \frac{p(x')}{\hbar} dx' + n\pi + \pi/2, \quad \text{(in region } ii) \qquad (6.21)\\
&\frac{\zeta_2}{2} \cos\varphi_2 = \zeta_3 \sin\varphi_3 \exp\left(\int_{x_3'}^{x_1} \frac{|p(x')|}{\hbar} dx'\right), \quad \text{(in region } iii)\\
&\zeta_2 \sin\varphi_2 = \frac{\zeta_3}{2} \cos\varphi_3 \exp\left(-\int_{x_3'}^{x_1} \frac{|p(x')|}{\hbar} dx'\right), \quad \text{(in region } iii)\\
&\zeta_4 = \zeta_3 \cos(\pi m), \quad \varphi_3 = -\int_{x_1}^{x_2} \frac{p(x')}{\hbar} dx' + m\pi + \pi/2, \quad \text{(in region } iv), \quad n, m \in \mathbb{Z}.
\end{aligned}$$

These conditions lead to the following condition for the quantized trajectories

$$\cot\left(\int_{x_1}^{x_2} \frac{p(x')}{\hbar} dx'\right) \cdot \cot\left(\int_{x_4'}^{x_3} \frac{p(x')}{\hbar} dx'\right) = \frac{1}{4} \exp\left(-2\int_{x_3'}^{x_1} \frac{|p(x')|}{\hbar} dx'\right). \qquad (6.22)$$

6.6.2 Analytic formulas for the action

In the following we give the full analytic formulae for S_{ij}. Due to the relative position of $p_{L,S}(X,E)^2$ to 0, we may have a transition from one branch to the other even without tunneling, which affects the limits of integration. In the following, index sign refers to the $\mathrm{sign}(p_{L,S}(X,E)^2)$.

$$\begin{aligned}
\partial_E S_{12} &= -\sqrt{\frac{2}{3}} \frac{8\mathbb{i}AB\left(\sqrt{AB} + \sqrt{AB-1}\right) m\Omega}{\sqrt{L}\sqrt{F_0\beta}\hbar} \\
&\times \mathcal{F}\left(\arcsin\left(\frac{\mathbb{i}}{\sqrt{AB} + \sqrt{AB-1}}\right) \middle| \frac{\left(\sqrt{AB} + \sqrt{AB-1}\right)^2}{\left(\sqrt{AB-1} - \sqrt{AB}\right)^2}\right), \qquad (6.23)\\
\partial_E S_{34+} &= -\sqrt{\frac{2}{3}} \frac{2\mathbb{i}m\Omega}{\sqrt{F_0 L\beta}\hbar} \left(\mathcal{F}\left(\arcsin\sqrt{\frac{A}{C}} \middle| \frac{1}{AB}\right) - \mathcal{F}\left(\arcsin\sqrt{BC} \middle| \frac{1}{AB}\right)\right) - \frac{2p(X)}{F_0\hbar},\\
\partial_E S_{34-} &= -\sqrt{\frac{2}{3}} \frac{2\mathbb{i}m\Omega}{\sqrt{F_0 L\beta}\hbar} \left(\mathcal{F}\left(\arcsin\sqrt{AB} \middle| \frac{1}{AB}\right) - \mathcal{K}(\frac{1}{AB})\right),
\end{aligned}$$

$$
\begin{aligned}
S_{31+} &= \frac{m\Omega}{4\sqrt{L}\hbar}\left(3cL\ \mathcal{E}(\frac{1}{AB}) + (8br_2+Q)\mathcal{K}(\frac{1}{AB}) + 8b(r_1-r_2)\Pi\left(\frac{1}{B}\middle|\frac{1}{AB}\right)\right), \\
S_{31-} &= \frac{m\Omega}{4\sqrt{L}\hbar}\Bigg(-3c\sqrt{Lr_3r_4}\left(\sqrt{C}+\frac{1}{\sqrt{C}}\right) + 4X\sqrt{-Lp_{L,S}(X)^2} \\
&+ 3cL\left(-\mathcal{E}\left(\arcsin\sqrt{AB}\middle|\frac{1}{AB}\right) + \mathcal{E}\left(\arcsin\sqrt{\frac{A}{C}}\middle|\frac{1}{AB}\right) + \mathcal{E}\left(\sin^{-1}\left(\sqrt{BC}\right)\middle|\frac{1}{AB}\right)\right) \\
&+ (Q+8br_1)\left(\mathcal{F}\left(\arcsin\sqrt{\frac{A}{C}}\middle|\frac{1}{AB}\right) - \mathcal{F}\left(\arcsin\sqrt{AB}\middle|\frac{1}{AB}\right)\right) \\
&+ (Q+8br_2)\mathcal{F}\left(\arcsin\sqrt{BC}\middle|\frac{1}{AB}\right) \\
&+ 8b(r_1-r_2)\left(\Pi\left(\frac{1}{A};\arcsin\sqrt{AB}\middle|\frac{1}{AB}\right) - \Pi\left(\frac{1}{A};\arcsin\sqrt{\frac{A}{C}}\middle|\frac{1}{AB}\right)\right. \\
&+ \left.\left.\Pi\left(\frac{1}{B};\arcsin\sqrt{BC}\middle|\frac{1}{AB}\right)\right)\right),
\end{aligned}
$$

where

$$
b = \frac{2\delta m\Omega^2}{3\beta},\ c = \sqrt{\frac{8F_0}{3\beta}},\ A = \frac{(r_1-r_3)}{(r_2-r_3)},\ B = \frac{(r_2-r_4)}{(r_1-r_4)},\ C = \frac{r_1}{r_2}, \tag{6.24}
$$

$$
L = (r_1-r_3)(r_2-r_4),\ Q = c(3(r_2r_3+r_1r_4)+2X), \tag{6.25}
$$

and r_j are the solutions of $-\left(r^2+X\right)^2 + b - cr = 0$. The elliptic integrals are given by

$$
\mathcal{F}(\phi|m) = \int_0^\phi d\theta \frac{1}{\sqrt{1-m\sin^2(\theta)}},\ \mathcal{K}(m) = \mathcal{F}\left(\frac{\pi}{2}|m\right), \tag{6.26}
$$

$$
\mathcal{E}(\phi|m) = \int_0^\phi d\theta\sqrt{1-m\sin^2(\theta)}, \tag{6.27}
$$

$$
\Pi(n;\phi|m) = \int_0^\phi \frac{d\theta}{(1-n\sin^2(\theta))\sqrt{1-m\sin^2(\theta)}},\ \Pi(n|m) = \Pi\left(n;\frac{\pi}{2}|m\right). \tag{6.28}
$$

The values of the elliptic integrals entering Eq. (6.22), taken at the energies of the extremal points, are

$$
\partial_E S_{3'4'}(E_{\mathrm{m}}) = \partial_E S_{12}(E_{\mathrm{m}}) = \sqrt{\frac{2}{3}}\frac{\pi m\Omega}{\sqrt{F_0L\beta}\hbar}, \tag{6.29}
$$

$$
\partial_E S_{3'4'}(E_{\mathrm{s}}) = \partial_E S_{12}(E_{\mathrm{s}}) = \infty,\ S_{3'1}(E_{\mathrm{s}}) = 0, \tag{6.30}
$$

$$
S_{3'1}(E_{\mathrm{m}}) = \frac{3c\sqrt{L}m\Omega}{4\hbar} + \frac{m\Omega}{2\hbar}\left(\frac{2X}{m\Omega}\sqrt{-p(X)^2} - 3c\sqrt{r_3r_4}\right). \tag{6.31}
$$

Chapter 7

Qubit relaxation due to a dissipative Duffing oscillator trapped in one of its attractors

I. Serban and F. K. Wilhelm

We investigate the relaxation of a superconducting flux qubit for the case when its detector, the Josepshon bifurcation amplifier, remains in the off-state. We observe a qualitatively different behavior for the two different attractors, and interpret the result as an effect of the effective curvature of the detector's basins of attraction in a rotating frame, in the proximity of the stable points.

This chapter presents work done in collaboration M. I. Dykman

7.1 Introduction

The Josepshon bifurcation amplifier (JBA) has been succesfully used as a high resolution, quantum nondemolition flux qubit detector [82]. In this case, the switching rate between its metastable states is strongly sensitive to the state of the qubit. Its detection profits from the very different amplitudes of the oscillator's response to the driving and the formally infinite gain at the bifurcation. Nevertheless, during the detection process several mechanisms contribute to reduce the resolution of the readout. One of them, the switching of the JBA due to its internal, quantum mechanical dynamics, independent on the state of the qubit, has already been investigated in chapter 6. We now focus on another possible mechanism, which is the qubit relaxation between the switching events of the dissipative JBA, when the detector remains trapped in one of its attractors. This relaxation can have various origins. On one hand, the JBA is a dissipative system, and thus represents an environment to the qubit even between the switching events. On the other hand, the JBA drives the qubit off-resonantly, which, in the presence of another environment, such as electromagnetic noise, may affect the relaxation of the qubit.

In this section we describe the relaxation of a flux qubit coupled inductively to the SQUID. The model has already been presented and the effective Hamiltonian has been derived in chapter 3. We assume the same limits, in particular the driving current I_B should remain much smaller than the critical current $I_{\rm c}^{\rm eff}$ of the SQUID. Unlike chapter 3, the driving strength should be large enough for the SQUID to enter the bistability regime but the qubit-SQUID coupling will be treated as a weak perturbation. Moreover, in this case we do explicitly take the $\hat{\sigma}_x$ term in the qubit Hamiltonian into account.

7.2 The model

The qubit Hamiltonian reads

$$\hat{H}_{\rm q} = \hbar w_0 \hat{\sigma}_z + \delta_0 \hat{\sigma}_x. \tag{7.1}$$

The qubit couples linearly to a noisy electromagnetic environment. Following the Caldeira-Leggett approach, we assume an Ohmic bath of harmonic oscillators

$$\hat{H}_{B\rm e} = \sum_i \left(\frac{m_i \omega_i^2 \hat{y}_i^2}{2} + \frac{\hat{p}_i^2}{2m_i} \right), \;\; \hat{H}_{I\rm e} = \hat{\sigma}_x \sum_i \lambda_{\rm ei} \hat{y}_i, \tag{7.2}$$

with spectral density $J_{\rm e}(\omega) = \pi \sum_i \lambda_{\rm ei}^2 \delta(\omega - \omega_i)/(2m_i\omega_i) = \alpha\omega\Theta(\omega - \omega_{\rm e})$ where Θ is the Heaviside step function and $\omega_{\rm e}$ a high frequency cutoff. The inductive coupling of the qubit to the dissipative SQUID is, according to the derivation presented in chapter 3, quadratic

$$\hat{H}_{I\rm d} = \frac{m\Delta^2}{2} \hat{\sigma}_z \hat{x}^2, \tag{7.3}$$

where $\hat{x}$ represents the external phase degree of freedom γ_+. The strongly driven dissipative SQUID is modeled by a Duffing oscillator in contact with an Ohmic bath of harmonic oscillators (see also chapter 6)

$$\hat{H}_{\rm d}(t) = \underbrace{\frac{\hat{p}^2}{2m} + \frac{m\Omega^2}{2}\hat{x}^2 - \beta\hat{x}^4 + F(t)\hat{x}}_{\hat{H}_S} + \sum_i \left(\underbrace{\frac{m_i\omega_i^2\hat{x}_i^2}{2} + \frac{\hat{p}_i^2}{2m_i}}_{\hat{H}_B} + \hat{x}^2\frac{\lambda_i^2}{2m_i\omega_i^2} + \underbrace{\hat{x}\lambda_i\hat{x}_i}_{\hat{H}_I} \right) \quad (7.4)$$

where $F(t) = F_0(\mathbb{e}^{\mathbb{i}\nu t} + \mathbb{e}^{-\mathbb{i}\nu t})$ is the driving field with frequency ν. The spectral density is here $J_{\rm d}(\omega) = \pi\sum_i \lambda_{{\rm d}i}^2\delta(\omega-\omega_i)/(2m_i\omega_i) = m\kappa_{\rm d}\omega\Theta(\omega-\omega_{\rm d})$ with $\omega_{\rm d}$ a high frequency cutoff.

In the following we address the decoherence produced by the electromagnetic environment and the detector separately. For now, in the case of the detector, we aim to describe the qubit relaxation for the case when the SQUID remains in one of the stable states of motion.

7.3 Relaxation from detector noise

In a first step, we approximate the interaction with the electromagnetic environment by its expectation value (mean field approximation). The effect of the fluctuations can be treated separately, and this approach is mentioned in the last section of this chapter. Effectively the Hamiltonian becomes

$$\hat{H}_{\rm q} = \hbar w_0\hat{\sigma}_z + \hbar\delta\hat{\sigma}_x, \quad (7.5)$$

where $\delta = \delta_0 + \langle\sum_i \lambda_{{\rm e}i}\hat{y}_i\rangle_{\rm e}$ and for unbiased noise we simply have $\delta = \delta_0$. The Bloch-Redfield relaxation rate [115, 189], after a secular approximation, is given by

$$\begin{aligned}\Gamma_{\rm r} &= \frac{m^2\Delta^4}{4\hbar^2}\int_0^\infty d\tau\,\left(\langle\hat{x}^2(t)\hat{x}^2(t-\tau)\rangle + \langle\hat{x}^2(t-\tau)\hat{x}^2(t)\rangle - 2\langle\hat{x}^2(t)\rangle\langle\hat{x}^2(t-\tau)\rangle\right)\\ &\cdot \left(\mathbb{e}^{2\mathbb{i}\tau\sqrt{w_0^2+\delta^2}} + \mathbb{e}^{-2\mathbb{i}\tau\sqrt{w_0^2+\delta^2}}\right)\frac{\delta^2}{w^2+\delta^2}, \end{aligned}\quad (7.6)$$

where one must take into consideration the fact that the noise caused by the detector is biased $\langle\hat{x}^2(t)\rangle \neq 0$. The noise bias is removed by the term $\langle\hat{x}^2(t)\rangle\langle\hat{x}^2(t-\tau)\rangle$ in Eq. (7.6). In this approach the correlation function, containing information about the internal, quasi-equilibrium dynamics of the detector, identifies a rate in the master equation of the system.

Here $\hat{x}(t) = \hat{U}_{\rm d}^\dagger(t)\hat{x}\hat{U}_{\rm d}(t)$ and

$$\hat{U}_{\rm d}(t) = \mathcal{T}\exp\left(\int_0^t dt'\frac{\hat{H}_{\rm q}+\hat{H}_{\rm d}(t')}{\mathbb{i}\hbar}\right). \quad (7.7)$$

Henceforth the goal of this section is to evaluate Eq. (7.6). As a first step, we remove the time-dependence of the Hamiltonian describing the Duffing oscillator, by transforming the total system into a rotating frame as shown in the previous chapter.

7.3.1 The rotating frame

We transform the total Hamiltonian into a rotating frame $\hat{H}_{\mathrm{q}}+\hat{H}_{I\mathrm{d}}+\hat{H}_{\mathrm{d}}(t)$ using the unitary operator $\hat{U}_{\mathrm{r}}(t) = \exp(\mathrm{i}\nu t(\hat{a}^\dagger\hat{a} + \sum_i \hat{b}_i^\dagger\hat{b}_i)$. Here $\hat{a}$ and $\hat{b}_i$ are the annihilation operators for the system and bath oscillators.

$$\hat{H}_{\mathrm{dr}} = \mathrm{i}\hbar\partial_t\hat{U}_{\mathrm{r}}\hat{U}_{\mathrm{r}}^\dagger + \hat{U}_{\mathrm{r}}(\hat{H}_q + \hat{H}_{\mathrm{d}}(t))\hat{U}_{\mathrm{r}}^\dagger. \tag{7.8}$$

We define the unitary operator $\hat{U}_{\mathrm{dr}}(t) = \hat{U}_{\mathrm{r}}(t)\hat{U}_{\mathrm{d}}(t)$, and using Eq. (7.11) we obtain

$$\mathrm{i}\hbar\partial_t\hat{U}_{\mathrm{dr}}(t) = \hat{H}_{\mathrm{dr}}\hat{U}_{\mathrm{dr}}(t). \tag{7.9}$$

Thus $\hat{U}_{\mathrm{dr}}(t)$ represents the evolution operators of the detector in the rotating frame. Using this unitary transformation we rewrite the correlation function involved in Eq. (7.6) as follows

$$\langle\hat{x}^2(t_1)\hat{x}^2(t_2)\rangle = \mathrm{Tr}_{\mathrm{d}}\left\{\hat{U}_{\mathrm{dr}}^\dagger(t_1-t_2)\hat{x}_{\mathrm{r}}^2(t_1)\hat{U}_{\mathrm{dr}}(t_1-t_2)\hat{x}_{\mathrm{r}}^2(t_2)\hat{U}_{\mathrm{dr}}(t_2)\hat{\rho}_{\mathrm{d}}(0)\hat{U}_{\mathrm{dr}}^\dagger(t_2)\right\}, \tag{7.10}$$

where $\hat{x}_{\mathrm{r}}(t) = \hat{U}_{\mathrm{r}}(t)\hat{x}\hat{U}_{\mathrm{r}}^\dagger(t)$. Dropping the fast rotating terms in the rotating wave approximation the Hamiltonian (7.8) becomes time independent

$$\hat{H}_{\mathrm{dr}} = \hat{H}_{S\mathrm{r}} + \underbrace{-\sum_i \frac{\hbar\lambda_i}{2\sqrt{m\Omega m_i\omega_i}}(\hat{a}^\dagger\hat{b}_i + \hat{a}\hat{b}_i^\dagger)}_{\hat{H}_{I\mathrm{r}}} + \underbrace{\sum_i \hbar(\omega_i-\nu)(\hat{b}_i^\dagger\hat{b}_i + 1/2)}_{\hat{H}_{B\mathrm{r}}}, \tag{7.11}$$

where, up to a constant we have

$$\hat{H}_{S\mathrm{r}} = \frac{\tilde{m}\tilde{\Omega}^2}{2}\hat{x}^2 + \frac{\hat{p}^2}{2\tilde{m}} - \frac{6\beta}{4\tilde{m}^2\tilde{\Omega}^4}\left(\frac{\tilde{m}\tilde{\Omega}^2}{2}\hat{x}^2 + \frac{\hat{p}^2}{2\tilde{m}}\right)^2 + F_0\hat{x}. \tag{7.12}$$

This transformation reduces the frequency $\tilde{\Omega} = \Omega d$ and increases the mass $\tilde{m} = m/d$ of the oscillators by a factor

$$d = \frac{\Omega-\nu}{\Omega} + \frac{\kappa\omega_{\mathrm{d}}}{\pi\Omega^2}. \tag{7.13}$$

$\hat{x}_{\mathrm{r}}$ becomes

$$\hat{x}_{\mathrm{r}}(t) = \sqrt{\frac{\hbar}{2m\Omega}}(\hat{a}\mathrm{e}^{-\mathrm{i}\nu t} + \hat{a}^\dagger\mathrm{e}^{\mathrm{i}\nu t}). \tag{7.14}$$

Assuming that initially the total system is described by the factorized density matrix $\hat{\rho}(0) = \hat{\rho}_{\mathrm{q}}(0)\otimes\hat{\rho}_{\mathrm{d}}(0)$ and that $\hat{\rho}_{\mathrm{d}}(0)$ commutes with $\hat{H}_{\mathrm{dr}}$, i. e. the detector is initially in a stationary state in the rotating frame, we obtain

$$\langle\hat{x}^2(t_1)\hat{x}^2(t_2)\rangle_{\mathrm{d}} = \mathrm{Tr}_S\left\{\hat{x}_{\mathrm{r}}^2(t_1)\mathrm{Tr}_B\left\{\hat{U}_{\mathrm{dr}}(t_1-t_2)\hat{x}_{\mathrm{r}}^2(t_2)\hat{\rho}_{\mathrm{d}}(0)\hat{U}_{\mathrm{dr}}^\dagger(t_1-t_2)\right\}\right\}. \tag{7.15}$$

We assume the system to be evolving in the proximity of one of the attractors, and thus the Hamiltonian (7.11) can be approximated further by

$$\hat{H}_{\mathrm{dr}} = m_{\mathrm{a}}\Omega_{\mathrm{a}}^2\frac{(\hat{x}-x_a)^2}{2}+\frac{\hat{p}^2}{2m_{\mathrm{a}}}+\sum_i \hbar(\omega_i-\nu)(\hat{b}_i^\dagger\hat{b}_i+1/2)+\sum_i \frac{\hbar\lambda_i}{2\sqrt{m\Omega m_i\omega_i}}(\hat{a}\hat{b}_i^\dagger+\hat{a}^\dagger\hat{b}_i), \quad (7.16)$$

where x_{a} is the position of the attractor, Ω_{a} and m_{a} are obtained from the local curvature of the Hamiltonian (7.11) in p and x direction in the proximity of this attractor.

7.3.2 The initial state

We assume the undriven system to be in equilibrium with the environment. After turning on the driving, the system will reach a new steady state. This will be the initial state used to evaluate Eq. (7.6). Physically, this means we are not looking at the influence of transients on qubit relaxation, but only at the fluctuations of the detector which has reached its long time limit.

The steady state without driving

Before the driving is being turned on, at sufficiently low temperature, the SQUID behaves like a harmonic oscillator. A potential factorized initial state $\hat{\rho}_{\mathrm{d}}(0) = \hat{\rho}_S(0)\otimes\hat{\rho}_B(0)$ evolves towards equilibrium with the environment.

In the laboratory frame, described by Hamiltonian $\hat{H}_{\mathrm{d}}$ in the absence of driving and for $\beta = 0$, the dynamics of a reduced density matrix $\hat{\rho}_S = \mathrm{Tr}_B\hat{\rho}$ describing the oscillator alone is given in the Born-Markov approximation by a master equation

$$\partial_t\hat{\rho}_S(t) = \frac{1}{\mathbb{i}\hbar}[\hat{H}_S,\hat{\rho}_S(t)] + \frac{1}{(\mathbb{i}\hbar)^2}\int_0^t dt'\ \mathrm{Tr}_B\ \left[\hat{H}_I,[\hat{H}_I(t,t'),\hat{\rho}_S(t)\otimes\hat{\rho}_B(0)]\right] \quad (7.17)$$

Similar to chapters 3, 4 and 5, we use the Wigner representation [27]

$$\hat{\rho}_S(t) = \frac{1}{\pi}\int d^2\alpha\ \chi(\alpha,t)\hat{D}(-\alpha), \quad (7.18)$$

where $\hat{D}(-\alpha) = \exp(-\alpha\hat{a}^\dagger + \alpha^*\hat{a})$ is the displacement operator and χ the Wigner characteristic function. The master equation (7.17) becomes

$$\dot{\chi}(\alpha,t) = \left((\mathbb{i}\Omega-\kappa)\alpha\partial_\alpha - (\mathbb{i}\Omega-\kappa)\alpha^*\partial_{\alpha^*} - (1+2n)\kappa|\alpha|^2\right)\chi(\alpha,t), \quad (7.19)$$

and the thermal state

$$\chi(\alpha) = \frac{1}{4\pi}\exp\left(-|\alpha|^2(n+1/2)\right), \quad (7.20)$$

with $n = n(\Omega)$ the Bose function at the bath temperature T is the steady state solution.

The steady state after turning on driving

We now turn on the driving and move into the rotating frame described in the previous section. Starting in the state described by Eq. (7.20) the system evolves towards a new steady state. In the proximity of one of the attractors the system evolves according to the Hamiltonian (7.16). In this frame the dynamics of a reduced density matrix

$$\hat{\rho}_{S\mathrm{r}}(t) = \mathrm{Tr}_{B\mathrm{r}}\hat{\rho}_{\mathrm{dr}}(t) = \mathrm{Tr}_{B\mathrm{r}}\left\{\hat{U}_{\mathrm{dr}}(t)\rho_{\mathrm{dr}}(0)\hat{U}^{\dagger}_{\mathrm{dr}}(t)\right\} = \hat{\mathcal{L}}_t\hat{\rho}_{S\mathrm{r}}(0), \tag{7.21}$$

describing the Duffing oscillator, is determined by an equation similar to (7.17). Here we define $\hat{\mathcal{L}}$ as the non-unitary superoperator that propagates $\hat{\rho}_{S\mathrm{r}}$ in time. We use the Wigner representation again

$$\hat{\rho}_{S\mathrm{r}}(t) = \frac{1}{\pi}\int d^2\alpha \;\; \chi_{\mathrm{r}}(\alpha,t)\hat{D}(-\alpha). \tag{7.22}$$

Defining $\hat{A}$ as the annihilation operator for the effective harmonic oscillator with effective mass and frequency m_{a} and Ω_{a}, we obtain

$$\hat{A} = \sqrt{\frac{m_{\mathrm{a}}\Omega_{\mathrm{a}}}{m\Omega}}\hat{a} - x_{\mathrm{a}}\sqrt{\frac{m_{\mathrm{a}}\Omega_{\mathrm{a}}}{2\hbar}}, \;\; \hat{A}(t) = \hat{A}\mathbb{e}^{\mathbb{i}\Omega_{\mathrm{a}}t}, \tag{7.23}$$

$$\hat{a}(t) = \hat{a}\mathbb{e}^{\mathbb{i}\Omega_{\mathrm{a}}t} + \xi(1-\mathbb{e}^{\mathbb{i}\Omega_{\mathrm{a}}t}), \;\; \xi = x_{\mathrm{a}}\sqrt{\frac{m\Omega}{2\hbar}}. \tag{7.24}$$

The initial state is $\chi_{\mathrm{r}}(\alpha,0) = \chi(\alpha)$ determined in Eq. (7.20). This state evolves in time according to the master equation

$$\begin{aligned}\dot{\chi}_{\mathrm{r}}(\alpha,t) &= \Big(((\mathbb{i}\upsilon_1-\kappa_1)\alpha+\mathbb{i}\upsilon_2\alpha^*)\partial_\alpha - ((\mathbb{i}\upsilon_1+\kappa_1)\alpha^*+\mathbb{i}\upsilon_2\alpha)\partial_{\alpha^*} \\ &- \eta\kappa_1|\alpha|^2 + \xi\left((\kappa_2+\mathbb{i}\upsilon_3)\alpha-(\kappa_2-\mathbb{i}\upsilon_3)\alpha^*\right)\Big)\chi_{\mathrm{r}}(\alpha,t),\end{aligned} \tag{7.25}$$

where

$$\kappa_1 = \frac{J_{\mathrm{d}}(\Omega_{\mathrm{a}}+\nu)}{2m\Omega}, \;\; \kappa_2 = \frac{J_{\mathrm{d}}(\Omega_{\mathrm{a}})}{2m\Omega}, \;\; \eta = 1+2n(\Omega_{\mathrm{a}}+\nu), \tag{7.26}$$

$$\upsilon_1 = \frac{m_{\mathrm{a}}\Omega_{\mathrm{a}}^2}{2m\Omega} + \frac{m\Omega}{2m_{\mathrm{a}}}, \;\; \upsilon_2 = \frac{m_{\mathrm{a}}\Omega_{\mathrm{a}}^2}{2m\Omega} - \frac{m\Omega}{2m_{\mathrm{a}}}, \;\; \upsilon_3 = \frac{m_{\mathrm{a}}\Omega_{\mathrm{a}}^2}{m\Omega}. \tag{7.27}$$

This equation can be solved by an appropriate variable transformation

$$\begin{aligned}\partial_s\alpha(s,z) &= -((\mathbb{i}\upsilon_1-\kappa_1)\alpha+\mathbb{i}\upsilon_2\alpha^*), \\ \partial_s\alpha^*(s,z) &= (\mathbb{i}\upsilon_1+\kappa_1)\alpha^*+\mathbb{i}\upsilon_2\alpha, \\ \alpha(0,z) &= z, \;\; \alpha^*(0,z^*) = z^*, \quad s=t,\end{aligned} \tag{7.28}$$

which removes the partial derivatives on the right-hand side of Eq. (7.25), and the resulting equation reads

$$\begin{aligned}\dot{\chi}_{\mathrm{r}}(z,s) &= \big(-\eta\kappa_1|\alpha(z,s)|^2+\xi\big((\kappa_2+\mathbb{i}\upsilon_3)\alpha(z,s)-(\kappa_2-\mathbb{i}\upsilon_3)\alpha(z,s)^*\big)\big)\chi_{\mathrm{r}}(z,s)\\ &= F(z,s)\chi_{\mathrm{r}}(z,s),\end{aligned}\tag{7.29}$$

and is directly solvable by a simple integration

$$\chi_{\mathrm{r}}(z,s) = \chi_{\mathrm{r}}(z,0)\exp\left(\int_0^s d\tau F(z,\tau)\right).\tag{7.30}$$

The inverse variable transformation of $\chi_{\mathrm{r}}(z,s)$ gives the full time dependent solution of Eq. (7.25), which will not be detailed here due to its length. The steady state solution reads

$$\chi_{\mathrm{r}}(\alpha) = \frac{1}{4\pi}\exp(-R_2|\alpha|^2-R_1\alpha^2-R_1^*\alpha^{*2}+R_0\alpha-R_0^*\alpha^*),\tag{7.31}$$

$$R_1=\frac{(\upsilon_1-\mathbb{i}\kappa_1)\upsilon_2\eta}{4\left(\kappa_1^2+\Omega_{\mathrm{a}}^2\right)},\ R_2=\frac{\eta\left(\kappa_1^2+\upsilon_1^2\right)}{2\left(\kappa_1^2+\Omega_{\mathrm{a}}^2\right)},\ R_0=\frac{(\kappa_2(\kappa_1+\mathbb{i}(\upsilon_1+\upsilon_2))+(\mathbb{i}\kappa_1-\upsilon_1+\upsilon_2)\upsilon_3)\xi}{\kappa_1^2+\Omega_{\mathrm{a}}^2}.$$

Here R_0 represents the displacement of the Gaussian state in the phase-space and $R_{1,2}$ describe the uncertainty of position and momentum and their correlation.

7.3.3 Using the quantum regression theorem

We consider the Duffing oscillator to be in the steady state $\hat{\rho}_{S\mathrm{r}}$ characterized by $\chi_{\mathrm{r}}(\alpha)$ in (7.31). To evaluate the correlators in Eq. (7.15) we use the quantum regression theorem. According to this theorem (see appendix A), given the Markovian evolution (7.21) one can use the superoperator $\hat{\mathcal{L}}$ to evaluate (7.15) as follows

$$\langle\hat{x}^2(t_1)\hat{x}^2(t_2)\rangle_{\mathrm{d}} = \mathrm{Tr}_{S\mathrm{r}}\left\{\hat{x}_{\mathrm{r}}^2(t_1)\hat{\mathcal{L}}_{t_1-t_2}\left(\hat{x}_{\mathrm{r}}^2(t_2)\hat{\rho}_{S\mathrm{r}}\right)\right\}.\tag{7.32}$$

The evolution $\hat{\mathcal{L}}_{t_1-t_2}$ propagates the operator $\hat{x}_{\mathrm{r}}^2(t_2)\hat{\rho}_{S\mathrm{r}}$ in time in the same fashion it would describe the evolution of a density matrix. Usually $\hat{\mathcal{L}}$ is used to propagate only forwards in time as it describes the irreversible evolution of the reduced density matrix. If $t_2>t_1$ a similar formula can be used

$$\langle\hat{x}^2(t_1)\hat{x}^2(t_2)\rangle_{\mathrm{d}} = \mathrm{Tr}_{S}\left\{\hat{x}_{\mathrm{r}}^2(t_2)\hat{\mathcal{L}}_{t_2-t_1}\left(\hat{\rho}_{S\mathrm{r}}\hat{x}_{\mathrm{r}}^2(t_1)\right)\right\}.\tag{7.33}$$

Since we restrict the evolution to the proximity of one of the attractors, we expect that the norm of the operator $\hat{x}_{\mathrm{r}}^2(t_2)\hat{\rho}_{S\mathrm{r}}$ remains finite, such that we can use the Wigner representation again

$$\begin{aligned}\hat{\mathcal{L}}_{t-\tau}\left(\hat{x}_{\mathrm{r}}^2(\tau)\hat{\rho}_{S\mathrm{r}}\right) &= \frac{1}{\pi}\int d^2\alpha\ \chi_L(\alpha,\tau,t-\tau)\hat{D}(-\alpha),\\ \hat{\mathcal{L}}_{t-\tau}\left(\hat{\rho}_{S\mathrm{r}}\hat{x}_{\mathrm{r}}^2(\tau)\right) &= \frac{1}{\pi}\int d^2\alpha\ \chi_R(\alpha,\tau,t-\tau)\hat{D}(-\alpha),\end{aligned}\tag{7.34}$$

According to the quantum regression theorem, the functions $\chi_{L,R}(\alpha,\tau,t)$ will obey the same equation of motion in time t as the density matrix (7.25) with the initial condition $\chi_L(\alpha,\tau,0)=\chi^{\{0\}}_{L,R}(\alpha,\tau)$ where

$$\hat{x}_{\mathrm{r}}^2(\tau)\hat{\rho}_{S\mathrm{r}}=\frac{1}{\pi}\int d^2\alpha\ \chi_L^{\{0\}}(\alpha,\tau)\hat{D}(-\alpha),\quad \hat{\rho}_{S\mathrm{r}}\hat{x}_{\mathrm{r}}^2(\tau)=\frac{1}{\pi}\int d^2\alpha\ \chi_R^{\{0\}}(\alpha,\tau)\hat{D}(-\alpha). \quad (7.35)$$

The same method can be employed to evaluate also the expectation value of $\hat{x}^2(t)$ as required in Eq. (7.6). Thus one can evaluate Γ_{r}. Essential for this type of calculation was the assumption that the bath oscillators remain in thermal equilibrium in the lab frame, and do not evolve under the influence of the coupling to the system. The Duffing oscillator provides an energy bottleneck between the qubit and the bath, such that the qubit is affected by the fluctuations of the environment taken at the oscillator frequency.

This bottleneck strategy is motivated by the assumption of an infinite bath, such that any excitations received from the oscillator are rapidly dispersed and never return to the quantum system. Physically, the bath, i. e. the dissipative element of the measurement circuitry, is in contact with further baths (phonons in the substrate, helium bath etc.) which contribute to dissipate these excitations.

Summarizing, our calculation is valid for $(\Omega-\nu)/\Omega \ll 1$ (rotating wave approximation), $\kappa \ll \Omega$ and $\kappa_1 \ll \Omega_a$ (Born approximation in both laboratory and rotating frame).

7.3.4 Results

Fig. 7.1 shows the dependence of the qubit relaxation rate on the parameters of the driving and on the quality factor. We observe qualitatively different behavior of the relaxation rate depending the attractor in which the oscillator remains trapped. We give the results in the following interpretation. The qubit relaxes due to fluctuations of the oscillator in the proximity of an attractor. Depending on the curvature of the potential around x_{a}, and also on the effective mass (determined by the curvature of the Hamilton function in the $p-$ direction), the oscillator responds differently to the fluctuations of the environment. In a narrow potential, the excursions of the coordinate around x_{a} are going to be small. For a wide potential, they will be large, and cause more decoherence. The plots show this behavior, see also Fig. 7.2.

We observe that the large amplitude attractor causes more noise than the small amplitude attractor. This is a consequence of the quadratic dependence of the relaxation rate on the attractor position in phase-space x_{a}. The positions of the two attractors meet at the bifurcation points. Accordingly, we see that also the relaxation rates approach each other in the proximity of the bifurcation points. The parameters given in Fig. 7.1 (d) relate to circuit parameters in the same manner as described in chapter 3.

Preliminary results indicate a good qualitative agreement between theory and experiment [190], although the parameters used in Fig. 7.1, in order to describe the experiment, go somewhat beyond the limitations posed by the various approximations used in the derivation.

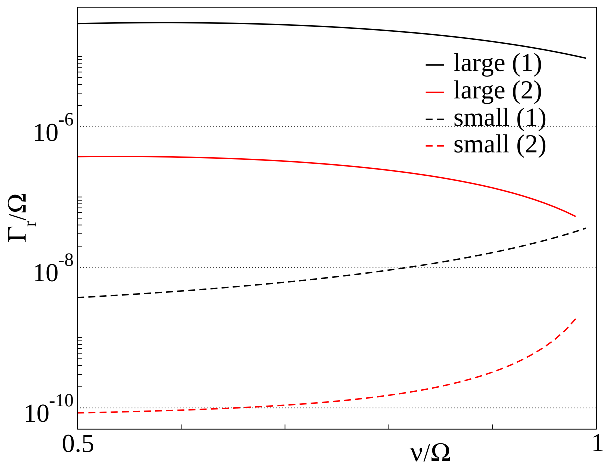

(a)

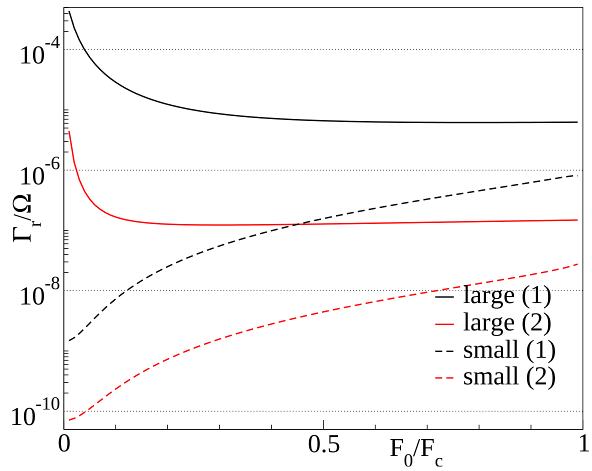

(b)

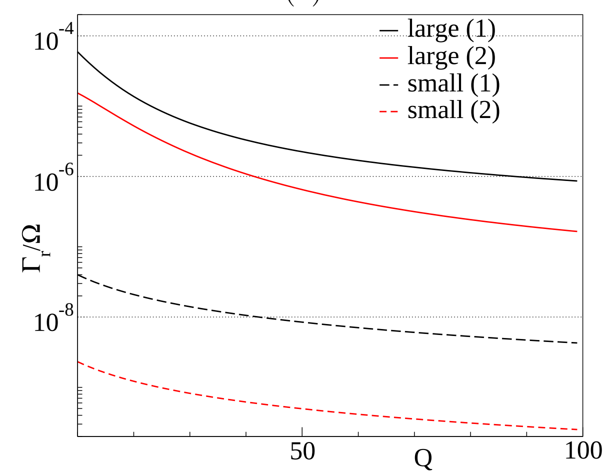

(c)

	set (1)	set (2)
Ω	$1.5 \cdot 10^9 Hz$	$0.8 \cdot 10^9 Hz$
ν	$1.4 \cdot 10^9 Hz$	$0.7 \cdot 10^9 Hz$
Q	20	100
I_B	$30 \cdot 10^{-9} A$	$8 \cdot 10^{-9} A$
I_c^{eff}	$10^{-6} A$	$0.8 \cdot 10^{-6} A$
w_0	$14 \cdot 10^9 Hz$	$20 \cdot 10^9 Hz$
δ_0	$5 \cdot 10^9 Hz$	$5 \cdot 10^9 Hz$
Δ/Ω	0.05	0.05
T	$30mK$	$30mK$

(d)

Figure 7.1: Relaxation rate for the qubit coupled to the Duffing oscillator as a function of driving frequency ν, panel (a), driving strength F_0, panel (b) and quality factor $Q = \kappa_{\mathrm{d}}/\Omega$, panel (c). Continuous lines represent the case when the oscillator is trapped in the large amplitude attractor, while dashed lines correspond to the small amplitude. In each case, two parameter sets similar to experiments [82] (1) and [80] (2) have been used, panel (d).

7.4 Outlook

Currently work is being done in collaboration with the Delft group to identify and describe the qubit relaxation mechanisms and compare theoretical and experimental results. Further possible relaxation mechanisms that remain to be investigated are e. g. the "hooked-up" relaxation. Here we consider an electromagnetic environment, other that the measurement circuitry which includes the Duffing oscillator. Due to the coupling to the damped Duffing oscillator, the qubit appears to have a time dependent energy splitting. Approxi-

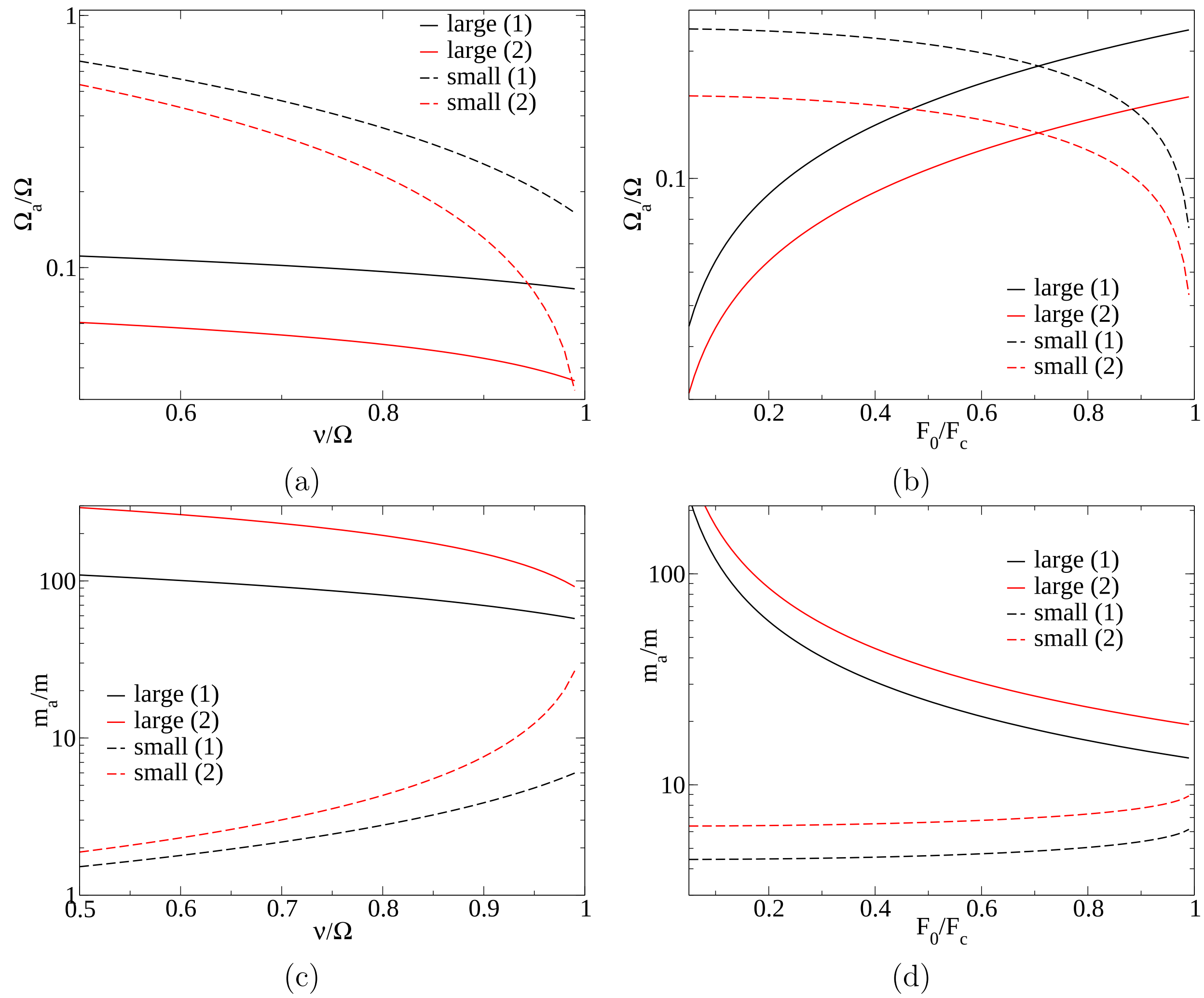

Figure 7.2: Effective mass and frequency of the Duffing oscillator in the proximity of the two attractors.

mating $\hat{H}_I$ by its expectation value we obtain the effective Hamiltonian

$$\hat{H}_q(t) \quad = \quad \hbar w(t)\hat{\sigma}_z + \hbar\mathfrak{d}_0\hat{\sigma}_x \tag{7.36}$$

where $w(t) = w_0 + m\Delta^2\hat{\sigma}_z\langle\hat{x}^2(t)\rangle/(2\hbar)$. A relaxation rate from this environment can be obtained in a Bloch-Redfield fashion similar to previous calculation

Chapter 8

Optimal control of a qubit coupled to a two-level fluctuator

A central challenge for implementing quantum computing in the solid state is decoupling the qubits from the intrinsic noise of the material. We investigate the implementation of quantum gates for a paradigmatic model, a single qubit coupled to a two-level system exposed to a heat bath. For this open system, an optimal control algorithm is applied in the search for the best pulse to achieve the desired gate. We show and explain that next to the known optimal bias point of this model, there are optimal shapes which refocus unwanted terms in the Hamiltonian. We study the limitations of control set by the decoherence properties, which go beyond a simple random telegraph noise model. This can lead to a significant improvement of quantum operations in hostile environments.

Parts of this chaper have been submitted to *Physical Review Letters* and are currently under review. The work presented has been done in collaboration with P. Rebentrost, T. Schulte-Herbrüggen and F. K. Wilhelm

8.1 Introduction

Devices based on Josephson junctions are a promising class of candidates for the practical realization of scalable quantum computers. Due to their mesoscopic dimensions, these systems suffer from decoherence resulting from a large number of environmental degrees of freedom. Previous chapters have focused on the measurement of a superconducting qubit, and the detailed description of the decoherence originating in its measurement circuitry. This type of noise originates in electromagnetic noise produced by macroscopic systems and can be modeled by oscillator baths. The qubit itself, in the absence of a detector, was assumed to be a coherent two level system, obeying the unitary laws of quantum mechanics.

However, it has been experimentally demonstrated that the (amorphous) tunnel barrier of a Josephson junction can host a number of two-level fluctuators [191]. The number of such fluctuators depends on the junction dimensions, fabrication, material etc. Futher examples of few-level noise origins are background charges, trapped in the substrate of the qubit setup which can hop between a charged and an empty trap [192], or trapped fluxes in superconducting devices. They are an intrinsic source of decoherence to qubits based on the Josephson effect and produce a low-frequency noise. The origin and nature of the flux noise remains subject of investigation [193]. A different system i. e. a nitrogen vacancy center in diamond (the qubit), coupled to a proximal electronic spin (the fluctuator) [51, 194] can be described by a model similar to the one presented in the following for charge/flux qubits subject to charge/flux noise.

As explained by the Dutta-Horn model [195, 196] the superposition of randomly flipping two level fluctuators (TLFs) results in $1/f$ noise. Compared to e. g. external decoherence sources, which can be engineered by usual cooling or shielding techniques, the intrinsic slow noise originating from TFLs is harder to avoid. A number of methods, such as dynamical decoupling [197, 198] or the optimum working point strategy [53, 107, 199] have been suggested.

The optimal working point strategies [200] rely on keeping the qubit at a degeneracy point where the dependence of its energy levels on external parameters (flux for the flux qubit and charge for the charge qubit) is minimal. There the qubit is insensitive (at least in the first order) to fluctuations in external control parameters. Thus, the sensitivity to noise in these external parameters can be minimized, but remains limited by $1/f$ noise [159].

In search for even better strategies, the numerical methods of optimal control may prove useful. Within this approach, taking the effects of a hostile environment into account can significantly contribute to expanding the limits of quantum control for solid state systems.

In this chapter we present a model which takes into account the influence of a randomly flipping two level fluctuator on the qubit. Under these conditions, the optimal control theory is applied in search for the best pulse to achieve a Z gate.

We focus on a qubit coupled to a single TLF, a situation achievable in small, clean samples, where the noise originating from a single dominating fluctuator [107, 192] can be resolved. The noise from TFLs can no longer be modeled by a bosonic bath but the source of the random flipping of the TLF can be assumed to be an Ohmic heath bath.

We treat both two level systems as a reduced quantum system exposed to the heath bath by means of the usual Born-Markov master equation. After averaging over the TLF, the qubit experiences a complex environment leading to non-Markovian qubit dynamics and non-Gaussian noise.

8.2 Decoherence model

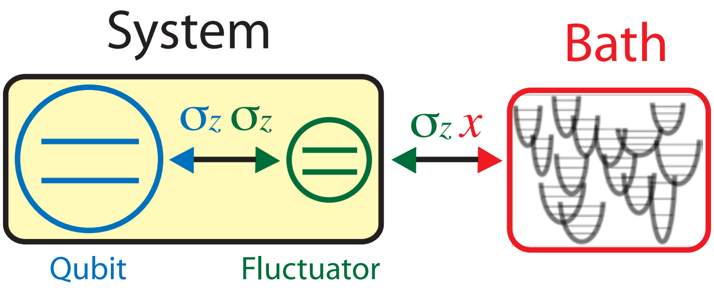

Figure 8.1: Illustration of the coupled system qubit-fluctuator-bath.

We specifically model a qubit coupled to a single TLF, see Fig. 8.1, by $\hat{H} = \hat{H}_S + \hat{H}_I + \hat{H}_B$. $\hat{H}_S$ consists of the qubit and the coupled two-state system, i.e.

$$\hat{H}_S \quad = \quad E_1(t)\hat{\sigma}_z + \Delta\hat{\sigma}_x + E_2\hat{\tau}_z + \Lambda\hat{\sigma}_z\hat{\tau}_z. \tag{8.1}$$

$\hat{\sigma}_i$ and $\hat{\tau}_i$ are the usual Pauli matrices operating in qubit and fluctuator Hilbert space respectively. The initial state is factorized

$$\hat{\rho}_S \quad = \quad \hat{\rho}_{\mathrm{q}} \otimes \hat{\rho}_{\mathrm{TLF}}, \quad \hat{\rho}(0) = \hat{\rho}_S(0) \otimes \hat{\rho}_B(0). \tag{8.2}$$

$E_1(t)$ is time-dependent and serves as an external control. The source of decoherence is the coupling of the fluctuator to the heat bath, which leads to incoherent transitions between the fluctuator eigenstates,

$$\hat{H}_I = \sum_i \lambda_i(\hat{\tau}^+\hat{b}_i + \hat{\tau}^-\hat{b}_i^\dagger), \quad \hat{H}_B = \sum_i \hbar\omega_i\hat{b}_i^\dagger\hat{b}_i. \tag{8.3}$$

Here $\hat{\tau}^\pm$ are the raising and lowering operators of the TLF. We introduce an Ohmic bath spectrum $J(\omega) = \sum_i \lambda_i^2\delta(\omega-\omega_i) = \kappa\omega\Theta(\omega-\omega_c)$ containing the couplings λ_i, the dimensionless damping κ, and a high frequency cutoff ω_c. The usual Born-Markov master equation for the reduced system, valid at finite temperatures $k_BT \gg \hbar\kappa$ and times $t \gg 1/\omega_c$ reads

$$\dot{\hat{\rho}}_S(t) \quad = \quad \frac{1}{\mathrm{i}\hbar}\left[\hat{H}_S, \hat{\rho}_S(t)\right] - \frac{1}{\hbar^2}\int_0^t dt' \mathrm{Tr}_B\left[\hat{H}_I, \left[\hat{H}_I(t, t-t'), \hat{\rho}_S(t) \otimes \hat{\rho}_B(0)\right]\right],$$

We are mostly interested in the qubit evolution in the limit of slow TLF flipping. We arrive at the equation

$$\dot{\hat{\rho}}_S(t) = \frac{1}{\mathrm{i}\hbar}[\hat{H}_S, \hat{\rho}_S(t)] + [\hat{\tau}^+, \hat{\Sigma}_1^-\hat{\rho}_S(t)] + [\hat{\tau}^-, \hat{\Sigma}_0^+\hat{\rho}_S(t)] - [\hat{\tau}^-, \hat{\rho}_S(t)\hat{\Sigma}_1^+] - [\hat{\tau}^+, \hat{\rho}_S(t)\hat{\Sigma}_0^-], \tag{8.4}$$

with the different rate tensors ($s = 0, 1$)

$$\hat{\Sigma}_s^{\pm} = \frac{1}{(\mathbb{i}\hbar)^2} \int_0^{\infty} dt' \int_0^{\infty} d\omega J(\omega) \left(n(\omega) + s\right) \mathbb{e}^{\pm \mathbb{i}\omega t'} \hat{\tau}^{\pm}(t'). \tag{8.5}$$

Here, $n(\omega)$ is the Bose function. The rate tensors depend explicitly on the control $E_1(t)$ due to the interaction representation of the operators $\hat{\tau}^{\pm}$ in Eq. (8.5). The time dependence of $\hat{H}_I(t, t')$, as shown in Appendix A yields

$$\tau^{\pm}(t) = \tau^{\pm} \otimes \hat{O}^{\pm}(t), \tag{8.6}$$

where $O^{\pm}(t)$ is a time-dependent operator in the Hilbert space of the qubit

$$\begin{aligned} \langle \sigma | \hat{O}^{\pm}(t) | \sigma' \rangle &= \sum_{i=1}^{4} c_{i\pm}^{\{\sigma,\sigma'\}} \mathbb{e}^{\mathbb{i}t\Omega_i}, \quad \sigma, \sigma' \in \{\uparrow, \downarrow\}, && (8.7) \\ \hbar\Omega_i &= \pm\sqrt{\Delta^2 + (\Lambda - E_1)^2} \pm \sqrt{\Delta^2 + (\Lambda + E_1)^2} - 2E_2. && (8.8) \end{aligned}$$

The coefficients c_i have analytic, but rather lengthy expressions. Thus, the Bosonic environment is sampled at the frequencies of the the qubit-TLF coupled system, making the operators $\hat{\Sigma}_s^{\pm}$ dependent also on the qubit energy E_1. Since tracing out the TLF at this stage would lead to an intricate non-Markovian master equation, we treat the qubit-TLF interactions exactly, i. e. the rate tensors act on the combined qubit-TLF system. Relaxation and dephasing will eventually bring the initial state into a classical mixture of eigenstates of $\hat{H}_S$ with thermal weights.

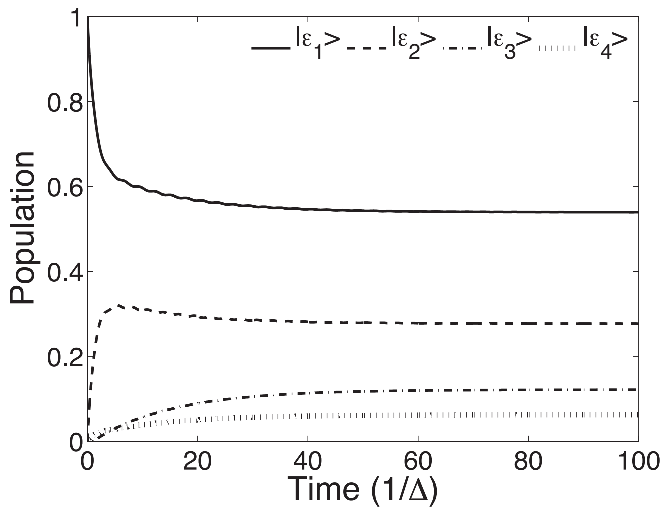

Figure 8.2: Typical behavior of relaxation in the coupled qubit⊗TLF system. ε_i denote the eigenstates of the Hamiltonian $\hat{H}_S$. Image from Ref. [201]

Our model goes far beyond a simple random telegraph noise (RTN) model, which describes a TLF randomly jumping between its two states [198], and captures the correlations between qubit and TLF [104, 202]. Still, as a way to characterize the system, it is useful to introduce the parameters of the RTN which would result for $\Lambda \to 0$ from Eq. (8.4). The

TLF flipping rate thus obtained is $\gamma = 2\kappa E_2 \coth(E_2/T)$, the sum of the excitation and relaxation rate. Thus the effective qubit Hamiltonian in this limit is

$$\hat{H}_{\mathrm{q}}^{\mathrm{eff}} = E_1\hat{\sigma}_z + \Delta\hat{\sigma}_x + \sigma_z F(t)\Lambda\hat{\tau}_z(t), \tag{8.9}$$

with the random force $F(t)$ [203] given by the randomly flipping fluctuator $F(t) = \Lambda\hat{\tau}_z(t)$. The Fourier transformed correlator of the random force $\langle F(t)F(0)\rangle$ gives the two-point noise spectrum of random telegraph noise

$$S(\omega) = \int_{-\infty}^{\infty} dt\; \mathrm{e}^{-\mathrm{i}\omega t}\Lambda^2\langle\tau_z(t)\tau_z(0)\rangle_{\mathrm{eq}} = \Lambda^2\frac{\gamma}{\omega^2+\gamma^2}. \tag{8.10}$$

This is the Fourier transform of the interaction representation of τ_z assuming the bath in equilibrium. In this limit, Eq. (8.4), yields the qubit relaxation and dephasing rates $1/T_1 = S(2E)\Delta^2/E^2$ and $1/T_2 = 1/2T_1 + S(0)E_1^2/E^2$ with $E = \sqrt{\Delta^2+E_1^2}$. For our Hamiltonian, there is no entanglement between qubit and the TLF if the latter is in an incoherent mixture of τ_z eigenstates. It has been shown in [53], that qubit coherence can be protected at the optimum working point by keeping $|E_1| \ll \Delta$ during all manipulations. In that case, pure dephasing is ruled out and $1/T_1$-relaxation is suppressed as $S(2\Delta) \simeq \Lambda^2/2\Delta$ for $2\Delta \gg \gamma$.

8.3 Optimal control and results

Optimal control theory (OCT) represents strategies for maximizing a performance measure as the state of a dynamic system evolves. The goal is to find a time-dependent control variable that drives the considered dynamical system from its initial to its final state, optimizing the performance measure at the same time. As mathematical theory, OCT dates back to the late 1950s, starting with Pontryagin's maximum principle [204]. In physics and chemistry, due to techniques recently developed in the shaping of laser fields [205], the control of chemical reactions became possible. In the field of quantum computing, the theory of optimal control finds a natural application in the manipulation of qubits, necessary for the achievement of quantum gates.

In this chapter we focus on the optimization of a single qubit Z gate. Thus, the goal is to find a time dependent control pulse $E_1(t)$, $t \in (0, t_{\mathrm{g}})$ such that the time evolution of the system, described by the unitary operator

$$\hat{U}(t_{\mathrm{g}}) = \mathcal{T}\exp\left(\int_0^{t_{\mathrm{g}}} \frac{\hat{H}(t)}{\mathrm{i}\hbar}dt\right), \tag{8.11}$$

induces a Z gate to the reduced system of the qubit at the end of the gate time t_{g}

$$\mathrm{Tr}_{B+\mathrm{TFL}}\left\{\hat{U}(t_{\mathrm{g}})\hat{\rho}(0)\hat{U}^\dagger(t_{\mathrm{g}})\right\} = \hat{\sigma}_z\hat{\rho}_{\mathrm{q}}(0)\hat{\sigma}_z. \tag{8.12}$$

The closed systems GRAPE (gradient ascent pulse engineering) algorithm [206] has proven useful in coupled Josephson devices already [207]. It was recently extended to open systems in the strictly Markovian domain [208]. Using the model presented in the previous section, this method has been generalized [209] to include the complex environment consisting of the TFL and leading to non-Markovian qubit dynamics and non-Gaussian noise. For the optimization the evolution of the reduced system Eq. (8.4) has been employed, tracing out the TLF at the end. The model of a qubit coupled to a TFL has been used by P. Rebentrost et al. to implement an optimal control scheme for the qubit. This research is focused on finding the optimal external control pulse for the noisy qubit, that achieves a Z gate. The main achievements of this work are briefly listed below while the complete mathematical formulation of the control problem and a more detailed discussion can be found in Refs. [201, 209].

Fig. 8.3 (top) shows the accessible gate performance as a function of the duration t_g of the gate. Excellent gate performance can be achieved for pulse time $t_g \gtrsim \pi/\Delta$. This corresponds to the static $\Delta\sigma_x$ inducing at least a full loop around the Bloch sphere, hence removing unwanted free evolution. Indeed, we see on the Bloch sphere in Fig. 8.4 that at $t_g = 3.375/\Delta$, the pulse consists of a quarter z rotation, a full loop around x, and the second quarter of the z-rotation leading to the total half rotation around z necessary for the Z gate. At shorter times, the pulses cannot use the physical resource provided by the drift to refocus the qubit. At longer times the gate performance mildly deteriorates, depending on the value of κ. This indicates that the optimal pulses are essentially limited by T_1 processes at the optimal working point. By explicitly including the non-unitary evolution of the qubit into the optimization process, this approach has demonstrated an improvement on gate error, compared to naive approaches such as Rabi pulses. Fig. 8.3 (bottom) demonstrates an improvement of around one order of magnitude over conventional Rabi pulses. Fig. 8.5 gives an analysis of the gate error dependence on the bath parameters. It shows a non-monotonic dependence of the gate error obtained with the optimized pulse on the TLF flipping rate γ. At low flipping rate the error increases with increasing γ, accounting for the increasing probability for the TLF to flip at a random time during the evolution. For a high flipping rate, the non-monotonic behavior is explained by the physics of motional narrowing. This limits the low frequency noise and hence the pure dephasing to $S(\omega < \gamma) = \Lambda^2/\gamma$ which vanishes for $\gamma \to \infty$. The high-γ part of the error is described by a law $c+d/\gamma$. The finite limiting value c captures the residual decoherence which occurs even though the RTN model Eq. (8.10) suggests absence of noise.

8.4 Conclusion

We have investigated an important model for decoherence in solid-state systems, a qubit coupled to a two-level fluctuator which itself is coupled to a heat bath. Our study is the first to exploit the explicit dynamics of a complex non-Markovian environment in optimal control of open systems for implementing quantum gates. For a wide range of parameters, we have identified self-refocusing effects, which are usually only visible at specific optimal pulse durations but can now be achieved more robustly. Both for fast and slow flipping of the TLF high-fidelity control can be achieved.

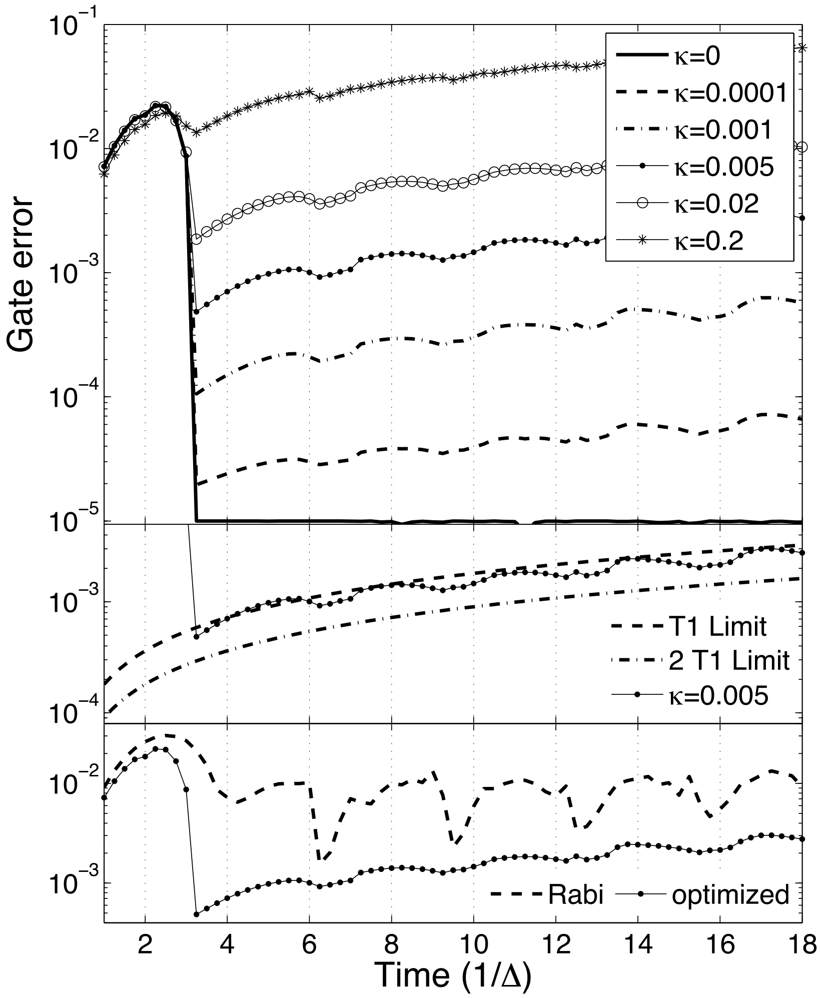

Figure 8.3: Top: gate error for optimal Z-gate pulses with different values of κ. There is a periodic sequence of minima around $t_n = \pi/\Delta$. Middle: the gate error of optimized pulses approaches a limit set by T_1 and $2T_1$ as shown with $\kappa = 0.005$. Bottom: optimized pulses reduce the error rate by approximately one order of magnitude compared to Rabi pulses for $\kappa = 0.005$. In all panels the system parameters are $E_2 = 0.1\Delta$, $\Lambda = 0.1\Delta$ and $T = 0.2\Delta$.

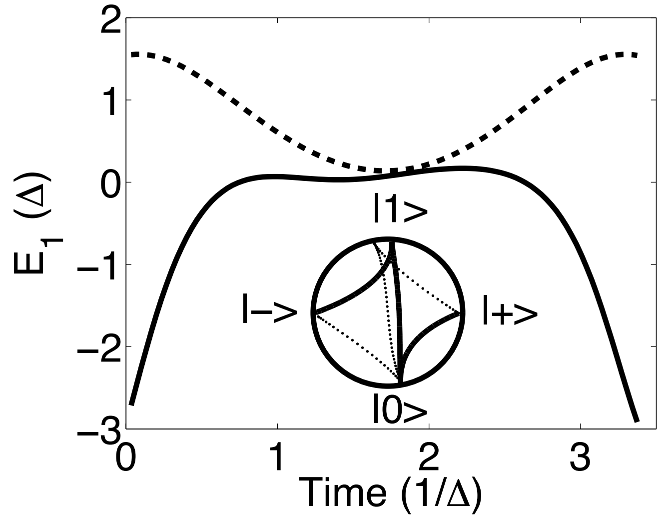

Figure 8.4: Rabi (- -) and optimized pulse (—) at $t_g = 3.375/\Delta$ and $\kappa = 0.05$. Inset shows the evolution of initial state $\rho = |+\rangle\langle+|$, $|\pm\rangle = (|0\rangle \pm |1\rangle)/\sqrt{2}$ on the Bloch sphere under these pulses. $E_2 = 0.1\Delta$, $\Lambda = 0.1\Delta$, $T = 0.2\Delta$.

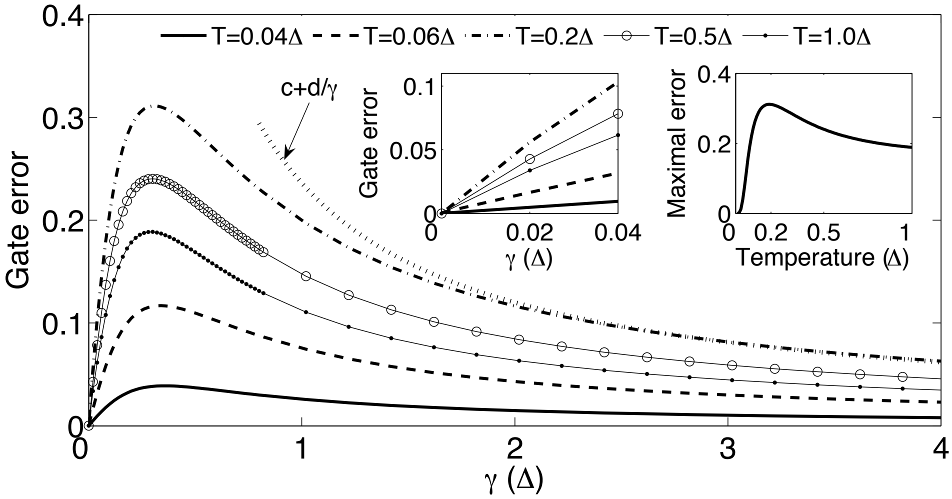

Figure 8.5: Gate error versus TLF rate γ for various temperatures for a long optimized pulse ($t_g = 60/\Delta$, $E_2 = 0.1\Delta$ and $\Lambda = 0.1\Delta$). A high γ fit with $c + d/\gamma$ is also pictured. The left inset is a magnification of the low γ part of the main plot and reveals the linear behaviour. The right inset shows the maximum of the curves versus temperature.

Conclusion

This thesis investigates the decoherence of solid-state devices with application as quantum bits. It consists of series of studies of different qubit measurement protocols, describing the backaction of the measurement onto the measured system and the dynamics of the detector. Insight into the internal working of the Josephson bifurcation amplifier (JBA), a promising candidate for a superconducting qubit detector is provided. Moreover, the optimal control theory is applied to a qubit subject to decoherence from a two-level fluctuator.

Chapter 3 studies a qubit coupled arbitrarily strongly to a nonlinear, non-Markovian environment using a phase-space method. This enables a theoretical description of the dispersive readout protocol of Ref. [1]. Here the qubit is coupled to a complex environment (weakly damped harmonic oscillator) with a quadratic coupling. The prominent degree of freedom of the environment, i. e. the main oscillator, is considered as part of the reduced quantum mechanical system and its dynamics is explicitly solved. In this chapter new measurement protocols are proposed, that make explicit use of the strong coupling between qubit and detector. The measurement and decoherence times are compared and parameter regimes where single shot, quasi-instantaneous measurement could be performed are identified.

Chapter 4 presents a concise theory of the dephasing of a qubit coupled dispersively to a damped oscillator, spanning both strong and weak coupling regimes. It discusses the dominating decoherence mechanism at weak qubit-oscillator coupling, where the linewidth of the damped oscillator plays the main role, analogous to the Purcell effect. At strong qubit-oscillator coupling a qualitatively different behavior of the qubit dephasing is identified and discussed in terms of the onset of the qubit-oscillator dressed states. A criterion delimitating the parameter range at which these processes dominate the qubit dephasing is provided.

Chapter 5 investigates a non-QND readout scheme which can induce a close to QND backaction on the qubit, despite arbitrarily strong interaction with the environment, provided that the interaction time is very short, i. e. the measurement is quasi-instantaneous. The readout scheme proposed here consists of two steps. In the first step the qubit information is transferred into an damped oscillator. In the second step this oscillator is read out. The relaxation of the qubit has been described in the first order in time. The readout time for the oscillator is restricted only by the ring-down of the two possible oscillations of its momentum. The results indicate the possibility of a fast, QND-like, single shot readout.

Chapter 6 focuses on the internal dynamics of a strongly driven Josephson junction. It investigates the quantum phenomenon of macroscopic dynamical tunneling and compares this process with the classical activation over the barrier using the mean first passage time approach. The results suggest that dynamical tunneling can be singled out from the background of activation processes. An experiment realizable within existing technology to demonstrate dynamical tunneling is being proposed.

Chapter 7 describes the relaxation of the qubit in contact with the JBA. We investigate this under the assumption that the Duffing oscillator remains trapped in one of its attractors. A scenario where the oscillator provides an energy "bottleneck" is studied. The resulting relaxation rate is interpreted in terms of the fluctuations around the attractors, induced by the JBA's coupling with an Ohmic environment.

Chapter 8 describes an important model for decoherence in solid-state systems, a qubit coupled to a two-level fluctuator which itself is coupled to a heat bath. This study exploits the explicit dynamics of a complex non-Markovian environment in an optimal control scheme of open systems for implementing quantum gates. Self-refocusing effects, visible at specific optimal pulse durations have been identified. Both for fast and slow flipping of the TLF high-fidelity control can be achieved. The full qubit-fluctuator correlations, embodied in the Hamiltonian are an important influence on the result.

Appendix A

System-bath model

In this section we give a derivation of the Born-Markov master equation for the reduced density matrix $\hat{\rho}_S(t) = \mathrm{Tr}_B \rho(t)$ of a system S coupled linearly to a bath B of harmonic oscillators. This is described by the Hamiltonian $\hat{H} = \hat{H}_S + \hat{H}_I + \hat{H}_B$. We have the free evolution operator

$$\hat{U}_t \;\; = \;\; \hat{\mathcal{T}} \exp\left(\int_0^t dt' \frac{\hat{H}_S + \hat{H}_B}{\mathbb{i}\hbar} \right). \tag{A.1}$$

In the interaction picture each operator $\hat{A}$ becomes $\hat{A}^I(t) = \hat{U}_t^\dagger \hat{A} \hat{U}_t$, and the Schrödinger equation reads

$$|\Psi^I(t)\rangle = U_t^\dagger |\Psi(t)\rangle, \qquad \hat{\rho}^I(t) = \hat{U}_t^\dagger \hat{\rho}(t) \hat{U}_t, \tag{A.2}$$

$$\mathbb{i}\hbar |\dot{\Psi}^I(t)\rangle = \hat{H}_I^I |\Psi^I(t)\rangle, \qquad \dot{\hat{\rho}}^I(t) = \frac{1}{\mathbb{i}\hbar}[\hat{H}_I^I(t), \hat{\rho}^I(t)], \tag{A.3}$$

with the formal solution

$$\hat{\rho}^I(t) \;\; = \;\; \hat{\rho}^I(0) + \frac{1}{\mathbb{i}\hbar} \int_0^t dt' [\hat{H}_I^I(t'), \hat{\rho}^I(t')]. \tag{A.4}$$

Up to the second order in the coupling Hamiltonian this becomes

$$\dot{\hat{\rho}}^I(t) \;\; = \;\; \frac{1}{\mathbb{i}\hbar}[\hat{H}_I^I(t), \hat{\rho}(0)] + \frac{1}{(\mathbb{i}\hbar)^2} \int_0^t dt' [\hat{H}_I^I(t), [\hat{H}_I^I(t'), \hat{\rho}(0)]] + \mathcal{O}(H_I^3). \tag{A.5}$$

We are interested in the dynamics of the reduced reduced system described by $\hat{\rho}_S = \mathrm{Tr}_B \hat{\rho}$ and in the interaction picture by $\hat{\rho}_S^I = \mathrm{Tr}_B \hat{\rho}^I$

$$\dot{\hat{\rho}}_S^I(t) \;\; = \;\; \frac{1}{\mathbb{i}\hbar} \mathrm{Tr}_B [\hat{H}_I^I(t), \hat{\rho}^I(t)], \tag{A.6}$$

$$\hat{\rho}_S^I(t) \;\; = \;\; \hat{\rho}_S^I(0) + \frac{1}{\mathbb{i}\hbar} \int_0^t dt' \; \mathrm{Tr}_B [\hat{H}_I^I(t'), \hat{\rho}^I(t')], \tag{A.7}$$

$$\dot{\hat{\rho}}_S^I(t) \;\; = \;\; \frac{1}{\mathbb{i}\hbar} \mathrm{Tr}_B [\hat{H}_I^I(t), \hat{\rho}(0)] + \frac{1}{(\mathbb{i}\hbar)^2} \int_0^t dt' \mathrm{Tr}_B [\hat{H}_I^I(t), [\hat{H}_I^I(t'), \hat{\rho}(0)]] + \mathcal{O}(H_I^3). \tag{A.8}$$

The exact equation of motion for the reduced density matrix in Schrödinger picture reads

$$\begin{aligned}\dot{\hat{\rho}}_S(t) &= \mathrm{Tr}_B\left\{\partial_t\left(\hat{U}_t\hat{\rho}^I(t)\hat{U}_t^\dagger\right)\right\} = \mathrm{Tr}_B\left\{\frac{1}{\mathbb{i}\hbar}[\hat{H}_S+\hat{H}_B,\hat{\rho}(t)] + \hat{U}_t\dot{\hat{\rho}}^I(t)\hat{U}_t^\dagger\right\} \\ &= \frac{1}{\mathbb{i}\hbar}\mathrm{Tr}_B[\hat{H}_S+\hat{H}_B,\hat{\rho}(t)] + \frac{1}{\mathbb{i}\hbar}\mathrm{Tr}_B\left\{\hat{U}_t[\hat{H}_I^I(t),\hat{\rho}^I(t)]\hat{U}_t^\dagger\right\}, \end{aligned} \tag{A.9}$$

which can be rewritten using Eq. (A.4) as follows

$$\begin{aligned}\dot{\hat{\rho}}_S(t) &= \frac{1}{\mathbb{i}\hbar}\mathrm{Tr}_B[\hat{H}_S+\hat{H}_B,\hat{\rho}(t)] + \frac{1}{\mathbb{i}\hbar}\mathrm{Tr}_B\left\{\hat{U}_t[\hat{H}_I^I(t),\hat{\rho}(0)]\hat{U}_t^\dagger\right\} \\ &+ \frac{1}{(\mathbb{i}\hbar)^2}\int_0^t dt'\mathrm{Tr}_B\left\{\hat{U}_t[\hat{H}_I^I(t),[\hat{H}_I^I(t'),\hat{\rho}^I(t')]]\hat{U}_t^\dagger\right\}. \end{aligned} \tag{A.10}$$

Eq. (A.10) is still exact. To approximate this equation up to second order in the interaction Hamiltonian $\hat{H}_I$ we make the ansatz

$$\hat{\rho}^I(t) = \hat{\rho}_S^I(t)\hat{\rho}_B(0) + \tilde{\rho}(t), \tag{A.11}$$

where $\tilde{\rho}(0)=0$ since we assume a system-bath factorized initial condition $\hat{\rho}(0)=\hat{\rho}_S(0)\hat{\rho}_B(0)$. It follows from Eqs. (A.5,A.8) that the time evolution for the nonseparable part of the density matrix $\tilde{\rho}$ is given by

$$\begin{aligned}\dot{\tilde{\rho}}(t) &= \dot{\hat{\rho}}^I(t) - \dot{\hat{\rho}}_S^I(t)\hat{\rho}_B(0) \\ &= \frac{1}{\mathbb{i}\hbar}[\hat{H}_I^I(t),\hat{\rho}(0)] + \frac{1}{(\mathbb{i}\hbar)^2}\int_0^t dt'[\hat{H}_I^I(t),[\hat{H}_I^I(t'),\hat{\rho}(0)]] \\ &- \frac{\hat{\rho}_B(0)}{\mathbb{i}\hbar}\mathrm{Tr}_B[\hat{H}_I^I(t),\hat{\rho}(0)] - \frac{\hat{\rho}_B(0)}{(\mathbb{i}\hbar)^2}\int_0^t dt'\mathrm{Tr}_B[\hat{H}_I^I(t),[\hat{H}_I^I(t'),\hat{\rho}(0)]] + \mathcal{O}(H_I^3). \end{aligned} \tag{A.12}$$

This equation can be integrated and we obtain

$$\begin{aligned}\tilde{\rho}(t) &= \frac{1}{\mathbb{i}\hbar}\int_0^t dt'\left[\left(\hat{H}_I^I(t') - \langle\hat{H}_I^I(t')\rangle_{B0}\right),\hat{\rho}_S(0)\right] - \frac{1}{\hbar^2}\int_0^t\int_0^{t'} dt'dt"[\hat{H}_I^I(t'),[\hat{H}_I^I(t"),\hat{\rho}(0)]] \\ &- \frac{\hat{\rho}_B(0)}{(\mathbb{i}\hbar)^2}\int_0^t\int_0^{t'} dt'dt"\mathrm{Tr}_B[\hat{H}_I^I(t'),[\hat{H}_I^I(t"),\hat{\rho}(0)]] + \mathcal{O}(H_I^3), \end{aligned} \tag{A.13}$$

It follows from Eq. (A.13) that $\mathrm{Tr}_B\tilde{\rho}(t) = 0 + \mathcal{O}(H_I^3)$. Assuming a linear coupling $\hat{H}_I = \sum_i \hat{S}_i\hat{B}_i$ with $\hat{S}_i \in \mathbb{S}$ and $\hat{B}_i \in \mathbb{B}$ we obtain from Eq. (A.13) that $\hat{U}_t\tilde{\rho}\hat{U}_t^\dagger = \sum_i \hat{\mathcal{S}}_i\hat{\mathcal{B}}_i + \mathcal{O}(\hat{H}_I^3)$ with $\hat{\mathcal{S}}_i \in \mathbb{S}$ and $\hat{\mathcal{B}}_i \in \mathbb{B}$. Using this observation and noting that

$$\mathrm{Tr}_B[\hat{H}_S,\hat{U}_t\tilde{\rho}\hat{U}_t^\dagger] = [\hat{H}_S,\mathrm{Tr}_B\{\hat{U}_t\tilde{\rho}\hat{U}_t^\dagger\}] = [\hat{H}_S,\mathrm{Tr}_B\tilde{\rho}] = 0, \tag{A.14}$$

$$\mathrm{Tr}_B[\hat{H}_B,\hat{\mathcal{S}}_i\hat{\mathcal{B}}_i] = \hat{\mathcal{S}}_i\mathrm{Tr}_B[\hat{H}_B,\hat{\mathcal{B}}_i] = 0, \tag{A.15}$$

$$\mathrm{Tr}_B[\hat{H}_S,\hat{\rho}_S(t)\hat{\rho}_B(0)] = [\hat{H}_S,\hat{\rho}_S(t)]\mathrm{Tr}_B\hat{\rho}_B(0) = [\hat{H}_S,\hat{\rho}_S(t)], \tag{A.16}$$

$$\mathrm{Tr}_B[\hat{H}_B,\hat{\rho}_S(t)\hat{\rho}_B(0)] = \mathrm{Tr}_B[\hat{H}_B,\hat{\rho}_B(0)]\hat{\rho}_S(t) = 0, \tag{A.17}$$

one can show that from the first commutator in Eq. (A.10) remains only $[\hat{H}_S, \hat{\rho}_S(t)]$.

Observing that

$$\mathrm{Tr}_B\{\hat{U}_t\hat{U}_t^\dagger \hat{H}_I \hat{U}_t \hat{\rho}(0)\hat{U}_t^\dagger - \hat{U}_t\hat{\rho}(0)\hat{U}_t^\dagger \hat{H}_I \hat{U}_t \hat{U}_t^\dagger\} = \mathrm{Tr}_B[\hat{H}_I, \hat{U}_t\hat{\rho}(0)\hat{U}_t^\dagger], \tag{A.18}$$

and assuming unbiased noise

$$\langle \hat{H}_I \rangle = 0 \tag{A.19}$$

we show that also the second commutator in Eq. (A.10) vanishes. Thus, for linear $\hat{H}_I$ Eq. (A.19) implies that the commutator (A.18) vanishes. As one can easily see from Eq. (A.13), $\tilde{\rho}$ is of the order $\hat{H}_I^2$, i.e. we need not take it into account in the double commutator in Eq. (A.10). We expand this commutator as follows

$$\begin{aligned}
&\hat{U}_t\,[\hat{H}_I^I(t), [\hat{H}_I^I(t'), \hat{\rho}_S^I(t')\hat{\rho}_B(0)]]\hat{U}_t^\dagger = \hat{U}_t\hat{U}_t^\dagger \hat{H}_I \hat{U}_t \hat{U}_{t'}^\dagger \hat{H}_I \hat{U}_{t'} \hat{\rho}_S^I(t')\hat{\rho}_B(0)\hat{U}_t^\dagger \\
-\;\; &\hat{U}_t\hat{U}_{t'}^\dagger \hat{H}_I \hat{U}_{t'} \hat{\rho}_S^I(t')\hat{\rho}_B(0)\hat{U}_t^\dagger \hat{H}_I \hat{U}_t \hat{U}_t^\dagger - \hat{U}_t\hat{U}_t^\dagger \hat{H}_I \hat{U}_t \hat{\rho}_S^I(t')\hat{\rho}_B(0)\hat{U}_{t'}^\dagger \hat{H}_I \hat{U}_{t'} \hat{U}_t^\dagger \\
+\;\; &\hat{U}_t\hat{\rho}_S^I(t')\hat{\rho}_B(0)\hat{U}_{t'}^\dagger H_I \hat{U}_{t'} \hat{U}_t^\dagger \hat{H}_I \hat{U}_t \hat{U}_t^\dagger,
\end{aligned} \tag{A.20}$$

and after appropriate permutations under the trace we obtain

$$\mathrm{Tr}_B\left\{\hat{U}_t[\hat{H}_I^I(t), [\hat{H}_I^I(t'), \hat{\rho}_S^I(t')\hat{\rho}_B(0)]]\hat{U}_t^\dagger\right\} = \mathrm{Tr}_B\left\{[\hat{H}_I, [\hat{H}_I(t,t'), \hat{U}_t\hat{\rho}_S^I(t')\hat{\rho}_B(0)\hat{U}_t^\dagger]]\right\}, \tag{A.21}$$

where $\hat{H}_I(t,t') = \hat{U}_t\hat{U}_{t'}^\dagger \hat{H}_I U_{t'} \hat{U}_t^\dagger$. For the annihilation operator $\hat{b}_i$, associated with one of the bath oscillators of frequency ω_i we have the following time-dependence

$$\begin{aligned}
\hat{b}_i(t,t')|n\rangle &= \hat{U}_{t'}^t \hat{b}_i (U_{t'}^t)^\dagger |n\rangle = \hat{U}_{t'}^t \hat{b}_i \hat{U}_t^{t'} |n\rangle = \hat{U}_{t'}^t \hat{b}_i \mathbb{e}^{-\mathbb{i}\omega_i(n+1/2)(t'-t)} |n\rangle\rangle \\
&= \hat{U}_{t'}^t \mathbb{e}^{-\mathbb{i}\omega_i(n+1/2)(t'-t)} \sqrt{n}|n-1 = \mathbb{e}^{-\mathbb{i}\omega_i(t'-t)}\sqrt{n}|n-1\rangle = \mathbb{e}^{-\mathbb{i}\omega_i(t'-t)}\hat{b}_i|n\rangle.
\end{aligned} \tag{A.22}$$

After all these considerations Eq. (A.10) becomes

$$\dot{\hat{\rho}}_S(t) = \frac{1}{\mathbb{i}\hbar}[\hat{H}_S, \hat{\rho}_S(t)] + \frac{1}{(\mathbb{i}\hbar)^2}\int_0^t dt' \mathrm{Tr}_B[\hat{H}_I, [\hat{H}_I^I(t,t'), \hat{U}_t\hat{\rho}_S^I(t')\hat{\rho}_B(0)\hat{U}_t^\dagger]] + \mathcal{O}(\hat{H}_I^3). \tag{A.23}$$

At this point one makes the Markov approximation [115] assuming that the bath has so many degrees of freedom that the effects of the interaction with the system dissipate away and do not react back. The bath remains in equilibrium, while the system is damped such that $\dot{\hat{\rho}}_S(t)$ depends only on its present value $\hat{\rho}_S(t)$ (the system loses all memory of its past). Finally, assuming that the correlations in the environment decay fast and after a variable transformation $t" = t - t'$, we can extend the integration to infinity and obtain the standard Born-Markov master equation in the Schrödinger picture

$$\dot{\hat{\rho}}_S(t) = \frac{1}{\mathbb{i}\hbar}[\hat{H}_S, \hat{\rho}_S(t)] + \frac{1}{(\mathbb{i}\hbar)^2}\int_0^\infty dt" \mathrm{Tr}_B[\hat{H}_I, [\hat{H}_I^I(t, t-t"), \rho_S(t)\hat{\rho}_B(0)]]. \tag{A.24}$$

Coupling to the environment

Within the scope of this thesis the coupling to the environment will be linear, having the form

$$\hat{H}_I = \hat{x}\sum \lambda_i \hat{x}_i,\ \hat{H}_I(t,t') = \hat{x}(t,t')\sum \lambda_i \hat{x}_i(t,t'), \tag{A.25}$$

$$\langle \hat{x}_i(t,t')\rangle_{B,eq} = \langle \hat{x}_i(t'-t)\rangle_{B,eq}. \tag{A.26}$$

Written in the second quantization this becomes

$$\hat{H}_I = \hat{x}\sum_i \lambda_i \hat{x}_i = g(\hat{a}+\hat{a}^\dagger)\sum_i g_i\lambda_i(\hat{b}_i+\hat{b}_i^\dagger) = \sum_i \lambda_i g g_i\left(\hat{a}\hat{b}_i^\dagger + \hat{a}^\dagger\hat{b}_i + \mathcal{R}\hat{a}^\dagger\hat{b}_i^\dagger + \mathcal{R}\hat{a}\hat{b}_i\right), \tag{A.27}$$

where for $\mathcal{R}=1$ we have the Hamiltonian Eq. (A.25) while for $\mathcal{R}=0$ the rotating wave approximation (RWA) has been made and

$$g = \sqrt{\frac{\hbar}{2m\Omega}},\ \ g_i = \sqrt{\frac{\hbar}{2m_i\omega_i}}. \tag{A.28}$$

In the following we evaluate the double commutator in the master equation (A.24) using for the bath operators the time evolution calculated in Eq. (A.22) and remembering that the bath remains in thermal equilibrium

$$\begin{aligned}
&\mathrm{Tr}_B[H_I,[H_I(t,t'),\rho_S(t)\rho_B(0)]] = \qquad\qquad (A.29)\\
&\mathrm{Tr}_B\, g^2\sum_i g_i^2\lambda_i^2\Big([(\hat{a}+\mathcal{R}\hat{a}^\dagger)\hat{b}_i^\dagger,[(\hat{a}^\dagger(t,t-t")+\mathcal{R}\hat{a}(t,t-t"))\hat{b}_i \mathrm{e}^{\mathrm{i}\omega_i t"},\hat{\rho}_S(t)\hat{\rho}_B(0)]]\\
&+ \quad [(\hat{a}^\dagger+\mathcal{R}\hat{a})\hat{b}_i,[(\hat{a}(t,t-t")+\mathcal{R}\hat{a}^\dagger(t,t-t"))\hat{b}_i^\dagger \mathrm{e}^{-\mathrm{i}\omega_i t"},\hat{\rho}_S(t)\hat{\rho}_B(0)]]\Big)\\
&= \quad g^2\mathrm{Tr}_B\sum_i g_i^2\lambda_i^2\Big([\hat{a}+\mathcal{R}\hat{a}^\dagger,(\hat{a}^\dagger(t,t-t")+\mathcal{R}\hat{a}(t,t-t"))\hat{\rho}_S(t)]n_i \mathrm{e}^{\mathrm{i}\omega_i t"}\\
&- \quad [\hat{a}+\mathcal{R}\hat{a}^\dagger,\hat{\rho}_S(t)(\hat{a}^\dagger(t,t-t")+\mathcal{R}\hat{a}(t,t-t"))](n_i+1)\mathrm{e}^{\mathrm{i}\omega_i t"}\\
&- \quad [\hat{a}^\dagger+\mathcal{R}\hat{a},(\hat{a}(t,t-t")+\mathcal{R}\hat{a}^\dagger(t,t-t")\hat{\rho}_S(t)](n_i+1)\mathrm{e}^{-\mathrm{i}\omega_i t"}\\
&+ \quad [\hat{a}^\dagger+\mathcal{R}\hat{a},\hat{\rho}_S(t)(\hat{a}(t,t-t")+\mathcal{R}\hat{a}^\dagger(t,t-t")]n_i \mathrm{e}^{-\mathrm{i}\omega_i t"}\Big),
\end{aligned}$$

where n_i is the Bose function for the bath oscillator with frequency ω_i at the environment temperature T

$$n_i = \frac{1}{\mathrm{e}^{\hbar\omega_i/k_BT}-1}. \tag{A.30}$$

The spectral density of the bath [16] is given by

$$J(\omega) = \pi\sum_i \frac{\lambda_i^2}{2m_i\omega_i}\delta(\omega-\omega_i), \tag{A.31}$$

such that

$$\sum_i \frac{\hbar\lambda_i^2}{2m_i\omega_i}f(\omega_i) = \frac{\hbar}{\pi}\int d\omega J(\omega)f(\omega). \tag{A.32}$$

A.1 The quantum regression theorem

A direct consequence of the linearity of master equations such as the one derived in the Born-Markov approximation is that a *quantum regression theorem* (see Ref. [103] and the references therein) can be derived. If, for some operator $\hat{O}$ it holds that

$$\langle \hat{O}(t+\tau) \rangle = \sum_j a_j(\tau) \langle \hat{O}(t) \rangle, \tag{A.33}$$

then the two-time correlation function of the same observable reads

$$\langle \hat{O}(t)\hat{O}(t+\tau) \rangle = \sum_j a_j(\tau) \langle \hat{O}(t)\hat{O}(t)) \rangle. \tag{A.34}$$

Appendix B

Wigner representation

For any operator $\hat{\rho}$ with finite norm (here one uses the trace norm $\parallel \hat{\rho} \parallel = \left(\mathrm{Tr}\left\{\hat{\rho}^\dagger \hat{\rho}\right\}\right)^{1/2}$) has been shown [27] that following representation is possible

$$\hat{\rho} = \frac{1}{\pi} \int d^2\alpha\, \chi(\alpha) \hat{D}(-\alpha). \tag{B.1}$$

For both a thermal state and a coherent state the phase-space function χ has a gaussian shape

$$\chi_{\mathrm{thermal}}(\alpha) = \frac{1}{4\pi} \exp\left(-\frac{|\alpha|^2}{2}(1 + 2n(\Omega)),\right) \tag{B.2}$$

$$\chi_{\mathrm{coherent}}(\alpha) = \frac{1}{4\pi} \exp(-|\lambda|^2 + \lambda\alpha_0^* - \lambda^*\alpha_0), \tag{B.3}$$

where $n(\Omega)$ is the Bose function.

From the phase function χ one can evaluate the expectation value of any observable of the system. Of particular interest are the quadratures x and p. The probability distributions are given by

$$P_p(p_0) = \sqrt{\frac{m\Omega\hbar}{2}} \langle \delta(\hat{p} - p_0) \rangle = 2 \int_{-\infty}^{+\infty} d\alpha_x \chi(\alpha_x) \exp\left(\sqrt{\frac{2}{m\Omega\hbar}} \mathbb{i} p_0 \alpha_x\right), \tag{B.4}$$

$$P_x(x_0) = \sqrt{\frac{\hbar}{2m\Omega}} \langle \delta(\hat{x} - x_0) \rangle = 2 \int_{-\infty}^{+\infty} d\alpha_y \chi(\mathbb{i}\alpha_y) \exp\left(-\sqrt{\frac{2m\Omega}{\hbar}} \mathbb{i} x_0 \alpha_y\right), \tag{B.5}$$

$$\alpha = \alpha_x + \mathbb{i}\alpha_y. \tag{B.6}$$

It follows that

$$\langle \hat{p}^n \rangle(t) = \left(\sqrt{\frac{m\Omega\hbar}{2}}\right)^n \frac{4\pi}{\mathbb{i}^n}(-1)^n(\partial_{\alpha_x})^n \chi(\alpha_x)|_{\alpha_x=0}, \tag{B.7}$$

$$\langle \hat{x}^n \rangle(t) = \left(\sqrt{\frac{\hbar}{2m\Omega}}\right)^n \frac{4\pi}{\mathbb{i}^n}(\partial_{\alpha_y})^n \chi(\mathbb{i}\alpha_y)|_{\alpha_y=0}, \tag{B.8}$$

$$\langle xp \rangle = \frac{\mathbb{i}4\pi\hbar}{2}(\partial^2_{\alpha,\alpha} - \partial^2_{\alpha^*,\alpha^*} - \alpha^*\partial_\alpha - \alpha\partial_{\alpha^*} + \alpha^{*2}/4 - \alpha^2/4 + 1)\chi(\alpha)|_{\alpha=0}. \tag{B.9}$$

If one uses the Wigner representation of a density operator in the master equation outlined in section A one reduces this equation to a partial differential equation for the function $\chi(\alpha, t)$. If the "system" is just a harmonic oscillator, this equation becomes a Fokker-Plank equation [28], which can be easily solved analytically. Usually in this thesis the "system" is a composite system, consisting of a two level system (qubit) coupled in various ways to a harmonic oscillator. The density operator of this system represented in the qubit basis is a 2×2 matrix with elements that are operators in the oscillator Hilbert space. Although not all of these operators have the properties of a density operators, they can usually still be represented by means of the Wigner characteristic function χ.

B.1 Useful relations

For the derivation of the partial differential equations for χ following relations may prove useful.

Using the Baker-Campbell-Hausdorff formula one can rewrite the displacement operator

$$\begin{aligned}\hat{D}(\alpha) &= \exp\left(\alpha\hat{a}^\dagger - \alpha^*\hat{a}\right) = \exp\left(-\frac{|\alpha|^2}{2}\right)\exp\left(\hat{a}^\dagger\alpha\right)\exp\left(-\alpha^*\hat{a}\right) \\ &= \exp\left(\frac{|\alpha|^2}{2}\right)\exp(-\alpha^*\hat{a})\exp(\hat{a}^\dagger\alpha). \end{aligned}\tag{B.10}$$

One can show that following relation holds

$$\hat{D}(\alpha+\beta) = \hat{D}(\alpha)\hat{D}(\beta)\exp\left(\frac{1}{2}(\alpha^*\beta - \alpha\beta^*)\right) \tag{B.11}$$

It can be shown that

$$\hat{D}(-\alpha)\hat{a} = (\hat{a}+\alpha)\,\hat{D}(-\alpha),\;\; \hat{D}(-\alpha)\hat{a}^\dagger = \left(\hat{a}^\dagger + \alpha^*\right)\hat{D}(-\alpha). \tag{B.12}$$

Thus, for some arbitrary function $f(\alpha)$ in the phase-space, we have

$$\hat{a}\int d^2\alpha f(\alpha)\hat{D}(-\alpha) = \int d^2\alpha f(\alpha)\exp\left(\frac{|\alpha|^2}{2}\right)\frac{\partial}{\partial\alpha^*}\exp\left(\alpha^*\hat{a}\right)\exp\left(-\alpha\hat{a}^\dagger\right) \tag{B.13}$$

$$= -\int d^2\alpha\, \mathbb{e}^{\alpha^*\hat{a}}\mathbb{e}^{-\alpha\hat{a}^\dagger}\frac{\partial}{\partial\alpha^*}\left(f(\alpha)\mathbb{e}^{|\alpha|^2/2}\right) = -\int d^2\alpha\,\hat{D}(-\alpha)\left(\frac{\partial}{\partial\alpha^*}+\frac{\alpha}{2}\right)f(\alpha).$$

The derivation involved an integration by parts, and assumed that $\chi(\alpha)$ vanishes for $|\alpha| \to \infty$ which is a legitimate assumption for the situations discussed in this thesis. A similar derivation for the creation operator leads to

$$\begin{aligned}
&\hat{a}^\dagger \int d^2\alpha\, f(\alpha)\hat{D}(-\alpha) = -\int d^2\,\alpha f(\alpha) \exp\left(-\frac{|\alpha|^2}{2}\right) \frac{\partial}{\partial\alpha} \exp\left(-\alpha\hat{a}^\dagger\right) \exp\left(\alpha^*\hat{a}\right) \\
&= \int d^2\alpha\, \mathrm{e}^{-\alpha\hat{a}^\dagger} \mathrm{e}^{\alpha^*\hat{a}} \frac{\partial}{\partial\alpha}\left(f(\alpha)\mathrm{e}^{-|\alpha|^2/2}\right) = \int d^2\alpha\, \hat{D}(-\alpha)\left(\frac{\partial}{\partial\alpha} - \frac{\alpha^*}{2}\right) f(\alpha). \qquad \text{(B.14)}
\end{aligned}$$

Using these equations one can derive similar relations for products of annihilation and creation operators. For our purposes, the second order terms will be sufficient

$$\begin{aligned}
\hat{a}^2 \int d^2\alpha\, f(\alpha)\hat{D}(-\alpha) &= \int d^2\alpha\, \hat{D}(-\alpha)\left(\frac{\partial^2}{(\partial\alpha^*)^2} + \alpha\frac{\partial}{\partial\alpha^*} + \frac{\alpha^2}{4}\right) f(\alpha), \\
\hat{a}^{\dagger 2} \int d^2\alpha\, f(\alpha)\hat{D}(-\alpha) &= \int d^2\alpha\, \hat{D}(-\alpha)\left(\frac{\partial^2}{(\partial\alpha)^2} - \alpha^*\frac{\partial}{\partial\alpha} + \frac{\alpha^{*2}}{4}\right) f(\alpha), \qquad \text{(B.15)} \\
\hat{a}^\dagger\hat{a} \int d^2\alpha\, f(\alpha)\hat{D}(-\alpha) &= \int d^2\alpha\hat{D}(-\alpha)\left(\frac{\alpha^*}{2}\frac{\partial}{\partial\alpha^*} - \frac{\alpha}{2}\frac{\partial}{\partial\alpha} - \frac{1}{2} + \frac{|\alpha|^2}{4} - \frac{\partial^2}{\partial\alpha\partial\alpha^*}\right) f(\alpha).
\end{aligned}$$

Appendix C

Floquet states

As discussed above, the pointer states are those vectors in the Hilbert space that are singled out by decoherence, during a measurement. In this section we are interested in the appropriate pointer states for a driven system, in particular a driven harmonic oscillator. They would represent an appropriate basis to represent the system during its evolution towards equilibrium with the environment.

For a driven harmonic oscillator the Fock states are no longer appropriate pointer states. A promising candidate are the so-called Floquet modes.

We start by considering the Schroedinger equation with a time-dependent Hamiltonian

$$\mathbb{i}\hbar\partial_t \Psi(x,t) = \hat{H}(t)\Psi(x,t), \tag{C.1}$$

where the potential is periodic in time $\hat{V}(\hat{x},t) = \hat{V}(\hat{x},t+T)$. The Floquet-state solutions to this problem has the property

$$\Psi_n(x,t) = \Phi_n(x,t)\exp(-\mathbb{i}E_n t/\hbar), \tag{C.2}$$

where $\Phi_n(x,t)$ is periodic in time

$$\Phi_n(x,t) = \Phi_n(x,t+T), \tag{C.3}$$

end eigenfunction to the operator $\hat{H}(t) - \mathbb{i}\hbar\partial_t$ corresponding to eigenvalue E_n. These eigenvalues can be mapped into a *first Brillouin zone* similar to the case of space-periodic potentials, where $-\hbar\Omega/2 \leq E \leq \hbar\Omega/2$ and $\Omega = 2\pi/T$.

In the case of the driven harmonic oscillator the Floquet modes have an exact analytical expression [16]

$$\Psi_n(x,t) = \varphi_n(x-\xi(t))\exp\left(\frac{\mathbb{i}}{\hbar}\left(m\dot{\xi}(t)(x-\xi(t)) - E_n t + \int_0^t dt'\mathcal{L}(t',\xi(t'),\dot{\xi}(t'))\right)\right) \tag{C.4}$$

where ξ is the classical trajectory of the driven harmonic oscillator and obeys the equation of motion

$$m\ddot{\xi}(t) + m\Omega^2\xi(t) \quad = \quad F(t), \tag{C.5}$$

$\varphi_n(x-\xi(t))$ is the Fock state centered around the classic trajectory $\xi(t)$ and $\mathcal{L}$ is the classical Lagrangian of the driven oscillator

$$\mathcal{L}(t,\xi(t),\dot{\xi}(t)) = \frac{1}{2}m\dot{\xi}^2(t) - \frac{1}{2}m\Omega^2\xi^2(t) + \xi F(t) \tag{C.6}$$

Due to the properties of the Fock states, at each time t the Floquet modes build an orthonormal basis in the Hilbert space of the harmonic oscillator. One can map the Floquet modes onto Fock states by a simple unitary transformation

$$\mathbb{e}^{\mathbb{i}\int_0^t dt'\mathcal{L}(t')/\hbar}\mathbb{e}^{-\mathbb{i}\xi(t)\hat{p}/\hbar}\mathbb{e}^{\mathbb{i}m\dot{\xi}(t)\hat{x}/\hbar}\varphi_n(x) = \Phi_n(x,t). \tag{C.7}$$

We are now interested in the action of a creation/annihilation operator on a Foquet mode, in particular because these operators are usually involved in the coupling of the driven oscillator to an environment. We consider $\hat{U}_t$ the evolution operator for the driven harmonic oscillator, such that $\hat{U}_t\hat{U}^\dagger_{t'}\Psi(x,t') = \Psi(x,t)$. A term that often appears in the derivation of a master equation is $\hat{a}(t,t') = \hat{U}_t\hat{U}^\dagger_{t'}\hat{a}\hat{U}_{t'}\hat{U}^\dagger_t$. We define the annihilation operator $\hat{A}$ for Floquet modes as follows

$$\hat{a} = \hat{A} + \zeta(t) = \sqrt{\frac{m\Omega}{2\hbar}}\left(\hat{x} + \frac{\hbar}{m\Omega}\frac{\partial}{\partial x}\right) \tag{C.8}$$

where $\zeta(t) = \sqrt{m/(2\hbar\Omega)}(\mathbb{i}\dot{\xi}(t) + \Omega\xi(t))$ represents the classical phase-space trajectory (real and imaginary parts corresponds to position and momentum, respectively). One can show that

$$\hat{A}\Psi_n(x,t) = e^{-\mathbb{i}\Omega t}\sqrt{n}\Psi_{n-1}(x,t), \tag{C.9}$$

and also

$$\hat{a}(t,t')\Psi_n(x,t) = \mathbb{e}^{-\mathbb{i}\Omega t'}\sqrt{n}\Psi_{n-1}(x,t) + \zeta(t')\Psi_n(x,t). \tag{C.10}$$

and since the Floquet modes build an orthonormal basis at any time t one concludes that also

$$\hat{a}(t,t') = e^{\mathbb{i}\Omega(t-t')}\hat{A} + \zeta(t') \tag{C.11}$$

must hold. Using these relations in the Born-Markov master equation for a driven damped harmonic oscillator, and representing the density operator for this system in a basis of Floquet modes one can, after a rather tedious calculation which will not be reproduced here, show that the Floquet modes are indeed a good approximation for the correct pointer states. These states are selected by the interaction with the environment and survive decoherence.

Bibliography

[1] A. Lupascu, C.J.M. Verwijs, R. N. Schouten, C.J.P.M. Harmans, and J. E. Mooij. Nondestructive readout for a superconducting flux qubit. *Phys. Rev. Lett.*, 93:177006, 2004.

[2] S.L. Adler. Why decoherence has not solved the measurement problem. *Studies in history and philosophy of modern physics*, 34:135, 2003.

[3] M.A. Nielsen and I.L. Chuang. *Quantum Computation and Quantum Information*. Cambridge University Press, Cambridge, UK, 2000.

[4] C.M. Caves, K.S. Thorne, R.W. P. Drever, V.D. Sandberg, and M. Zimmermann. On the measurement of a weak classical force coupled to a quantum-mechanical oscillator. I. Issues of principle. *Rev. Mod. Phys.*, 52(2):341–392, 1980.

[5] V.B. Braginsky, F. Ya. Khalili, and K.S. Thorne. *Quantum Measurement*. Cambridge University Press, Cambridge, 1995.

[6] J.R. Friedman, V. Patel, W. Chen, S.K. Tolpygo, and J.E. Lukens. Quantum superposition of distinct macroscopic states. *Nature*, 46:43, 2000.

[7] A.J. Leggett. Testing the limits of quantum mechanics: motivation, state of play, prospects. *Journal of Physics: Condensed Matter*, 14(15):R415, 2002.

[8] F. Marquardt, B. Abel, and J. von Delft. Measuring the size of a schroedinger cat state, 2006. quant-ph/0609007.

[9] W.H. Zurek. Pointer basis of quantum apparatus: Into what mixture does the wave packet collapse? *Phys. Rev. D*, 24:1516, 1981.

[10] W.H. Zurek. Preferred states, predictability, classicality and the environment-induced decoherence. *Prog. Theor. Phys.*, 89:281, 1993.

[11] Juan Pablo Paz and Wojciech Hubert Zurek. Quantum limit of decoherence: Environment induced superselection of energy eigenstates. *Phys. Rev. Lett.*, 82(26):5181–5185, 1999.

[12] Yakir Aharonov, David Z. Albert, and Lev Vaidman. How the result of a measurement of a component of the spin of a spin-1/2 particle can turn out to be 100. *Phys. Rev. Lett.*, 60(14):1351–1354, 1988.

[13] Yu. Makhlin, G. Schön, and A. Shnirman. Quantum-state engineering with Josephson-junction devices. *Rev. Mod. Phys.*, 73:357, 2001.

[14] R.P. Feynman and F.L. Vernon. The theory of a general quantum system interacting with a linear dissipative system. *Ann. Phys. (N.Y.)*, 24:118, 1963.

[15] A.O. Caldeira and A.J. Leggett. Quantum tunneling in a dissipative system. *Ann. Phys. (NY)*, 149:374, 1983.

[16] G.L. Ingold. *Quantum transport and dissipation*, chapter Dissipative quantum systems. Wiley-VCH, Weinheim, 1998.

[17] H.B. Callen and T.A. Welton. Irreversibility and generalized noise. *Phys. Rev. B*, 83:34, 1951.

[18] J. von Delft and H. Schoeller. Bosonozation for beginners - refermionization for experts. *Ann. Phys. (Leipzig)*, 7:225, 1998.

[19] U. Weiss. *Quantum Dissipative Systems.* Number 10 in Series in modern condensed matter physics. World Scientific, Singapore, 2 edition, 1999.

[20] M. V. S. Bonanca and M. A. M. de Aguiar. Quantum dissipation and decoherence via interaction with low-dimensional chaos: A feynman-vernon approach. *Phys. Rev. A*, 74(1):012105, 2006.

[21] S. Nakajima. On quantum theory of transport phenomena - steady diffusion. *Prog. Theor. Phys.*, 20:948, 1958.

[22] R. Zwanzig. Ensembe method in the theory of irreversibility. *J. Chem. Phys.*, 33:1338, 1960.

[23] G. Lindblad. On the generators of quantum dynamical semigroups. *Commun. Math. Phys.*, 48:119, 1976.

[24] R. Alicki and K. Lendi. *Quantum dynamical semigroups and applications.* Number 286 in Lecture notes in physics. Springer, Berlin, 1976.

[25] R.J. Glauber. Coeherent and incoherent states of the radiation field. *Phys. Rev.*, 131:2766, 1963.

[26] E. C. G. Sudarshan. Equivalence of semiclassical and quantum mechanical descriptions of statistical light beams. *Phys. Rev. Lett.*, 10(7):277–279, 1963.

[27] K.E. Cahill and R.J. Glauber. Density operators and quasiprobability distributions. *Phys. Rev.*, 177:1882, 1969.

[28] H. Risken. *The Fokker-Planck Equation : Methods of Solutions and Applications*. Springer series in synergetics. Springer, Heidelberg, 2nd edition, 1996.

[29] L.K. Grover. Quantum mechanics helps in searching for a needle in a haystack. *Proceedings of the 28'th Annual ACM Symposium on the Theory of Computing*, 79:325, 1997.

[30] P. Shor. Algorithms for quantum computation: Discrete logarithms and factoring. *Proceedings 35th Annual Symposium on Foundations of Computer Science*, page 124, 1994.

[31] R.P. Feynman. Simulating physics with computers. *International Journal of Theoretical Physics*, 21:467, 1981.

[32] C. H. Bennett and G. Brassard. Quantum cryptography: Public key distribution and coin tossing. In *Proceedings of IEEE International Conference on Computers, Systems, and Signal Processing, Bangalore, India*, pages 175–179, New York, 1984. IEEE.

[33] G. Vidal and C. M. Dawson. Universal quantum circuit for two-qubit transformations with three controlled-not gates. *Phys. Rev. A*, 69(1):010301, 2004.

[34] D.P. DiVincenzo. Quantum computation. *Science*, 270:255, 1995.

[35] D.P.DiVincenzo and D. Loss. Quantum information is physical. *Superlattices and Microstructures*, 23:419, 1998.

[36] D.P. DiVincenzo. The physical implementation of quantum computation. *Fortschr. Phys.*, 48:771, 2000.

[37] E. Knill, R. Laflamme, and G. J. Milburn. A scheme for efficient quantum computation with linear optics. *Nature*, 409(6816):46–52, 2001.

[38] B. P. Lanyon, T. J. Weinhold, N. K. Langford, M. Barbieri, D. F. V. James, A. Gilchrist, and A. G. White. Experimental demonstration of a compiled version of shor's algorithm with quantum entanglement. *Phys. Rev. Lett.*, 99(25):250505, 2007.

[39] J. I. Cirac, P. Zoller, H. J. Kimble, and H. Mabuchi. Quantum state transfer and entanglement distribution among distant nodes in a quantum network. *Phys. Rev. Lett.*, 78(16):3221–3224, 1997.

[40] J. I. Cirac and P. Zoller. Quantum computations with cold trapped ions. *Phys. Rev. Lett.*, 74(20):4091–4094, 1995.

[41] C. Monroe, D. M. Meekhof, B. E. King, W. M. Itano, and D. J. Wineland. Demonstration of a fundamental quantum logic gate. *Phys. Rev. Lett.*, 75(25):4714–4717, 1995.

[42] S. Gulde, M. Riebe, G.P. T. Lancaster, C. Becher, J. Eschner, H. Haffner, F. Schmidt-Kaler, I.L. Chuang, and R. Blatt. Implementation of the deutsch-jozsa algorithm on an ion-trap quantum computer. *Nature*, 421(6918):48–50, 2003.

[43] J. Chiaverini, D. Leibfried, T. Schaetz, M. D. Barrett, R. B. Blakestad, J. Britton, W. M. Itano, J. D. Jost, E. Knill, C. Langer, R. Ozeri, and D. J. Wineland. Realization of quantum error correction. *Nature*, 432(7017):602–605, 2004.

[44] G.K. Brennen, C.M. Caves, P.S. Jessen, and I.H. Deutsch. Quantum logic gates in optical lattices. *Phys. Rev. Lett.*, 82(5):1060–1063, 1999.

[45] L.M.K. Vandersypen, M. Steffen, G. Breyta, C.S. Yannoni, M.H. Sherwood, and I.L. Chuang. Experimental realization of shor's quantum factoring algorithm using nuclear magnetic resonance. *Nature*, 414(6866):883–887, 2001.

[46] E. Knill, R. Laflamme, R. Martinez, and C. Negrevergne. Benchmarking quantum computers: The five-qubit error correcting code. *Phys. Rev. Lett.*, 86(25):5811–5814, 2001.

[47] P. M. Platzman and M. I. Dykman. Quantum Computing with Electrons Floating on Liquid Helium. *Science*, 284(5422):1967–1969, 1999.

[48] D. Loss and D.P. DiVincenzo. Quantum computation with quantum dots. *Phys. Rev. A*, 57:120, 1998.

[49] C. Stampfer, J. Güttinger, F. Molitor, D. Graf, T. Ihn, and K. Ensslin. Tunable coulomb blockade in nanostructured graphene. *Applied Physics Letters*, 92(1):012102, 2008.

[50] B. E. Kane. A silicon-based nuclear spin quantum computer. *Nature*, 393(6681):133–137, 1998.

[51] M. V. Gurudev Dutt, L. Childress, L. Jiang, E. Togan, J. Maze, F. Jelezko, A. S. Zibrov, P. R. Hemmer, and M. D. Lukin. Quantum Register Based on Individual Electronic and Nuclear Spin Qubits in Diamond. *Science*, 316(5829):1312–1316, 2007.

[52] Y. Nakamura, Y.A. Pashkin, and J.S. Tsai. Coherent control of macroscopic quantum states in a single-Cooper-pair box. *Nature*, 398:786, 1999.

[53] D. Vion, A. Aassime, A. Cottet, P. Joyez, H. Pothier, C. Urbina, D. Esteve, and M.H. Devoret. Manipulating the quantum state of an electrical circuit. *Science*, 296:286, 2002.

[54] J.M. Martinis, S. Nam, J. Aumentado, and C. Urbina. Rabi oscillations in a large Josephson-junction qubit. *Phys. Rev. Lett.*, 89(11):117901, 2002.

[55] T. Yamamoto, Yu.A. Pashkin, O. Astafiev, Y. Nakamura, and J.S. Tsai. Demonstration of conditional gate operation using superconducting charge qubits. *Nature*, 425:941, 2003.

[56] J. H. Plantenberg, P. C. de Groot, C. J. P. M. Harmans, and J. E. Mooij. Demonstration of controlled-not quantum gates on a pair of superconducting quantum bits. *Nature*, 447(7146):836–839, 2007.

[57] M. Steffen, M. Ansmann, Radoslaw C. Bialczak, N. Katz, Erik Lucero, R. McDermott, Matthew Neeley, E. M. Weig, A. N. Cleland, and J.M. Martinis. Measurement of the Entanglement of Two Superconducting Qubits via State Tomography. *Science*, 313(5792):1423–1425, 2006.

[58] C.H. van der Wal. *Quantum Superpositions of Persistent Josephson Currents*. PhD thesis, Technische Universiteit Delft, 2001.

[59] J. Bardeen, L. N. Cooper, and J. R. Schrieffer. Theory of superconductivity. *Phys. Rev.*, 108(5):1175–1204, 1957.

[60] B.D. Josephson. Possible new effects in superconductive tunneling. *Phys. Lett.*, 1(7):251, 1962.

[61] M.H. Devoret. Quantum fluctuations in electrical circuits. In *Quantum Fluctuations*, number LXIII in Les Houches Session, page 351, Amsterdam, 1995. Elsevier.

[62] B. Yurke and J.S. Denker. Quantum network theory. *Phys. Rev. A*, 29(3):1419–1437, 1984.

[63] R.F. Voss and R.A. Webb. Macroscopic quantum tunneling in $1-\mu$ m nb Josephson junctions. *Phys. Rev. Lett.*, 47(4):265–268, 1981.

[64] M.H. Devoret, J.M. Martinis, and J. Clarke. Measurements of macroscopic quantum tunneling out of the zero-voltage state of a current-biased Josephson junction. *Phys. Rev. Lett.*, 55(18):1908–1911, 1985.

[65] J.M. Martinis, M.H. Devoret, and J. Clarke. Energy-level quantization in the zero-voltage state of a current-biased Josephson junction. *Phys. Rev. Lett.*, 55(15):1543–1546, 1985.

[66] A. J. Leggett and Anupam Garg. Quantum mechanics versus macroscopic realism: Is the flux there when nobody looks? *Phys. Rev. Lett.*, 54(9):857–860, 1985.

[67] Y. Nakamura, C. D. Chen, and J. S. Tsai. Spectroscopy of energy-level splitting between two macroscopic quantum states of charge coherently superposed by Josephson coupling. *Phys. Rev. Lett.*, 79(12):2328–2331, 1997.

[68] C.H. van der Wal, A.C.J. ter Haar, F.K. Wilhelm, R.N. Schouten, C.J.P.M.Harmans, T.P. Orlando, S. Lloyd, and J.E.Mooij. Quantum superposition of macroscopic persistent-current states. *Science*, 290:773, 2000.

[69] J. Koch, T.M. Yu, J. Gambetta, A. A. Houck, D. I. Schuster, J. Majer, A. Blais, M. H. Devoret, S. M. Girvin, and R. J. Schoelkopf. Charge-insensitive qubit design derived from the cooper pair box. *Phys. Rev. A*, 76(4):042319, 2007.

[70] I. Chiorescu, Y. Nakamura, C. J. P. M. Harmans, and J. E. Mooij. Coherent Quantum Dynamics of a Superconducting Flux Qubit. *Science*, 299(5614):1869–1871, 2003.

[71] J.C. Lee, W.D. Oliver, T.P. Orlando, and K.K. Berggren. Resonant readout of a persistent current qubit. *IEEE Trans. Appl. Superc.*, 15:841, 2005.

[72] E. Il'ichev, N. Oukhanski, A. Izmalkov, Th. Wagner, M. Grajcar, H.-G. Meyer, A.Yu. Smirnov, Alec Maassen van den Brink, M.H.S. Amin, and A.M. Zagoskin. Continuous observation of Rabi oscillations in a Josephson flux qubit. *Phys. Rev. Lett.*, 91:097906, 2003.

[73] M. Tinkham. *Introduction to Superconductivity.* McGraw-Hill, New York, 1996.

[74] J. Clarke and A.I. Braginski, editors. *The SQUID Handbook.* Wiley-VCH, Weinheim, 2004.

[75] J.E. Mooij, T.P. Orlando, L. Levitov, L. Tian, C.H. van der Wal, and S. Lloyd. Josephson persistent current qubit. *Science*, 285:1036, 1999.

[76] C.H. van der Wal, A.C.J. ter Haar, F.K. Wilhelm, R.N. Schouten, C.J.P.M. Harmans, T.P. Orlando, S. Lloyd, and J.E. Mooij. Quantum superposition of macroscopic persistent-current states. *Science*, 290:773, 2000.

[77] M. Grajcar, A. Izmalkov, E. Il'ichev, Th. Wagner, N. Oukhanski, U. Hübner, T. May, I. Zhilyaev, H. E. Hoenig, Ya. S. Greenberg, V. I. Shnyrkov, D. Born, W. Krech, H.-G. Meyer, Alec Maassen van den Brink, and M. H. S. Amin. Low-frequency measurement of the tunneling amplitude in a flux qubit. *Phys. Rev. B*, 69(6):060501, 2004.

[78] A. Wallraff, D. I. Schuster, A. Blais, L. Frunzio, J. Majer, M. H. Devoret, S. M. Girvin, and R. J. Schoelkopf. Approaching unit visibility for control of a superconducting qubit with dispersive readout. *Phys. Rev. Lett.*, 95(6):060501, 2005.

[79] I. Siddiqi, R. Vijay, M. Metcalfe, E. Boaknin, L. Frunzio, R. J. Schoelkopf, and M. H. Devoret. Dispersive measurements of superconducting qubit coherence with a fast latching readout. *Phys. Rev. B*, 73(5):054510, 2006.

[80] A. Lupascu, E. F. C. Driessen, L. Roschier, C. J. P. M. Harmans, and J. E. Mooij. High-contrast dispersive readout of a superconducting flux qubit using a nonlinear resonator. *Phys. Rev. Lett.*, 96(12):127003, 2006.

[81] I. Siddiqi, R. Vijay, F. Pierre, C. M. Wilson, M. Metcalfe, C. Rigetti, L. Frunzio, and M. H. Devoret. Rf-driven Josephson bifurcation amplifier for quantum measurement. *Phys. Rev. Lett.*, 93(20):207002, 2004.

[82] A. Lupascu, S. Saito, T. Picot, P. C. de Groot, C. J. P. M. Harmans, and J. E. Mooij. Quantum non-demolition measurement of a superconducting two-level system. *Nat. Phys.*, 3(2):119–125, 2007.

[83] A. Peres. *Quantum Theory: Concept and Methods*. Kluwer, Dordrecht, 1993.

[84] P.W. Anderson. Science: A 'dappled world' or a 'seamless web'. *Studies in history and philosophy of modern physics*, 32:487, 2001.

[85] P.W. Anderson. Reply to Cartwright. *Studies in history and philosophy of modern physics*, 32:499, 2001.

[86] M.H. Devoret, A. Wallraff, and J.M. Martinis. Superconducting qubits: A short review. cond-mat/0411174.

[87] M.R. Geller, E.J. Pritchett, A.T. Sornborger, and F.K. Wilhelm. *Quantum computing with superconductors I: Architectures*. NATO Science Series II: Mathematics, Physics and Chemistry. Springer, Dordrecht, 2007.

[88] F.K. Wilhelm and K. Semba. Superconducting qubits, status and prospects. In M. Nakahara, S. Kanemitsu, and M.M. Salomaa, editors, *Physical Realizatinons of Quantum Computing: Are the DiVincenzo Criteria Fulfilled in 2004?*, Singapore, 2006. WorldScientific.

[89] C. Cohen-Tannoudji, B. Diu, and F. Laloë. *Quantum Mechanics*. Wiley Interscience, Weinheim, 1992.

[90] J. von Neumann. *Mathematical Foundations of Quantum Mechanics*. Princeton University Press, 1955.

[91] J. Clarke, T.L. Robertson, B.L.T. Plourde, A. Garcia-Martinez, P.A. Reichardt, D.J. van Harlingen, B. Chesca, R. Kleiner, Y. Makhlin, G. Schoen, A. Shnirman, and F.K. Wilhelm. Quiet readout of superconducting flux states. *Phys. Scr.*, T102:173, 2002.

[92] C.H. van der Wal, F.K. Wilhelm, C.J.P.M. Harmans, and J.E. Mooij. Engineering decoherence in Josephson persistent-current qubits. *Eur. Phys. J. B*, 31:111, 2003.

[93] M. Steffen, M. Ansmann, R. McDermott, N. Katz, R.C. Bialczak, E. Lucero, M. Neeley, E. M. Weig, A. N. Cleland, and J. M. Martinis. State tomography of capacitively shunted phase qubits with high fidelity. *Phys. Rev. Lett.*, 97(5):050502, 2006.

[94] J.M. Martinis, M.H. Devoret, and J. Clarke. Experimental tests for the quantum behavior of a macroscopic degree of freedom: The phase difference across a Josephson junction. *Phys. Rev. B*, 35(10):4682–4698, 1987.

[95] F. K. Wilhelm. Asymptotic von neumann measurement strategy for solid-state qubits. *Phys. Rev. B*, 68(6):060503, 2003.

[96] P. Joyez, D. Vion, M. Goetz, M.H. Devoret, and D. Esteve. The Josephson effect in nanoscale tunnel junctions. *Journal of superconductivity*, 12:757, 1999.

[97] T.L. Robertson, B.L.T. Plourde, T. Hime, S. Linzen, P.A. Reichardt, F.K. Wilhelm, and J. Clarke. Superconducting quantum interference device with frequency-dependent damping: Readout of flux qubits. *Phys. Rev. B*, 72(2):024513, 2005.

[98] A. Blais, R-S. Huang, A. Wallraff, S.M. Girvin, and R.J. Schoelkopf. Cavity quantum electrodynamics for superconducting electrical circuits: An architecture for quantum computing. *Phys. Rev. A*, 69:062320, 2004.

[99] D.I. Schuster, A. Wallraff, A. Blais, L. Frunzio, R.S. Huang, J. Majer, S.M. Girvin, and R.J. Schoelkopf. ac stark shift and dephasing of a superconducting qubit strongly coupled to a cavity field. *Phys. Rev. Lett.*, 94:123602, 2005.

[100] I. Siddiqi, R. Vijay, F. Pierre, C.M. Wilson, L. Frunzio, M. Metcalfe, C. Rigetti, R.J. Schoelkopf, M.H. Devoret, D. Vion, and D. Esteve. Direct observation of dynamical bifurcation between two driven oscillation states of a Josephson junction. *Phys. Rev. Lett.*, 94:027005, 2005.

[101] F.K. Wilhelm, U. Hartmann, M.J. Storcz, and M.R. Geller. *Quantum computing with superconductors II: Decoherence.* NATO Science Series II: Mathematics, Physics and Chemistry. Springer, Dordrecht, 2007.

[102] M. Keil and H. Schoeller. Real-time renormalization-group analysis of the dynamics of the spin-boson model. *Phys. Rev. B*, 63:180302, 2001.

[103] D.F. Walls and G.J. Milburn. *Quantum Optics.* Springer, Berlin, 1994.

[104] E. Paladino, L. Faoro, G. Falci, and R. Fazio. Decoherence and 1/f noise in Josephson qubits. *Phys. Rev. Lett.*, 88:228304, 2002.

[105] M. Thorwart, E. Paladino, and M. Grifoni. Dynamics of the spin-boson model with a structured environment. *Chem. Phys.*, 296:333, 2004.

[106] M.I. Dykman and M.A. Krivoglaz. Profiles of no-phonon lines of impurity centers interacting with local or quasilocal vibrations. *Fiz. Tverd. Tela*, 29:368, 1987.

[107] P. Bertet, I. Chiorescu, G. Burkard, K. Semba, C. J. P. M. Harmans, D. P. DiVincenzo, and J. E. Mooij. Dephasing of a superconducting qubit induced by photon noise. *Phys. Rev. Lett.*, 95(25):257002, 2005.

[108] A. N. Korotkov and D. V. Averin. Continuous weak measurement of quantum coherent oscillations. *Phys. Rev. B*, 64(16):165310, 2001.

[109] R. Ruskov and A.N. Korotkov. Quantum feedback control of a solid-state qubit. *Phys. Rev. B*, 66(4):041401, 2002.

[110] A.O. Caldeira and A.J. Leggett. Influence of dissipation on quantum tunneling in macroscopic systems. *Phys. Rev. Lett.*, 46:211, 1981.

[111] A. J. Leggett. Quantum tunneling in the presence of an arbitrary linear dissipation mechanism. *Phys. Rev. B*, 30(3):1208–1218, 1984.

[112] A.J. Leggett, S. Chakravarty, A.T. Dorsey, M.P.A. Fisher, A. Garg, and W. Zwerger. Dynamics of the dissipative two-state system. *Rev. Mod. Phys.*, 59:1, 1987.

[113] A. Garg, J.N. Onuchic, and V. Ambegaokar. Effect of friction on electron-transfer in biomolecules. *J. Chem. Phys.*, 83:4491, 1985.

[114] V. Ambegokar. Dissipation and decoherence in a quantum oscillator, 2005. quant-ph/0506087.

[115] K. Blum. *Density Matrix Theory and Applications*. Plenum, New York, 1996.

[116] R. Alicki, D. Lidar, and P. Zanardi. Internal consistency of fault-tolerant quantum error correction in light of rigorous derivaqtions of the quantum markovian limit. *Phys. Rev. A*, 73:052311, 2006.

[117] P. Hänggi. *Quantum Transport and Dissipation*, chapter 6. Wiley-VCH, Weinheim, 1998.

[118] M. Grifoni and P. Hänggi. Driven quantum tunneling. *Phys. Lett.*, 304:229, 1998.

[119] W.P. Schleich. *Quantum Optics in Phase Space*. Wiley-VCH, Weinheim, 2001.

[120] A. A. Clerk, S. M. Girvin, and A. D. Stone. Quantum-limited measurement and information in mesoscopic detectors. *Phys. Rev. B*, 67(16):165324, 2003.

[121] Frank K. Wilhelm. Reduced visibility of quantum oscillations in the spin-boson model, 2005. cond-mat/0507526.

[122] Q. Zhang, A.G. Kofman, J.M. Martinis, and A.N. Korotkov. Analysis of measurement errors for a superconducting phase qubit. *Phys. Rev. B*, 74(21):214518, 2006.

[123] H. Walther P. Lougovski and E. Solano. Measurement of field quadrature moments and entanglement with a two-level probe. *Eur. Phys. J. D*, 38:685, 2006.

[124] J. von Zanthier T. Bastin and E. Solano. Measure of phonon-number moments and motional quadratures through infinitesimal-time probing of trapped ions. *Journal of Physics B*, 39(3):685–693, 2006.

[125] M. Franca Santos, G. Giedke, and E. Solano. Noise-free measurement of harmonic oscillators with instantaneous interactions. *Phys. Rev. Lett.*, 98(2):020401, 2007.

[126] R.H. Koch, G.A. Keefe, F.P. Williken, J.R. Rozen, C.C. Tsuei, J.R. Kirtley, and D.P. DiVincenzo. Experimental demonstration of an oscillator stabilized Josephson flux qubit. *Phys. Rev. Lett.*, 96:127001, 2006.

[127] E.M. Purcell. Spontaneous emission probabilities at radio frequencies. *Phys. Rev.*, 69:681, 1946.

[128] A.G. Fowler, W.F. Thompson, Z. Yan, A. M. Stephens, B.L.T. Plourde, and F.K. Wilhelm. Long-range coupling and scalable architecture for superconducting flux qubits, 2007.

[129] J.M. Raimond, M. Brune, and S. Haroche. Manipulating quantum entanglement with atoms and photons in a cavity. *Rev. Mod. Phys.*, 73:565, 2001.

[130] A. Balodato, K. Hennessy, M. Atature, J. Dreiser, E. Hu, P.M. Petroff, and A. Imamoglu. Deterministic coupling of single quantum dots to single nanocavity modes. *Science*, 308:1158, 2005.

[131] A. Wallraff, D.I. Schuster, A. Blais, L. Frunzio, R.S. Huang, J. Majer, S. Kumar, S.M. Girvin, and R.J. Schoelkopf. Strong coupling of a single photon to a superconducting qubit using circuit quantum electrodynamics. *Nature*, 431:162, 2004.

[132] T. Duty, D. Gunnarsson, K. Bladh, and P. Delsing. Coherent dynamics of a Josephson charge qubit. *Phys. Rev. B*, 69:140503, 2004.

[133] Y.A. Pashkin, T. Yamamoto, O. Astafiev, Y. Nakamura, D.V. Averin, and J.S. Tsai. Quantum oscillations in two coupled charge qubits. *Nature*, 421:823, 2003.

[134] R. McDermott, R.W. Simmonds, M. Steffen, K.B. Cooper, K. Cicak, K.D. Osborn, S. Oh, D.P. Pappas, and J.M. Martinis. Simultaneous state measurement of coupled Josephson phase qubits. *Science*, 307:1299, 2005.

[135] W.D. Oliver, Y. Yu, J.C. Lee, K.K. Berggren, L.S. Levitov, and T.P. Orlando. Mach-zehnder interferometry in a strongly driven superconducting qubits. *Science*, 310:5754, 2005.

[136] T.L. Robertson B. L. Plourde, P.A. Reichardt, T. Hime, S. Linzen, C.E. Wu, and J. Clarke. Flux qubits and readout device with two independent flux lines. *Phys. Rev. B*, 72:060506, 2005.

[137] O. Buisson and F.W.J. Hekking. Entangled states in a Josephson charge qubit coupled to a superconducting resonator. In D.V. Averin, B. Ruggerio, and P. Silvestrini, editors, *Macroscopic Quantum Coherence and Quantum Computing*, page 137, New York, 2001. Kluwer.

[138] J.Q. You and F. Nori. Quantum information processing with superconducting qubits in a microwave field. *Phys. Rev. B*, 68:064509, 2003.

[139] M.C. Goorden, M. Thorwart, and M. Grifoni. Entanglement spectroscopy of a driven solid-state qubit and its detector. *Phys. Rev. Lett.*, 93:267005, 2004.

[140] S. Kleff, S. Kehrein, and J. von Delft. Exploiting environmental resonances to enhance qubit quality factors. *Phys. Rev. B*, 70:014516, 2004.

[141] C.P. Yang, S.I. Chu, and S.Y. Han. Quantum information transfer and entanglement with squid qubits in cavity qed: A dark-state scheme with tolerance for nonuniform device parameter. *Phys. Rev. Lett.*, 92:117902, 2004.

[142] M. Sarovar, H.S. Goan, T.P. Spiller, and G.J. Milburn. High-fidelity measurement and quantum feedback control in circuit qed. *Phys. Rev. A*, 72:062327, 2005.

[143] M. Mariantoni, M.J. Storcz, F.K. Wilhelm, W.D. Oliver, A. Emmert, A. Marx, R. Gross, H. Christ, and E. Solano. On-chip microwave fock states and quantum homodyne measurements. cond-mat/0509737.

[144] P. Bertet, I. Chiorescu, C.J.P.M. Harmans, and J.E. Mooij. Dephasing of a flux qubit coupled to a harmonic oscillator. cond-mat/0507290.

[145] D. I. Schuster, A. A. Houck, J. A. Schreier, A. Wallraff, J. M. Gambetta, A. Blais, L. Frunzio, J. Majer, B. Johnson, M. H. Devoret, S. M. Girvin, and R. J. Schoelkopf. Resolving photon number states in a superconducting circuit. *Nature*, 445(7127):515–518, 2007.

[146] D. Leibfried, R. Blatt, C. Monroe, and D. Wineland. Quantum dynamics of single trapped ions. *Rev. Mod. Phys.*, 75(1):281–324, 2003.

[147] J. Gambetta, A. Blais, D.I. Schuster, A. Wallraff, L. Frunzio, J. Majer, M.H. Devoret, S.M. Girvin, and R.J. Schoelkopf. Qubit-photon interaction in a cavity: Measurement induced dephasing and number splitting. *Phys. Rev. A*, 74:042318, 2006.

[148] S. Haroche and D. Kleppner. Cavity quantum electrodynamics. *Physics Today*, page 24, 1989.

[149] C.P. Slichter. *Principles of magnetic resonance.* Number 1 in Series in Solid State Sciences. Springer, Berlin, 3. edition, 1996.

[150] L. Bulaevskii, M. Hruška, A. Shnirman, D. Smith, and Yu. Makhlin. Nondemolition measurements of a single quantum spin using Josephson oscillations. *Phys. Rev. Lett.*, 92(17):177001, 2004.

[151] D. V. Averin. Quantum nondemolition measurements of a qubit. *Phys. Rev. Lett.*, 88(20):207901, 2002.

[152] A.N. Jordan and M. Buttiker. Quantum nondemolition measurement of a kicked qubit. *Phys. Rev. B*, 71(12):125333, 2005.

[153] A.N. Jordan and A.N. Korotkov. Qubit feedback and control with kicked quantum nondemolition measurements: A quantum bayesian analysis. *Phys. Rev. B*, 74(8):085307, 2006.

[154] G. J. Milburn and D. F. Walls. Quantum nondemolition measurements via quadratic coupling. *Phys. Rev. A*, 28(4):2065–2070, 1983.

[155] B. C. Sanders and G. J. Milburn. Complementarity in a quantum nondemolition measurement. *Phys. Rev. A*, 39(2):694–702, 1989.

[156] M. Brune, S. Haroche, V. Lefevre, J. M. Raimond, and N. Zagury. Quantum nondemolition measurement of small photon numbers by rydberg-atom phase-sensitive detection. *Phys. Rev. Lett.*, 65(8):976–979, 1990.

[157] N. Boulant, G. Ithier, P. Meeson, F. Nguyen, D. Vion, D. Esteve, I. Siddiqi, R. Vijay, C. Rigetti, F. Pierre, and M. Devoret. Quantum nondemolition readout using a Josephson bifurcation amplifier. *Phys. Rev. B*, 76(1):014525, 2007.

[158] M. Boissonneault, J. Gambetta, and A. Blais. Non-linear dispersive regime of circuit qed: The dressed dephasing model, 2008. arXiv.org:0803.0311.

[159] M. Metcalfe, E. Boaknin, V. Manucharyan, R. Vijay, I. Siddiqi, C. Rigetti, L. Frunzio, R. J. Schoelkopf, and M. H. Devoret. Measuring the decoherence of a quantronium qubit with the cavity bifurcation amplifier. *Phys. Rev. B*, 76(17):174516, 2007.

[160] T. Bastin, J. Zanthier, and E. Solano. Measure of photon-number moments and motional quadratures through infinitesimal-time probing of trapped ions. *J. Phys. B.*, 39:685, 2006.

[161] M. Franca Santos, G. Giedke, and E. Solano. Noise-free measurement of harmonic oscillators with instantaneous interactions. *Phys. Rev. Lett.*, 98(2):020401, 2007.

[162] M.J. Storcz, M. Mariantoni, H. Christ, A. Emmert, A. Marx, W. D. Oliver, R. Gross, F. K. Wilhelm, and E. Solano. Orthogonally-driven superconducting qubit in circuit qed, 2006. cond-mat/0612226.

[163] T. P. Orlando, J. E. Mooij, L. Tian, C.H. van der Wal, L. S. Levitov, S. Lloyd, and J. J. Mazo. Superconducting persistent-current qubit. *Phys. Rev. B*, 60:15398, 1999.

[164] L. Tian, S. Lloyd, and T.P. Orlando. Decoherence and relaxation of a superconducting quantum bit during measurement. *Phys. Rev. B*, 65:144516, 2002.

[165] V. Lefevre-Seguin, E. Turlot, C. Urbina, D. Esteve, and M.H. Devoret. Thermal activation of a hysteretic dc superconducting quantum interference device from its different zero-voltage states. *Phys. Rev. B*, 46(9):5507–5522, 1992.

[166] I. Serban, E. Solano, and F. K. Wilhelm. Phase-space theory for dispersive detectors of superconducting qubits. *Phys. Rev. B*, 76(10):104510, 2007.

[167] P. Bertet, I. Chiorescu, G. Burkard, K. Semba, C. J. P. M. Harmans, D. P. DiVincenzo, and J. E. Mooij. Dephasing of a superconducting qubit induced by photon noise. *Phys. Rev. Lett.*, 95(25):257002, 2005.

[168] M. Mück. Private communication, 2008.

[169] M. Muck, C. Welzel, and J. Clarke. Superconducting quantum interference device amplifiers at gigahertz frequencies. *Appl. Phys. Lett.*, 82(19):3266–3268, 2003.

[170] M. Mück, J.B. Kycia, and J. Clarke. Superconducting quantum interference device as a near-quantum-limited amplifier at 0.5 ghz. *Appl. Phys. Lett.*, 78:967, 2001.

[171] E.J. Heller. The many faces of tunneling. *J. Phys. Chem. A*, 103:10433, 1999.

[172] E.J. Heller and M.J. Davis. Quantum dynamical tunneling in large molecules. a plausible conjecture. *J. Phys. Chem.*, 85(4):307–309, 1981.

[173] W. K. Hensinger, H. Haffner, A. Browaeys, N. R. Heckenberg, K. Helmerson, C. McKenzie, G. J. Milburn, W. D. Phillips, S. L. Rolston, H. Rubinsztein-Dunlop, and B. Upcroft. Dynamical tunnelling of ultracold atoms. *Nature*, 412(6842):52–55, 2001.

[174] D.A. Steck, W.H. Oskay, and M.G. Raizen. Observation of Chaos-Assisted Tunneling Between Islands of Stability. *Science*, 293(5528):274–278, 2001.

[175] J.C. Lee, W.D. Oliver, K.K. Berggren, and T.P. Orlando. Nonlinear resonant behavior of a dispersive readout circuit for a superconducting flux qubit. *Phys. Rev. B*, 75:144505, 2007.

[176] M. Marthaler and M.I. Dykman. Quantum interference in the classically forbidden region: A parametric oscillator. *Phys. Rev. A*, 76:010102, 2007.

[177] M. Marthaler and M.I. Dykman. Switching via quantum activation: A parametrically modulated oscillator. *Phys. Rev. A*, 73:042108, 2006.

[178] M.I. Dykman. Critical exponents in metastable decay via quantum activation. *Phys. Rev. E*, 75:011101, 2007.

[179] M.I. Dykman and V.N. Smelyanskiy. Quantum theory of transitions between stable states of a nonlinear oscillator interacting with a medium in a resonant field. *Zh. Eksp. Teor. Fiz.*, 94:61, 1988.

[180] V. Peano and M. Thorwart. Nonlinear response of a driven vibrating nanobeam in the quantum regime. *New. J. Phys*, 8:21, 2006.

[181] V. Peano and M. Thorwart. Dynamics of the quantum duffing oscillator in the driving induced bistable regime. *Chem. Phys.*, 322:135, 2006.

[182] J.R. Almog, S. Zaitsev, O.Shtempluck, and E. Buks. Noise squeezing in a nanomechanical duffing resonator. *Phys. Rev. Lett*, 98:078103, 2007.

[183] J.S. Aldridge and A.N. Cleland. Noise-enabled precision measurements of a duffing nanomechanical resonator. *Phys. Rev. Lett*, 94:156403, 2005.

[184] L.D. Landau and E.M. Lifshitz. *Mechanics*, volume 1 of *Course of Theoretical Physics*. Butterworth-Heinemann, Burlington, MA, 1982.

[185] P. Hanggi, P. Talkner, and M. Borkovec. Reaction-rate theory: fifty years after kramers. *Rev. Mod. Phys.*, 62:252, 1990.

[186] W. G. Unruh. Notes on black-hole evaporation. *Phys. Rev. D*, 14(4):870–892, 1976.

[187] W. Nolting. *Quantenmechanik-Methoden und Anwendungen*, volume 5 of *Grundkurs Theoretische Physik*. Springer, Berlin, 2004.

[188] R.E. Langer. On the connection formulas and the solutions of the wave equation. *Phys. Rev.*, 51(8):669–676, Apr 1937.

[189] F.K. Wilhelm, S. Kleff, and J. von Delft. The spin-boson model with a structured environment: A comparison of approaches. *Chem. Phys.*, 296:345, 2004.

[190] T. Picot. Private communication, 2008.

[191] R. W. Simmonds, K. M. Lang, D. A. Hite, S. Nam, D. P. Pappas, and J.M. Martinis. Decoherence in Josephson phase qubits from junction resonators. *Phys. Rev. Lett.*, 93(7):077003, 2004.

[192] R.T. Wakai and D.J. van Harlingen. Direct lifetime measurements and interactions of charged defect states in submicron Josephson junctions. *Phys. Rev. Lett.*, 58:1687, 1987.

[193] R.H. Koch, D.P. DiVincenzo, and J. Clarke. Model for 1/f flux noise in squids and qubits. *Physical Review Letters*, 98(26):267003, 2007.

[194] L. Jiang, M. V. Gurudev Dutt, E. Togan, L. Childress, P. Cappellaro, J. M. Taylor, and M. D. Lukin. Coherence of an optically illuminated single nuclear spin qubit. *Phys. Rev. Lett.*, 100(7):073001, 2008.

[195] P. Dutta and P.M. Horn. Low-frequency fluctuations in solids: 1/f-noise. *Rev. Mod. Phys.*, 53:497, 1981.

[196] M.B. Weissman. 1/f noise and other slow, nonexponential kinetics in condensed matter. *Rev. Mod. Phys.*, 60:537, 1988.

[197] L. Faoro and L. Viola. Dynamical suppression of 1/f noise processes in qubit systems. *Phys. Rev. Lett.*, 92:117905, 2004.

[198] H. Gutmann, W.M. Kaminsky, S. Lloyd, and F.K. Wilhelm. Compensation of decoherence from telegraph noise by means of an open loop quantum-control technique. *Phys. Rev. A*, 71:020302(R), 2005.

[199] G. Ithier, E. Collin, P. Joyez, P. J. Meeson, D. Vion, D. Esteve, F. Chiarello, A. Shnirman, Y. Makhlin, J. Schriefl, and G. Schon. Decoherence in a superconducting quantum bit circuit. *Phys. Rev. B*, 72(13):134519, 2005.

[200] Y. Makhlin and A. Shnirman. Dephasing of solid-state qubits at optimal points. *Phys. Rev. Lett.*, 92(17):178301, Apr 2004.

[201] P.Rebentrost. *Optimal control of solid state qubits in presence of leakage and decoherence*. PhD thesis, Ludwig Maximilians Universität, Munich, 2007.

[202] A. Grishin, I.V. Yurkevich, and I.V. Lerner. Low-temperature decoherence of qubit coupled to background charges. *Phys. Rev. B*, 72(6):060509, 2005.

[203] R. J. Schoelkopf, A. A. Clerk, S. M. Girvin, K. W. Lehnert, and M. H. Devoret. *Quantum Noise*, chapter Qubits as spectrometers of quantum noise. Nato ASI. Kluwer, Dordrecht, 2002. edited by Yu.V. Nazarov and Ya.M. Blanter.

[204] L.S. Pontryagin, V.G. Boltyanskii, R.V. Gamkrelidtze, and E.F. Mischenko. *The mathematical theory of optimal processes*, volume 4. 1986.

[205] A.M. Weiner, D.E. Leaird, J.S. Patel, and II Wullert, J.R. Programmable shaping of femtosecond optical pulses by use of 128-element liquid crystal phase modulator. *Quantum Electronics, IEEE Journal of*, 28(4):908, 1992.

[206] N. Khaneja, T. Reiss, C. Kehlet, T. Schulte-Herbrüggen, and S.J. Glaser. Optimal control of coupled spin dynamics: Design of nmr pulse sequences by gradient ascent algorithms. *J. Magn. Reson.*, 172:296, 2005.

[207] A. Spoerl, T. Schulte-Herbrueggen, S.J. Glaser, V. Bergholm, M.J. Storcz, J. Ferber, and F.K. Wilhelm. Optimal control of coupled josephson qubits. quant-ph/0504202.

[208] T. Schulte-Herbrueggen, A. Spoerl, N. Khaneja, and S. J. Glaser. Optimal control for generating quantum gates in open dissipative systems, 2006. quant-ph/0609037.

[209] P. Rebentrost, I. Serban, T. Schulte-Herbrueggen, and F. K. Wilhelm. Optimal control of a qubit coupled to a two-level fluctuator, 2006. quant-ph/0612165.

List of publications

- “Qubit relaxation due to a dissipative Duffing oscillator trapped in one of its attractors”,
  I. Serban, M. I. Dykman, and F. K. Wilhelm,
  in preparation

- “Quantum nondemolition-like, fast measurement scheme for a superconducting qubit”,
  I. Serban, B. L. T. Plourde, and F. K. Wilhelm,
  arXiv:0803.0958 (2008), submitted to Phys. Rev. B.

- “Dynamical tunneling in macroscopic systems”,
  I. Serban and F. K. Wilhelm,
  Phys. Rev. Lett. 99, 137001 (2007)

- “Crossover from weak to strong coupling regime in dispersive circuit QED”,
  I. Serban, E. Solano, and F. K. Wilhelm,
  Europhys. Lett. 80, 40011 (2007).

- “Phase-space theory for dispersive detectors of superconducting qubits” ,
  I. Serban, E. Solano, and F. K. Wilhelm,
  Phys. Rev. B 76, 104510 (2007),
  figure selected for PRB Kaleidoscope Images: September 2007.

- “Optimal control of a qubit coupled to a two-level fluctuator”,
  P. Rebentrost, I. Serban, T. Schulte-Herbrueggen, F. K. Wilhelm,
  quant-ph/0612165 (2006), submitted to Phys. Rev. Lett.

Acknowledgment

I am much obliged to Professor Dr. Jan von Delft the opportunity to join his research group in Munich and for his constant support in my attending various conferences and workshops.

I am deeply grateful to my advisor, Prof. Dr. Frank K. Wilhelm, for his mentoring, for the many discussions, his unceasing and contagious optimism and his admirable patience with all my stupid questions. I am also grateful to him and to Prof. Dr. Jan von Delft and Prof. Dr. Raymond Laflamme, for the unique opportunity of an extended visit (2006-2008) at the Institute for Quantum Computing (IQC), in Waterloo, Canada.

The work presented in this thesis has benefited from the help and ideas of many great collaborators. I would like to thank to

- Prof. Dr. Enrique Solano for many insightfull discussions and for some very valuable pieces of advice which guided me through the jungle of phase-space representations and quantum optical methods,
- Prof. Dr. Britton Plourde (Syracuse University) for sharing his expertise in qubit readout and a valuable collaboration,
- Prof. Dr. Kees Harmans, Prof. Dr. Hans Mooij and their group, especially Dr. Adrian Lupaşcu and Thomas Picot (TU Delft) for their help in understanding some experimental issues in superconducting qubit detection, for sharing some of their not yet published results and their hospitality during my stay in Delft,
- Sir Anthony Leggett (University of Illinois at Urbana-Champaign) for sharing some of his broad experience and overview, which helped enlarge the scope of this work,
- Prof. Dr. Mark Dykman (Michigan State University) for interesting discussions about nonlinear systems and the joint work,
- Patrick Rebentrost for a fruitful collaboration on optimal control of open systems,
- Dr. Florian Marquardt for his interest in my work, and many very helpful suggestions,
- Dr. Henryk Gutmann for his help with my very first attempts at understanding open quantum systems,

- Prof. Dr. Eihab Abdel-Rahman, Prof. Dr. Aashish Clerk, Dr. Bill Coish, Dr. Christophe Couteau, Dr. Austin Fowler, Dr. Jay Gambetta, Prof. Dr. Milena Grifoni, Prof. Dr. Evgeni Il'ichev, Dr. Sigmund Kohler, Michael Marthaler, Prof. Dr. Yasunobu Nakamura for useful remarks and stimulating discussions,

- Hauke Häseler for being an attentive listener whenever I was stuck with some physics problem, which helped sort out my ideas, and for his help with some of the more complex figures of this thesis,

- Deutsche Forschungsgemeinschaft and SFB 631 (Festkörperbasierte Quanteninformationsverarbeitung: Physikalische Konzepte und Materialaspekte), the Center for NanoScience (International Doctorate Program NanoBioTechnology) and EuroSQIP (Integrated Project for developing a "European Superconducting Quantum Information Processor") for financial support,

- Mike Ditty, Peter Routledge and Ralph Simmler for computer related technical support.

For creating an enjoyable work atmosphere, I would like to thank, in addition to those mentioned above, to all members of both the Munich group (Benjamin Abel, Peter Fritsch, Dr. Udo Hartmann, Theresa Hecht, Ferdinand Helmer, Andreas Holzner, Prof. Dr. Stefan Kehrein, Michael Möckel, Hamed Saberi, Dr. Markus Storcz) and the Waterloo group (Peter Groszkowski, Georg Heinrich, Felix Motzoi, Brendan Osberg, Ed Platt, Marcus Silva, Geoff Stanley, Will Thompson).

On a more personal note I would like to thank to Hauke Häseler and Austin Fowler for their friendship which made it easier to adapt to the new Canadian environment and to my parents for their constant moral support.

Zusammenfassung

Diese Arbeit präsentiert Ergebnisse zur Messung, Dekohärenz und Kontrolle von Quantenbits (Qubits), die aus supraleitenden Komponenten bestehen und deren Arbeitsweise auf der Nichtlinearität des Josephson-Effekts basiert. Sowohl der Einfluss der Messung auf das gemessene Objekt als auch die interne, quantenmechanische Dynamik des Detektors wird für verschiedene Messmethoden untersucht.

Der erste Teil gibt eine Einführung in die Physik von supraleitenden Qubits und in die Theorie von offenen Quantensystemen, die erfolgreich Teile des Messprozesses beschreibt. Im zweiten Teil, basierend auf Methoden aus der Quantenoptik, adaptiert zur Beschreibung von Festkörpersystemen, wird die beliebig starke und nichtlineare Wechselwirkung eines Qubits mit seiner komplexen Umgebung in einem dispersiven Messprotokol untersucht. Dadurch werden neue Einsichten in die Qubitdekohärenz im Regime starker Kopplung gewonnen. Parameterregionen mit qualitativ unterschiedlichem Verhalten der Qubitdephasierung werden identifiziert, z. B. der Phasen-Purcell-Effekt, und erklärt. Diese Erkenntnisse öffnen neue Wege, bessere Messprotokole zu entwerfen, die die starke, nichtlineare Wechselwirkung zwischen Qubit und Detektor voll ausnutzen. Experimentell realisierbare Protokole werden vorgeschlagen. Diese Idee, kombiniert mit der einer quasi-instantanen Messung wird in einem leicht abgeänderten Aufbau weiter verfolgt, und eröffnet die Möglichkeit einer Quanten-Nondemolition-Detektion.

Da der Qubitdetektor auf der gleichen Technologie wie das Qubit basiert, muss er quantenmechanisch untersucht werden. Die interne, nicht-klassische Dynamik spielt eine wichtige Rolle im Messprozess. So wird weiter das dynamische Tunneln in einem Josephson Bifurkationsverstärker (JBA) untersucht. Diese Sorte Tunneln tritt zwichen verschiedenen Bewegungsmustern auf, die duch eine klassisch verbotene Phasenraumregion separiert sind. Dies ist ein Effekt, dessen Ursprung in der Nichtlinearität des stark angetriebenen Systems liegt, und dessen Quantennatur sogar in einem makroskopischen und verrauschten System beobachtbar sein kann. Das Ergebnis dieser Untersuchung kann nicht nur zu einer besseren Messmethode für supraleitende Qubits verhelfen, sondern auch den experimentellen Nachweis quantenmechanischer Effekte in Systemen mit ähnlichen Nichtlinearitäten unterstützen, wie z. B. in der Nanomechanik. Für den ersten Fall wird zusätzlich die Qubitrelaxation untersucht, die durch die Wechselwirkung mit dem dissipativen JBA entsteht, und den Kontrast der Messung begrenzt.

Weiterhin wird die Kontrolltheorie verwendet, um Pulssequenzen zu optimieren, die bei der Steuerung von Qubits nötig sind. Diese Optimierung berücksichtigt, und nutzt die Tatsache aus, dass in einem realistischen Fall das Qubit nicht vollständig von Rauschquellen isoliert werden kann. Eine wichtige solche Rauschquelle sind intrinsische Zwei-Niveau-Fluktuatoren, typischerweise in der Tunnelbarierre eines Josepshon Kontakts zu finden. Die optimierten Pulse stellen eine Verbesserung zur naiven Rabi-Pulse-Methode dar. Refokussierungseffekte werden sichtbar bei spezifischen Pulslängen.

Curriculum vitae

Ioana Şerban

born	August 31, 1981	in Bucharest, Romania
school	1996-2000	Colegiul National "Sf. Sava", Bucharest (high-school)
	08/2000	Baccalaureate
study	09/2000-06/2001	Study of Electronic Engineering at the Politechnic University, Bucharest
	10/2001-10/2003	Study of Physics at the Freie Universität Berlin
	04/2002	*Vordiplom* in Physics (Freie Universität Berlin)
	10/2003-10/2004	*Diplomarbeit* (Freie Universität Berlin)
	11/2004	*Diplom* in Physics (Freie Universität Berlin)
	01/2005-05/2008	Ph.D. studies in Theoretical Condensed Matter Physics, supervised by Prof. Dr. Frank K. Wilhelm and Prof. Dr. Jan von Delft, Physics Department, ASC and CeNS, Ludwig-Maximilians-Universität München
Thesis	2004	"Optimal control of time-dependent targets" (*Diplomarbeit*) supervised by Prof. Dr. Eberhard Gross, Freie Universität Berlin